US Army Corps of Engineers

AN EVALUATION OF THE SEPARATED BAY CONCEPT FOR A MUNITION ASSEMBLY COMPLEX; AN EXPERIMENTAL INVESTIGATION OF THE DEPARTMENT OF ENERGY BUILDING 12-64 COMPLEX

by

Robert D. Volz, Sam A. Kiger

Structures Laboratory
U. S. Army Engineer Waterways Experiment Station
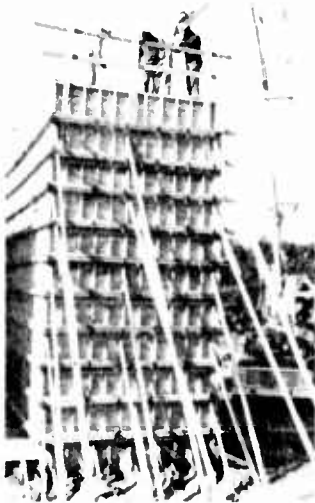P. O. Box 631, Vicksburg, Miss. 39180

AD A137467

September 1983
Final Report

Approved for Public Release; Distribution Unlimited

DTIC
ELECTE
FEB 0 3 1984
E

DTIC FILE COPY

STRUCTURES LABORATORY

84 02 03 049

Destroy this report when no longer needed. Do not
return it to the originator.

The findings in this report are not to be construed as an
official Department of the Army position unless so
designated by other authorized documents.

The contents of this report are not to be used for
advertising, publication, or promotional purposes.
Citation of trade names does not constitute an
official endorsement or approval of the use of such
commercial products.

REPORT DOCUMENTATION PAGE		READ INSTRUCTIONS BEFORE COMPLETING FORM
1. REPORT NUMBER Technical Report SL-83-6	2. GOVT ACCESSION NO.	3. RECIPIENT'S CATALOG NUMBER
4. TITLE *(and Subtitle)* AN EVALUATION OF THE SEPARATED BAY CONCEPT FOR A MUNITION ASSEMBLY COMPLEX; AN EXPERIMENTAL INVESTIGATION OF THE DEPARTMENT OF ENERGY BUILDING 12-64 COMPLEX		5. TYPE OF REPORT & PERIOD COVERED Final report
		6. PERFORMING ORG. REPORT NUMBER
7. AUTHOR(s) Robert D. Volz Sam A. Kiger		8. CONTRACT OR GRANT NUMBER(s)
9. PERFORMING ORGANIZATION NAME AND ADDRESS U. S. Army Engineer Waterways Experiment Station Structures Laboratory P. O. Box 631, Vicksburg, Miss. 39180		10. PROGRAM ELEMENT, PROJECT, TASK AREA & WORK UNIT NUMBERS
11. CONTROLLING OFFICE NAME AND ADDRESS Department of Energy, Albuquerque Operations Amarillo Area Office, P. O. Box 30030 Amarillo, Tex. 79120		12. REPORT DATE September 1983
		13. NUMBER OF PAGES 325
14. MONITORING AGENCY NAME & ADDRESS(*If different from Controlling Office*)		15. SECURITY CLASS. *(of this report)* Unclassified
		15a. DECLASSIFICATION/DOWNGRADING SCHEDULE

16. DISTRIBUTION STATEMENT *(of this Report)*

Approved for public release; distribution unlimited.

17. DISTRIBUTION STATEMENT *(of the abstract entered in Block 20, if different from Report)*

19. KEY WORDS *(Continue on reverse side if necessary and identify by block number)*

Accidental explosions	Soil-structure interaction
Airblast	Structural response
Blast effects	Vibration testing
Ground shock	

20. ABSTRACT *(Continue on reverse side if necessary and identify by block number)*

The Munition Assembly Complex, Building 12-64, located at Pantex, Tex., uses the separated bay concept to isolate adjacent bays from one another. Tests were conducted by the U. S. Army Engineer Waterways Experiment Station to investigate the possibility of an accidental explosion in one bay causing personnel injury in an adjacent bay, and to collect data that can be used to improve future designs of this type. Tests, simulating an accidental

(Continued)

DD FORM 1473 EDITION OF 1 NOV 65 IS OBSOLETE

20. ABSTRACT (Continued):

explosion, were conducted in a full size donor with a partially completed adjacent acceptor bay, and in a 1/2-scale donor bay with a complete adjacent acceptor bay, access tunnels, and blast doors.

Data from these tests indicate the separated bay concept is a cost efficient way to insure the safety of adjacent bays in case of an accidental explosion.

PREFACE

The study reported herein was conducted from May 1981 through May 1982 by personnel of the U. S. Army Engineer Waterways Experiment Station (WES) Structures Laboratory (SL). The study was sponsored by the Amarillo Area Office (AAO) of the Department of Energy (DOE). The contracting officer was Mr. L. M. Paradee, AAO, and Mr. Larry Skeen of Mason & Hanger--Silas Mason Co., Inc. was the project monitor. Mason & Hanger--Silas Mason Co., Inc. is the operating contractor for the DOE Pantex plant. Test plans and specifications were prepared by Mr. Norval Dobbs of Gibbs & Hill/Ammann & Whitney, a joint venture firm, under contract to the DOE to design a new weapon assembly bay complex at the DOE Pantex facility.

Work at WES was under the general supervision of Messrs. W. J. Flathau, Assistant Chief, SL, and J. T. Ballard, Chief, Structural Mechanics Division (SMD), SL, and under the direct supervision of Dr. S. A. Kiger and CPT Robert D. Volz, SMD, SL. The test site construction was supervised by Mr. R. S. Cummins, SMD, SL. Mrs. Patricia S. Jones, SMD, SL, designed and supervised construction of the Phase II blast doors and assisted in conducting the test and reducing the data. This report was prepared by CPT Volz and Dr. Kiger, SMD, SL.

COL Tilford C. Creel, CE, was the Commander and Director of WES during the study and preparation of this report. Mr. F. R Brown was Technical Director.

1

CONTENTS

LIST OF ILLUSTRATIONS

LIST OF TABLES

CONVERSION FACTORS, NON-SI TO SI (METRIC)
UNITS OF MEASUREMENT

Non-SI units of measurement used in this report can be converted to SI (metric) units as follows:

Multiply	By	To Obtain
cubic feet	0.02831685	cubic metres
degrees (angle)	0.01745329	radians
feet	0.3048	metres
feet per second	0.3048	metres per second
foot-pounds (force)	1.355818	joules
inches	25.4	millimetres
kips (force) per square inch	6.894757	megapascals
miles (U. S. statute)	1.609347	kilometres
pounds (mass)	0.4535924	kilograms
pounds (mass) per cubic foot	16.01846	kilograms per cubic metre
pounds per square inch	6894.757	kilopascals
pounds per square inch-second	6894.757	kilopascal-second
square inches	6.451600	square centimetres

AN EVALUATION OF THE SEPARATED BAY CONCEPT FOR A MUNITION
ASSEMBLY COMPLEX; AN EXPERIMENTAL INVESTIGATION OF THE
DEPARTMENT OF ENERGY BUILDING 12-64 COMPLEX

CHAPTER 1

INTRODUCTION

1.1 BACKGROUND

The Department of Energy (DOE) is planning an expansion program at its weapon assembly facility at the Amarillo, Texas, Pantex plant. The new Assembly Bay Complex is designated Building 12-84. The existing Assembly Bay Complex, known as Building 12-64, employs a concept used for weapon storage magazines where adjacent individual bays are separated by earth fill. The distance between adjoining bays is approximately equal to 2.0 times $W^{1/3}$, where W is equal to the actual weight of explosive contained in each bay.

The DOE requested the U. S. Army Engineer Waterways Experiment Station (WES) to conduct an experimental program to evaluate the Building 12-64 separated-bay concept. Data from this program will be used to evaluate the safety of the existing Building 12-64 complex and to design more cost-efficient facilities for new construction.

The basic test plan and specifications were prepared by Gibbs & Hill/ Ammann & Whitney.[1] The overall test program was divided into four phases: Phase I, Evaluation of Punching Failure of Unlaced Reinforced Concrete and Effects Produced by the Fragmentation of the Donor Structure Roof; Phase II, Evaluation of the Overall Blast Overpressure Resistant Capacity of Individual Bays of Existing Building 12-64; Phase III, Evaluation of the Fragment-Resistant Capacity of Individual Bays of Existing Building 12-64; and Phase IV, Evaluation of the Modification of Individual Bays of Building 12-64 to Resist the Blast and Fragment Dispersal of Phases I through III. Phases I and II would furnish the basic test data necessary to evaluate the design concept. The need to conduct Phases III and IV was to be determined after completion of the initial phases of the test program.

1.2 PURPOSE AND OBJECTIVES

The purpose of the test program was to verify the adequacy of the separated bays and unlaced wall reinforcement used in the design of Building 12-64. Validation of this design concept would allow continued use of present facilities as well as future construction of separated assembly bays.

The objectives of Phase I were to determine whether a punching shear failure would occur in adjacent bay walls, and to evaluate the missile hazard produced by the opening of a donor bay roof. The objective of Phase II was to evaluate the overall blast resistance of Building 12-64. Both test phases shared the experimental measurement objectives of determining the following:

a. Velocity, size, and distribution of secondary fragments.

b. Airblast environment in the donor bay.

c. Pressure leakage into acceptor bays.

d. External loads on acceptor bays.

e. Acceptor bay structural response.

1.3 SCOPE

To accomplish the objectives of the investigation, WES personnel constructed two model structures at Camp Shelby, Miss. The Phase I structure was a full-scale model of a donor bay and a partial acceptor bay. The Phase II structures were half-scale models that included two complete assembly bays, two partial bays, three air locks, and a retaining wall and ramp. Soil was placed as backfill between the donor and acceptor bays. The soil was selected and placed according to specifications that model the stiffness of the soil at the prototype facility at Pantex, Tex.

The test plan for Phase I called for a 300-lb* cylinder of PBX 9501 as the explosive charge. The charge weight equaled the explosive weight limit of the bay and was placed near the wall adjacent to the acceptor bay. The center of the charge corresponded to the center of a 390-lb sphere of TNT whose surface is 3 ft from the wall and 2 ft from the floor. The test plan for Phase II called for a 37.5-lb explosive charge placed half the distance of the Phase I charge from the wall and floor. Phase II explosive charge was half-scale.

---

* A table of factors for converting non-SI units of measurement to SI (metric) units is given on page 9.

Airblast pressures, soil and interface pressures, deflections, and acceler-
ations were measured by electronic instrumentation. The exterior of the struc-
ture and the interior of the acceptor bays were photographed by high-speed
cameras during the tests.

CHAPTER 2

PHASE I TEST PROCEDURES

Construction of the Phase I structures was begun in August 1981 and was completed on 14 December 1981. Appendix A lists significant events in the test program.

2.1 TEST SITE

The Phase I structures were constructed and tested on Ash Range, Camp Shelby, Miss., which is approximately 20 miles south of Hattiesburg, Miss. Figure 2.1 is a site layout map of the test area. The elevation of the test site is approximately 240 ft above mean sea level. Sachs's Scaling Laws can be used to convert the various blast parameters measured in these tests to pressure at other elevations.[2,3]

2.2 DESCRIPTION OF STRUCTURES

Phase I of the Building 12-64 Test Program consisted of two full-scale structures--a donor bay in which detonation occurred and an acceptor bay adjacent to the donor bay (Figure 2.2).

The design of the model donor bay was identical to that of Building 12-64 except that the rectangular concrete air-lock entrance was replaced by a 9-ft-diameter corrugated pipe. The cross-sectional area of the pipe approximated the area of door openings in the prototype structure. Its volume was 2003.9 cu ft. The outside dimensions of the donor bay were 31 ft long, 27 ft wide, and 22.67 ft high with all walls 1.5 ft thick (see Figures 2.2-2.5). The internal volume of the bay was 13,442.6 cu ft. The roof of the donor bay was designed to hinge upward and vent gases produced by an internal explosion. The roof was 1.5 ft thick at the walls, tapered to 0.75 ft thick in the center, and was covered with 2 ft of soil. Heating, ventilating, and air conditioning (HVAC) ductwork and a roof vent were included in the model.

The acceptor bay structure was a one-third section of a prototype bay adjacent to the donor bay. The bay wall facing the donor bay and its HVAC ductwork were identical to those in Building 12-64. The floor slab was extended and its footing deepened to minimize relative motion between the two bays (Figure 2.4). The roof was modified to support the top of the wall facing the donor bay but without the capability of disengaging due to internal

13

explosion. The back wall of the acceptor bay was a wooden partition supported by four W18 x 50 beams welded to connection seats embedded in the side walls. A 4-ft-diameter corrugated pipe was used as an access tunnel through the back wall. The acceptor bay structure was 10.5 ft long, 27 ft wide, and 22.67 ft high with walls 1.5 ft thick (see Figures 2.2-2.4). Grade 40 reinforcing steel and 4000-psi concrete were specified for construction. Reinforcing steel bar sizes and spacing are described in Tables 2.1 and 2.2.

2.3 CONSTRUCTION PROCEDURES

Design drawings and specifications used for construction of the bays were prepared by Gibbs & Hill/Ammann & Whitney.

2.3.1 Concrete Construction

The site was prepared by removal of topsoil and compaction of the sub-grade material (Figure 2.6). Footings for both donor and acceptor bay slabs were excavated and the sides lined with sheet metal to maintain dimensional control. A 6-in. layer of compacted sand was placed in the bottom of footing trenches and inside the slab forms. Figure 2.7 shows the base slab formwork with sand fill. Reinforcing steel was placed in the footings and slabs in ac-cordance with Tables 2.1 and 2.2. Figure 2.8 shows the completed formwork and reinforcing steel. Figure 2.9 shows formwork and reinforcing steel details at the corners of the slab and also the 6-in.-high by 18-in.-wide section of the slab around the perimeter which forms the base of the walls. The inside edge of the raised section was chamfered back to floor level at a 45-deg angle. A 3-in.-wide by 2-in.-deep keyway was formed in the top of each of these raised sections.. Typical bar layouts inside the slab are shown in Figure 2.10. Con-crete was placed directly from a ready-mix truck and was vibrated to fill all voids (Figure 2.11).

The walls were constructed by setting the interior wall forms and then placing the reinforcing steel. Rebar mats were tied on the ground and then raised into position by a crane. All rebar mats were spot-welded at 5-ft ver-tical and horizontal intervals (a procedure used during construction of the prototype facilities at the Pantex Plant). Views of the reinforcing steel in the north, east, south, and west walls of the donor bay are shown in Figure 2.12. Two 16-in.-diameter steel pipes were set in the north wall to provide penetrations for HVAC ductwork (Figure 2.12b). The east and west walls are

14

considerably more heavily reinforced than the other walls, as shown in Figure 2.12e. The corners were reinforced by extending the horizontal steel bars in the east and west walls, bending them 90 deg at the corners, and tying the bars to the outer mat of the north and south walls (Figure 2.13). After all reinforcement was tied in place, the 9-ft-diameter corrugated pipe was installed and outer forms were set. The four walls were cast monolithically using a concrete pump (Figure 2.14). The concrete was placed in 5-ft-high lifts, beginning at one corner and continuing around the walls. Total placement time was approximately five hours.

The acceptor bay was constructed in the same manner as the donor bay. An overall view of the reinforcing steel layout is shown in Figure 2.15. A total of nine interface pressure gage mounts were placed in the south wall as well as two 16-in.-diameter pipe penetrations. Four beam seats were placed in both east and west walls. Figure 2.16 shows a typical corner detail in the south wall. Figure 2.17 shows a corner detail at the base of the south wall. All wall steel was tack-welded at 5-ft intervals. The concrete was placed monolithically in the three walls with a concrete pump in the same manner as that for the donor bay (Figure 2.18).

The reinforcing steel in the roof of the donor bay was placed according to the specifications shown in Table 2.1. The No. 10 bars in the east-west direction were lapped 38 in. over the dowels from the walls and extended to the center of the roof. There was a distance of 3 in. between the ends of the No. 10 bars at the center line of the bay. Figure 2.19 shows the overall roof steel layout and details of the bar layouts at the walls. One 16-in.-diameter pipe penetration was placed in the roof as well as two anchor bolts to hold the explosive charge. Figure 2.20 shows the interior of the completed donor bay.

The dimensions of the steel in the acceptor bay roof are shown in Table 2.2. Since the acceptor bay roof was not designed to disengage, bars in the east-west direction were continuous over the roof. The concrete in both roofs was placed with a concrete pump.

The north wall of the acceptor bay consisted of both wood and steel construction. Four W18 by 50 steel beams were placed on the bearing seats cast into the north ends of both east and west walls, and were then welded in place. The north wall was enclosed with 3/4-in. plywood panels reinforced with 2 by 4 and 3 by 12 lumber. Access to the structure was provided by a 4-ft-diameter

15

corrugated metal pipe installed in the east wall.

Prior to backfill, 4-in. polystyrene foam panels were placed against the north wall of the donor bay, the south wall of the acceptor bay, and the donor bay roof. These panels were fastened to the concrete with Gulf Seal Corporation mastic.

2.3.2 Embankment Construction

Two different materials were used and two different specifications were followed in backfilling the structures. The material used between the donor and acceptor bays was chosen and placed to model the stiffness of the prototype soil at the Pantex facility. Details of the testing performed to select this soil and the backfill specifications are discussed in Section 2.4.3. The backfill around the sides of the bays was a clayey sand, native to the test site, placed to model the mass of the soil surrounding the Pantex bays.

A gravelly sand was placed between the two bays in 12-in. lifts using a scoop loader. This material was compacted with a vibratory compactor to achieve specified densities. The same material was used over the roofs of the bays since it was easier to place and to obtain uniform densities than the native material. Soil densities over the roofs were chosen to match the weight of soil on the roof of a prototype bay.

The backfill material around the other walls of the bays was hauled and dumped using Clark 290 tractors equipped with scraper pans. A bulldozer was then used to spread the material to form a lift 8 to 12 in. thick. Clark 290 tractors and a scoop loader were used to compact the material to desired density. Figure 2.21 shows the appearance of the structures with approximately 40 percent of the backfill in place; Figure 2.22 shows the completed backfill. Quality control checks were performed to insure that soil was placed at correct densities.

Wet soil densities were measured with a nuclear density gage and moisture contents were determined by oven drying. Table 2.3 lists the results of tests performed on the select sand backfill used between the bays and over the roofs. Table 2.4 shows the results of similar tests performed on the native backfill material around the bay wall.

2.3.3 Appurtenances

Once the backfill was completed and shaped, a 6-in.-thick concrete slab

was placed between the two bays as shown in Figure 2.5. The purpose of the slab was to model the floor slab mass of the building used to house HVAC equipment on prototype bays.

The soil over the roofs of the structure was covered with 1/2-in.-thick Gulf Seal Corporation asphalt planks. Each plank was lapped 6 in. over adjacent planks, and the laps were bonded with Gulf Seal Corporation 626 U catalytically blown asphalt.

Three wooden poles were erected on the north side of the acceptor bay. Two by four's were nailed to the poles on 2-ft centers to provide dimensional scale for high-speed photography. Figure 2.23 shows this camera background as well as the concrete HVAC slab and the asphalt planks on the top of the bays.

2.4 CONSTRUCTION MATERIALS

2.4.1 Concrete

The results of compressive tests on 6- by 12-in. concrete control cylinders for the donor bay and acceptor bay are summarized in Table 2.5. The compressive strengths at 7 and 28 days and on the day of the Phase I event, 18 December 1981, are shown. Average compressive strengths also are listed for 28 days and on 18 December. However, only 28-day compressive strengths were determined for the roof slabs since these cylinders were tested on 16 December 1981. The control cylinders for the entire donor bay structure and acceptor bay structure indicated average 28-day compressive strengths of 4308 and 4536 psi, respectively. Average compressive strengths on 18 December for the donor bay and acceptor bay structures were 4294 and 4405 psi, respectively.

2.4.2 Reinforcing Steel

All reinforcing steel used in the structure was Grade 40. Bar sizes were Nos. 4, 5, 6, 8, 9, and 10. Results of the static tensile tests on samples of the steel reinforcement are presented in Table 2.6. Stress-strain curves are shown in Appendix B. The first digit in each specimen number listed in the table and the appendix corresponds to the bar size of the specimen. The reinforcement bar mats were spot-welded as a required feature of the facility grounding and lightning protection system design.

17

2.4.3 Soil

The soil used for backfill at Pantex was examined by Amarillo Testing and Engineering, Inc.[4] Their investigation consisted of subsurface exploration, laboratory testing, and analysis leading to a determination of in situ soil conditions between Building 12-64 assembly bays and over the bay roofs. Over the roofs, they found a thin layer (0 to 6 in.) of gravelly sand followed by a layer (18 to 24 in.) of reddish brown silty clay with a dry density of about 113 to 114 lb/ft^3 at an in situ moisture content of 16 to 17 percent. Between the bays, gravelly sand was found immediately below the silty-clay layer and extending to the floor level of the structure. The gravelly-sand stratum had an in situ moisture content of 4 to 6 percent and an in-place dry density of 100 to 120 lb/ft^3.

Gradation curves for candidate backfill materials from the Hattiesburg area were compared with the gradations of the Pantex gravelly sand. The best match was a river-run material obtained from the American Sand and Gravel Company in Hattiesburg (Figure 2.24). Uniaxial strain tests were then conducted at WES on remolded specimens of the Pantex backfill, and the axial stress versus axial strain was plotted (Figure 2.25). Uniaxial strain tests were also performed on the select sand backfill, and the stress versus strain was plotted (Figure 2.26). These curves were compared and a dry density of 107 lb/ft^3 was recommended for the select sand backfill placement. No specific moisture content was required since any moisture content encountered in field conditions would make the backfill at least as stiff as the Pantex backfill. The select sand backfill material was used only between the bays and over the bay roofs. The remainder of the backfill material was a clayey sand obtained at the test site.

2.5 INSTRUMENTATION

Electronic data measurements were made to obtain airblast pressures, soil pressures, interface pressures, and structural deflections. A measurement list is shown in Table 2.7, and gage locations are illustrated in Figures 2.2-2.5. Six airblast gages were located in the donor bay to record pressures on the floor (BP1), the four walls (BP2-5), and in the corrugated pipe which represented an air lock (BP6). Two gages were located at ground surface level (BP7 and 8), and one gage was in the HVAC ductwork in the acceptor bay (BP9). Gage mounts for BP2-5 were equipped with a debris shield to protect the

transducers during the blast. Soil pressures between the bay were measured by four soil stress gages. Pressures acting on the acceptor bay were measured by nine interface pressure gages mounted flush with the surface of the wall. All of these gages were covered by the 4-in. polystyrene foam panels placed against the wall during construction. Deflection gages D1 and D2 were used to measure acceptor bay wall deflections and gage D3 was used to measure the acceptor bay slab movement.

The location of the recording equipment relative to the structure is shown in the site layout (Figure 2.1). Individually shielded cables were used between the gages and the instrumentation trailer. Cables routed through the concrete walls or floor were protected by 1/2-in.-diameter steel pipe. Average cable lengths were approximately 700 ft.

Signal conditioning and amplification were accomplished using WES-built amplifiers. Airblast data were recorded on an 80-kHz, Sangamo Sabre V, 32-track, FM magnetic tape recorder at a speed of 120 in./sec. A 20-kHz, Sangamo Sabre III recorder was used to record all other data at a speed of 60 in./sec.

Four high-speed movie cameras and two sequence cameras were used to view the exterior of the structures at camera stations 1 through 3. Three high-speed movie cameras were located inside the acceptor bay at station 4. Camera information is listed in Table 2.8, and camera relative locations are shown in Figure 2.27. Cameras at stations 1 and 2 were mounted on scaffolding at approximately the same elevation as the bay roofs (Figure 2.28). The three cameras in the acceptor bay are shown in Figure 2.29.

2.6 STRUCTURAL VIBRATION TESTING

The donor bay north wall and acceptor bay south wall were dynamically tested to determine their vibration characteristics. Each test was conducted in the following manner: the wall was marked with two lines passing through its horizontal and vertical center line. Drive points were established on the lines at 3-ft intervals in the horizontal direction and 2.46-ft intervals in the vertical direction. An accelerometer was mounted at one of the points at or near the center of the wall, and each of the points was excited by striking it with a PCB Piezotronics 086BSO impulse hammer. The hammer generates an impulse load which is measured by a piezoelectric load cell in the device. Acceleration is simultaneously measured at the accelerometer location. Force

and acceleration measurements were digitally recorded and processed by a
Hewlett Packard 5423A structural dynamics analyzer. The data obtained during
each test were recorded on magnetic tape as transfer functions. To minimize
the possibility of "missing" a mode, test personnel moved the accelerometer to
another location away from the center, and the procedure was repeated for each
wall test. This procedure was used on each wall both before and after
backfill.

2.7 EXPLOSIVE CHARGE ASSEMBLY AND PLACEMENT

The explosive charge was a 300-lb cylinder of PBX 9501, with nominal
dimensions of 14-1/2 in. in diameter and 27-1/2 in. long. It consisted of six
14-1/2-in.-diameter wafers which were pressed and machined to dimensions at
the DOE Pantex Plant and then glued together at Camp Shelby to form the charge.
A detailed account of charge fabrication and performance is given in Refer-
ence 5. The charge was suspended from the ceiling of the donor bay by a com-
bination of two steel cables, a wooden beam, and nylon straps as shown in Fig-
ure 2.30. The center of the charge was 3.97 ft from the north wall and
2.97 ft above the floor.

A 9-ft-square by 3.5-in.-thick concrete slab was placed over the entrance
of the corrugated pipe to model the mass of blast doors in the prototype struc-
ture (Figure 2.31). Detonation was accomplished with an SE-1 detonator
located on the west end of the charge. At the time of detonation, the air
temperature was $37^\circ F$ and the barometric pressure was 30.41 in. of mercury.

Table 2.1. Donor bay concrete reinforcing steel.

Component	Mat Face	Bar Orientation	Bar Size No.	Bar Spacing in.	Remarks
Footing*	Outer and inner	Horizontal	6	--	Four per footing
		Vertical	4	36	Stirrups
Floor slab*	Bottom	N-S	5	11	
		E-W	8	11	
	Top	N-S	5	11	
		E-W	10	7	
North and south walls	Outer	Horizontal	4	9	
		Vertical	4	12	
	Inner	Horizontal	4	9	
		Vertical	8	6	
East and west walls	Outer	Horizontal	5	11	
		Vertical	8	8	
	Inner	Horizontal	5	11	
		Vertical	9	7	
Floor-to-wall dowels	Bottom/outer		8	8	L shaped
	Top/inner		8	11	L shaped
Wall-to-roof dowels**	Outer/top		10	6	L shaped
	Inner/bottom		5	12	L shaped
Roof slab	Bottom	N-S	5	12	Four bars on each side
		E-W	†		
	Top	N-S	5	11	
		E-W	10	6	

* Footing and floor slab were monolithic.
** Wall-to-roof dowels were installed in east and west walls only.
† Reinforcement in this direction provided by wall-to-roof dowels.

21

Table 2.2. Acceptor bay reinforcing steel.

Component	Mat Face	Bar Orientation	Bar Size No.	Bar Spacing in.	Remarks
Footing*	Outer and inner	Horizontal	6	--	Four per footing
		Vertical	4	11	Stirrups
Floor slab*	Bottom	N-S	5	11	
		E-W	8	11	
	Top	N-S	5	11	
		E-W	10	7	
South wall	Outer	Horizontal	4	9	
		Vertical	4	12	
	Inner	Horizontal	4	9	
		Vertical	8	6	
East and west walls	Outer	Horizontal	5	11	
		Vertical	8	8	
	Inner	Horizontal	5	11	
		Vertical	9	7	
Floor-to-wall dowels	Bottom/outer		8	8	L shaped
	Top/inner		8	11	L shaped
Wall-to-roof dowels**	Outer/top		10	6	L shaped
	Inner/bottom		10	6	L shaped
Roof slab	Bottom	N-S	5	11	
		E-W	5	12	
	Top	N-S	5	11	
		E-W	10	6	

* Footing and floor slab were monolithic.
** Wall-to-roof dowels were installed in east and west walls only.

Table 2.3. Results of soil tests on select sand material.

Location	Elevation Above Bay Floor ft	Average Dry Density lb/ft^3	Average Moisture Content percent	Average Wet Density lb/ft^3
Between bays	Grade	109.1	5.2	114.8
	1	108.8	4.2	113.4
	2	109.8	4.8	115.0
	3	113.4	4.4	118.4
	5.5	111.2	4.2	115.9
	6	110.2	4.5	115.2
	6.5	112.7	4.5	117.2
	7	111.4	4.7	117.1
	8	113.1	4.1	117.7
	9	110.3	4.7	115.4
	10	111.3	4.6	116.4
	12.5	106.4	4.2	110.9
	14	112.2	4.4	117.2
	15	112.5	4.3	117.3
	16	114.1	3.8	117.7
	17	111.4	3.6	115.4
	18	109.1	4.3	114.8
	19	111.4	4.2	116.0
	20.7	110.0	4.2	114.6
	22	110.6	5.0	116.2
	23	110.5	5.3	116.4
	Average	110.9	4.4	115.9
Over roofs	22	110.7	4.7	116.1
	23	110.4	4.7	115.5
	Average	110.6	4.7	115.8

Table 2.4. Results of soil tests on native material around bay walls.

Location	Elevation Above Bay Floor ft	Average Dry Density lb/ft^3	Average Moisture Content percent	Average Wet Density lb/ft^3
North side	0	100.8	15.1	
	10	109.7	11.9	122.8
	14	104.9	11.0	116.5
	20.7	103.6	16.6	120.8
	23	110.0	11.0	122.1
	Average	105.8	13.1	118.0
East side	8	107.3	14.6	123.0
	14	106.3	11.9	118.9
	15	104.2	11.6	116.3
	18	102.0	12.5	114.7
	20.7	105.2	14.6	120.6
	23	99.4	8.5	107.8
	Average	104.1	12.3	116.9
South side	5	111.2	12.6	125.2
	7	106.6	15.4	122.9
	8	111.5	14.6	127.8
	13	108.3	11.3	120.5
	16	104.0	11.3	115.7
	17	104.3	12.2	117.0
	20.7	108.1	14.5	123.8
	23	110.7	9.4	121.1
	Average	108.1	12.7	121.8
West side	6	110.4	14.5	126.4
	8	117.2	13.8	124.9
	10	108.6	12.2	122.0
	11	108.1	11.3	120.3
	14	113.6	11.3	126.4
	20.7	106.6	14.1	121.4
	23	101.6	7.0	108.7
	Average	109.4	12.0	121.4

Table 2.5. Concrete compressive strengths.

Structural Component	Specimen No.	Compressive Strength, psi	Specimen Age, days
Donor bay floor slab	I-12	3979	7
	I-13	4598	28
	I-14	4439	28
	I-15	3395	7
	I-16	4598	28
	I-17	4173	28
	I-18	3643	7
	I-19*	3855	28
	I-20	4244	28
	I-21	3448	7
	I-22	4527	28
	I-23	3890	91
	I-24	3643	7
	I-25	4403	28
	I-26	4598	91
	Average	4355	28
	Average	4244	91**
Acceptor bay floor slab	I-1	4067	7
	I-2	4881	28
	I-3	4951	28
	I-4	3625	7
	I-5	4739	28
	I-6	4810	28
	I-7	3678	7
	I-8	4209	28
	I-9	4598	28

(Continued)

* Showed signs of improper consolidation.
** Day of the Phase I event.

(Sheet 1 of 4)

Table 2.5. (Continued).

Structural Component	Specimen No.	Compressive Strength, psi	Specimen Age, days
Acceptor bay floor slab (cont'd)	I-10	4474	94
	I-11	4492	94
	Average	4698	28
	Average	4483	94**
Donor bay walls	I-27	3006	7
	I-28	4279	28
	I-29	3997	62
	I-30	2759	7
	I-31	3908	28
	I-32	4350	62
	I-33	3254	7
	I-34	4067	28
	I-35	4297	62
	I-36	2829	7
	I-37	4244	28
	I-38	4704	62
	I-39	2900	7
	I-40	4138	28
	I-41	3997	62
	I-42	2759	7
	I-43	3784	28
	I-44	3749	62
	I-45	2865	7
	I-46	3890	28
	I-47	4598	62
	I-47A	3254	62
	I-48	2847	7
	I-49	3714	28

(Continued)

** Day of the Phase I event.

(Sheet 2 of 4)

Table 2.5. (Continued).

Structural Component	Specimen No.	Compressive Strength, psi	Specimen Age, days
Donor bay walls (cont'd)	I-50	3820	62
	I-50A	3855	62
	I-51	3024	7
	I-52	4350	28
	I-53	4398	62
	I-54	3183	7
	I-55	3997	28
	I-56	4032	62
	I-56A	4704	62
	I-57	2829	7
	I-58	4244	28
	I-59	4403	62
	I-59A	3890	62
	I-60	2741	7
	I-61	4244	28
	I-62	4350	62
	Average	4072	28
	Average	4143	62**
Acceptor bay walls	I-63	3926	7
	I-64	4386	28
	I-65	4350	51
	I-66	3183	7
	I-67	4279	28
	I-68	4315	51
	I-69	3448	7
	I-70	4315	28
	I-71	3961	51
	I-72	4085	28

(Continued)

** Day of the Phase I event.

(Sheet 3 of 4)

27

Table 2.5. (Concluded).

Structural Component	Specimen No.	Compressive Strength, psi	Specimen Age, days
Acceptor bay walls (cont'd)	I-73	4439	28
	I-74	4173	51
	I-75	4421	28
	I-76	4209	51
	I-77	3855	51
	Average	4321	28
	Average	4144	51**
Donor bay roof	I-78	3448	7
	I-79	4598	28
	I-80	4492	28
	I-81	3537	7
	I-82	4598	28
	I-83	4598	28
	I-84	3254	7
	I-85	4421	28
	I-86	4456	28
	I-87	3360	7
	I-88	4545	28
	I-89	4262	28
	Average	4496	28
Acceptor bay roof	I-90	4704	28
	I-91	4739	28
	I-92	4315	28
	I-93	4598	28
	Average	4589	28

** Day of the Phase I event.

(Sheet 4 of 4)

Table 2.6. Properties of concrete reinforcing steel.

Specimen No.	Cross Sectional Area, in.^{2}	Percent Area Reduction at Failure	Yield Stress psi	Yield Strain μin./in.	Ultimate Stress psi	Modulus of Elasticity E, ksi
4-1	0.1450	52.41	68,400	2,240	105,862	30,535
4-2	0.1438	53.47	67,000	2,080	106,258	32,211
4-3	0.1461	52.05	67,700	2,280	106,502	29,693
4-4	0.1491	55.70	--*	--	105,566	--
Average	0.1460	53.40	67,700	2,200	106,047	30,813
5-1	0.2119	52.15	65,900	2,040	101,328	32,303
5-2	0.2161	53.59	67,000	2,080	101,960	32,211
5-3	0.2156	50.98	65,300	2,080	100,653	31,394
5-4	0.2130	54.45	66,800	2,120	101,650	31,509
Average	0.2141	52.79	66,250	2,080	101,397	31,854
6-1	0.3035	55.77	66,400	2,200	100,164	30,181
6-2	0.3024	55.44	64,000	2,000	97,883	32,000
6-3	0.3040	52.30	65,000	2,200	100,657	29,545
6-4	0.3034	54.60	66,000	2,120	100,856	31,132
Average	0.3033	54.52	65,350	2,130	99,890	30,714
8-1	0.5972	46.29	61,500	2,040	104,990	30,147
8-2	0.5973	45.56	63,000	2,000	105,139	31,500
8-3	0.6006	46.58	63,000	2,000	104,723	31,650
8-4	0.5936	47.05	62,600	2,040	104,952	30,686
Average	0.5971	46.37	62,600	2,020	104,952	30,995
9-1	0.7838	47.57	64,000	2,000	105,128	32,000
9-2	0.7775	44.40	62,400	2,160	105,209	28,888
9-3	0.7760	46.77	64,000	2,280	105,154	28,070
9-4	0.7822	46.03	65,200	2,080	105,088	31,346
Average	0.7798	47.19	63,900	2,130	105,144	30,076
10-1	0.9957	49.19	61,200	2,160	103,444	28,333
10-2	1.0028	49.25	66,100	2,200	105,704	30,045
10-3	0.9957	50.20	64,000	2,320	104,449	27,587
10-4	1.0028	48.15	65,200	2,320	105,704	28,017
Average	0.9980	49.18	63,466	2,266	104,532	27,978

* Strain gage failed.

Table 2.7. Measurement list for Phase I.

Type of Measurement	Gage No.	No. of Gages	Manufacturer	Model No.	Range	Natural Frequency Gage
Blast pressure	BP1, BP2	2	Kulite	HKS-1-375	5000 psi	675 kHz
	BP3, BP5	2	Kulite	HKS-1-375	2000 psi	650 kHz
	BP4	1	Kulite	HKS-1-375	1000 psi	500 kHz
	BP6-BP8	3	Kulite	XTS-190	200 psi	200 kHz
	BP9	1	Kulite	XTS-190	50 psi	130 kHz
Interface pressure	IP1-IP9	9	Kulite	VM-750	200 psi	28 kHz
Deflection	D1-D2	2	Trans-Tec	246-000	$\pm$ 3 in.	75 Hz
	D3	1	Trans-Tec	245-000	$\pm$ 2 in.	110 Hz
Soil stress	SS1-SS4	4	Kulite	LQ-080U	200 psi	17 kHz

Table 2.8. High-speed camera list.

Camera Station	Type of Camera	Frame Rate fps	Lens Focal Length mm
1	Milliken, 16-mm movie	350	35
2	Milliken, 16-mm movie	500	50
2	Photec, 16-mm movie	1000	45
2	Hulcher, 70-mm sequence	50	150
3	Milliken, 16-mm movie	500	25
3	Hulcher, 70-mm sequence	50	150
4	Milliken, 16-mm movie	500	5.9
4	Nova, 16-mm movie	2200	11
4	Nova, 16-mm movie	*	--

* No film recovery.
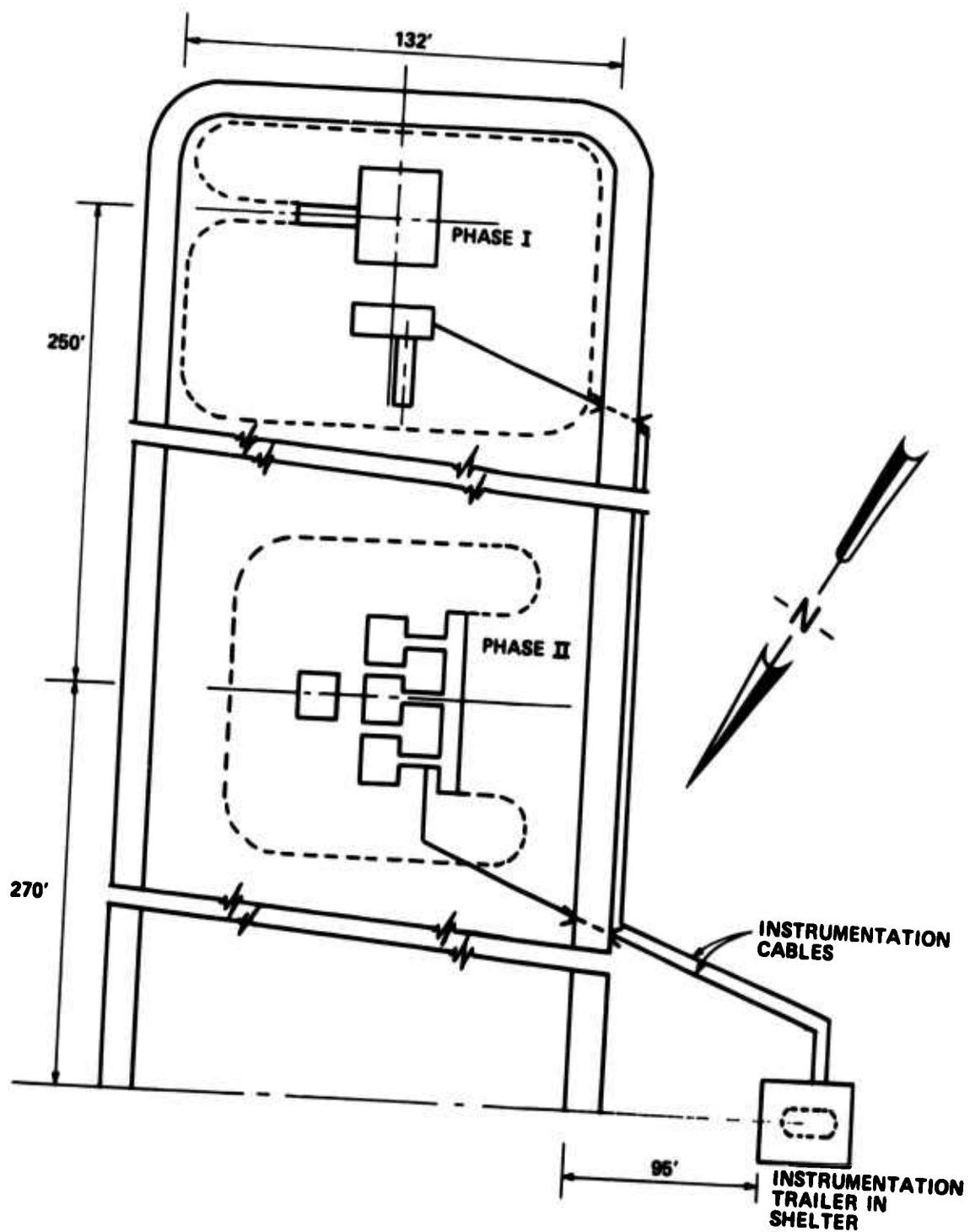
Figure 2.1. Test site layout at Camp Shelby, Miss.
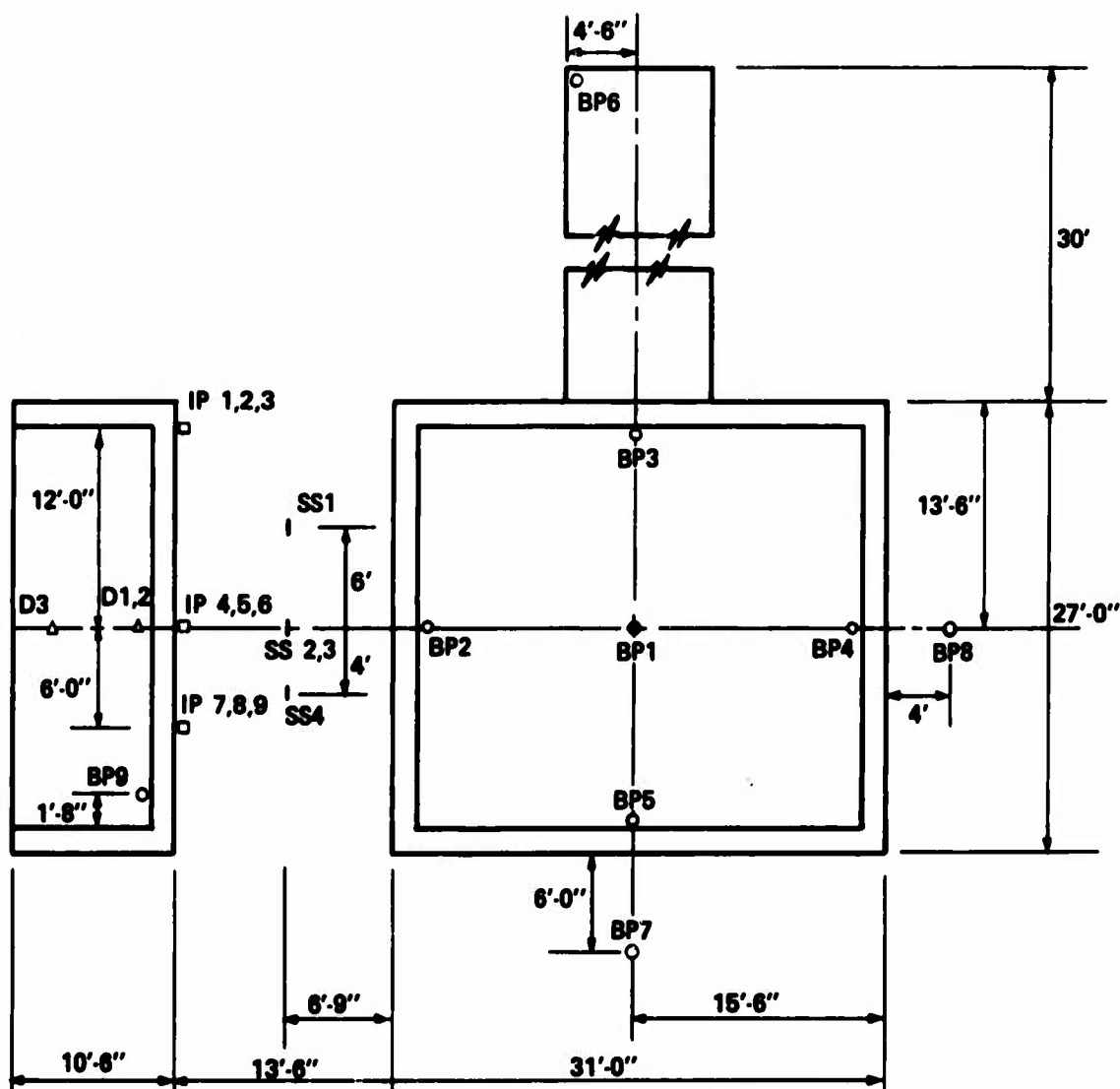
NOTE: ALL WALLS 18" THICK.

Figure 2.2. Plan view of donor and acceptor bays.

33

Figure 2.3. Elevation view of donor bay.

34

Figure 2.4. Elevation view of donor and acceptor bays.
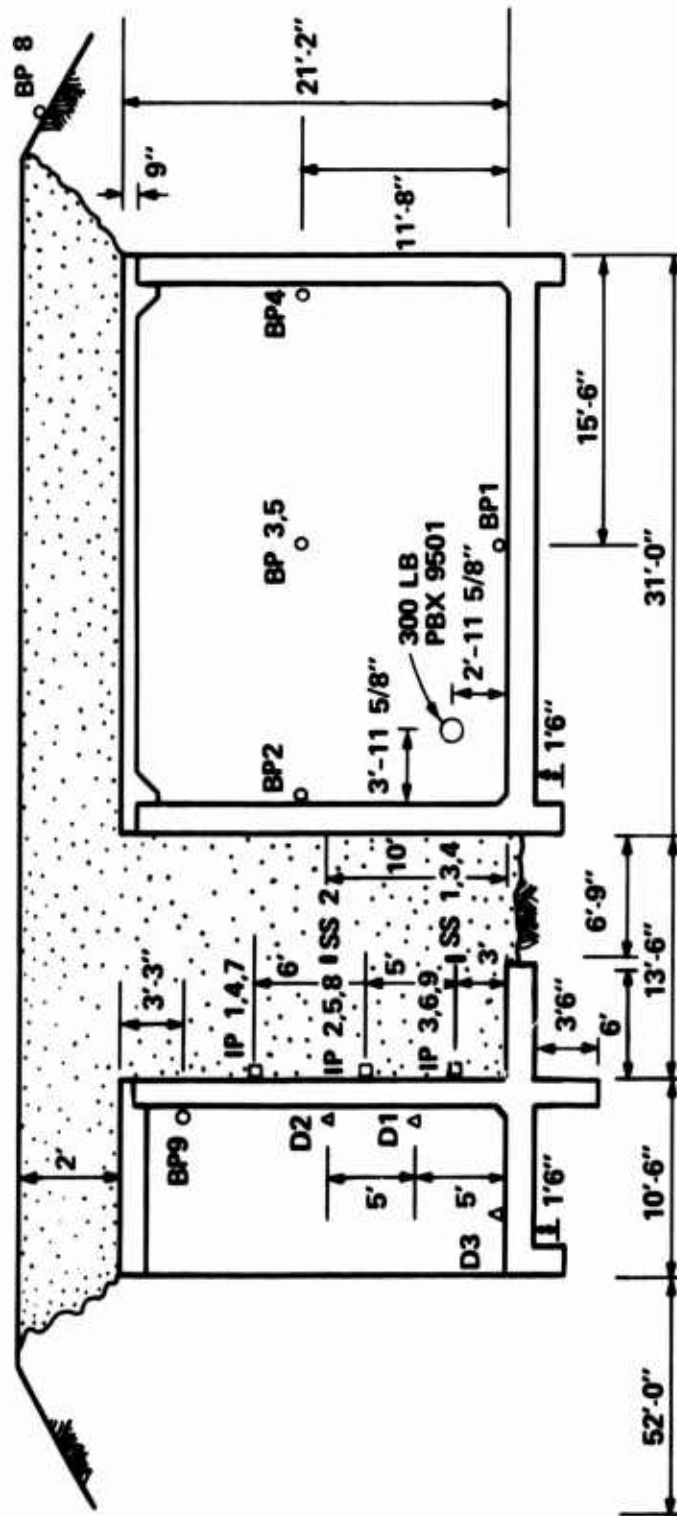
NOTE: 4" polystyrene on roofs
and adjoining walls
Sand backfill between
bays and over roofs

35

PLAN

NO. 2 REBAR 12" O.C.

VENT STACK

FIN. GRADE

BP 9

NOTE:
DUCTWORK - 14"⌀ SCHEDULE 10 STEEL PIPE
PENETRATIONS - 16"⌀ STEEL PIPE

ELEVATION
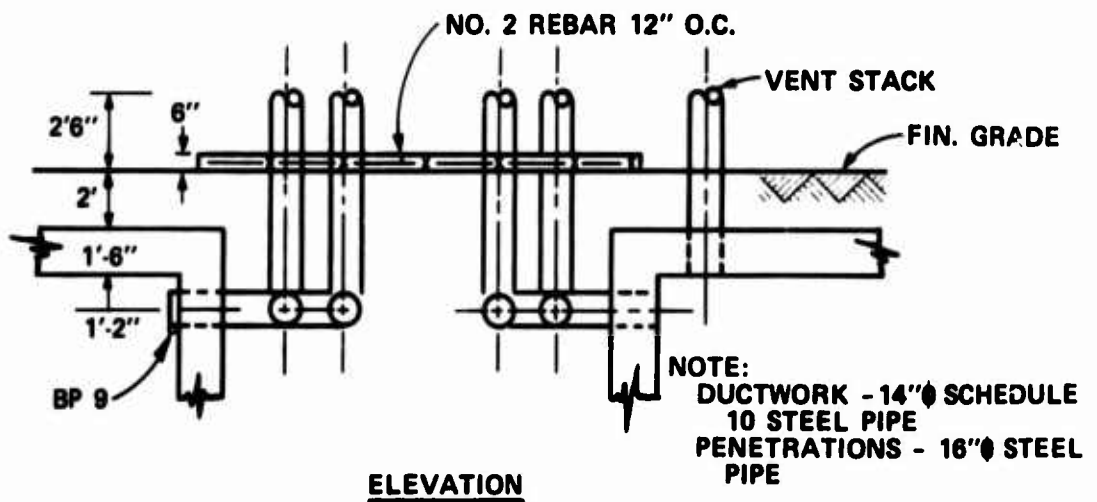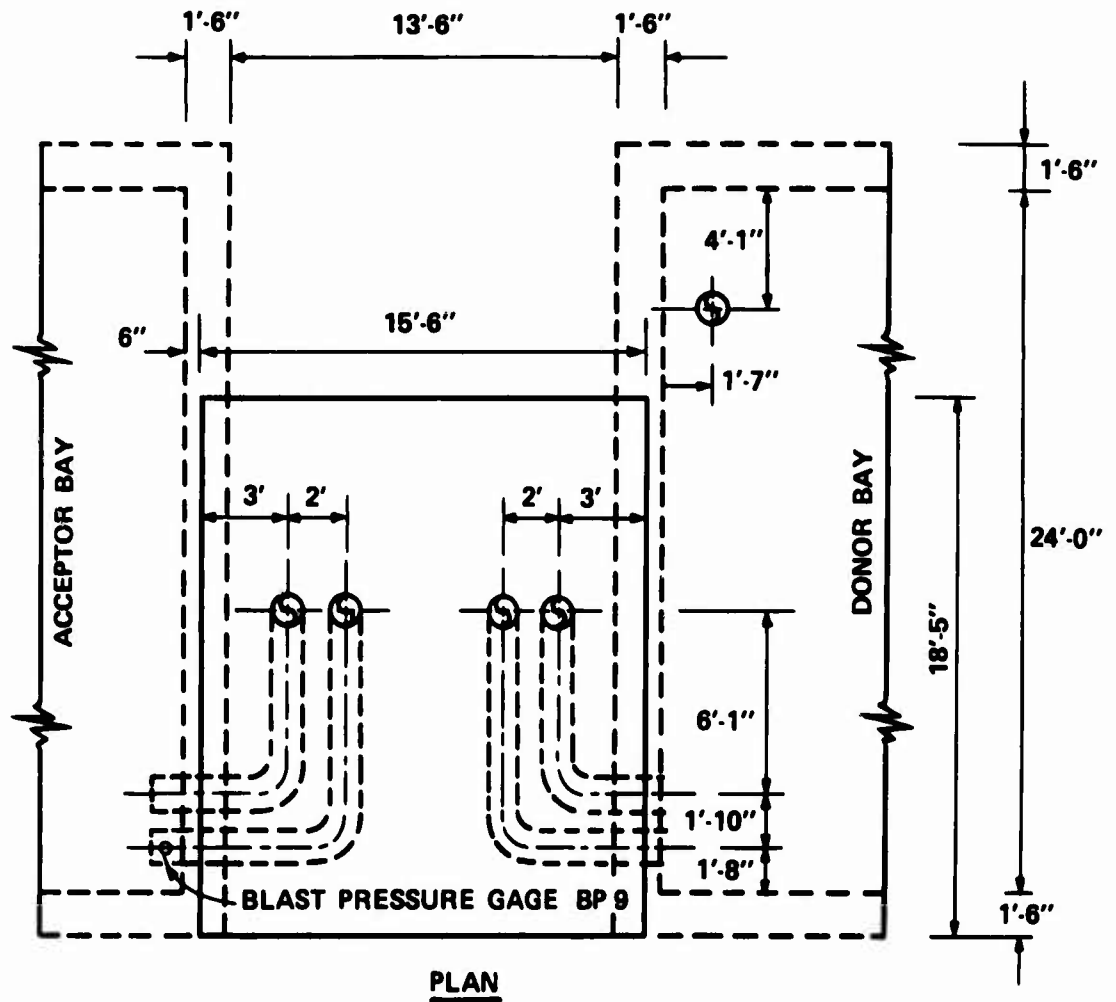
Figure 2.5. HVAC ductwork.

36

a. Clearing.

b. Compaction.

Figure 2.6. Site preparation.

a. Donor and acceptor bay formwork.

b. Acceptor bay formwork.

Figure 2.7. Base slab formwork.
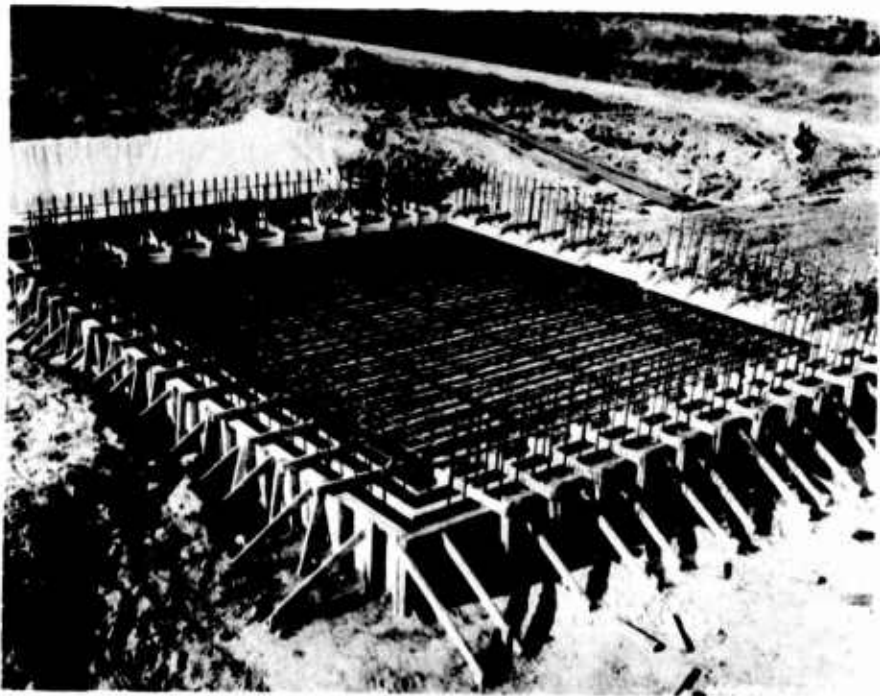
Figure 2.8.   Donor bay slab reinforcement.

Figure 2.9   Corner detail of donor slab reinforcement.

39

Figure 2.10.   Detail of slab reinforcement.
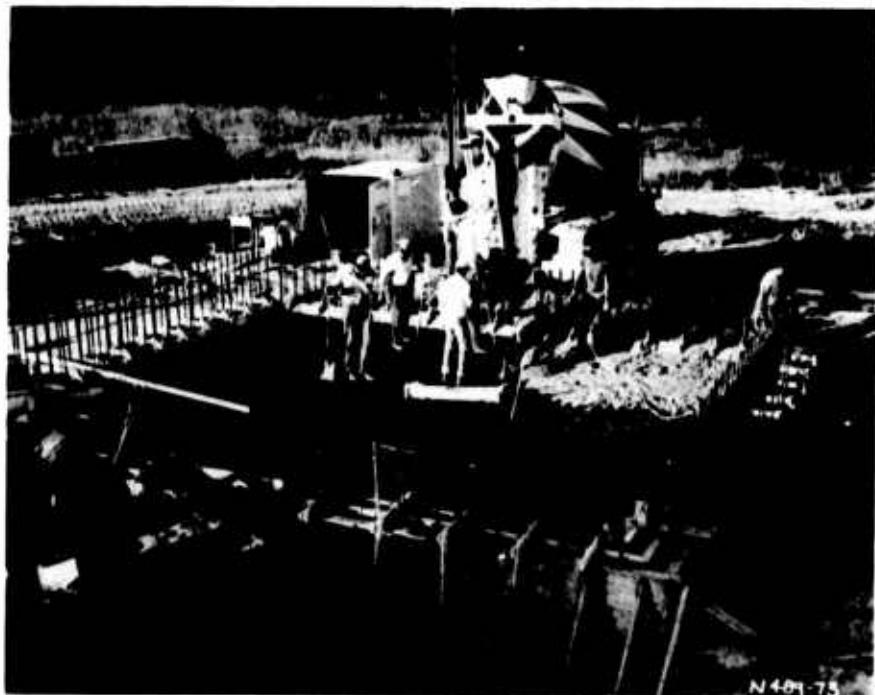
Figure 2.11.   Concrete placement in donor bay slab.

a. North wall.

b. Detail of ductwork penetration in north wall.

Figure 2.12. Donor bay wall reinforcing steel
(Sheet 1 of 3).
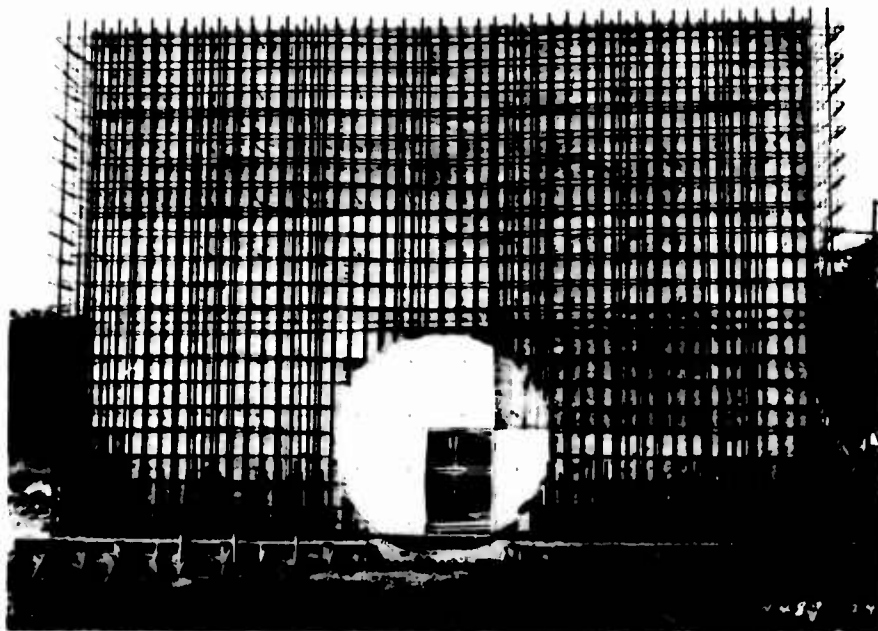
c.   East wall.
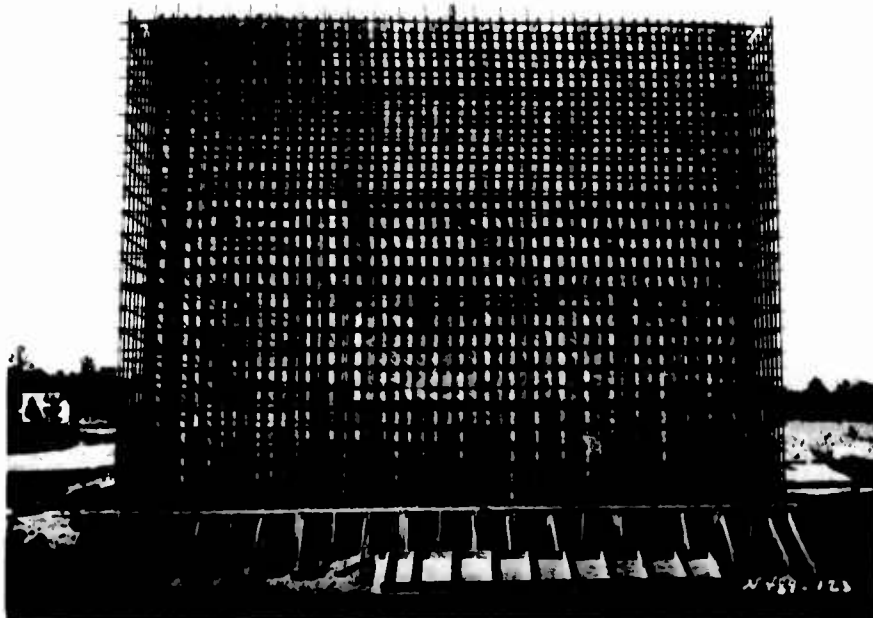
d.   South wall.

Figure 2.12.   (Sheet 2 of 3).

42
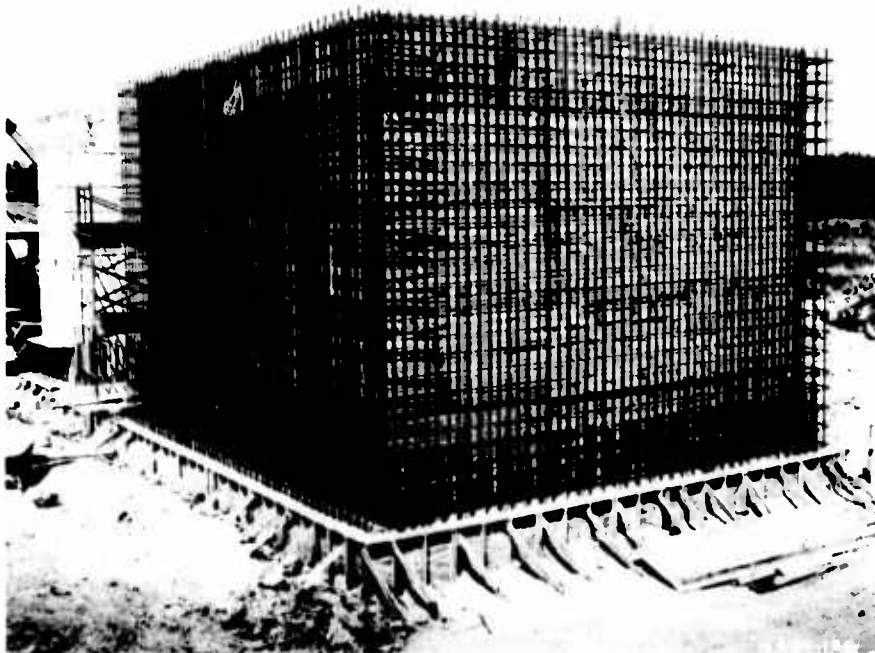
e. West and south walls.
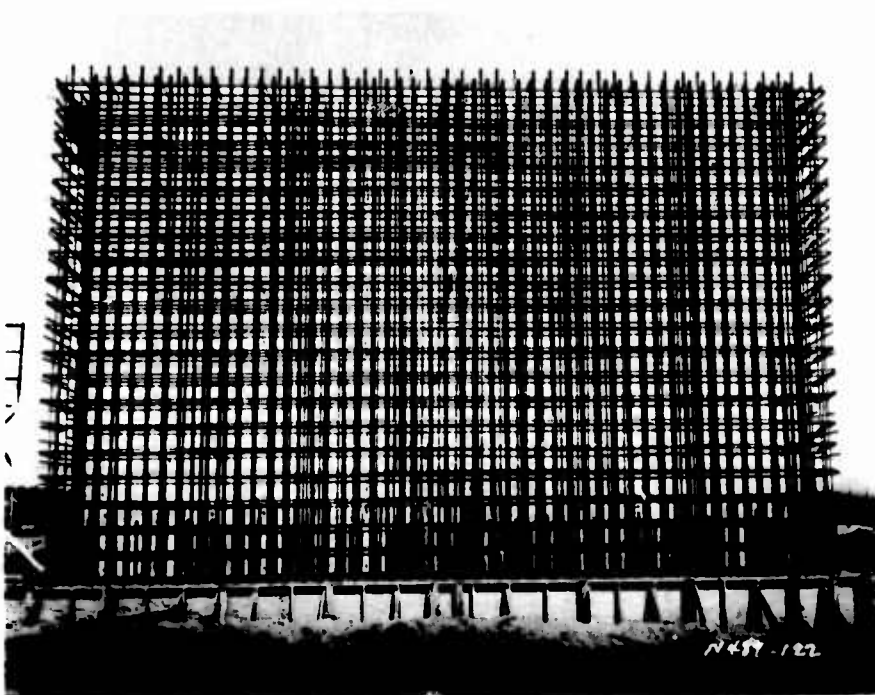
f. West wall.

Figure 2.12. (Sheet 3 of 3).

43
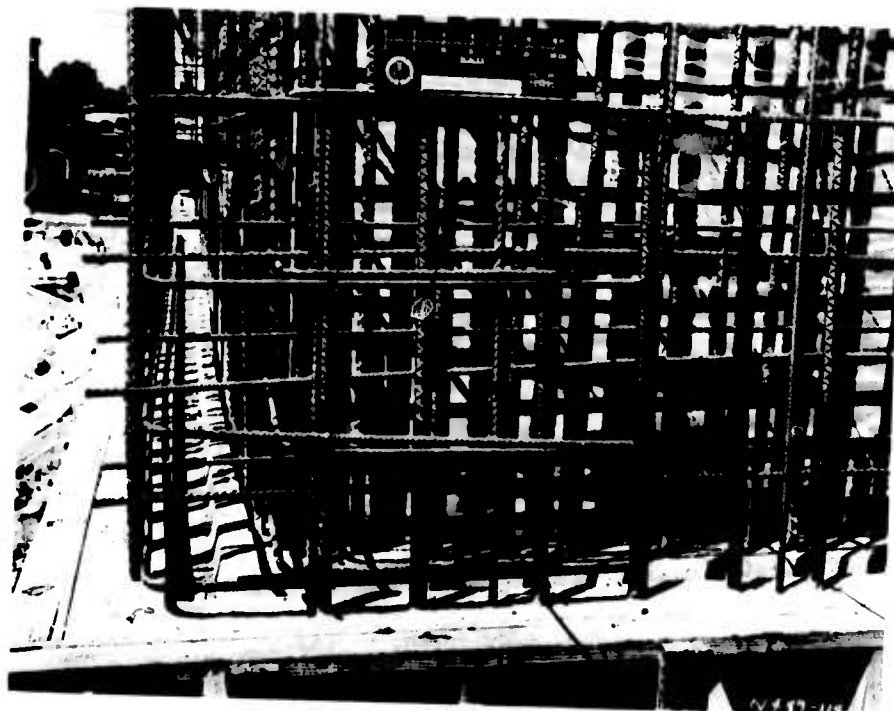
Figure 2.13. Corner reinforcement detail on south wall.
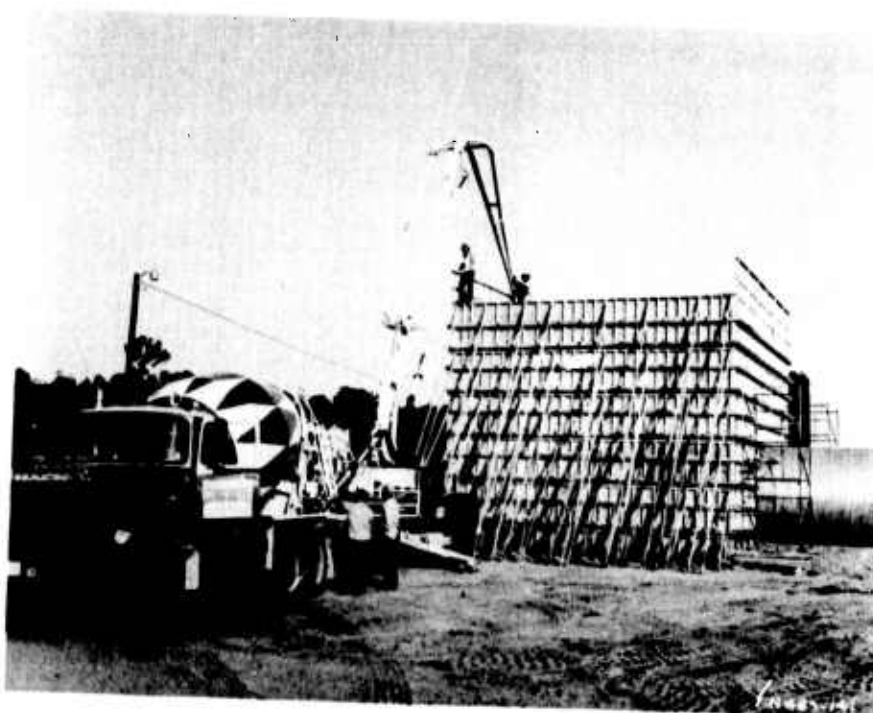
Figure 2.14. Concrete placement in donor bay walls with pump.
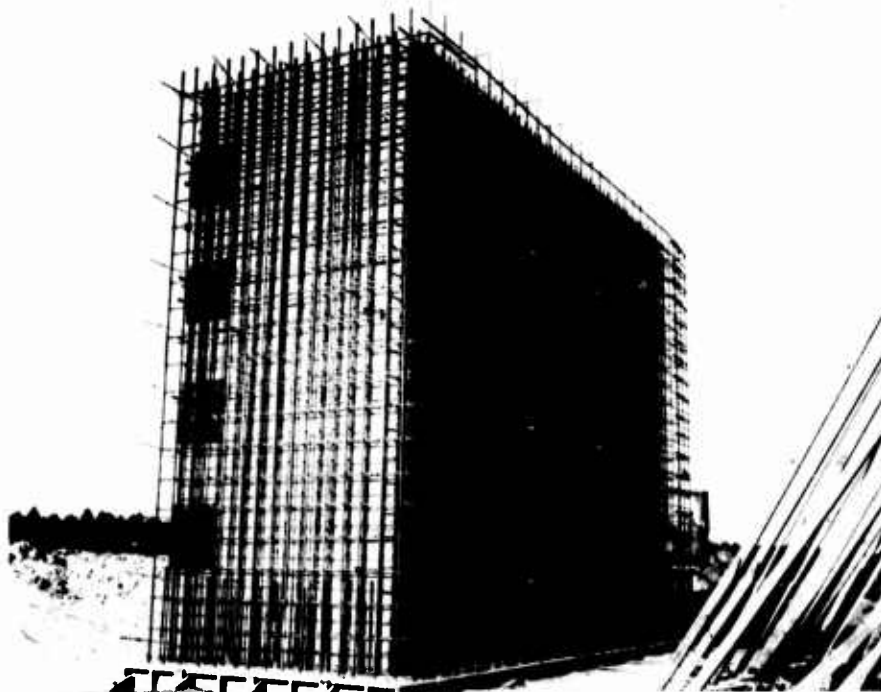
Figure 2.15. Acceptor bay west and south wall reinforcing steel.
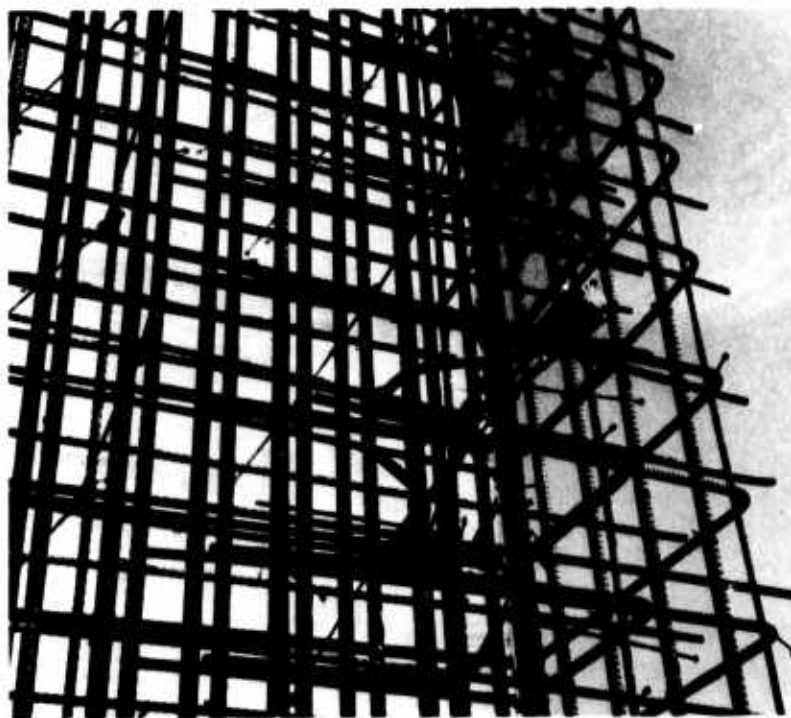
Figure 2.16. Corner reinforcing steel detail and interface pressure gage mount on acceptor bay wall.
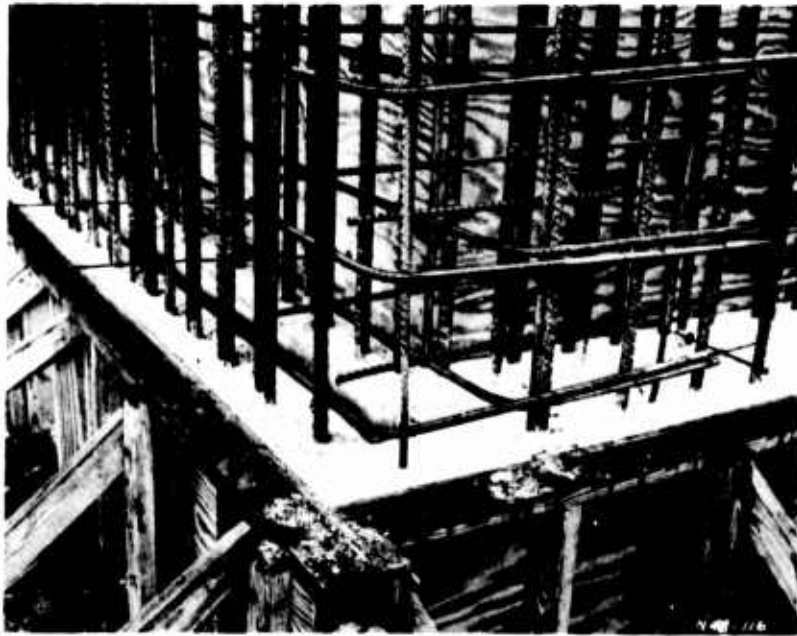
Figure 2.17. Corner reinforcing steel detail at base of acceptor bay wall.
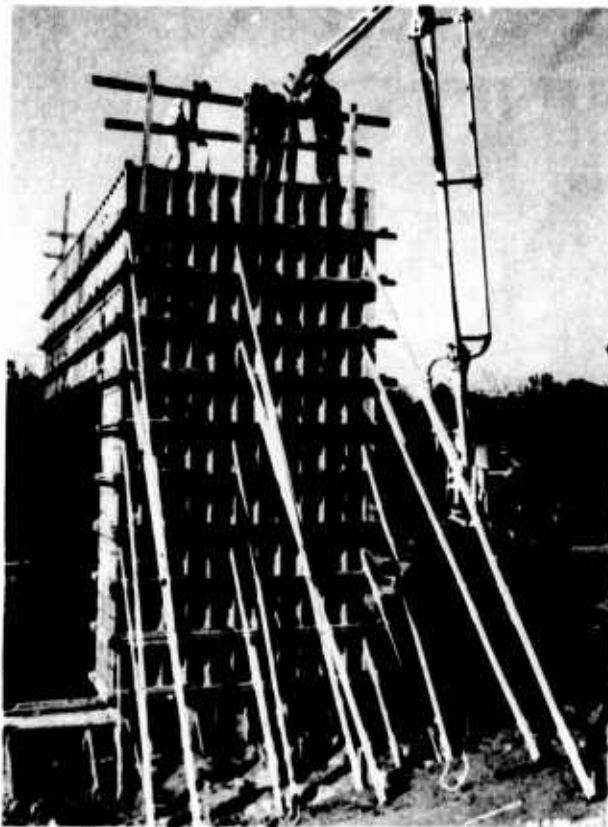
Figure 2.18. Concrete placement in acceptor bay walls with pump.
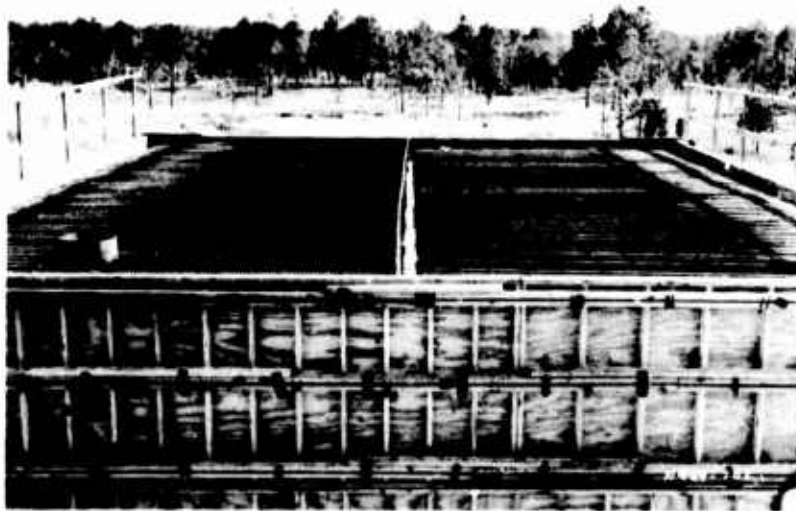
a. Overall view.

b. Centerline of bay.

Figure 2.19. Donor bay roof reinforcing steel
(Sheet 1 of 2).
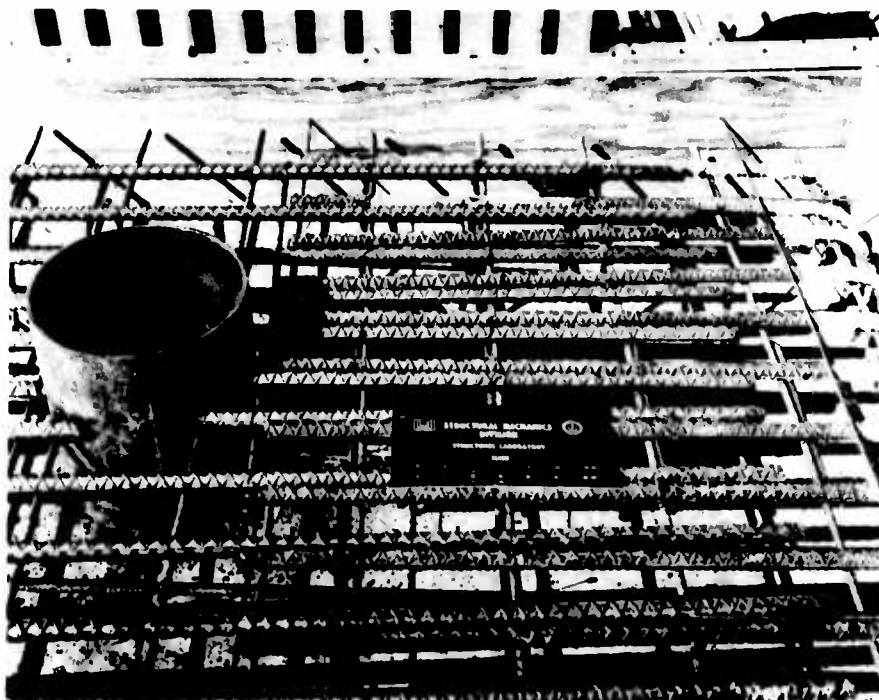
c. Detail of bar splices and duct penetration.

d. Edge detail.

Figure 2.19. (Sheet 2 of 2).
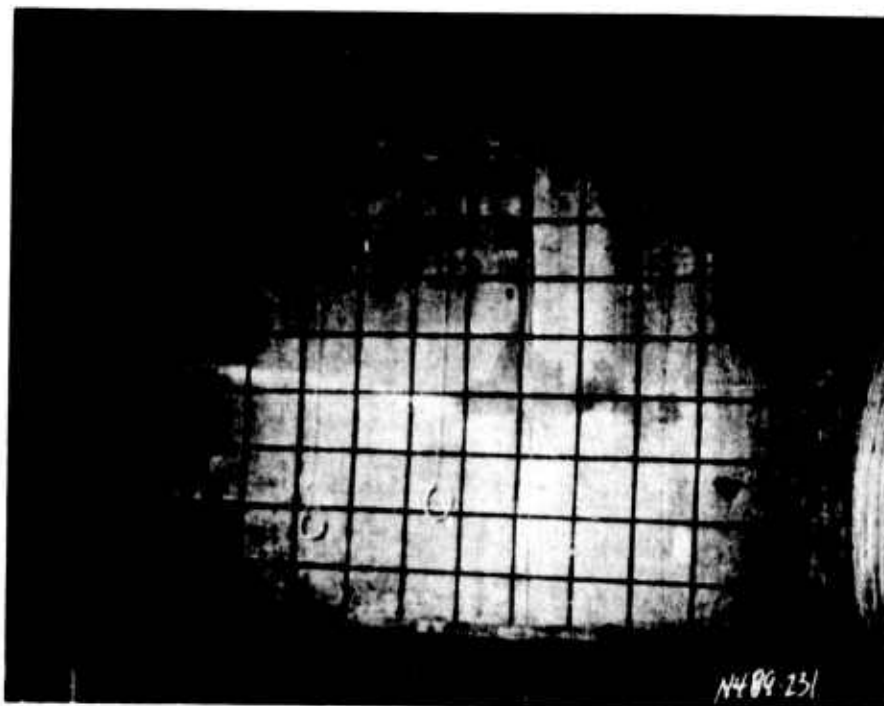
a. North wall.
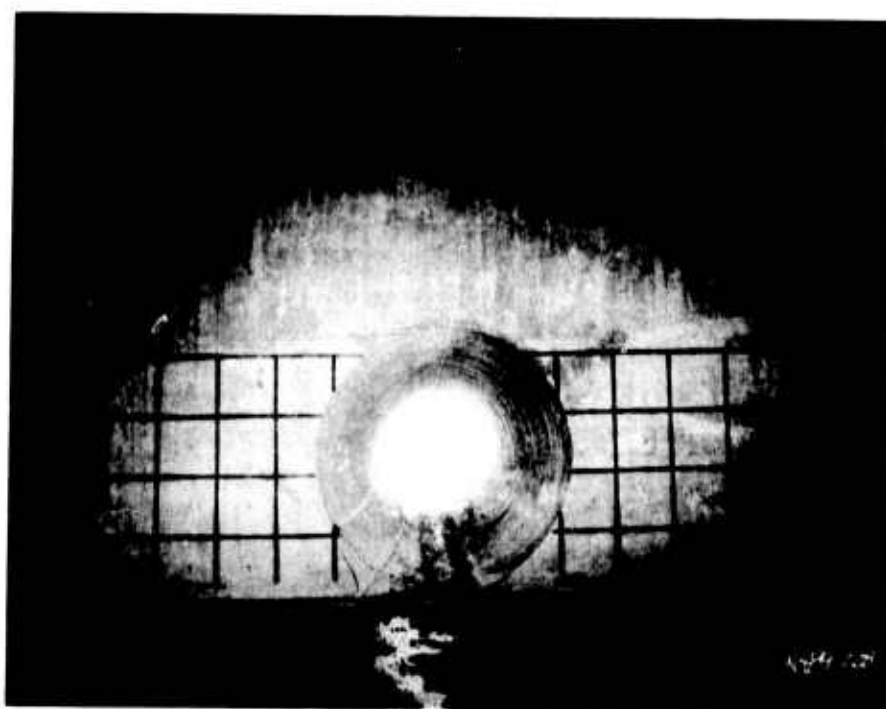
b. East wall.

Figure 2.20. Interior of completed donor bay (Sheet 1 of 2).
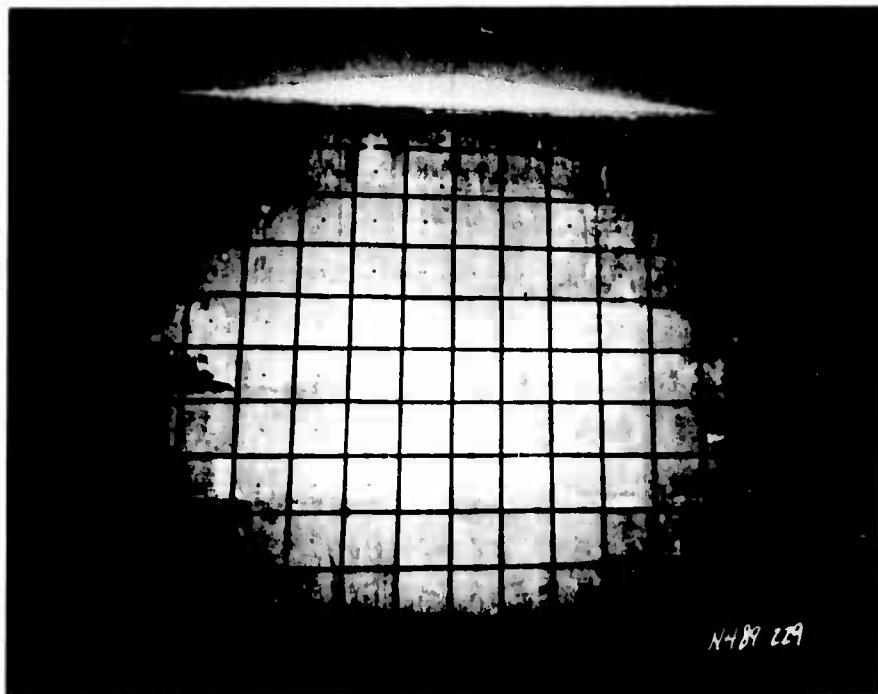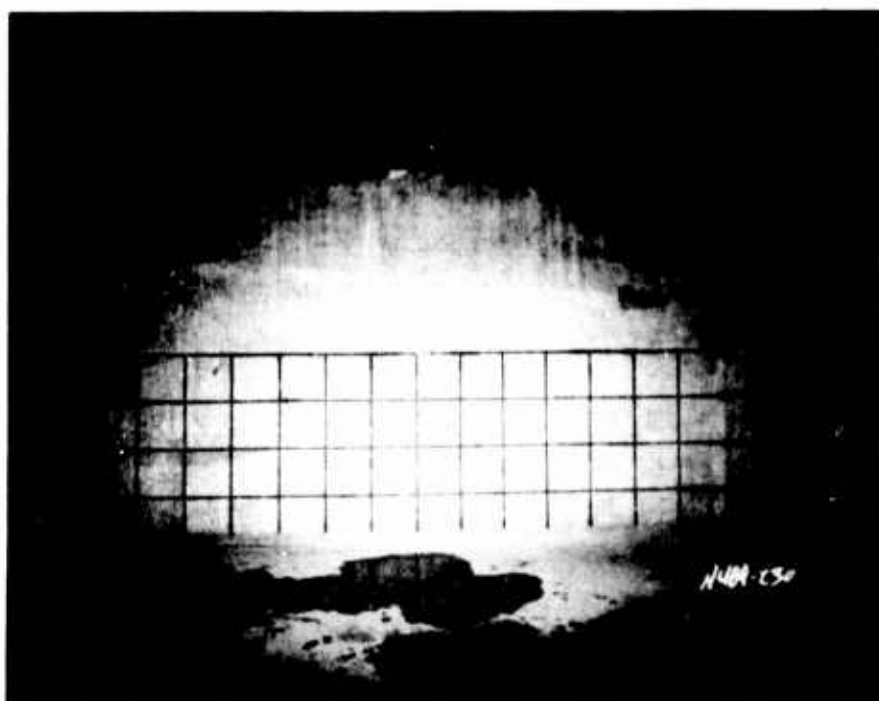
c. South wall.

d. West wall.

Figure 2.20. (Sheet 2 of 2).
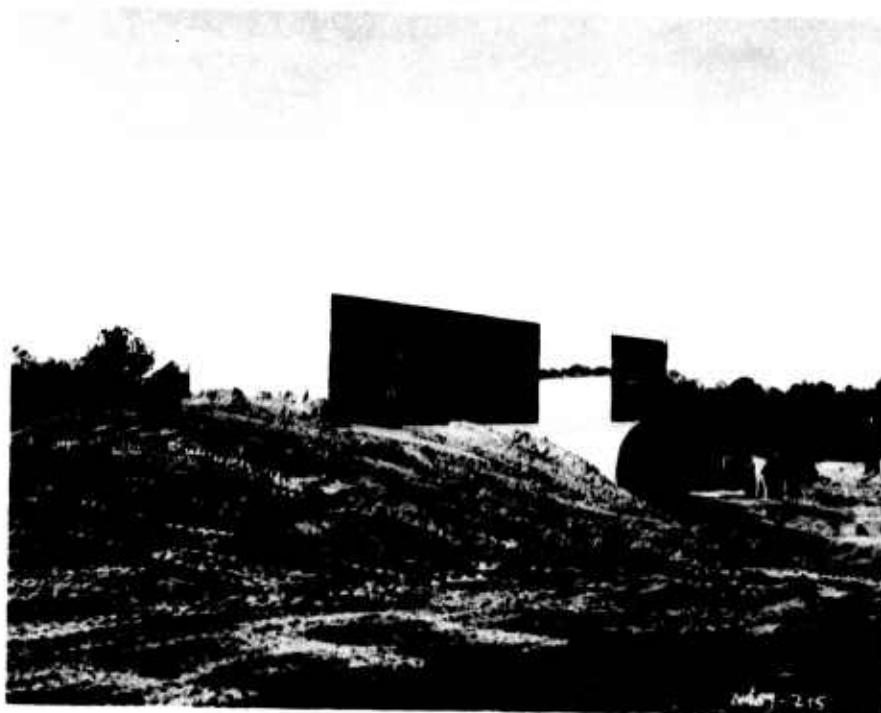
a. View facing northwest.
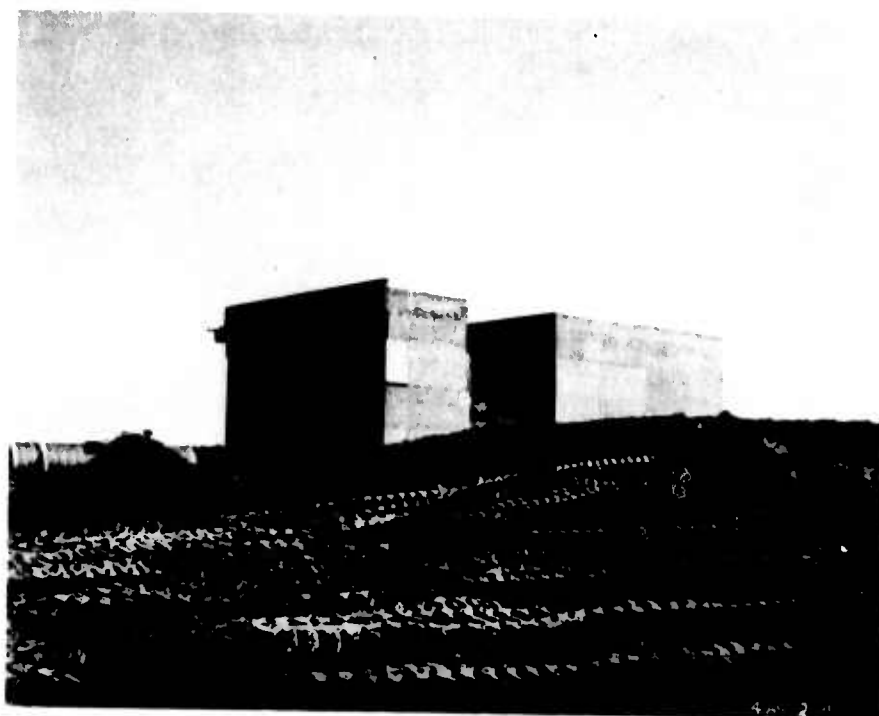
b. View facing southwest.

Figure 2.21. Structures during backfill.

51
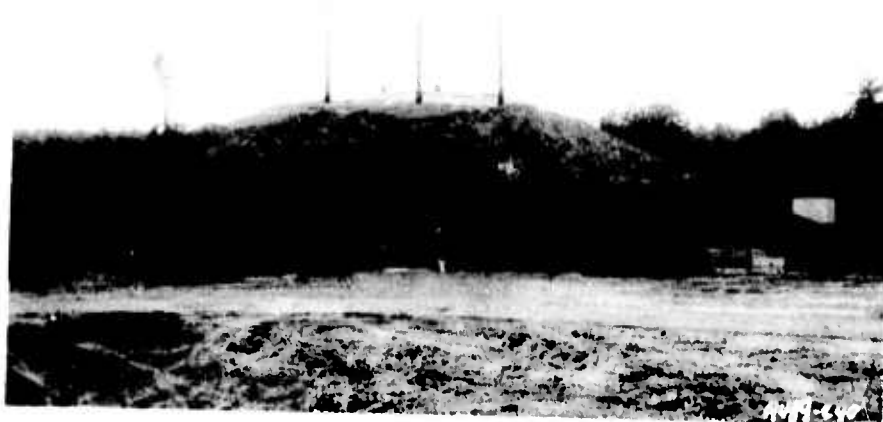
a. North side.

b. East side.

Figure 2.22. Exterior view of bays prior to
testing (Sheet 1 of 2).
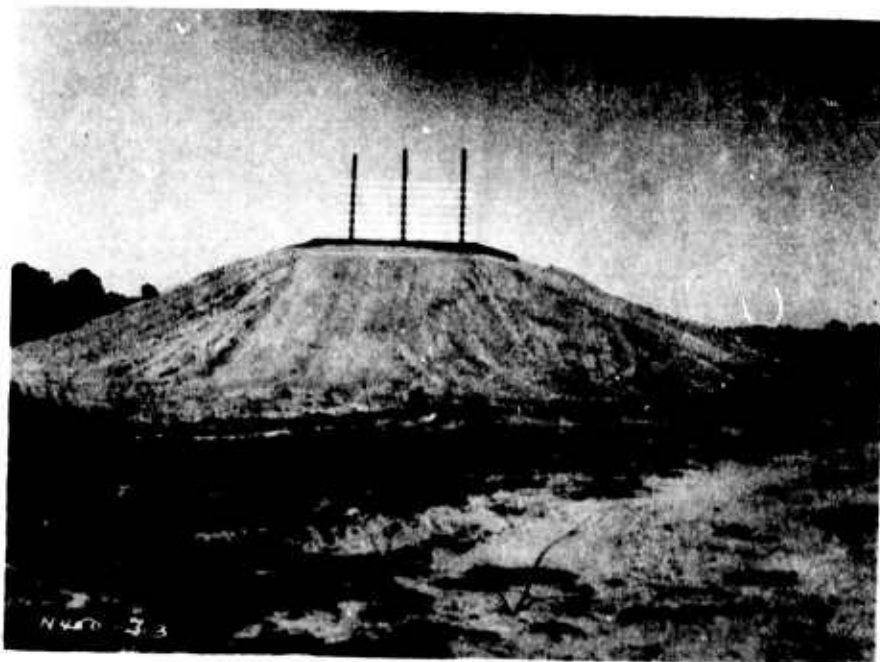
c.   South side.

d.   West side.

Figure 2.22 (Sheet 2 of 2).

53
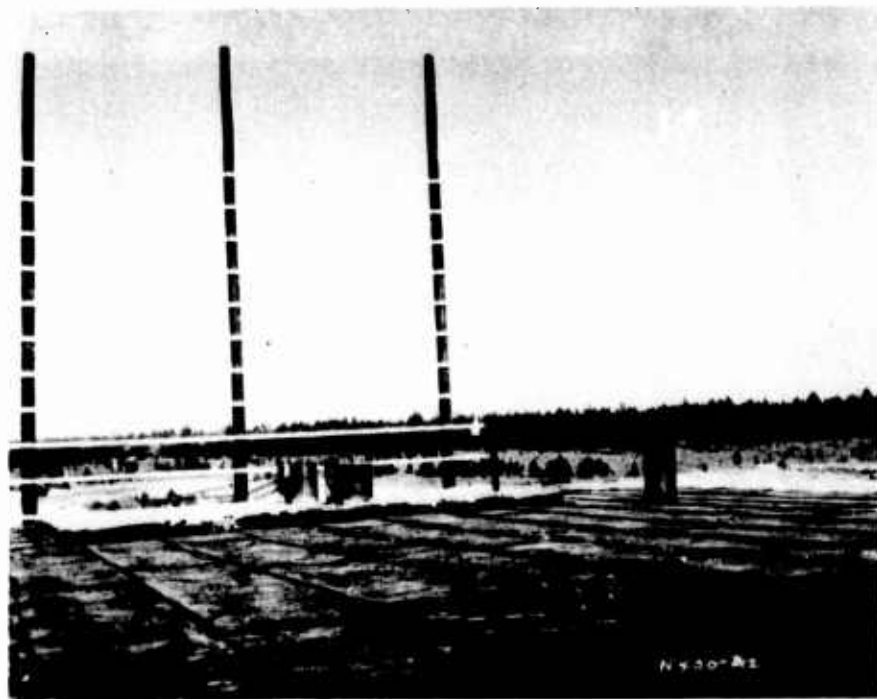
Figure 2.23.   Camera background and HVAC slab on top of bays.
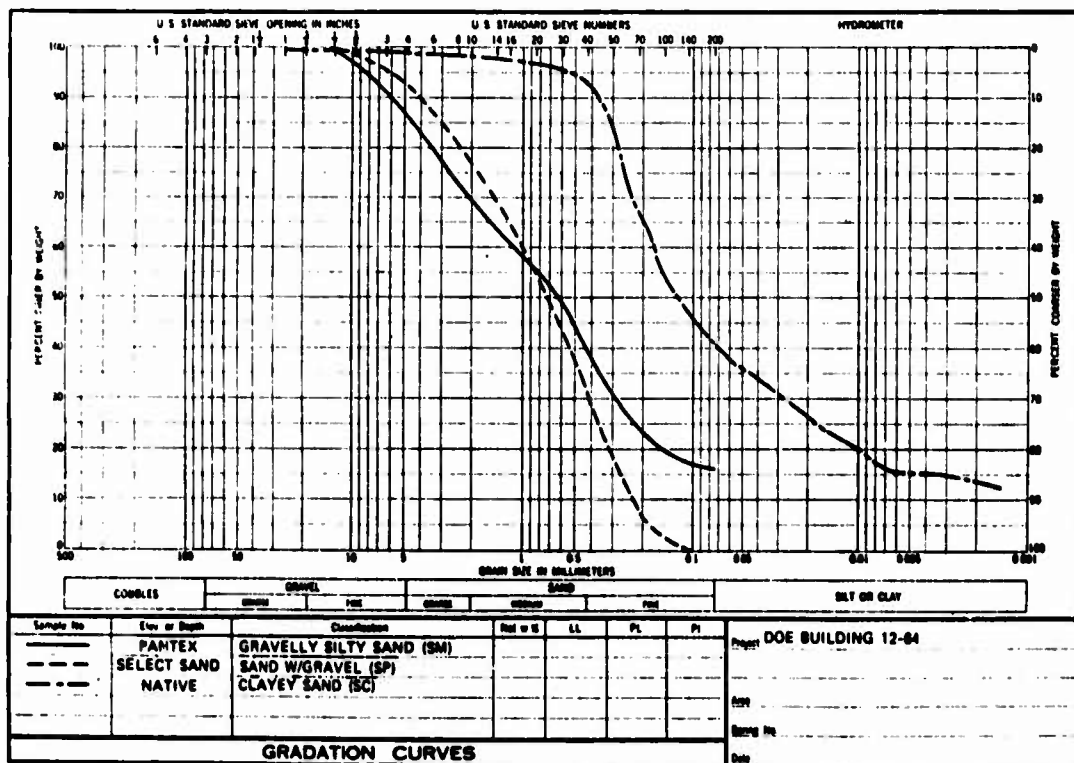
Figure 2.24.   Comparison of gradation curves for prototype, select
sand, and native backfill materials.

54
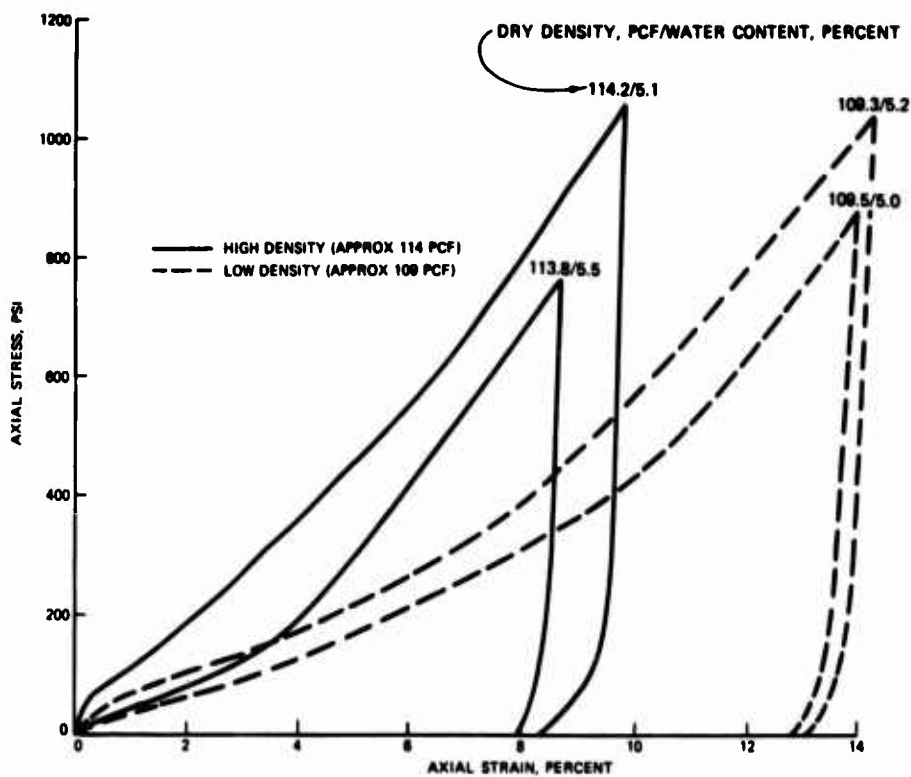
Figure 2.25. Results of uniaxial strain tests on soil from Pantex Building 12-64.
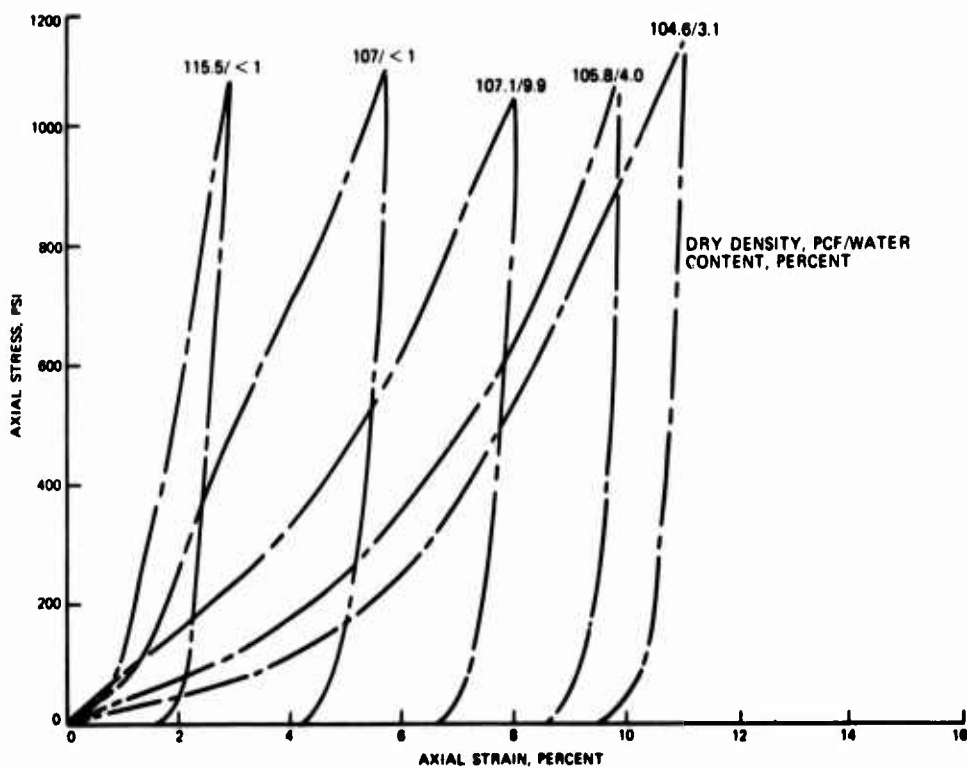
Figure 2.26. Results of uniaxial strain tests on select sand backfill material.
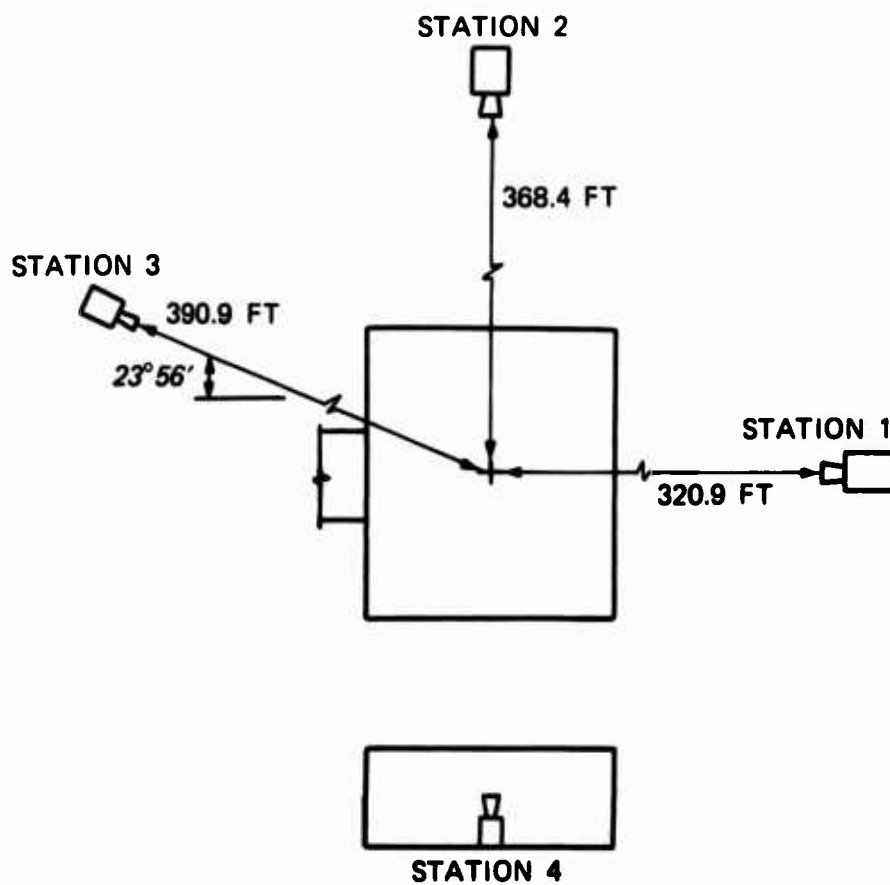
Figure 2.27. Movie camera locations.

Figure 2.28.   Camera station 2.

Figure 2.29.   Interior of acceptor bay.
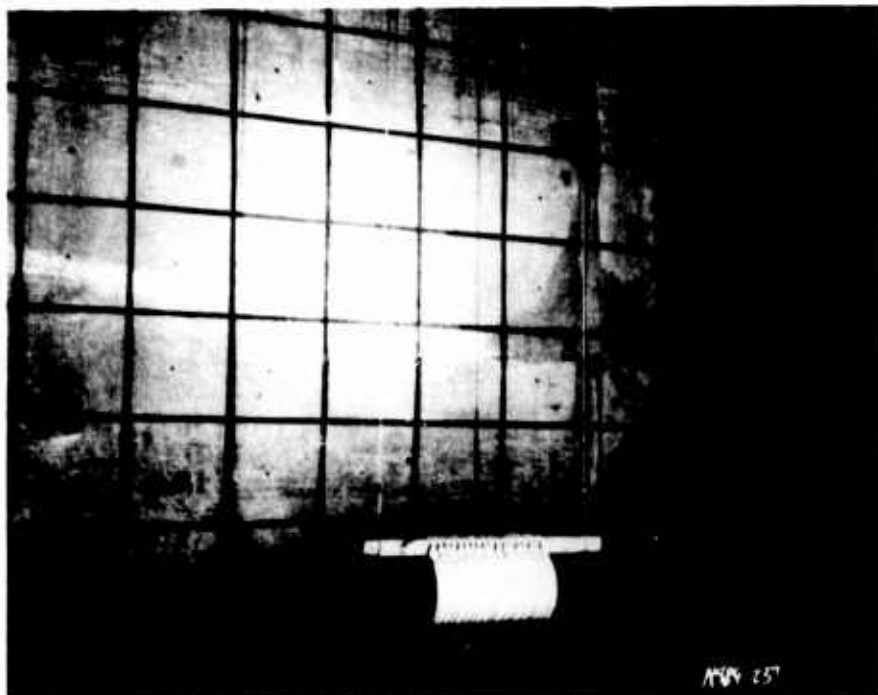
Figure 2.30. Explosive charge placement in donor bay.

Figure 2.31. Concrete slab placed in
donor bay entrance.

CHAPTER 3

PHASE II TEST PROCEDURES

Construction on the Phase II structures was begun in August 1981 and was completed on 22 January 1982. Appendix A lists significant events in the test program. Section 2.1 describes the test site.

3.1 DESCRIPTION OF STRUCTURES

The Phase II test structure was a half-scale model of a portion of Building 12-64 at the Pantex Plant. This model included two complete assembly bays with air locks, two simulated bay roofs, another air lock, and a retaining wall with ramp connecting the three air locks. A plan view of the Phase II structures is shown in Figure 3.1. The donor bay is in the center of the figure with the acceptor bay to the left. To simplify future discussion, directions will be referenced to the north arrow shown in Figure 2.1.

The model donor and acceptor bays duplicated all of the design and construction features of the prototype bays except they were built to half-scale. Exterior dimensions were 15.5 ft long, 13.5 ft wide, and 11.33 ft high with 0.75-ft-thick walls. The internal volume of the model bays was 1680.3 cu ft. Roofs were designed to hinge upward and vent gases produced by an internal explosion; they were connected to the walls along the east and west sides only. The roofs were 0.75 ft thick at the east and west walls and tapered to 0.38 ft thick at the center line. Figure 3.2 is an elevation view through both the donor and acceptor bays. The south wall of the acceptor bay, the north wall of the donor bay, as well as both roofs were covered with a 2-in.-thick layer of polystyrene foam of the type used to provide thermal insulation for the prototype. The void between the two bays was filled with a gravelly sand selected to model the stiffness of the prototype backfill material. The other sides of the bays were backfilled with native material. Reinforcing steel sizes and spacings used in the bays are listed in Table 3.1.

The west side of each bay was connected to an entrance air lock by steel dowels as shown in Figure 3.3. The other end of the air lock adjoined the retaining wall and ramp. Each air lock was 15.5 ft long, 8.5 ft wide, and 6 ft high; the wall and roof were 0.5 ft thick. The internal volume of each air lock from the bay to the bulkhead was 468.75 cu ft. Reinforcing steel sizes

and spacings in the air locks are listed in Table 3.2. The void between the donor and acceptor bay air locks was backfilled with the same gravelly sand used between the two bays.

The prototype air locks functioned as entrance tunnels to the bays and were equipped with two sets of blast doors, one set at the bay entrance and the other at a bulkhead in the air lock approximately 5 ft from the retaining wall. For the purposes of the test, the blast doors at the donor and acceptor bay entrances were assumed to be open, but the doors at the bulkheads to be closed. Thus, the air locks leading to the donor and acceptor bays were equipped with model blast doors at the bulkheads near the retaining wall but the bay entrances were not equipped with doors. The southernmost air lock represented the possibility of the first set of doors at the bulkhead being left open with the second set of doors at the bay left closed. In that air lock, there were no doors at the bulkhead and the other end was closed with a 1/2-in. steel plate.

The three air locks were connected by a retaining wall and ramp structure as shown in Figures 3.1, 3.3, and 3.4. The retaining wall was 9.3 ft high and 0.75 ft thick at the base, tapering to 0.5 ft at the top. Reinforcing bar sizes and spacings are listed in Table 3.3. The wall was connected by rebar dowels to the footing, the three air locks, and the ramp slab. The roof and west wall of the ramp were framed with steel S shapes and channels. Both the roof and wall were covered with 13/16-in.-thick cement-asbestos panels with an additional layer of corrugated sheet aluminum on the roof.

Two concrete slabs were placed to the east and south of the donor bay to simulate the roofs of adjacent bays in the prototype structure. These slabs are shown in both Figures 3.1 and 3.5.

HVAC ductwork was modeled to evaluate possible blast leakage into the acceptor bay and to properly model the vent area in the donor bay. Details of the model ductwork are shown in Figure 3.6. The "penthouse" in which the actual HVAC mechanical equipment was located was modeled with the concrete slab shown in Figure 3.6.

3.2 CONSTRUCTION PROCEDURES

3.2.1 Concrete Construction

All concrete placed in the models was cast in place at the test site.

60

Quality control was insured by casting standard cylinder specimens from concrete used to place each structural component. Specific test results are discussed in Section 3.3.1. Specimens of reinforcing steel were instrumented and tested as discussed in Section 3.3.2. Structural components were cured by coating all exposed surfaces with curing compound.

The site was prepared by removing all organic material from the subsoil and grading the area as shown in Figure 3.7. No fill operations were performed. Footings for the two bay slabs and retaining wall were excavated using a backhoe. Plywood exterior forms were set for the bays while sheet metal liners were used for interior forms to insure a chamfer between the footing and the floor slab. Earth forms were used for the retaining wall footing. A 3-in.-thick compacted sand layer was placed under all footings and floor slabs.

Formwork for the bay slabs included not only the footing and floor slab, but a 3-in.-high section of wall around the perimeter of each slab. The inside edge of the raised section was chamfered back to the floor slab at a 45-deg angle. A keyway was cast into the top of perimeter of the walls. An overall view of the acceptor bay formwork and reinforcing steel prior to concrete placement is shown in Figure 3.8. Details of the rebar placement are shown in Figure 3.9. Views of the reinforcing steel in the retaining wall footing are shown in Figure 3.10. Concrete was placed directly from ready-mix trucks into the forms as shown in Figure 3.11. Vibrators were used to insure proper consolidation. The bay slabs and wall footing after concrete placement are shown in Figure 3.12.

Reinforcing steel mats for the bay walls were laid out and tied on the ground and then raised into place. Figure 3.13 shows the steel layout for the four bay walls. Note that the long dowels shown as roof reinforcement in Figure 3.13a were cut as shown in Figure 3.17. Corners were reinforced with horizontal bars from the east and west faces which were bent 90 deg to lap over the steel in the north and south faces as shown in Figure 3.14. The rebar mats were tack welded on 2.5-ft centers to model the same practice used for prototype construction to insure adequate grounding. The four walls in each bay were cast monolithically by placing concrete with a pump as shown in Figure 3.15.

Following construction of the bay walls, outer retaining wall forms were set and reinforcing steel was tied in place as shown in Figure 3.16. Dowels

61

were placed to provide connections from the wall to the air locks and ramp slab. Steel plates with shear studs were set into the forms to provide connections for the steel beams to be used to frame the ramp roof. After completion of formwork, concrete was placed in the wall through a metal pipe.

Forms were then constructed inside the two bays to support the weight of the roof slabs. Reinforcing steel was tied in place as shown in Figure 3.17. The horizontal steel spanning the east/west direction was lapped 38 bar diameters onto the No. 5 dowels from the east and west walls. There was a 1-1/2-in. space running down the crest of the roof slab which was not reinforced. Since there were no dowels from the north and south walls, internal pressure would cause the slab to fracture along the crest, then each half of the roof would rotate along an axis parallel to the top of either the east or west wall. Placement of the roof slab concrete completed construction of the bays.

Floor slab forms were then set for both the air locks and the ramp. The perimeters of all slabs included an integral footing. A 3-in. compacted sand layer was placed under all slabs and footings. Reinforcing details of the air-lock slabs are shown in Figure 3.18. At the blast door bulkheads, a footing was included in the formwork. A steel plate was embedded at floor grade level to provide a threshold and an anchor for the locking bolt from the inactive door leaf. Dowels were provided to connect both walls and bulkheads to the slabs. Formwork and steel for the ramp slab are shown in Figure 3.19. The slab was 3 in. thick with a single reinforcing mat. Concrete was placed into the forms directly from ready-mix trucks.

Formwork for the air-lock walls, bulkheads, and roofs were constructed at the same time. Wall steel layout is shown in Figure 3.20 and typical roof steel details are shown in Figure 3.21. The two door frames for the blast doors were placed within the bulkhead forms. Concrete for the walls, bulkheads, and roofs was placed monolithically.

Completion of the air locks was followed by backfill placement which will be discussed in the following section. When soil elevations approached the top of the two bays, forms were set for the two simulated acceptor bay roof slabs to the east and west of the donor bay. The elevations at the top of these slabs were the same as the roofs of the two bays. Figure 3.22 shows one of the completed 6-in.-thick slabs.

With the completion of concrete construction, the interior of the donor

bay was painted with grid lines on 1-ft centers to aid in the survey of post-test damage. The interior of the completed donor bay is shown in Figure 3.23. The south wall of the acceptor bay was similarly marked and outfitted with equipment discussed in Section 3.4.

3.2.2 Embankment Construction

Two materials were used to backfill the structures, a select gravelly sand and the native clayey sand. The void between the donor and acceptor bays and the donor and acceptor air locks was filled with the select sand material which was compacted to specific density standards to model the shock transmissibility of the prototype material. Details of the prototype soil investigation and selection of the sand material are discussed in Section 2.4.3 The remaining areas were backfilled with the native soil which was compacted to model the mass of the prototype soil. Sand was also placed over the tops of the bays and the air locks in order to achieve uniform densities and allow accurate shaping of final soil profiles.

The select sand material was placed between the bays and air locks using a crane with clamshell attachment as shown in Figure 3.24a. Prior to placement, a 2-in. layer of polystyrene foam was cemented to the adjacent bay walls. The sand was spread with a backhoe and by hand into 1-ft-thick lifts and was compacted with vibratory compactors. Quality control was insured by frequent nuclear density measurements. Moisture contents were obtained by oven drying soil samples. The results of soil tests for the select sand material are summarized in Table 3.4.

The native material was placed around the perimeter of the bays with a bulldozer in 1-ft lifts and was compacted by multiple passes with rubber-tired equipment. The areas next to the bays and air locks were compacted with "wacker"-type portable compactors. Figure 3.24b shows the placement of native soil adjacent to the bays. The results of soil density measurements in the native backfill material are summarized in Table 3.5.

Once placement of backfill around and between the bays had been completed, the two simulated acceptor bay roofs were placed. Polystyrene foam 2 in. thick was cemented to the bay roofs, and a sand layer was then placed over the air locks and roofs. Following compaction, the sand was shaped to specified slopes as shown in Figure 3.25.

63

3.2.3 Blast Doors

The blast doors were a half-scale model of the blast doors used in Building 12-64. A set of doors consisted of an active leaf, an inactive leaf, and a door frame as shown in Figure 3.26. The door frame was fabricated from angle and channel sections and had overall dimensions of 4.34 ft high, 4.69 ft wide, and 0.5 ft thick. Shear studs were attached to the door frame's outer surface, and the door frame was cast in place in the air-lock bulkhead. The two door leaves each consisted of an internal framework of channels sandwiched between sheet steel skin plates. Both leaves were 4.07 ft high and 0.17 ft thick. The inactive leaf was the wider of the two (2.58 ft versus 1.63 ft) and its internal construction included a set of bolts which locked it to the door frame and the floor. Each of the door leaves was attached to the frame with three hinges. The 2- by 1/4-in. straps were welded to the doors, and the hinge pads were bolted to the door frame. Material properties are discussed in Section 3.3.3.

The blast doors were fabricated at WES. The door frame consisted of 3- by 2- by 3/16-in. angles and C4 by 5.4 channels. The end of the channel's flange was welded to the 2-in. angle leg, with a continuous fillet weld to form a door stop. Number 2 rebar shear studs 4 in. long were welded around the outside of the frame at 6-in. centers on both the angle and channel sides of the frame. Once the frame was cast in place, the long leg of the angle was flush with the front face of the bulkhead and the opposite channel flange was flush with the back of the bulkhead.

A 4-in.-wide by 1/4-in.-thick baseplate was also fabricated. Two rows of 4-in.-long No. 2 anchors were welded to the base at 6-in. centers. The baseplate was cast into the air-lock slabs. Holes were drilled into the door frame and baseplate to accommodate the inactive leaf-door bolts.

The door leaves were fabricated by fillet welding the internal framework of channels to the back skin plate as shown in Figure 3.27. Sixteen gage steel was used for the skin plates. The channels were cold formed from 10 gage steel with flanges 0.75 in. long and a web 1.5 in. wide. Channels were placed across the top and bottom of the door and along the outer edge of the door. Two channels were placed 4.38 in. apart at the inside edge of the doors. This area contained the locking mechanism in the inactive leaf. Five more channels were placed horizontally, spanning the remaining width of the door at a spacing of 0.68 ft. After the locking mechanism was in place on the inactive

64

leaves, the front skin plates for all leaves were plug-welded to the channels as shown in Figure 3.28. A 4.38-in.-wide by 3/16-in.-thick plate was then fillet-welded to the front and back skin plates at the inside edge of each leaf. All welds were tested with dye penetrant.

The locking mechanism used in the inactive leaf consisted of an 11/16-in.-diameter bolt which passed through two 3/16-in.-thick plates and the 1/8-in.-thick channel at the edge of the leaf, shown in Figure 3.29. The locking bolts extended 7/8 in. into both the door frame at the top and the base plate at the bottom. The active leaf was held shut with a 1/4-in.-diameter bolt through a hasp welded in the top right corner of the door leaf and the corresponding location on the door frame.

Commercial door hinges could not be ordered in a half scale so they were fabricated at WES. Hot rolled, merchant quality A-36 steel, 1/4 in. thick, was used for both the hinge pad and hinge strap. The pinned sections of the pads and straps were formed by heating and bending around a 1/2-in.-diameter pin. The hinge pads were 5 by 5 by 1/4 in. with four 3/8-in.-diameter bolts connecting the hinge pads to the door frame. The length of the 2- by 1/4-in. hinge straps welded to the front skin plate was 14.5 in. on the active leaf and 22.62 in. on the inactive leaf. A 1/2-in.-diameter bolt was used for a hinge pin.

After the doors were painted, 1/8-in.-thick neoprene rubber seals were glued around the door frame on the channel area that contacted the door. A rubber seal was also glued along the edge of the inactive leaf that lapped the active leaf. A neoprene rubber door sweep was attached to the bottom of each leaf.

3.2.4 Ramp and Appurtenance Construction

Provisions for the HVAC ductwork included the 8-in.-diameter pipes which were cast into the donor and acceptor bay walls (Figure 3.13c) and the roofs (Figure 3.17) to serve as ductwork penetrations. The ductwork was prefabricated at WES using 7-in.-diameter tubing and was placed in position as soon as the soil fill was at the proper elevation (Figure 3.30a). Once the soil fill was placed over the bay roofs, the model penthouse slab was cast in place as shown in Figure 3.30b.

The west wall and roof for the ramp were framed with steel components. Beams and columns were welded to one another and then put into position as

shown in Figure 3.24b. The beams were welded to clip angles which were attached to plates embedded in the retaining wall. Column baseplates were bolted to the ramp slab with two 1/2-in.-diameter bolts. Five steel purlins were welded to the beams to support the roof. Sag rods 1/4 in. in diameter were welded between the purlins at midspan. One girt spanned the length of the wall. Both the wall and the roof were covered with 13/16-in.-thick Johns Manville Transitop panels which were attached to the girts and purlins with No. 12 self-tapping screws. Vertical joints between the panels were connected by 1-in.-wide strips of 22-gage sheet metal attached to adjoining panels with screws. A 2- by 2-in., 22-gage sheet steel angle was screwed to the base of each panel and attached to the ramp slab with Ramset fasteners. A layer of corrugated aluminum roofing was placed over the roof.

The backfill material over the bays and the surrounding area was covered with 1/4-in.-thick W. R. Meadows Corporation protective course panels to simulate the mass of the 1/2-in.-thick Gulf Seal Corporation asphalt planks used in prototype construction. Joints were lapped 3 in. and sealed with Gulf Seal Corporation 626 U catalytically blown asphalt. The exterior appearance of the completed Phase II structure is shown in Figure 3.31.

3.3 CONSTRUCTION MATERIALS

3.3.1 Concrete

The results of the compressive tests on 6- by 12-in. control cylinders for the Phase II structures are summarized in Table 3.6. Compressive strengths were measured 7 and 28 days after placement and on 27 January 1982 for the remaining specimens. Average compressive strengths are listed for 28-day breaks and available 27 January breaks. The average 28-day compressive strength of the Phase II structure was 4336 psi.

3.3.2 Concrete Reinforcing Steel

Grade 40 reinforcing steel was used for the Phase II structures in bar sizes 2 through 5. Static tensile tests were performed on specimens of each bar size to determine the engineering properties of the actual material used for construction. Results of these tests are summarized in Table 3.7, and the stress-strain curves derived from the tests are shown in Appendix B. The first digit in each specimen number listed in the table and appendix

corresponds to the bar size of the specimen.

3.3.3 Structural Steel

Blast doors were fabricated of structural sheet and plate steel. Sheet steel was 16 and 10 gage hot-rolled commercial grade; plate steel was 3/16- and 1/4-in. thick A36 steel. Table 3.8 lists the results of static tensile tests on samples of these materials, and Appendix C includes the stress-strain curves from these tests.

3.4 INSTRUMENTATION

Fifty-six electronic transducers were used to record airblast pressures, soil pressures, interface pressures, deflections, and accelerations in the structures. A measurement list is shown in Table 3.9 and gage locations are illustrated in Figures 3.1-3.3, 3.5, and 3.6. Airblast instrumentation included four gages in the acceptor bay (BP1-4), ten gages in the air locks (BP5-8 and BP15-20), three gages on the retaining wall (BP9-11), three gages in the donor bay (BP12-14), eight gages on the surface (BP21-28), and one gage in the HVAC ductwork (BP29). Gages BP12 and 13 were equipped with debris shields. Soil pressures midway between the donor and acceptor bays were measured by four soil-stress gages. Interface pressures on the acceptor bay wall were measured by gages IP1-9. These gages were flush-mounted with the surface of the wall and covered with a 2-in. foam layer. Interface pressures acting on the two simulated acceptor bay roofs were measured by gages IP10-14. Acceptor bay wall deflections were measured by gages D1 and 2 and roof deflections by gages D3-5. The displacement of the acceptor bay floor slab was measured by gage D6. Acceptor bay wall accelerations were measured by gages A1 and A2 and floor accelerations by A3. Figure 3.32 shows the interior of the acceptor bay with all of the associated deflection gage mounts and accelerometers.

The locations of the structures, instrumentation cables, and recording equipment during the test are shown in Figure 2.1. Each transducer cable was individually shielded and was approximately 350 ft long. Cables embedded in concrete were protected by 1/2-in.-diameter steel pipe.

WES-built amplifiers were used for signal conditioning and amplification. Airblast data were recorded on a 80-kHz, Sangamo Sabre V, 32-track, FM magnetic tape recorder at a speed of 120 in./sec. All other data were recorded on a

67

20-kHz, Sangamo Sabre III, 32-track, FM tape recorder at a speed of 60 in./sec.

Four high-speed movie cameras and one sequence camera were used to view the exterior of the structures at camera stations 1 through 4. One high-speed movie camera was located inside the acceptor bay at station 5. This camera can be seen in Figure 3.32b. Camera information is listed in Table 3.10 and camera station locations are shown in Figure 3.33. The cameras at stations 1 and 2 were located on the roofs of existing structures and were elevated approximately 10 ft higher than the roofs of the Phase II structures. The camera at station 3 was placed at approximately the same elevation as the model roofs.

3.5 STRUCTURAL VIBRATION TESTING

The donor bay north wall and the acceptor bay south wall were dynamically tested to determine their vibration characteristics. These tests were conducted both before and after the structures were backfilled. The basic test procedure is discussed in Section 2.6. The only significant difference was that the drive points were located at 1.5-ft intervals in the horizontal direction and 1.23-ft intervals in the vertical direction.

3.6 EXPLOSIVE CHARGE ASSEMBLY AND PLACEMENT

The explosive charge was a 37.56-lb cylinder of PBX 9501, with nominal dimensions of 14.5 in. in diameter and 13.75 in. in length. The charge consisted of six cylindrical segments which were pressed and machined to proper size and weight and then glued together with Urethane 7200 adhesive. All fabrication was performed at the DOE Pantex plant.[5] The charge was suspended from the roof of the donor bay by a combination of two steel cables, a wood beam, and nylon straps as shown in Figure 3.34. The center of the charge was located 1.94 ft from the north wall and 1.48 ft above the floor. Detonation was accomplished with an SE-1 detonator located on the west end of the charge. At the time of detonation, the air temperature was 54° F and barometric pressure was 30.27 in. of mercury.

Table 3.1. Assembly bay concrete reinforcing steel.

Component	Mat Face	Bar Orientation	Bar Size No.	Bar Spacing in.	Remarks
Footing*	Outer and inner	Horizontal	3	--	Four per footing
		Vertical	2	18	Stirrups
Floor slab*	Bottom	N-S	3	8	
		E-W	4	5.5	
	Top	N-S	3	8	
		E-W	6	5	
North and south walls	Outer	Horizontal	2	4.5	
		Vertical	2	6	
	Inner	Horizontal	2	4.5	
		Vertical	4	3	
East and west walls	Outer	Horizontal	3	8	
		Vertical	4	4	
	Inner	Horizontal	3	8	
		Vertical	5	4.5	
Floor-to-wall dowels	Bottom/outer		4	4	L shaped
	Top/inner		4	5.5	L shaped
Wall-to-roof dowels**	Outer/top		5	3	L shaped
	Inner/bottom		3	9	L shaped
Roof slab	Bottom	N-S	3	13	Three bars on each side
		E-W	5	3	
	Top	N-S	3	8	
		E-W	5	3	

* Footing and floor slab were monolithic.
** Wall-to-roof dowels were installed in east and west walls only.

69

Table 3.2. Air-lock reinforcing steel.

Component	Mat Face	Bar Orientation	Bar Size No.	Bar Spacing in.	Remarks
Footing*	Outer and inner	Horizontal	3	--	Four per footing
		Vertical	2	18	Stirrups
Floor slab*	Bottom	N-S	2	6	
		E-W	2	6	
	Top	N-S	4	4	
		E-W	2	6	
North and south walls	Outer	Horizontal	2	6	
		Vertical	3	6	
	Inner	Horizontal	2	6	
		Vertical	3	4	
North and south bulk-head walls	Outer and inner	Horizontal	2	6	N and S sides of door
		Vertical	2	6	
Upper bulkhead wall	Outer and inner	Horizontal	3	--	Four per bulkhead
		Vertical	2	6	U-shaped stirrups
Floor-to-wall dowels	Bottom/outer		6	5	L shaped
	Top/inner		3	12	L shaped
Wall-to-roof dowels	Outer/top		6	5	L shaped
	Inner/bottom		3	12	L shaped
Roof slab	Bottom	N-S	4	4	
		E-W	2	6	
	Top	N-S	4	6	
		E-W	2	6	

* Footings and floor slab are monolithic.

Table 3.3. Retaining wall reinforcing steel.

Component	Mat Face	Bar Orientation	Bar Size No.	Bar Spacing in.	Remarks
Footing	Bottom	N-S	3	--	One bar
		Vertical	4	7	J-shaped dowel
	Intermediate	N-S	2	6	Six bars
		E-W/ Vertical	4	7	L-shaped dowel*
	Top	N-S	5	6.5	
		E-W	2	6	
Wall section between air lock	Inner	Horizontal	2	6	Bar lengths vary
		Vertical	4	3.5	
	Outer	Horizontal	2	6	
		Vertical	2	6	
Wall section over air lock	Inner	Horizontal	2	6	
		Vertical	4	10.5	
	Outer	Horizontal	2	6	
		Vertical	2	6	

* Bar shape changed and spacing changed to 10.5 in. under air-lock intersections.

Table 3.4. Results of soil tests on select sand material.

Location	Elevation Above Bay Floor ft	Average Dry Density lb/ft^3	Average Moisture Content percent	Average Wet Density lb/ft^3
Between bays	Grade	110.4	4.4	115.2
	1	109.3	4.4	114.0
	2	110.8	4.4	115.6
	3	113.0	4.2	117.8
	4	111.6	4.1	116.2
	5	111.2	4.0	115.6
	6	111.9	3.8	116.2
	7	111.1	3.9	115.4
	8	112.3	4.2	117.0
	9	112.8	3.5	116.7
	10	111.0	5.8	117.4
	10.6	110.9	5.8	117.3
	11.6	112.3	3.9	116.7
	Average	111.4	4.3	116.2
Between air locks	1	112.8	4.4	117.8
	2	111.1	3.9	115.4
	3	106.7	3.9	110.8
	4	110.6	3.8	114.8
	5	111.0	4.0	115.4
	5.5	111.4	4.3	116.1
	7	112.2	3.9	116.6
	8	111.1	4.0	115.5
	9	112.0	4.8	117.4
	Average	111.0	4.1	115.5
Over bay roofs	11.6	110.4	3.7	114.4
Over simulated bay roofs	11.6	105.2	4.5	110.0

Table 3.5. Results of soil tests on native material around structure.

Location	Elevation Above Bay Floor ft	Average Dry Density lb/ft^3	Average Moisture Content percent	Average Wet Density lb/ft^3
North side of acceptor bay	2	112.5	13.0	127.1
	4	110.1	14.2	125.7
	5	114.1	13.6	129.6
	6	109.2	15.8	126.5
	7	111.4	13.1	126.0
	8	110.8	16.3	128.9
	9	114.4	11.1	127.0
	9.5	113.7	10.9	126.1
	10.6	110.3	13.2	124.8
	Average	111.8	13.5	126.9
East side of bay	1	108.3	11.2	120.4
	3	109.9	11.8	122.8
	3.5	107.4	11.6	119.9
	4	109.8	11.6	122.5
	4.5	108.6	11.2	123.8
	6.5	110.9	11.7	119.0
	7	110.5	14.6	126.6
	8	108.5	14.6	124.4
	8.5	111.6	13.8	127.0
	9.5	112.3	14.0	127.9
	10.6	113.3	12.2	127.1
	Average	110.1	12.6	123.8
South side of donor bay	1	103.7	11.3	115.4
	2.5	110.4	12.0	123.6
	3	109.0	10.5	120.5
	4	109.6	12.4	123.2
	5	107.3	12.1	120.3
	6	108.3	12.3	121.7
	7	107.9	11.6	120.4
	8	110.6	15.8	128.1
	9	114.0	13.8	129.7
	10.6	109.5	16.9	128.0
	Average	109.0	12.9	123.1
South of donor air lock	Average	109.2	12.3	122.6
North of acceptor air lock	Average	111.8	13.3	126.8

Table 3.6. Concrete compressive strengths.

Structural Component	Specimen Number		Compressive Strength, psi	Specimen Age, days
Retaining wall footing	II-1		3749	7
	II-2		4562	28
	II-3		4669	28
	II-4		3997	7
		Average	4615	28
Donor bay floor slab	II-5		4739	28
	II-6		4279	28
	II-7		4085	7
	II-8		4775	28
	II-9		4810	28
		Average	4651	28
Acceptor bay floor slab	II-10		3466	7
	II-11		4067	28
	II-12		4527	28
	II-13		4562	138
		Average	4297	28
		Average	4562	138*
Acceptor bay walls	II-14		3236	7
	II-15		3890	28
	II-16		3731	28
	II-17		3395	7
	II-18		3678	28
		Average	3766	28
Donor bay walls	II-19		4067	28
	II-20		3431	7
	II-21		3979	28
	II-22		4527	121
	II-23		3413	7
	II-24		3855	28
	II-25		4439	121
		Average	3967	28
		Average	4483	121*

(Continued)

* Day of the Phase II event.

(Sheet 1 of 2)

Table 3.6. (Concluded).

Structural Component	Specimen Number		Compressive Strength, psi	Specimen Age, days
Retaining walls	II-26		3890	28
	II-27		4792	92
	II-28		4775	92
	II-29		4598	28
	II-30		5447	92
		Average	4244	28
		Average	5005	92*
Bay roofs	II-31		3678	7
	II-32		3307	7
	II-33		4492	28
	II-34		4598	28
	II-35		5517	84
	II-36		5553	84
	II-37		4598	28
	II-38		4598	28
	II-39		5730	84
		Average	4572	28
		Average	5600	84*
Air-lock slabs	II-40		3749	7
	II-41		4598	28
	II-42		4739	28
	II-43		5376	79
	II-44		3448	7
	II-45		4598	28
	II-46		5270	79
	II-47		5234	79
		Average	4645	28
		Average	5305	79*
Air-lock walls and roof	II-48		4456	28
	II-49		4067	28
	II-50		4969	57
	II-51		4244	28
	II-52		4173	28
	II-53		5058	57
		Average	4235	28
		Average	5014	57*

* Day of the Phase II event.

(Sheet 2 of 2)

Table 3.7. Properties of concrete reinforcing steel.

Speci-men No.	Cross-Sectional Area, in.^{2}	Percent Area Reduction at Failure	Yield Stress psi	Yield Strain μin./in.	Ultimate Stress psi	Modulus of Elasticity E , ksi
2-1	0.0467	53.19	60,000	2080	80,728	28,846
2-2	0.0479	54.16	61,200	2120	79,853	28,867
2-3	0.0475	58.33	64,000*	--	78,947	--
2-4	0.0483	54.16	64,000*	--	81,573	--
Average	0.0476	54.96	62,300	2100	80,275	28,856
3-1	0.0762	50.00	62,000	2120	99,737	29,245
3-2	0.0746	53.33	60,500**	2000	96,514	30,250
3-3	0.0735	52.05	62,800	2120	100,340	29,622
3-4	0.0740	51.35	62,900*	2080	100,000	30,240
Average	0.0745	51.68	62,050	2080	99,147	29,839
4-1	0.1450	52.41	68,400	2240	105,862	30,535
4-2	0.1438	53.47	67,000	2080	106,258	32,211
4-3	0.1461	52.05	67,700	2280	106,502	29,693
4-4	0.1491	55.70	--*	--	105,566	--
Average	0.1460	53.40	67,700	2200	106,047	30,813
5-1	0.2119	52.15	65,900	2040	101,328	32,303
5-2	0.2161	53.59	67,000	2080	101,960	32,211
5-3	0.2156	50.98	65,300	2080	100,653	31,394
5-4	0.2130	54.45	66,800	2120	101,650	31,509
Average	0.2141	52.79	66,250	2080	101,397	31,854
6-1	0.3035	55.77	66,400	2200	100,164	30,181
6-2	0.3024	55.44	64,000	2000	97,883	32,000
6-3	0.3040	52.30	65,000	2200	100,657	29,545
6-4	0.3034	54.60	66,000	2120	100,856	31,132
Average	0.3033	54.52	65,350	2130	99,890	30,714

* Gage failed.
** 0.02 percent offset.

Table 3.8. Properties of structural steel.

Nominal Thickness	Specimen No.	Cross-Sectional Area, in.²	Percent Area Reduction at Failure	Yield Stress psi	Yield Strain μin./in.	Ultimate Stress psi	Ultimate Strain μin./in.	Modulus of Elasticity E, ksi
16 gage	1	0.03309	36.23	45,330	1800	55,300	80,000	25,185
	2	0.03339	33.82	44,920	1800	56,450	85,000	24,955
	3	0.03354	40.31	45,020	1840	54,020	94,000	24,467
	Average	0.03334	36.78	45,090	1813	55,250	86,333	24,870
10 gage	4	0.06386	51.22	31,710	3100*	49,480	109,800	28,827
	5	0.06487	60.81	37,000	3300*	49,790	123,700	28,461
	6	0.06435	66.46	31,700	3850*	--	120,000	17,135
	Average	0.06436	59.49	33,470	3416*	49,630	117,833	23,637
3/16 in.	7	0.08946	59.67	38,450	3600*	58,680	95,000	24,031
	8	0.09194	58.83	44,370	3500*	61,720	115,000	29,580
	9	0.09027	56.75	39,880	3280*	59,710	96,000	31,156
	Average	0.09055	58.42	40,900	3460*	60,030	102,000	28,014
1/4 in.	10	0.11808	70.57	33,870	1180	49,120	117,300	28,703
	11	0.11592	67.86	34,590	1210	50,250	112,000	28,586
	12	0.11880	72.62	34,260	1180	49,450	117,500	29,034
	Average	0.11760	70.35	34,240	1190	49,600	119,600	28,773

* 0.2 percent offset.

Table 3.9. Measurement list for Phase II.

Type of Measurement	Gage No.	No. of Gages	Manufacturer	Model No.	Range	Natural Frequency Gage
Blast pressure	BP1-4, 21, 22, 29	7	Kulite	XTS-190	25 psi	100 kHz
	BP5, 6, 8, 15-20, 23, 24, 26-28	14	Kulite	XTS-190	50 psi	130 kHz
	BP7, 9-11, 25	5	Kulite	XTS-190	100 psi	160 kHz
	BP12, 13	2	Kulite	HKS-1-375	2000 psi	650 kHz
	BP14	1	Kulite	HKS-1-375	5000 psi	675 kHz
Interface pressure	IP1-IP14	14	Kulite	VM-750	200 psi	28 kHz
Deflection	D1, D2, D6	3	Trans-Tec	245-000	±2 in.	110 Hz
	D3-D5	3	Trans-Tec	246-000	±3 in.	75 Hz
Soil stress	SS1-SS4	4	Kulite	LQ-080U	200 psi	17 kHz
Acceleration	A1-A2	2	Endevco	2262C-1000	1000 g	6 kHz
	A3	1	Endevco	2262C-200	200 g	3.6 kHz

Table 3.10. High-speed camera list.

Camera Station	Type of Camera	Frame Rate fps	Lens Focal Length mm
1	Lo Cam, 16-mm movie	500	15
	Hulcher, 70-mm sequence	50	150
2	Lo Cam, 16-mm movie	500	10
3	Photec, 16-mm movie	2000	32
4	Milliken, 16-mm movie	500	25
5	Nova, 16-mm movie	4000	11

Figure 3.1. Plan view of Phase II structures.

Figure 3.2. Elevation view of Phase II donor and acceptor bays.

Figure 3.3. Elevation view of Phase II acceptor bay.

82

Figure 3.4. Elevation view of retaining wall and ramp.

Labels within figure:

ALUMINUM ROOFING

CEMENT ASBESTOS SANDWICH PANEL

½" φ SAG RODS MID-SPAN BETWEEN COLUMNS

5-C3x4.1 PURLINS EQ. SPACED

S 4x7.7 BEAM AND COLUMN

9" BASE THICKNESS

8'-3¾"

4'-8-3/16"

1"

6"

2'-3"

3"

6'-3¾"

12

3

6"

9"

6"

2'-10½"

3'-8½"

1'-1½"

Figure 3.5. Elevation view of simulated acceptor bay roof.

PLAN

VENT STACK   NO. 2 REBAR 12"O.C.   VENT STACK

FIN. GRADE

BP29

ELEVATION
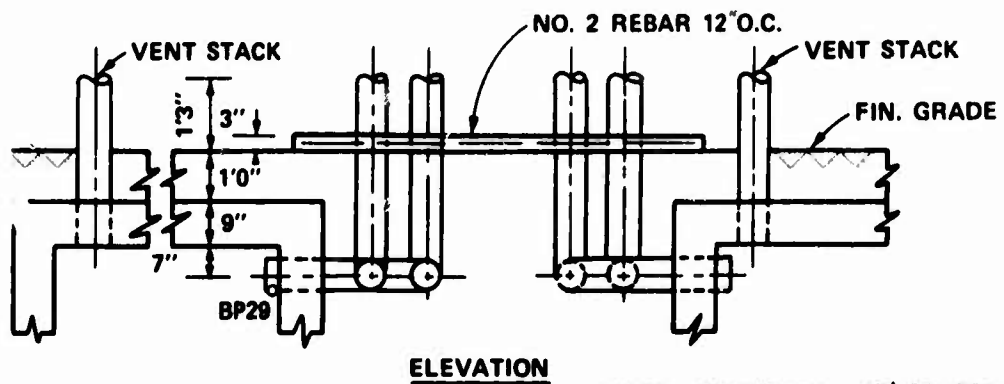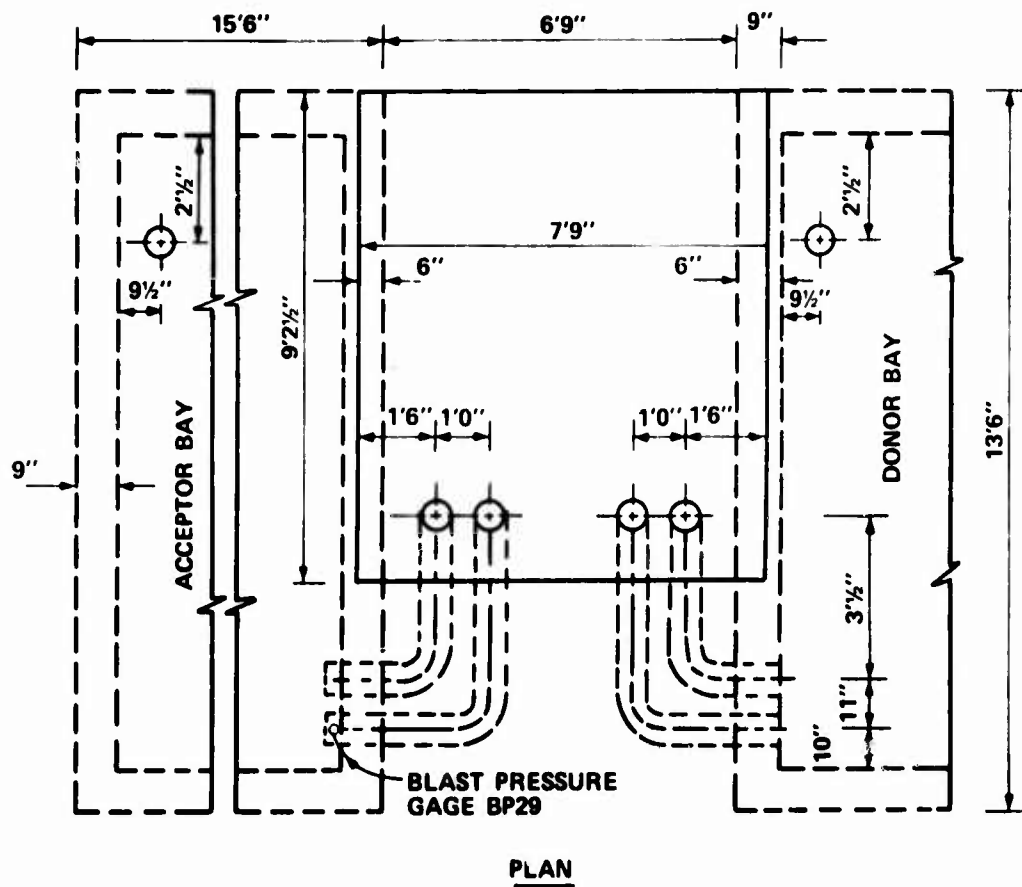
NOTE: DUCTWORK - 7"⌀ SCHEDULE
10 STEEL PIPE

PENETRATIONS - 8"⌀ STEEL
PIPE

Figure 3.6. Phase II HVAC ductwork.

Figure 3.7.   Site preparation.
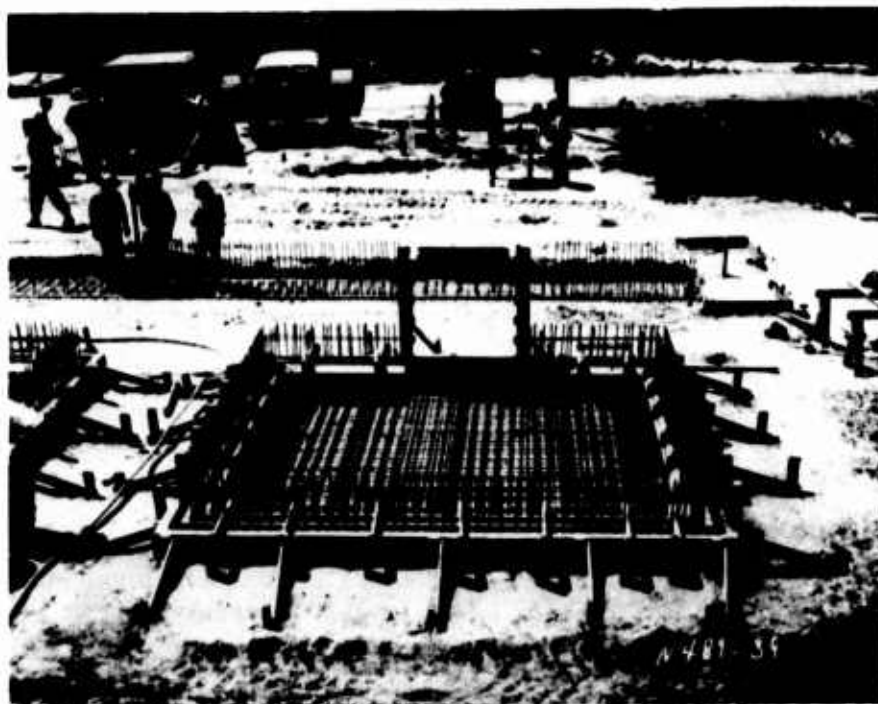
Figure 3.8.   Bay floor slab formwork and
reinforcing steel.

b. Corner.

a. Center of bay.

Figure 3.9. Details of bay floor slab reinforcing steel.

87

a.   Overall view.
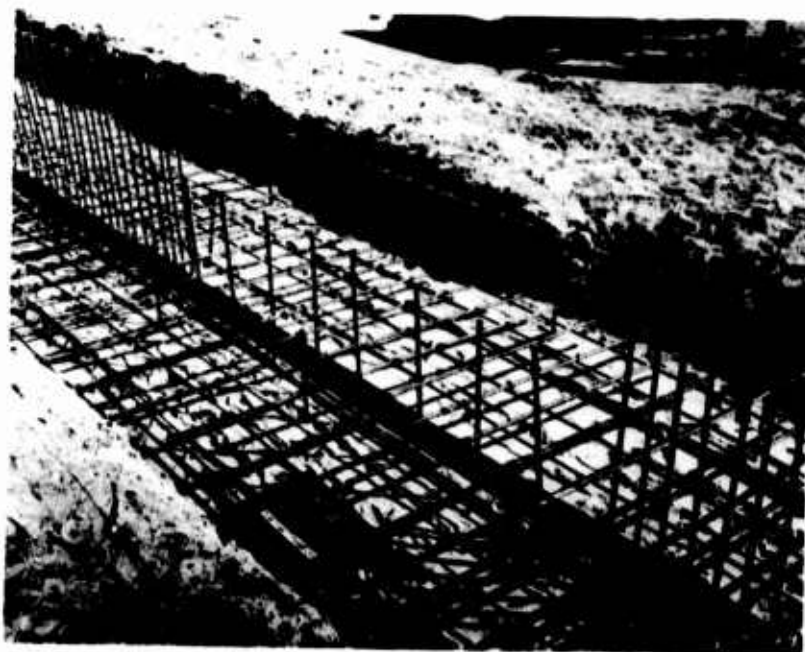
b.   Detail at airlock entrance.

Figure 3.10.   Retaining wall footing reinforcing steel.

Figure 3.11.   Concrete placement in bay floor.

Figure 3.12.   Completed bay floors and retaining wall footing.
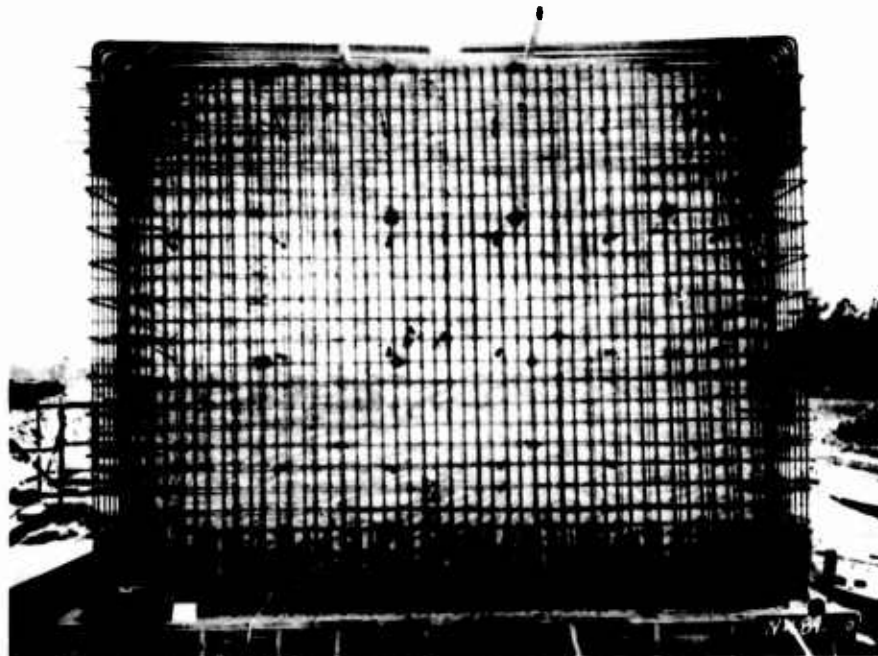
a. North wall.

b. East wall.

Figure 3.13. Acceptor bay wall reinforcing steel
(Sheet 1 of 2).
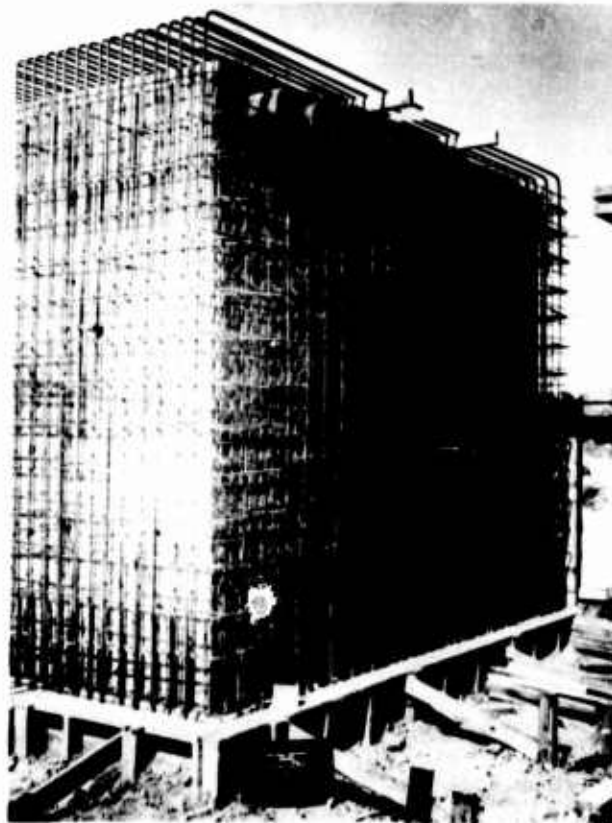
c. South wall.
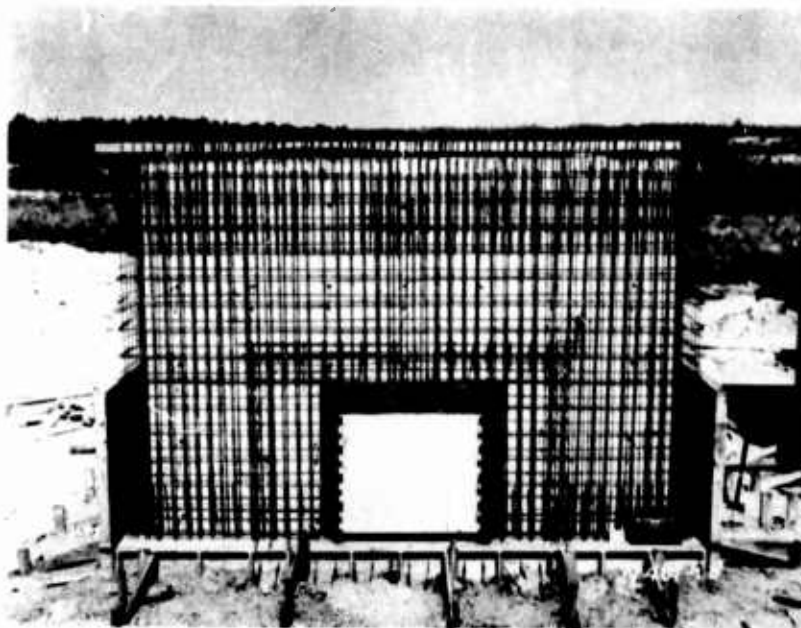
d. West wall.

Figure 3.13. (Sheet 2 of 2).
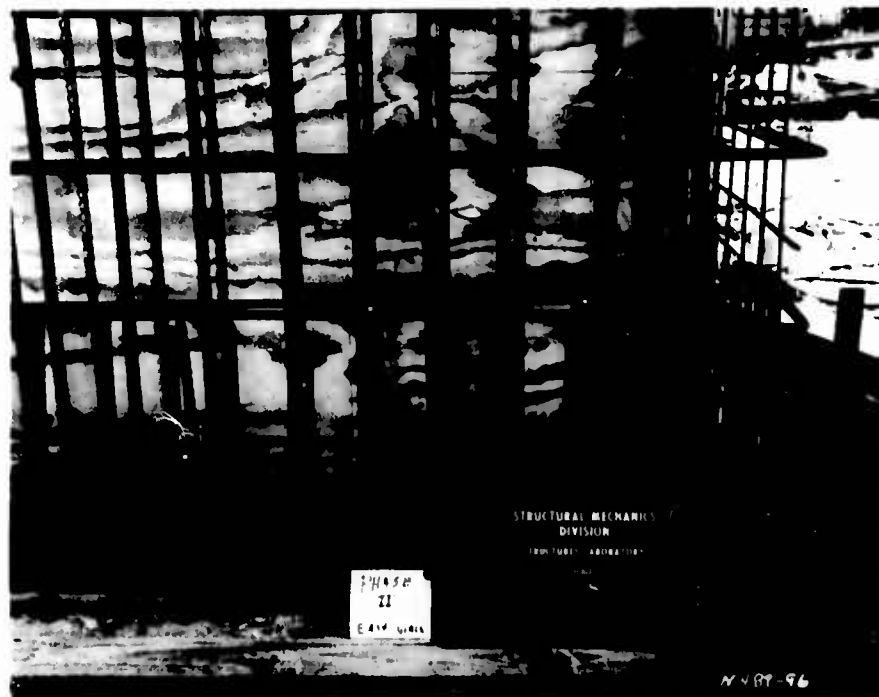
Figure 3.14. Corner reinforcement details.

Figure 3.15. Concrete placement in bay walls.

a. Overall view.
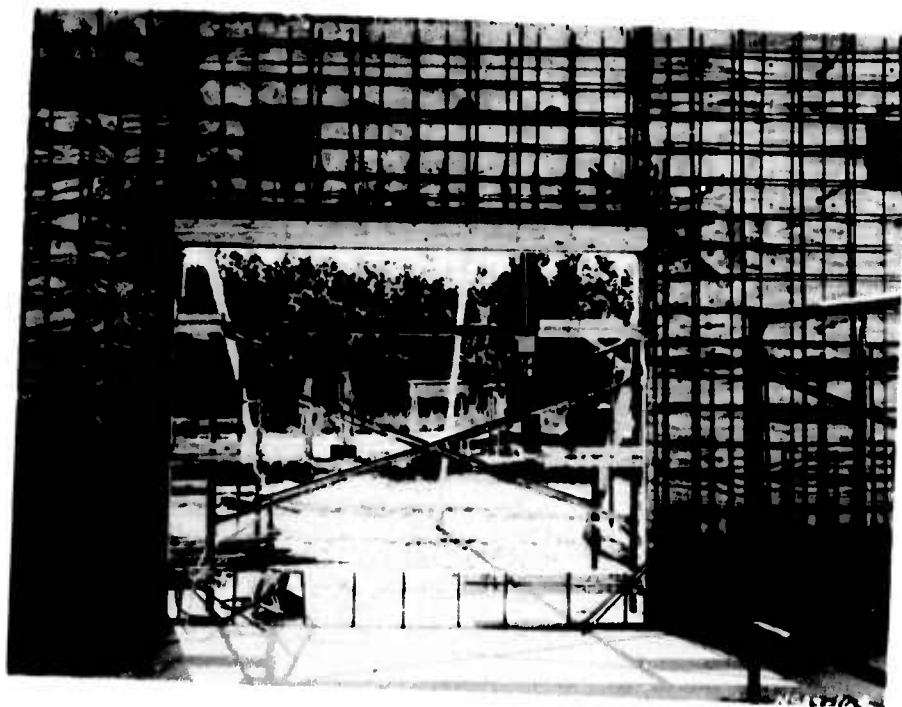
b. Detail at air-lock opening.

Figure 3.16. Retaining wall reinforcing steel.

93
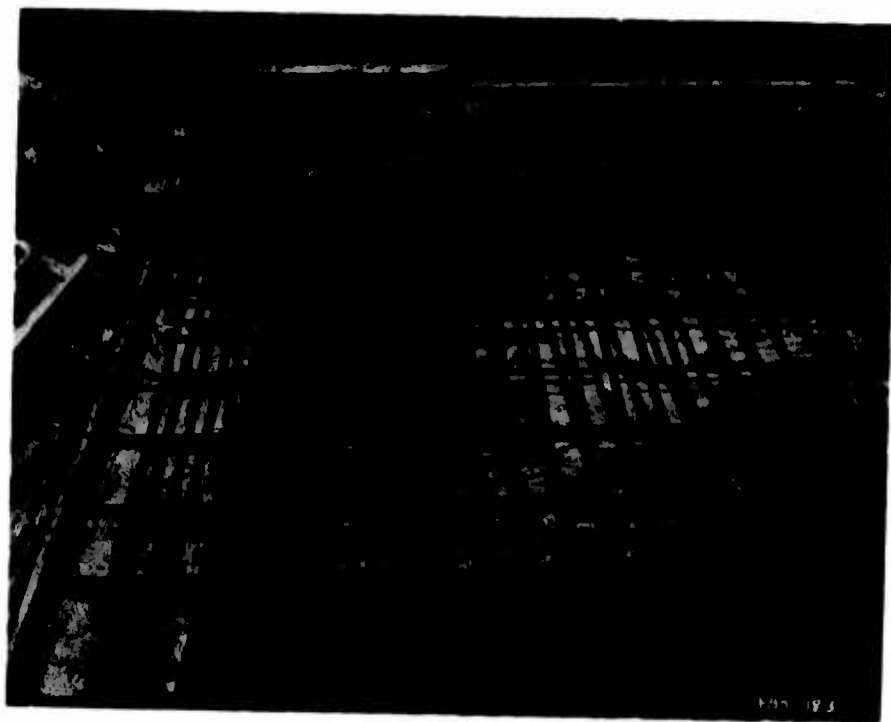
a. Overall view.

b. Detail at corner.

Figure 3.17. Bay roof reinforcing steel.

94

a. Overall view.

b. Detail at blast door bulkhead.

Figure 3.18. Air-lock floor reinforcing steel.
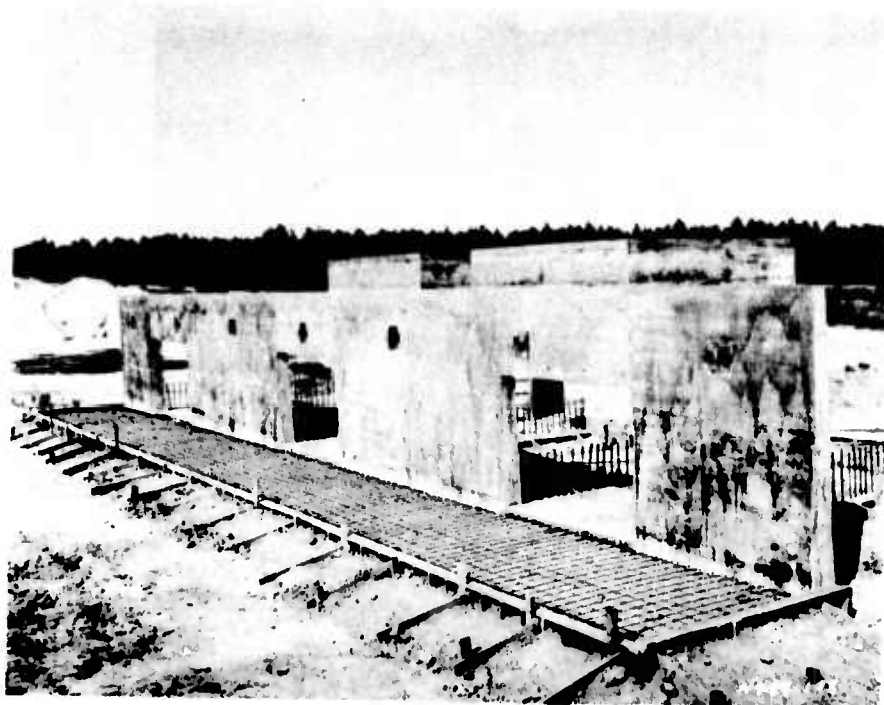
Figure 3.19. Ramp slab forms and reinforcing steel.
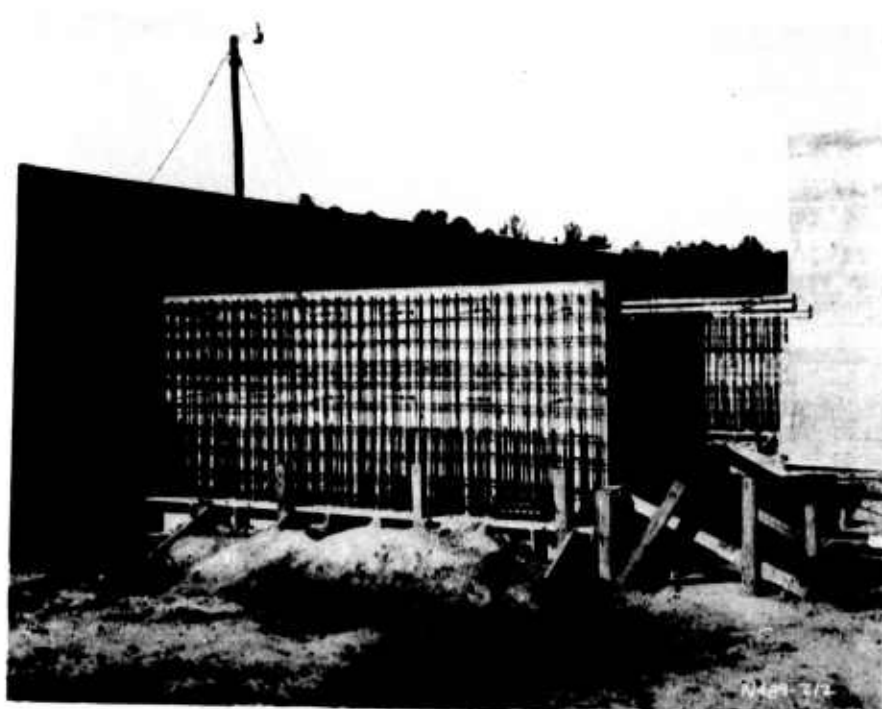
Figure 3.20. Air-lock wall reinforcing steel.
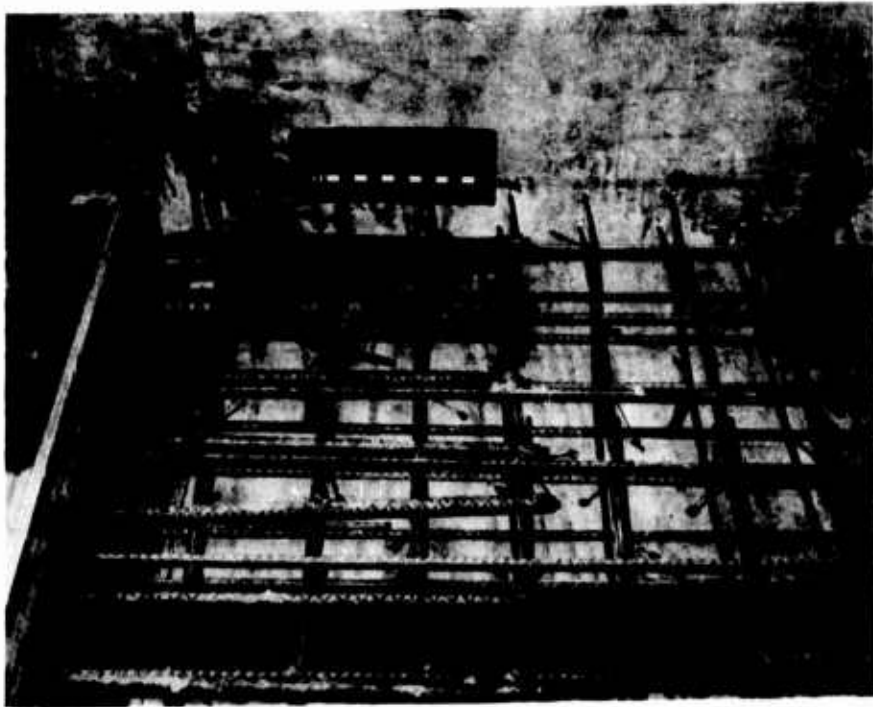
Figure 3.21. Air-lock roof steel reinforcement detail.
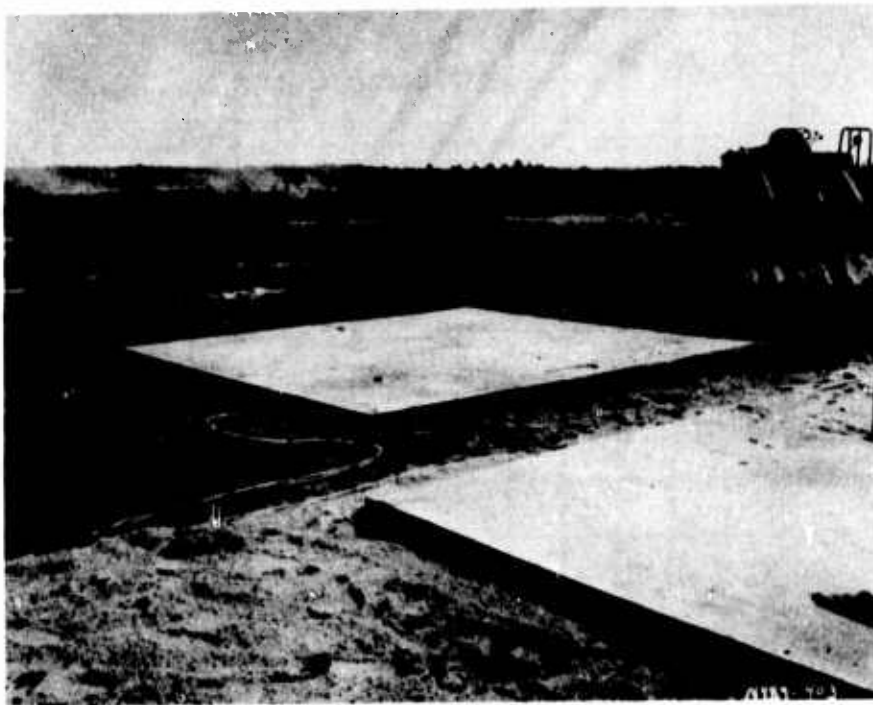
Figure 3.22. East simulated acceptor bay roof slab.

97
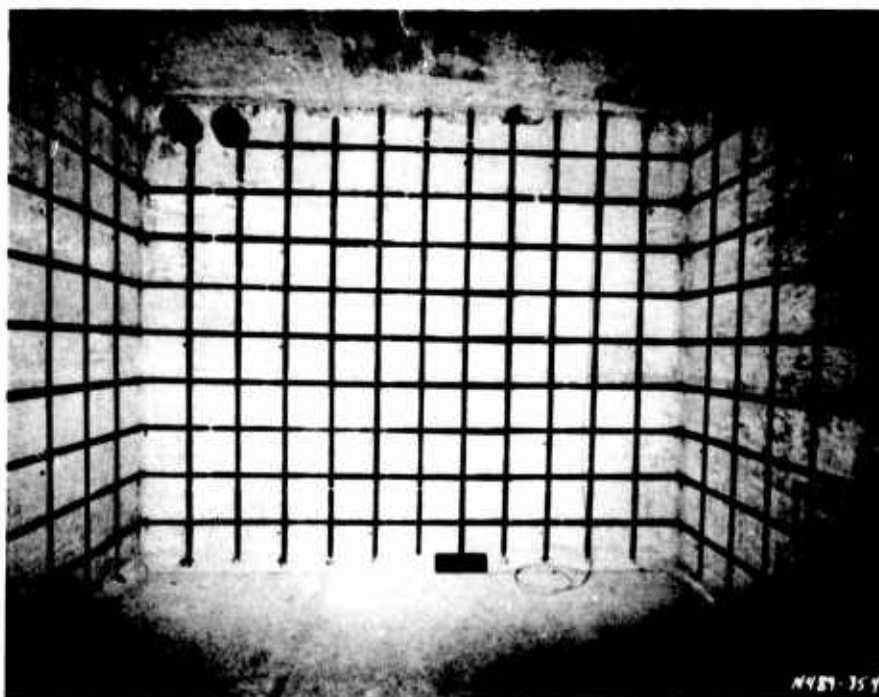
a. North wall.
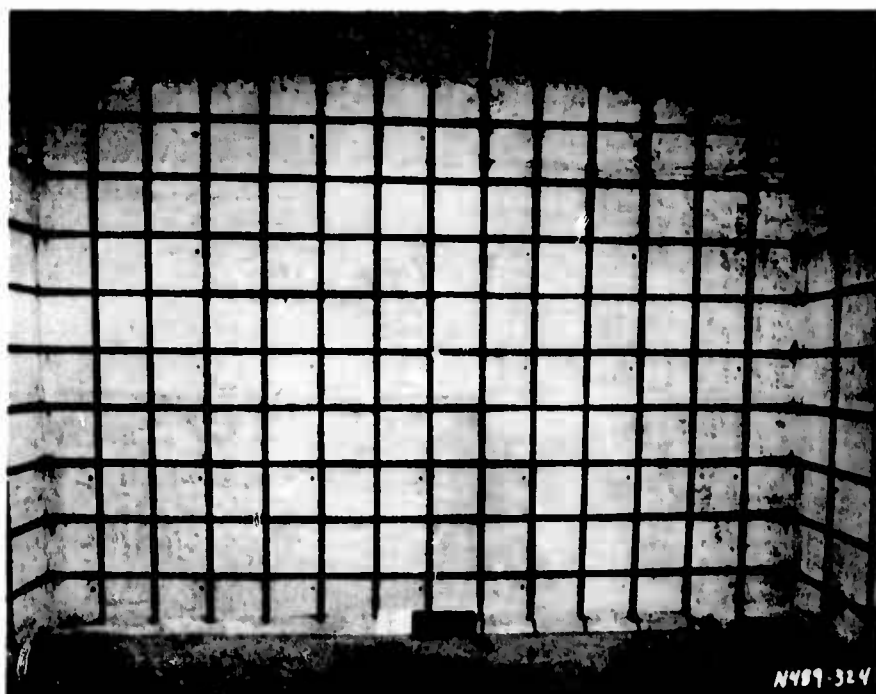
b. East wall.

Figure 3.23.   Interior view of completed donor bay
(Sheet 1 of 2).
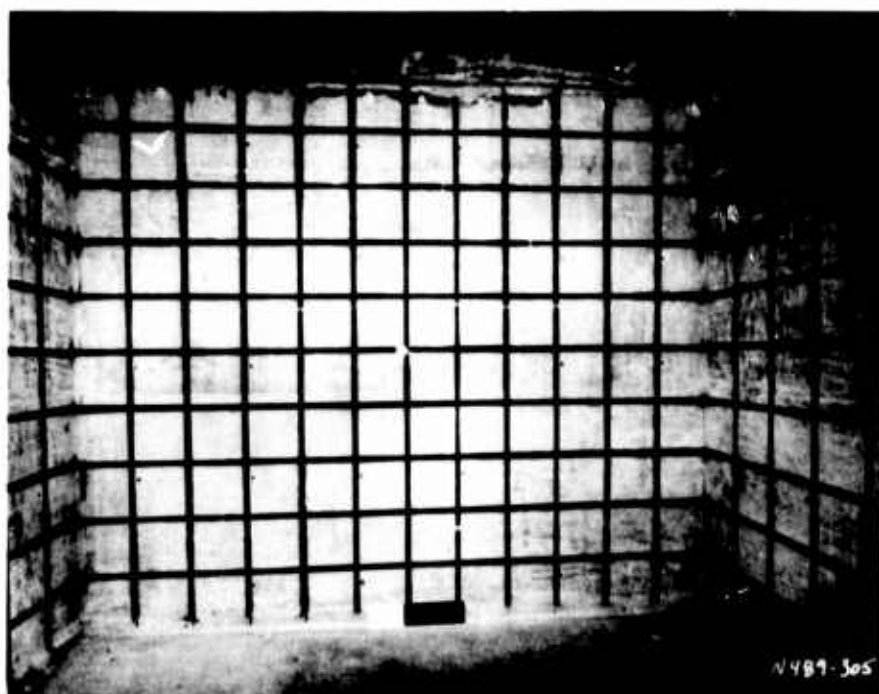
c. South wall.
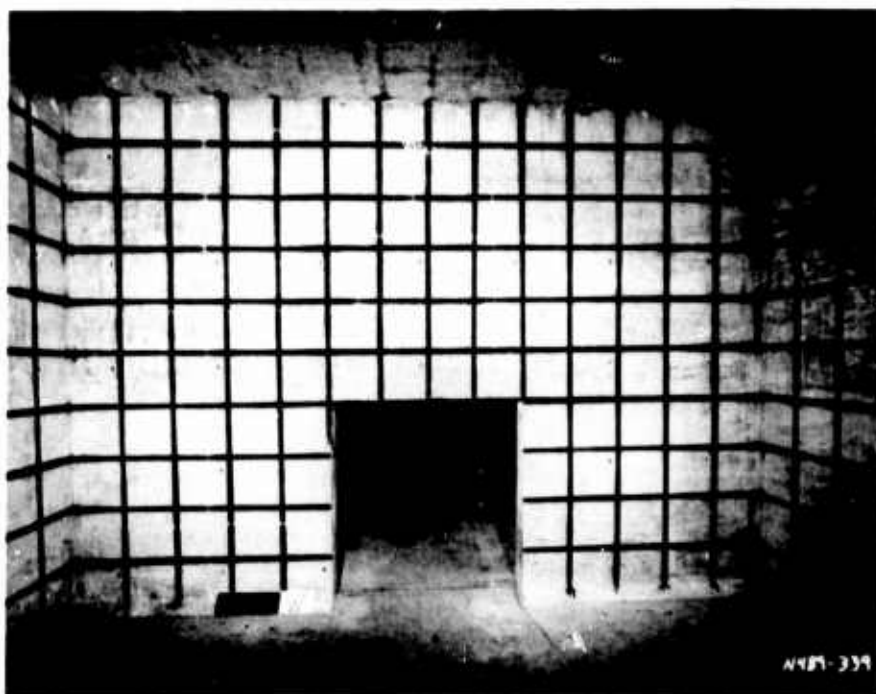
d. West wall.

Figure 3.23. (Sheet 2 of 2).

99

a. Placement of select sand between bays.

b. Native soil placed around bays.

Figure 3.24. Embankment construction.

Figure 3.25.   Sand layer over bays and air locks.

Figure 3.26.   Completed blast doors and frame.

Figure 3.27.   Internal construction of inactive
blast door leaf.
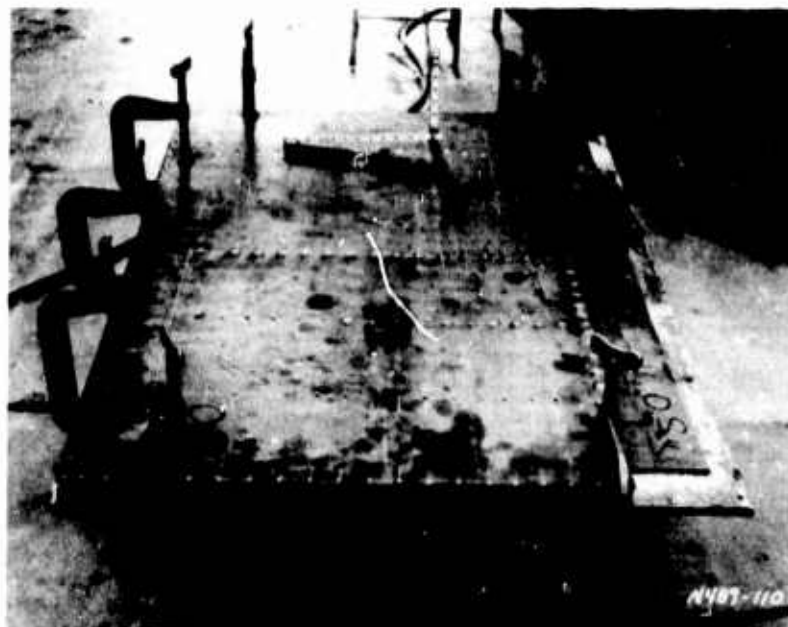
Figure 3.28.   Plug welds in blast door outer plate.
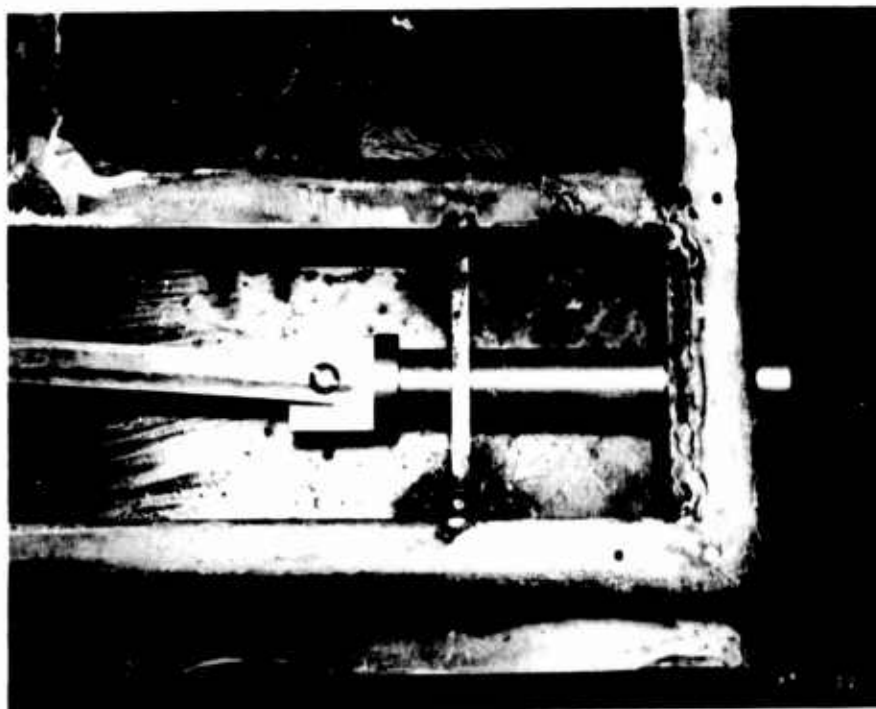
Figure 3.29.   Exposed view of inactive door leaf
locking pin.

103
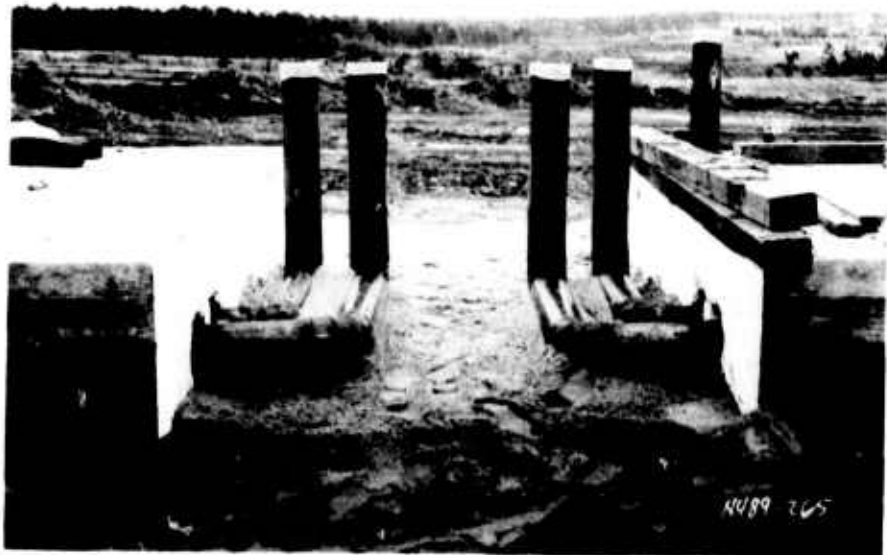
a. Installed ductwork.
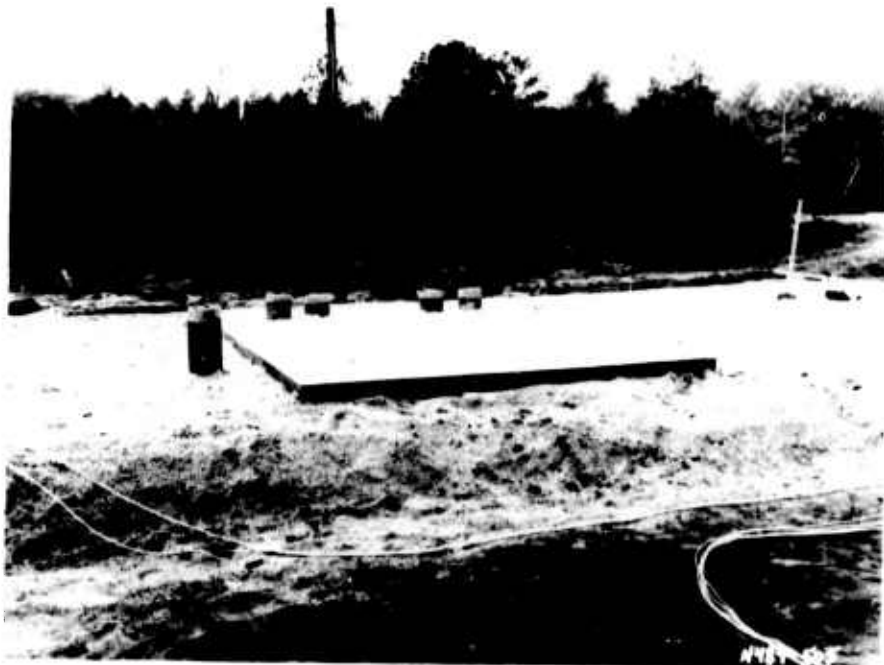
b. Completed penthouse slab.

Figure 3.30. Modeling of HVAC system.

104

a. View facing southeast.

b. View facing north.

Figure 3.31. Completed Phase II structure (Sheet 1 of 2).

105
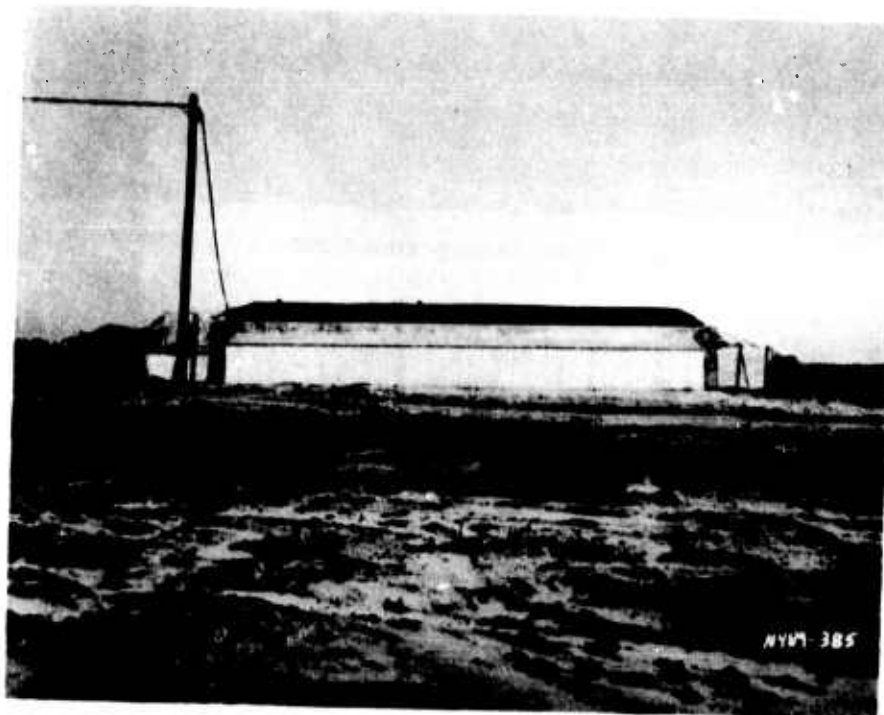
c. View facing east.

Figure 3.31. (Sheet 2 of 2).
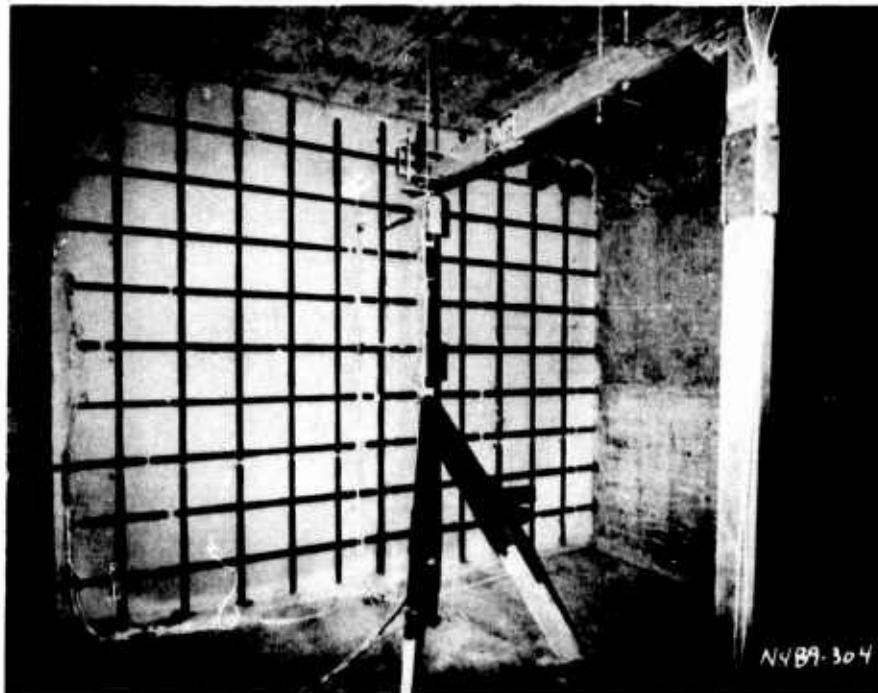
a.   South wall.
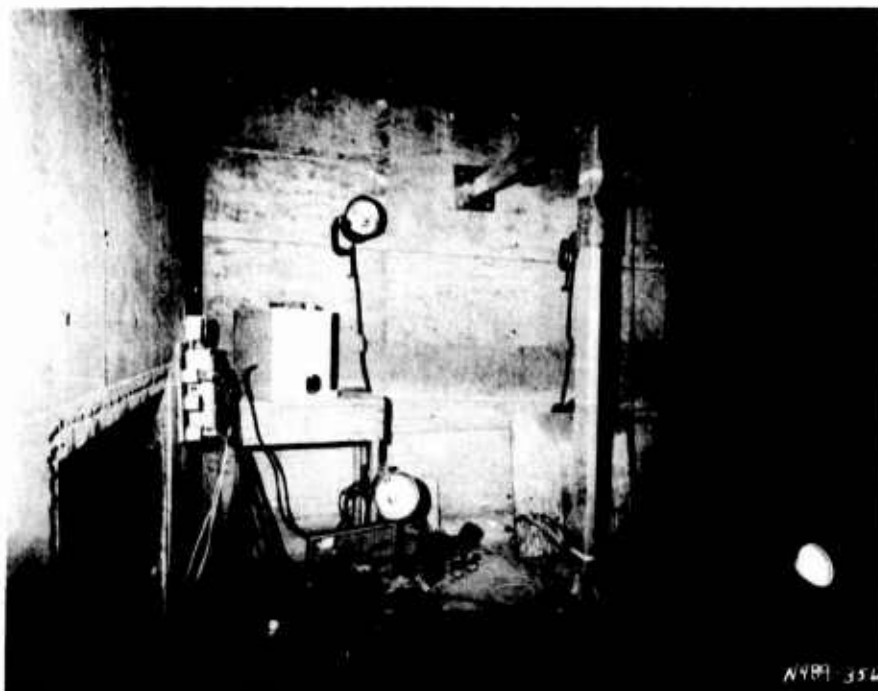
b.   North wall.

Figure 3.32.   Interior of acceptor bay.
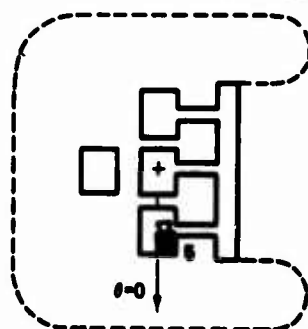
Figure 3.33.   Movie camera locations.
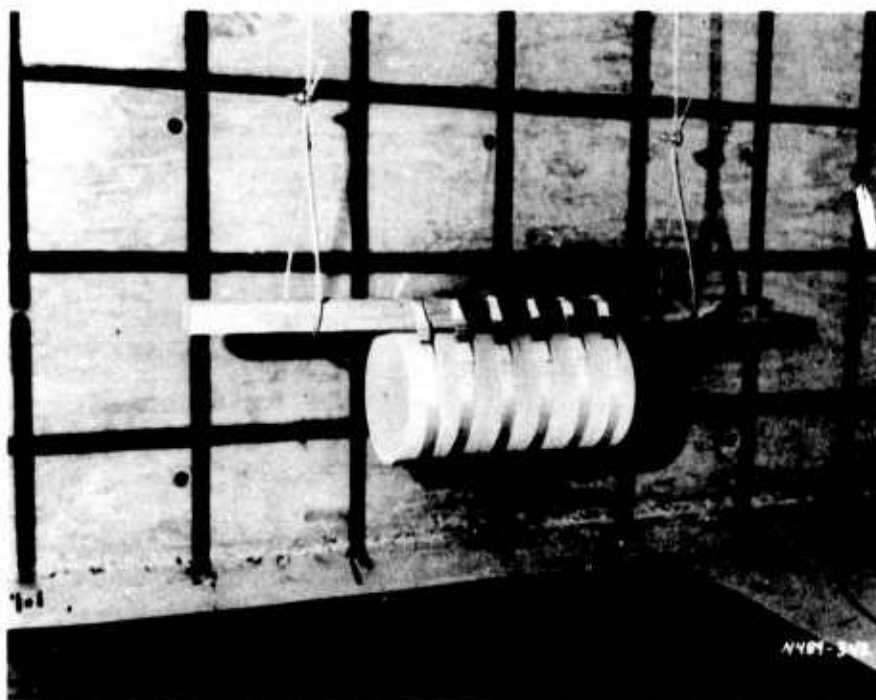
Figure 3.34.   Explosive charge in donor bay.

CHAPTER 4

PHASE I TEST RESULTS

4.1 STRUCTURAL VIBRATION TESTS

The four lowest resonant frequencies and associated modal damping ratios for the donor and acceptor bays are listed in Table 4.1. Typical transfer functions obtained during testing are shown in Appendix D. Test data were processed on a Hewlett-Packard 5423A structural dynamics analyzer. Frequency and damping ratio values were obtained from individual transfer function records and were averaged to obtain the values shown in Table 4.1.

4.2 ELECTRONIC DATA MEASUREMENTS

Data obtained from electronic transducers are displayed in Appendix E. The heading on each data graph in the appendix includes the test name, gage number, digitizing sampling rate, and calibration value. If the record was filtered, the type of filter and frequency response after filtering are included as an additional line. The amplitude response of the LP4 filter used on some of the records is shown in Figure 4.1.

The data record for gage IP4 indicated that the gage was not performing properly during the test and the record was omitted. Transducers BP2, BP3, BP4, and BP6 became inoperative during the test due to gage or instrument cable damage. Records from these instruments were truncated to the time of failure. The damaged transducers and cables shorted their excitation current to "ground," producing a phenomenon known as crosstalk. The noise spikes seen on many of the data records can be attributed to this source. Table 4.2 lists the peak values of pressures and displacements recorded during the event.

The permanent posttest deflections at gage positions D1 and D2 were lost because one of the beams supporting the acceptor bay north wall was sheared from its bearing seats and fell on the D1 and D2 deflection gage mount and gages. Gage D3 recorded a maximum deflection of 3.29 in. and a posttest deflection of 2.61 in. Posttest hand measurements showed a 3.63-in. permanent displacement. This measurement tends to confirm the peak value recorded by gage D3. The sensing element of the gage was attached by a 12-ft-long steel rod to a 4-in. by 6-ft angle embedded in the soil backfill of the bay as an anchor. Thus, the gage measured bay displacement relative to this anchor.

109

During the initial movement of the acceptor bay the anchor did not move and the gage recorded displacement relative to the anchor's "stationary" position. However, as the effects of the event propagated through the soil, this anchor was also permanently displaced. Test personnel believed that the discrepancy in measured and electronically recorded posttest displacements reflects the permanent displacement of the sensing probe anchor.

4.3 POSTTEST INSPECTION OF DONOR BAY

An overall view of the donor bay immediately after the test is shown in Figure 4.2. The roof disengaged and completely separated from the bay leaving only a few No. 5 bars which had pulled out of the roof slab. The roof slab broke into two major fragments which impacted to the east and west of the donor bay. The north wall completely separated from the floor and the east and west walls and fell back onto the bay floor. The east wall was displaced and rotated away from the center of the bay, and the corrugated entrance pipe was destroyed. The south and west walls suffered much less severe damage. Post-test donor bay relative displacements were measured between the east and west walls and are listed in Table 4.3.

4.3.1 Roof Damage and Fragment Distribution

The roof slab broke into two major fragments, approximately 9 by 31 ft in plan, which impacted 104 ft to the east and 102 ft to the west of the bay (Figure 4.3). Analysis of high-speed photography from camera station 1 revealed that the major roof fragment on the west side of the bay achieved a terminal velocity of 52 fps. The two major roof slab fragments are shown in Figures 4.4 and 4.5. The concrete covering the rebar splices at the east and west edges was spalled away from the bars. These secondary fragments were primarily distributed on the east and west backfill slopes, as shown in Figure 4.6.

Two other parts of the test structures produced fragments: the concrete slab covering the entrance pipe, and the HVAC slab. The concrete slab covering the entrance was fragmented by the explosion and produced fragments with a typical size of 8 by 4 by 3 in. Fragments from the slab were measured as far as 365 ft east of the structure. Other fragments were observed at distances up to 1200 ft but were not mapped since the slab was used to represent door mass, not to provide accurate blast door fragment information. Approximately

110

one half of the HVAC slab was broken into fragments. Eleven pieces, weighing 50 lb and over, were thrown as far as 279 ft to the north of the structure.

Individual fragment locations and fragment grid areas are shown relative to the Phase I structures in Figure 4.7. The figure shows the locations of all fragments which impacted outside of the five grids (E, E', W, w, and W'). The fragment content within these areas was too dense to produce a legible map. Grids E, W, and w represent the east and west backfill slopes. Grids E' and W' were impact areas for the two major roof slab fragments.

Each of these grids was subdivided into 6-ft-square areas as shown in Figure 4.8. Grids E and W are shown in Figures 4.9 and 4.10 after the grids were subdivided and the styrofoam was removed. The fragments which fell outside of the five grids were grouped according to the four quadrants shown in Figure 4.8. Tables 4.4-4.8 show the fragment distribution by weight in the fragment grid areas E, E', W, W', and w. Table 4.9 shows the fragment distribution by weight of the quadrants not included in grids. Table 4.10 itemizes all fragments weighing over 100 lb. All weights were calculated using a unit weight of 150 pcf.

4.3.2 North Wall Damage

Figure 4.11a shows the north wall shortly after the test event. The wall was excavated to remove the sand backfill which fell back into the bay. Figure 4.11b shows the exterior face of the north wall. The collapse of the wall left all No. 8 dowel bars joining the floor to the wall intact. The wall broke away from the floor slab as shown in Figure 4.11c. The portion of the wall left standing on either side of the center of the wall was 36 in. high and was broken flush with the top of the floor dowels. The wall's inside face vertical No. 8 rebar merely pulled away from the dowels without apparent deformation. Of the outside face vertical No. 4 rebar, 9 bars pulled out and 11 were broken. The center of the wall adjacent to the charge location was crushed and spalled. The distance from the top of the wall to the spalled and crushed area was 14 ft 10 in.

On the northwest edge, the wall opened up at the corner but it broke away approximately 2 ft from the edge leaving a section of the wall attached to the west wall (Figure 4.11e). At the separation point, all of the inside face steel rebars spalled their concrete cover and pulled away. All of the No. 4 rebars in the outer face horizontal direction failed in tension. Four No. 4

111

vertical bars were left embedded in the section of the wall still attached to
the west wall. At the corner between the north and west walls, the No. 4 bars
on the inside face of the north wall were failed but the No. 5 horizontal bars
which had been bent around the corner from the west wall were largely intact.

The northeast edge of the north wall separated from the east wall at the
corner as shown in Figure 4.11f. One No. 4 vertical rebar from the outside
face mat was left embedded at the east wall. The outside face No. 4 horizontal
rebar pulled out at the corner with minimal damage while all of the inside face
No. 4 horizontal bars were broken. The corner reinforcement details included
No. 5 horizontal steel from the east wall bent 90 deg around the corners into
the north wall (see Figure 2.13). On the outside face, 3 No. 5 bars were
broken and 13 pulled out of the north wall. On the inside face 4 No. 5's were
broken and 10 pulled out.

4.3.3 East Wall Damage

A pictorial view of the east wall is shown in Figure 4.12. Damage to the
wall is identified in Figure 4.13. The top of the wall was rotated away from
the center of the bay producing posttest angular displacements ranging from
5.4 deg at the north side to 11.1 deg at the base of the south side. This
rotation is evident in Figure 4.12a and caused the inner face reinforcing
steel mat to separate from the floor dowels as shown in Figure 4.12b. The
inward displacement of the No. 9 vertical rebar was 8.75 in. where the photo-
graph in the figure was taken. The concrete covering these bars was separated
from the wall to an elevation of approximately 8.5 ft from the floor. One
major vertical crack ran from near the crest of the entrance pipe to the top
of the wall.

The disengagement of the roof rotated the No. 10 roof dowels approximately
59 to 67 deg, leaving 53 dowels in place with 5 broken and 1 pulled out of the
corner. Six of the No. 5 dowels remained attached to the wall while all others
pulled out of the concrete.

4.3.4 South Wall Damage

The posttest condition of the south wall is shown in Figure 4.14 and dam-
age is detailed in Figure 4.15. The wall suffered significant damage at the
edges, but the remainder of the wall remained in relatively good condition.
Other than the edges, cracking was limited to one vertical hairline crack near

112

the center of the wall. The outward rotation of the wall was 1.3 deg measured near the center.

Details of the failure at the southeast corner of the wall are shown in Figure 4.14b, c, and d. Near the base slab, the east and south walls were separated only at the corner, but the damaged area widened from the base to the top. From the base to elevation 3 ft there was evidence of rebar yielding but no failures. Between elevations 3 and 8 ft, virtually all of the No. 4 inside face bars were failed in tension. The No. 5 bars from the east wall were deformed but only a few were broken. It was not possible to examine the condition of the outer face steel at the lower elevations. From elevation 8 ft to the top, both vertical and horizontal inner face steel pulled away from the corner without apparent damage. The concrete at the edge of the south wall was crushed above the 8-ft grid line. The No. 4 horizontal bars in the outer face reinforcement failed in tension approximately 2 ft 3 in. from the corner of the wall. The No. 5 horizontal reinforcement from the east wall was bent but none appeared to have been broken.

The corner separation at the southwest corner is shown in Figure 4.14e and f. All of the observed steel failures occurred at the corner. The south wall was cracked approximately 2 ft 8 in. from the edge but the concrete within this region was not crushed as it was on the opposite edge. The No. 4 inside face horizontal steel failed from elevation 5 ft to the top. The No. 5 inside face horizontal steel from the west wall was failed from elevation 16 ft to the top. The outer face horizontal No. 4 steel pulled out of the corner with minimal deformation. The No. 5 outer face horizontal bars bent but did not fail. The corner displacement at the top of the wall was 5.75 in.

4.3.5 West Wall Damage

The posttest condition of the west wall is shown in Figure 4.16. Damage to the wall is shown in Figure 4.17. The wall suffered two vertical cracks near the center line of the wall and was rotated outward 1.9 deg. Reinforcing steel was left exposed at the north portion of the wall at the bottom adjacent to the explosive charge location as shown in Figure 4.16b. All but six of the No. 5 roof dowels pulled out of the wall, and the No. 10 roof dowels were bent back in a manner analogous to those on the east wall. Fifty-seven No. 10 dowels remained in the wall, two were broken, and one pulled out of the wall at the north edge.

113

4.4 POSTTEST INSPECTION OF ACCEPTOR BAY

The acceptor bay suffered minor wall cracking and sustained a rigid body motion as a result of the test. Figure 4.18a shows a posttest view of the south wall. The largest crack in the wall was approximately 0.04 in. wide and was located 13 ft from the east wall and 11.5 ft from the floor (Figure 4.18b). The crack pattern for the entire wall is shown in Figure 4.19. With the exception of the area in the four grid squares near the center of the wall, the cracks were of hairline width. An overall view of the wall after excavation is shown in Figure 4.20. The cracks in the wall have been highlighted with a felt-tip pen for clarity.

Permanent displacements of the wall are listed in Table 4.11. The deflections correspond to locations of the grid intersections shown in Figures 4.19 and 4.20. A contour plot of these data is included as Figure 4.21. The acceptor bay sustained a permanent displacement of 3.63 in. away from the donor bay and 0.7-deg rotation.

During the test, one of the beams supporting the north wall sheared its welds to the beam seats and fell down the face of the wall, destroying deflection gages D1 and D2 and damaging a high-speed camera. The beam beneath it broke loose from one seat and came to rest on an aluminum ladder left in the bay. The other two high-speed cameras in the bay were attached to this beam and were displaced during the test. Figure 4.22 shows the condition of the acceptor bay north wall after the event.

Table 4.1. Lowest resonant frequencies and damping ratios
of Phase I donor and acceptor bays.

| | Before Backfill | | After Backfill | |
Bay	Frequency Hz	Damping Ratio % of Critical	Frequency Hz	Damping Ratio % of Critical
Donor	48.15	2.25	61.38	8.99
	53.55	3.43	79.63	5.37
	82.83	3.20	102.06	5.75
	109.24	4.46	123.71	9.22
Acceptor	48.46	3.40	66.50	7.76
	63.39	3.33	83.08	6.65
	82.46	2.98	100.55	3.81
	99.64	2.32	114.26	6.31

Table 4.2. Phase I peak electronic transducer measurements.

a. Peak pressures and impulses.

Transducer	Location	Maximum Pressure psi	Time of Maximum msec	Maximum Impulse psi × sec	Time of Maximum msec
BP-1	Center of donor bay floor	2323.4	0.74	7.969	129.33
BP-2	North donor bay wall	979	0.65	1.678*	18.3*
BP-3	East donor bay wall	724.8	0.97	3.534*	62.45*
BP-4	South donor bay wall	794.7	3.84	5.065*	79.30*
BP-5	West donor bay wall	571.3	3.28	7.289	150.99
BP-6	East end of entrance	432	11.29	0.644	18.0*
BP-7	Surface, west of bay	1.9	28.24	0.0314	172.73
BP-8	Surface, south of bay	2.2	29.44	0.0636	115.42
BP-9	Acceptor bay HVAC duct	2.2	31.4	0.0492	179.8
SS-1	Mid-distance between bays	36.35	26.68	2.338	204.8
SS-2	Mid-distance between bays	117.45	23.72	6.583	194.2
SS-3	Mid-distance between bays	94.50	26.46	5.036	196.9
SS-4	Mid-distance between bays	72.59	26.82	4.571	193.9
IP-1	East edge, acceptor bay wall	27.09	108.57	3.021	305.8
IP-2	East edge, acceptor bay wall	36.97	108.56	4.755	345.8
IP-3	East edge, acceptor bay wall	15.82	97.18	1.962	293.4
IP-4	Center, acceptor bay wall	--	--	--	--
IP-5	Center, acceptor bay wall	71.33	84.89	8.285	326.2
IP-6	Center, acceptor bay wall	43.45	94.63	5.477	314.7
IP-7	Quarter point, acceptor bay wall	51.77	108.57	5.908	292.9
IP-8	Quarter point, acceptor bay wall	51.39	88.50	5.873	276.8
IP-9	Quarter point, acceptor bay wall	32.62	98.68	4.124	262.1

b. Peak deflections.

Transducer	Location	Maximum Deflection in.	Time of Maximum msec
D-1	Quarter point, acceptor bay wall	1.00	130.06
D-2	Midpoint, acceptor bay wall	2.02	126.99
D-3	Acceptor bay floor	3.28	177.90

* Peak impulse occurred after transducer became inoperative.

Table 4.3. Phase I posttest donor bay displacements between east and west walls.

Location	Elevation ft	Displacement ft
North end	10.0	1.75
	19.6	2.38
Center	10.0	2.08
	19.6	2.71
South end	10.0	0.75
	19.6	2.83

Table 4.4. Fragment distribution by weight* in fragment area E.

Location	1-25 lb	26-50 lb	51-75 lb	76-100 lb	Over 100 lb
E(1,1)	--	--	--	--	--
E(1,2)	3	--	--	--	--
E(1,3)	5	2	--	--	--
E(1,4)	14	1	--	--	5
E(1,5)	1	--	--		1
E(1,6)	1				1
E(2,1)	6	--	--	--	
E(2,2)	16	3	1	--	
E(2,3)	15				
E(2,4)	14	2	1	1	2
E(2,5)	5				1
E(2,6)	2	--			
E(3,1)	3				
E(3,2)	18	2			1
E(3,3)	22	2			1
E(3,4)	8	3		3	
E(3,5)	3		5		2
E(3,6)	3				
E(4,1)	8	2			
E(4,2)	21	7	2	1	
E(4,3)	18	2	1	1	1
E(4,4)	2				1
E(4,5)	5	1	1		2
E(4,6)					1
E(5,1)	20	4			
E(5,2)	9	1	1		
E(5,3)	6	1			
E(5,4)	2				1
E(5,5)	2	1	1		
E(5,6)	1				
E(6,1)	6	--	--	--	--
E(6,2)	6	1	--	--	--
E(6,3)	14	--	--	--	--
E(6,4)	2	--	--	--	--
E(6,5)	--	--	--	--	--
E(6,6)	--	--	--	--	--
E(7,1)	2	--	--	--	--
E(7,2)	--	--	--	--	--
E(7,3)	1	--	--	--	--
E(7,4)	1	--	--	--	--
E(7,5)	--	--	--	--	--
E(7,6)	--	--	--	--	--

* Weights calculated using 150 pcf.

Table 4.5. Fragment distribution by weight* in fragment area E'.

Location	1-25 lb	26-50 lb	51-75 lb	76-100 lb	Over 100 lb
	* Number of Fragments				
E'(1,1)	--	--	--	--	--
E'(1,2)	6	--	--	--	--
E'(1,3)	3	--	--	--	--
E'(1,4)	--	--	--	--	--
E'(1,5)	--	--	--	--	--
E'(1,6)	--	--	--	--	--
E'(1,7)	--	--	--	--	--
E'(2,1)	--	--	--	--	--
E'(2,2)	Contained major roof slab fragment weighing ~46,000 lb				
E'(2,3)					
E'(2,4)					
E'(2,6)					
E'(3,2)					
E'(3,3)					
E'(3,4)					
E'(3,5)					
E'(3,6)					
E'(2,7)	--	--	--	--	--
E'(3,1)	4	1	--	--	1
E'(3,7)	1	--	--	--	--
E'(4,1)	4	--	--	--	--
E'(4,2)	30	3	1	--	3
E'(4,3)	14	--	--	--	1
E'(4,4)	14	1	--	--	--
E'(4,5)	--	--	--	--	--
E'(4,6)	1	--	--	--	--
E'(4,7)	1	--	--	--	--
E'(5,1)	1	1	--	--	--
E'(5,2)	6	--	--	--	--
E'(5,3)	13	1	--	--	--
E'(5,4)	11	--	--	--	--
E'(5,5)	2	--	--	--	--
E'(5,6)	--	--	--	--	--
E'(5,7)	--	--	--	--	--
E'(6,1)	--	--	--	--	--
E'(6,2)	--	--	--	--	--
E'(6,3)	2	--	--	--	--
E'(6,4)	2	--	--	--	--
E'(6,5)	1	--	--	--	--
E'(6,6)	1	--	--	--	--
E'(6,7)	1	--	--	--	--

* Weights calculated using 150 pcf.

119

Table 4.6. Fragment distribution by weight* in fragment area W.

Location	Number of Fragments				
	1-25 lb	26-50 lb	51-75 lb	76-100 lb	Over 100 lb
W(1,1)	2	--	--	--	--
W(1,2)	2	--	--	--	--
W(1,3)	6	1	--	--	--
W(1,4)	10	--	--	1	--
W(1,5)	9	--	--	--	2
W(1,6)	20	--	--	--	2
W(1,7)	16	1	--	--	--
W(1,8)	15	--	--	--	--
W(1,9)	2	--	--	--	--
W(2,1)	--	--	--	--	--
W(2,2)	3	1	--	--	--
W(2,3)	2	--	1	--	--
W(2,4)	1	1	--	--	--
W(2,5)	10	2	--	--	1
W(2,6)	10	3	1	--	--
W(2,7)	20	--	--	--	2
W(2,8)	19	1	--	--	--
W(2,9)	--	1	--	--	1
W(3,1)	--	--	--	--	--
W(3,2)	2	--	--	--	--
W(3,3)	7	1	--	--	--
W(3,4)	1	--	--	--	--
W(3,5)	10	3	--	--	--
W(3,6)	6	--	--	--	--
W(3,7)	9	1	--	--	--
W(3,8)	18	1	--	--	--
W(3,9)	2	--	--	--	--
W(4,1)	2	--	--	--	--
W(4,2)	3	--	--	--	--
W(4,3)	6	1	--	--	--
W(4,4)	4	1	--	--	--
W(4,5)	14	3	--	--	1
W(4,6)	3	--	1	--	2
W(4,7)	16	--	--	--	--
W(4,8)	17	--	--	--	--
W(4,9)	7	--	--	--	1
W(5,1)	1	--	--	--	1
W(5,2)	2	--	--	--	--
W(5,3)	6	1	--	--	--
W(5,4)	3	1	--	--	--

(Continued)

* Weights calculated using 150 pcf.

(Sheet 1 of 3)

120

Table 4.6. (Continued)

Location	Number of Fragments				
	1-25 lb	26-50 lb	51-75 lb	76-100 lb	Over 100 lb
W(5,5)	5	--	--	--	--
W(5,6)	9	1	--	--	1
W(5,7)	12	2	1	--	--
W(5,8)	8	1	1	--	--
W(5,9)	1	--	--	--	--
W(6,1)	--	--	--	--	--
W(6,2)	1	--	--	--	--
W(6,3)	3	1	--	--	--
W(6,4)	4	2	--	--	--
W(6,5)	5	1	--	--	1
W(6,6)	30	--	--	--	1
W(6,7)	14	--	--	--	--
W(6,8)	10	--	--	--	--
W(6,9)	6	--	--	--	--
W(7,1)	--	--	--	--	--
W(7,2)	1	--	--	--	--
W(7,3)	6	--	--	--	--
W(7,4)	4	--	--	--	--
W(7,5)	22	2	--	--	--
W(7,6)	17	4	--	2	--
W(7,7)	7	--	--	--	--
W(7,8)	4	1	--	--	--
W(7,9)	2	1	--	--	--
W(8,1)	--	1	--	--	--
W(8,2)	2	--	--	1	--
W(8,3)	--	1	--	--	--
W(8,4)	5	--	--	--	--
W(8,5)	1	--	--	--	--
W(8,6)	13	2	--	--	--
W(8,7)	4	--	--	--	2
W(8,8)	12	--	--	--	--
W(8,9)	--	--	--	--	--
W(9,1)	--	1	--	--	--
W(9,2)	--	1	--	--	--
W(9,3)	5	--	--	--	--
W(9,4)	8	1	--	--	--
W(9,5)	6	1	--	--	--
W(9,6)	13	2	--	--	--
W(9,7)	1	--	--	--	--
W(9,8)	2	--	--	--	--

(Continued)

(Sheet 2 of 3)

Table 4.6. (Concluded).

Location	Number of Fragments				
	1-25 lb	26-50 lb	51-75 lb	76-100 lb	Over 100 lb
W(9,9)	--	--	--	--	1
W(10,1)	--	1	--	--	--
W(10,2)	--	1	--	--	--
W(10,3)	1	--	--	--	--
W(10,4)	1	1	--	1	--
W(10,5)	2	--	--	--	--
W(10,6)	--	--	--	--	--
W(10,7)	5	--	--	--	--
W(10,8)	4	--	--	--	1
W(10,9)	3	--	--	--	--
W(11,1)	--	--	--	--	--
W(11,2)	1	--	--	--	--
W(11,3)	1	--	--	--	--
W(11,4)	1	1	1	--	--
W(11,5)	--	--	--	--	--
W(11,6)	1	--	--	--	--
W(11,7)	2	--	--	--	--
W(11,8)	2	--	--	--	--
W(11,9)	1	1	1	--	--

Table 4.7. Fragment distribution by weight* in fragment area W'.

Location	Number of Fragments				
	1-25 lb	26-50 lb	51-75 lb	76-100 lb	Over 100 lb
W'(1,1)	1	--	--	--	--
W'(1,2)	3	--	--	--	--
W'(1,3)	5	--	--	--	1
W'(1,4)	13	1	1	--	--
W'(1,5)	14	7	2	--	--
W'(1,6)	9	1	--	--	--
W'(1,7)					
W'(2,3)					
W'(2,4)	Contained major roof slab fragment weighing ~46,000 lb				
W'(2,5)					
W'(2,6)					
W'(2,7)					
W'(3,3)					
W'(3,4)					
W'(3,5)					
W'(3,6)					
W'(3,7)					
W'(2,1)	2	1	--	--	--
W'(2,2)	6	--	--	--	--
W'(3,1)	4	--	--	--	--
W'(3,2)	36	4	1	3	4
W'(4,1)	15	--	--	--	--
W'(4,2)	19	--	--	--	1
W'(4,3)	36	--	--	--	--
W'(4,4)	30	--	--	--	1
W'(4,5)	21	2	--	--	--
W'(4,6)	3	--	--	--	--
W'(4,7)	1	--	--	--	--
W'(5,1)	6	--	--	--	--
W'(5,2)	26	--	--	--	--
W'(5,3)	41	--	--	--	--
W'(5,4)	23	1	--	--	--
W'(5,5)	9	1	--	--	--
W'(5,6)	1	--	--	--	--
W'(5,7)	2	--	--	--	--
W'(6,1)	6	--	1	--	--
W'(6,2)	24	--	--	--	--
W'(6,3)	14	--	--	--	--
W'(6,4)	7	1	--	--	--
W'(6,5)	4	--	--	--	--
W'(6,6)	--	--	--	--	--
W'(6,7)	2	--	--	--	--

* Weights calculated using 150 pcf.

Table 4.8. Fragment distribution by weight* in fragment area w.

Location	1-25 lb	26-50 lb	51-75 lb	76-100 lb	Over 100 lb
w(1,1)	--	--	1	--	1
w(1,2)	--	--	--	--	--
w(1,3)	5	1	--	--	--
w(1,4)	10	2	--	--	--
w(1,5)	6	4	--	--	--
w(2,1)	--	--	--	--	1
w(2,2)	--	--	--	--	--
w(2,3)	--	--	--	--	--
w(2,4)	16	1	--	--	1
w(2,5)	10	1	--	--	--
w(3,1)	--	--	1	--	1
w(3,2)	--	--	--	--	--
w(3,3)	--	--	--	--	--
w(3,4)	2	--	--	--	--
w(3,5)	1	--	--	--	--

(Header spanning: Number of Fragments)

* Weights calculated using 150 pcf.

Table 4.9. Fragment distribution by weight* in quadrants N, S, E, W (excluding previously mentioned fragment areas).

Location	1-25 lb	26-50 lb	51-75 lb	76-100 lb	Over 100 lb
Quadrant N	12	--	3	1	7
Quadrant S	20	1	--	--	--
Quadrant E	125	7	1	2	4
Quadrant W	73	5	--	1	9

(Header spanning: Number of Fragments)

* Weights calculated using 150 pcf.

Table 4.10. Calculated fragment weight* over 100 lb excluding
the two major roof slab fragments.

Location	Weight, lb
E(1,4)	102, 253, 260, 389, 469
E(1,5)	109
E(1,6)	450
E(2,4)	199, 223
E(2,5)	415
E(3,2)	256
E(3,3)	116
E(3,5)	354, 594
E(4,3)	117
E(4,4)	113
E(4,5)	191, 486
E(4,6)	150
E(5,4)	109
E'(3,1)	244
E'(4,2)	190, 496, 812
E'(4,3)	661
W(1,5)	160, 219
W(1,6)	139, 286
W(2,5)	113
W(2,7)	115, 262
W(2,9)	384
W(4,5)	188
W(4,6)	130, 269
W(4,9)	212
W(5,1)	138
W(5,6)	188
W(6,5)	194
W(6,6)	207
W(8,7)	150, 172
W(9,9)	227
W(10,8)	136
W'(1,3)	142
W'(3,2)	105, 126, 153, 422
W'(4,2)	152
W'(4,4)	198
w(1,1)	153
w(2,1)	306
w(2,4)	218
w(3,1)	143
Quadrant N	188, 281, 282, 292, 450, 525, 750
Quadrant E	115, 119, 212, 292
Quadrant W	122, 124, 172, 208, 210, 218, 225, 410, 646

* Weights calculated using 150 pcf.

Table 4.11. Acceptor bay wall posttest deformation.

Vertical Scale ft	Horizontal Scale, ft												
	0	2	4	6	8	10	12	14	16	18	20	22	24
20	0	0	0	0	0	0	0	0	0	0	0	0	0
18	0	0	2.08	3.13	4.17	3.13	2.08	2.08	0	0	0	0	0
16	0	2.08	4.17	5.21	4.17	2.08	2.08	2.08	1.04	0	2.08	2.08	0
14	0	5.21	3.65	3.13	5.21	3.13	4.17	4.17	3.13	2.08	0	0	0
12	0	4.17	3.65	3.13	4.17	4.17	4.17	4.17	3.13	2.08	1.04	1.04	0
10	0	2.08	2.08	4.17	3.65	3.65	3.13	3.13	2.08	2.08	2.08	0	0
8	0	1.04	2.08	3.13	3.65	2.60	3.13	3.13	1.04	0	0	0	0
6	0	1.04	1.04	2.08	3.13	3.13	3.13	4.17	4.69	4.17	3.13	3.13	0
4	0	0	1.56	1.04	2.08	2.08	2.60	1.04	1.04	1.04	0.52	0.52	0
2	0	0.52	0.52	0.52	0	0.52	0.52	0	0	0	0	0	0
0	0	0	0	0	0	0	0	0	0	0	0	0	0

Note: All deformations in hundredths of a foot (0.01 ft).

126
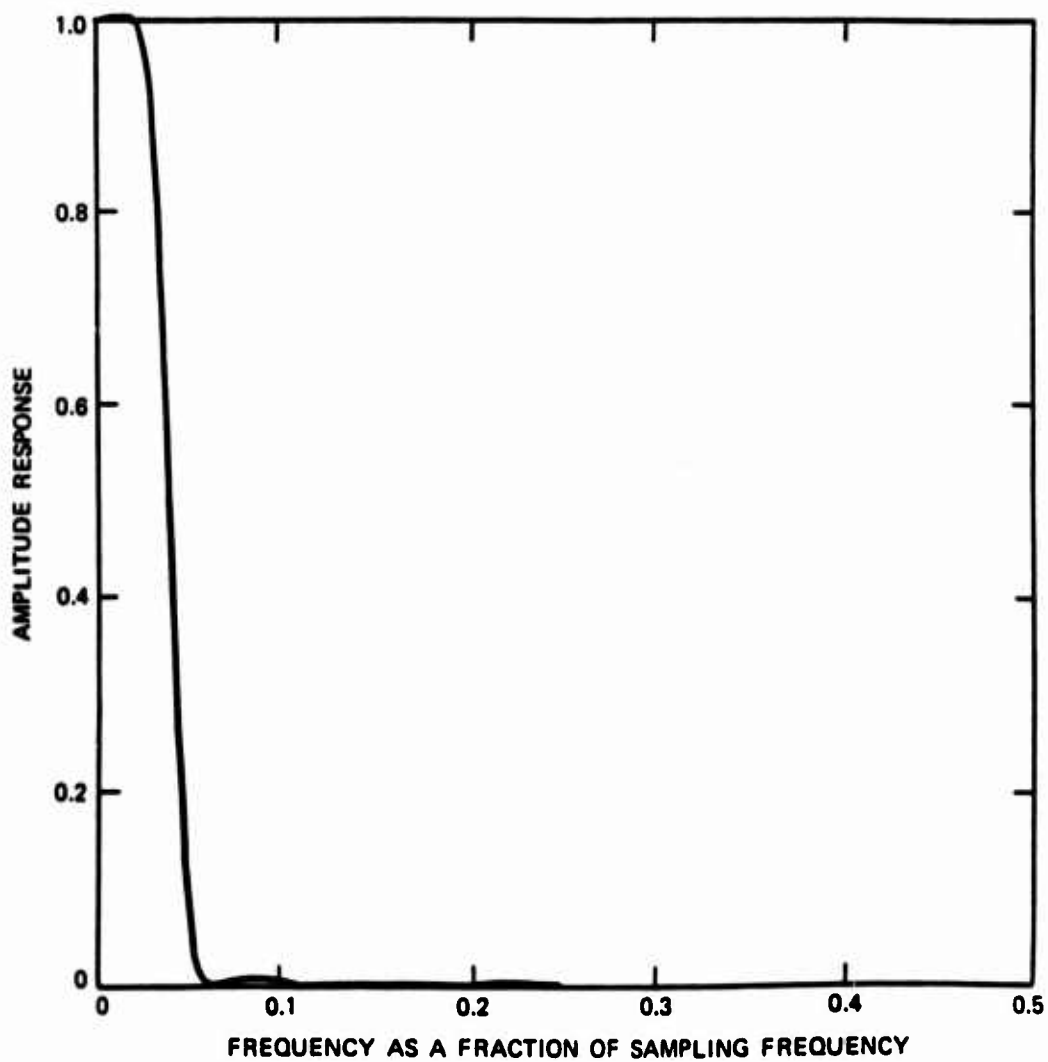
Figure 4.1.   Amplitude response of LP4 low-pass filter.

Figure 4.2. Posttest view of donor bay.

Figure 4.3. Posttest view of Phase I test site.

128
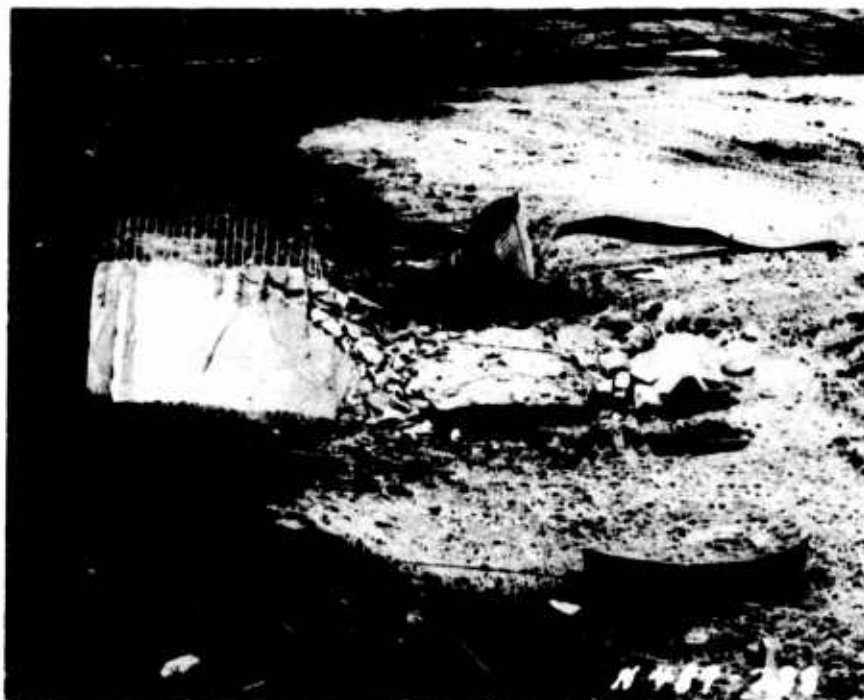
a. View facing east.

b. View facing northwest.

Figure 4.4. Major roof-slab fragment on east side of structure.

a. View facing west.

b. View facing north.

Figure 4.5. Major roof-slab fragment on west side of structure.

130
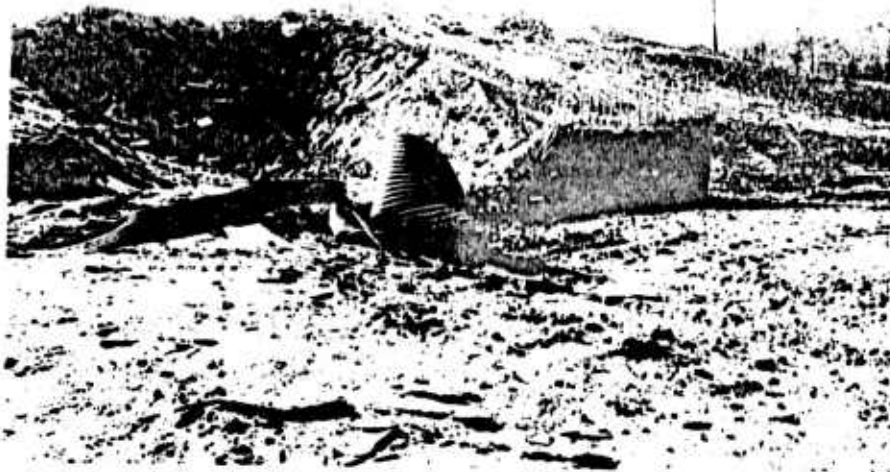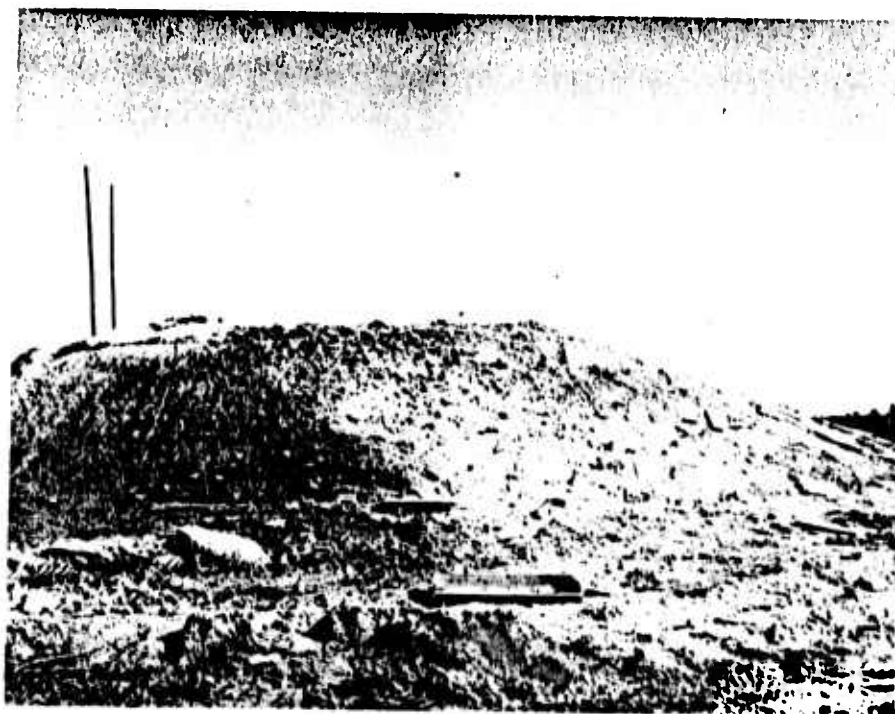
a. East slope.

b. West slope.

Figure 4.6. Posttest view of backfill slopes on Phase I structure.

131
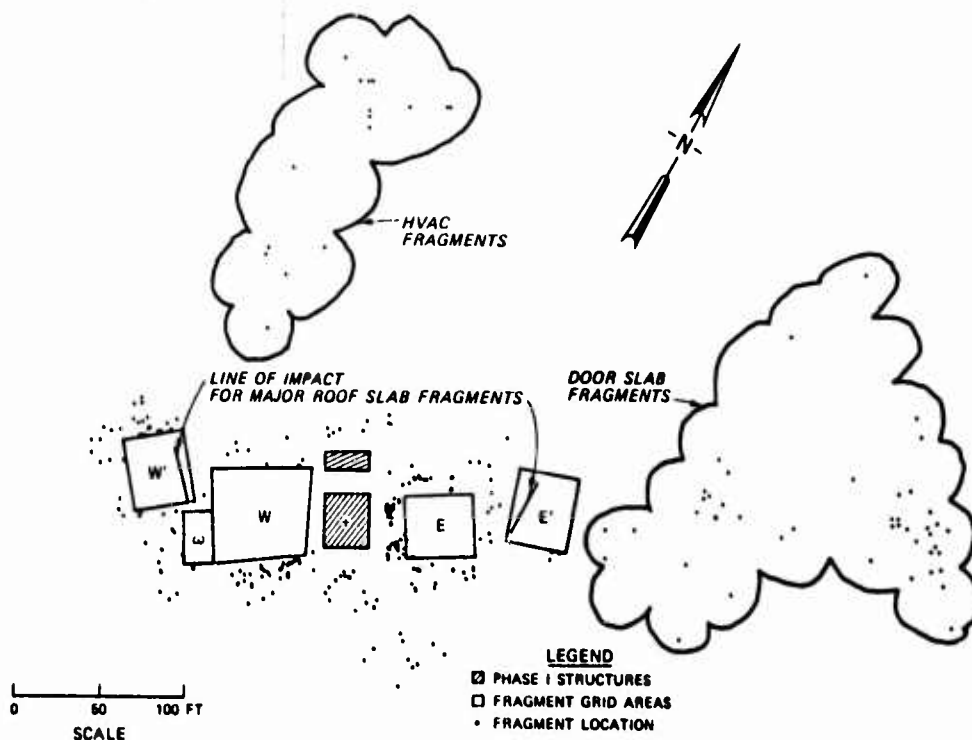
Figure 4.7. Individual fragments and grid areas relative to Phase I structures.
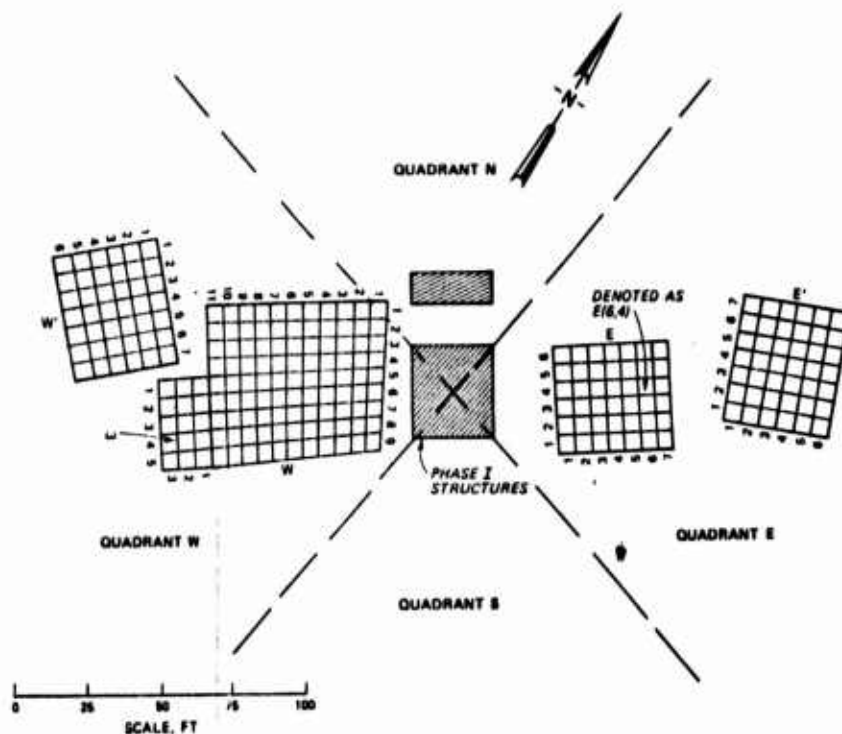
Figure 4.8. Fragment grid area and quadrant locations.

132

Figure 4.9.   East slope with E grid.

Figure 4.10.   West slope with W grid.

133
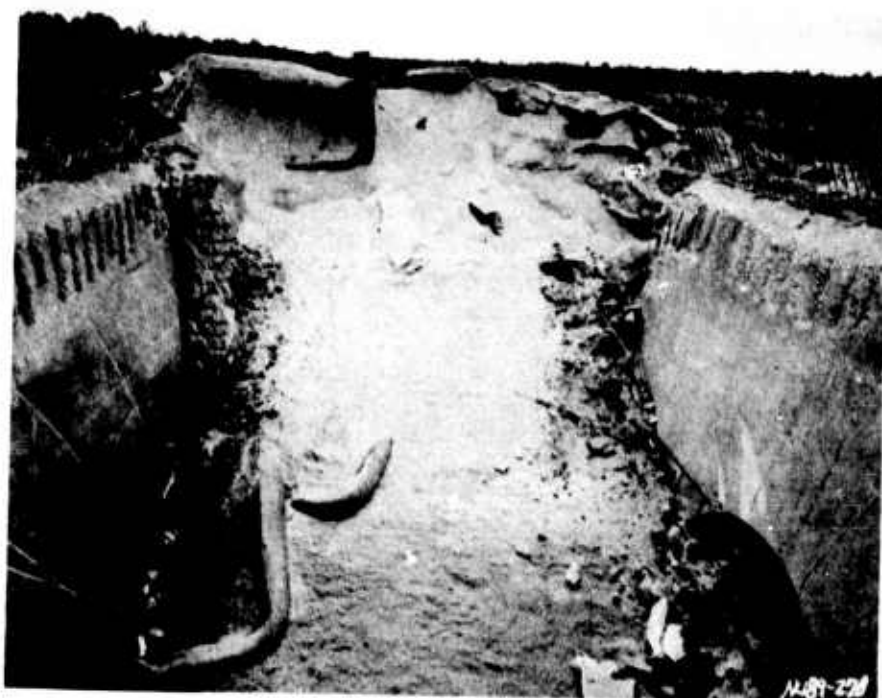
a.   Before excavation.
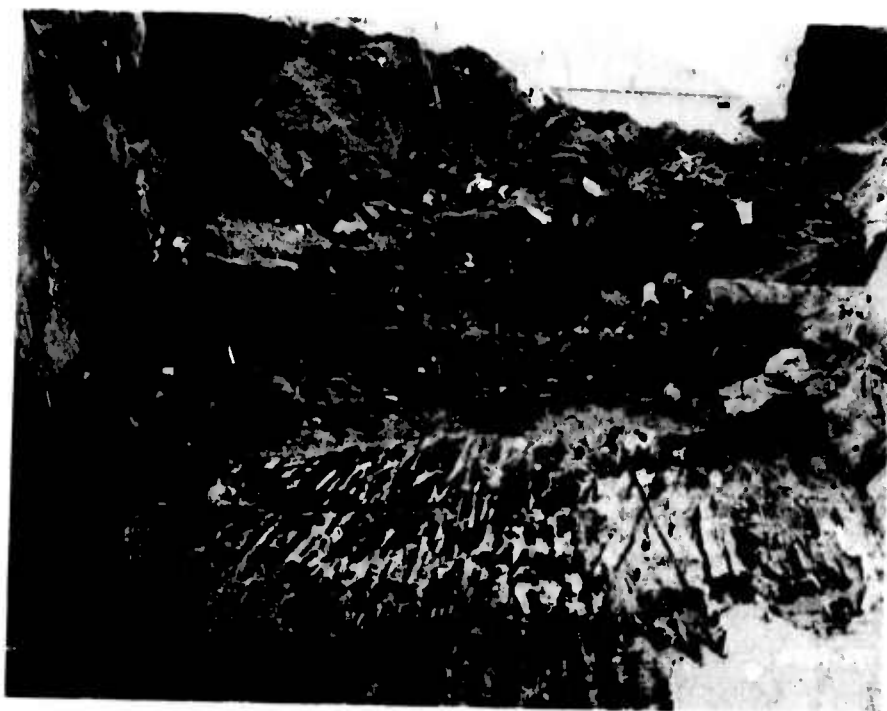
b.   North view after excavation.

Figure 4.11.   Posttest view of north donor bay wall
(Sheet 1 of 3).

134

c. South view after excavation.

d. West edge of wall.

Figure 4.11. (Sheet 2 of 3).

e. Northwest corner.

f. Northeast corner.

Figure 4.11. (Sheet 3 of 3).
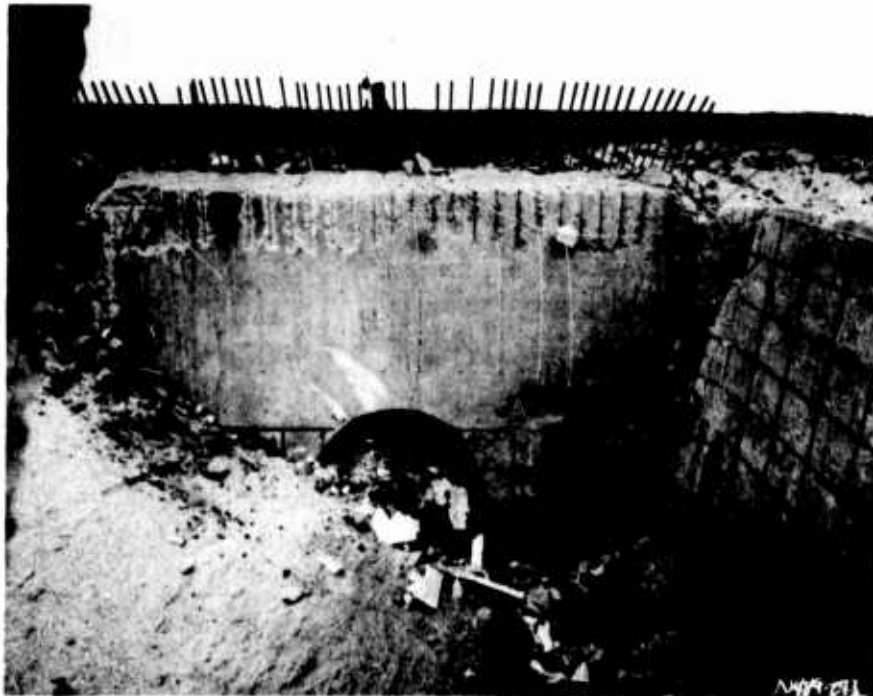
a. Overall view.

b. Reinforcement separation at base of wall.

Figure 4.12. Posttest view of east donor bay wall.
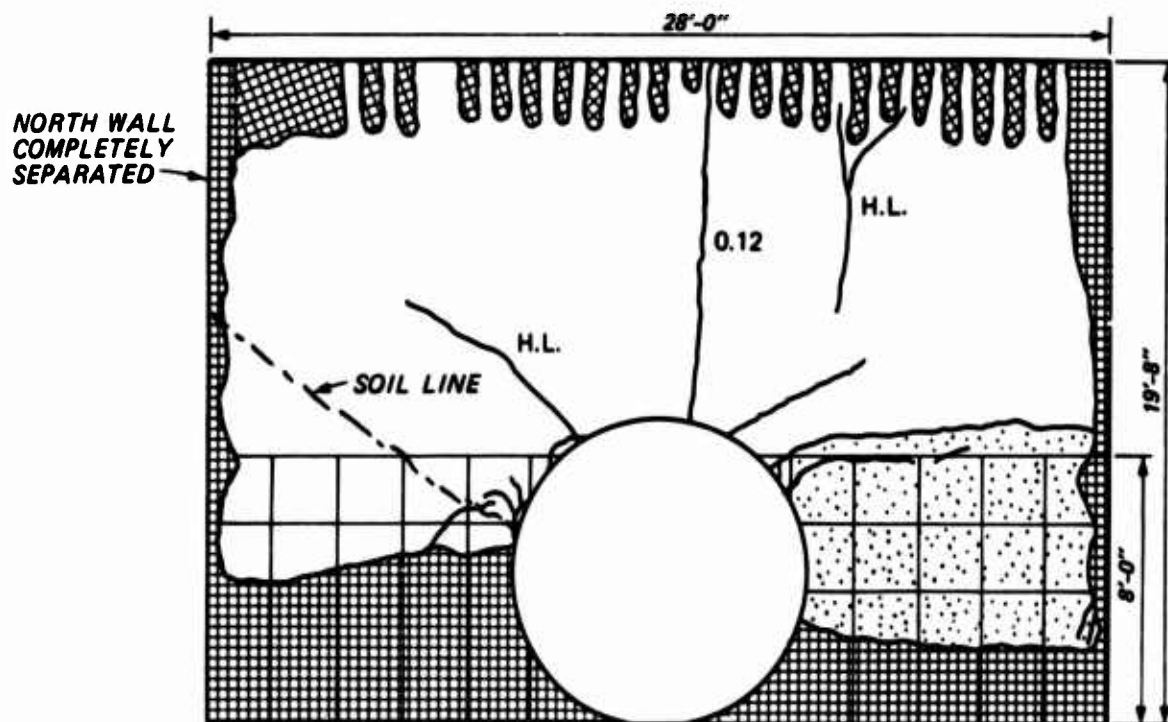
NOTE: CRACK DIMENSIONS IN INCHES
SIX #5 DOWELS REMAINED IN TOP OF WALL

LEGEND

▣ INNER FACE REINFORCEMENT EXPOSED
   DUE TO WALL ROTATION
▦ FRAGMENTED BUT NOT SPALLED
◈ REBAR PULLED OUT OF CONCRETE
H.L. HAIRLINE CRACKS

Figure 4.13.   Posttest damage to east donor bay wall.

138
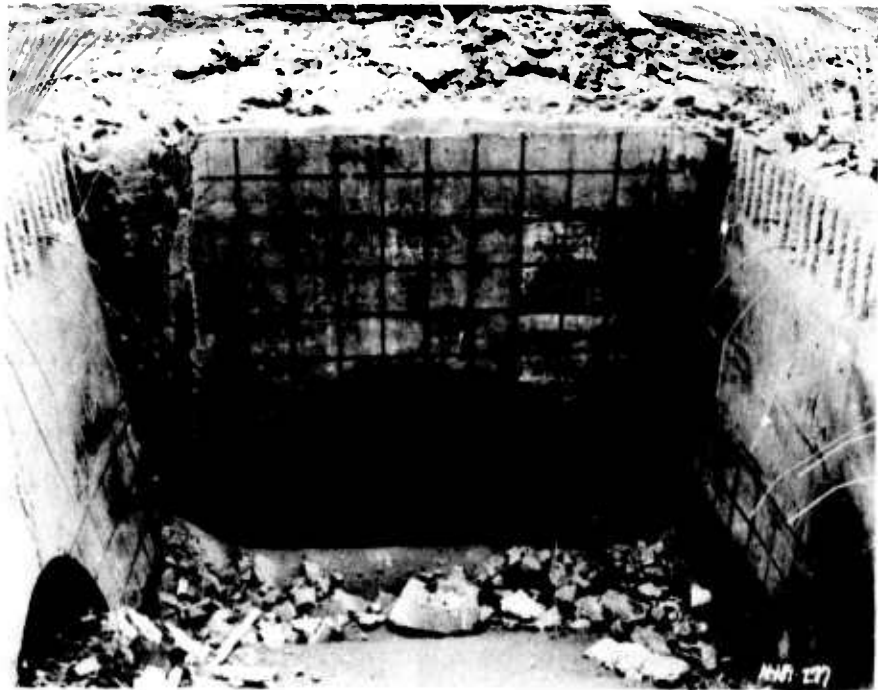
a. Overall view.
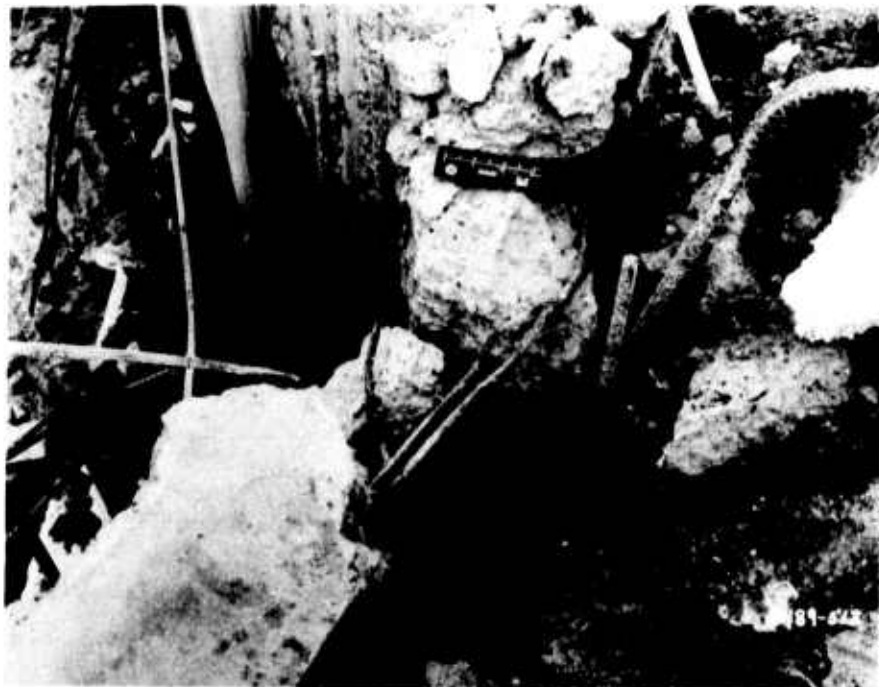
b. Exterior of southeast corner.

Figure 4.14. Posttest damage to donor bay south wall (Sheet 1 of 3).

139

c. Upper interior view of southeast corner.
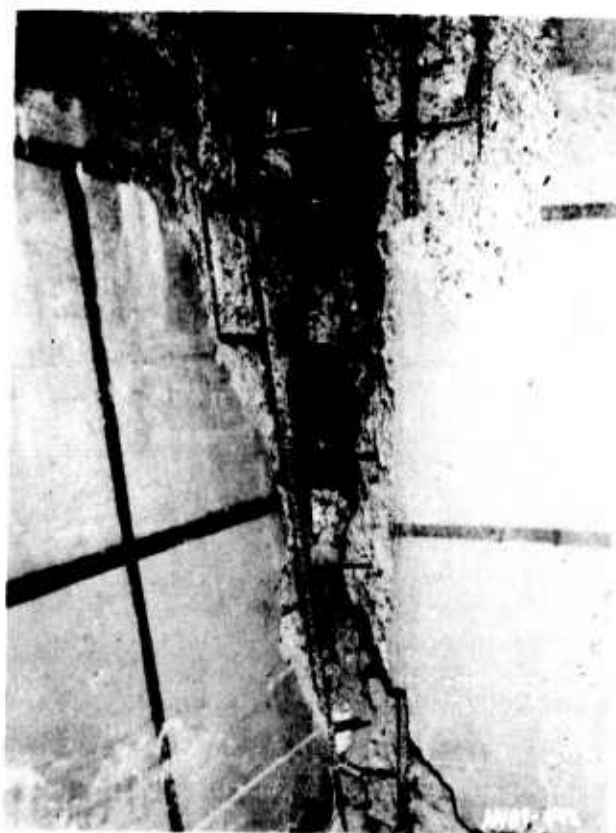
d. Lower interior view of southeast corner.

Figure 4.14. (Sheet 2 of 3).
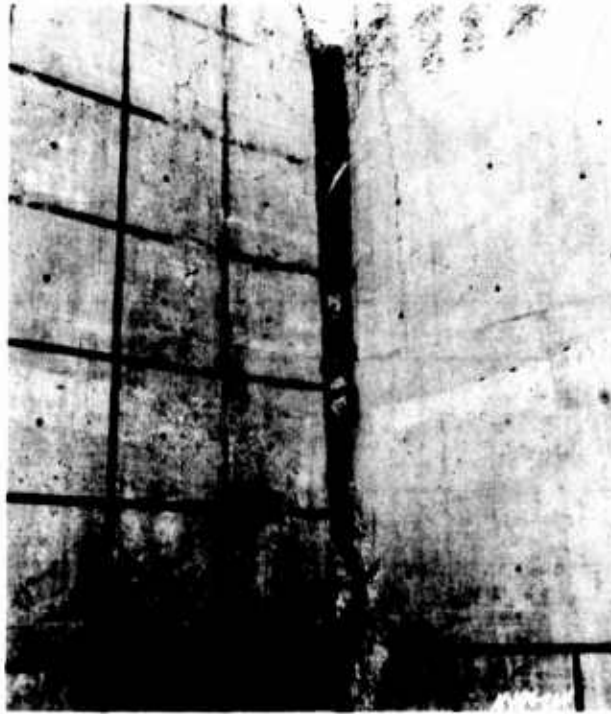
e.   Interior view of southwest corner.

f.   Exterior view of southwest corner.

Figure 4.14.   (Sheet 3 of 3).
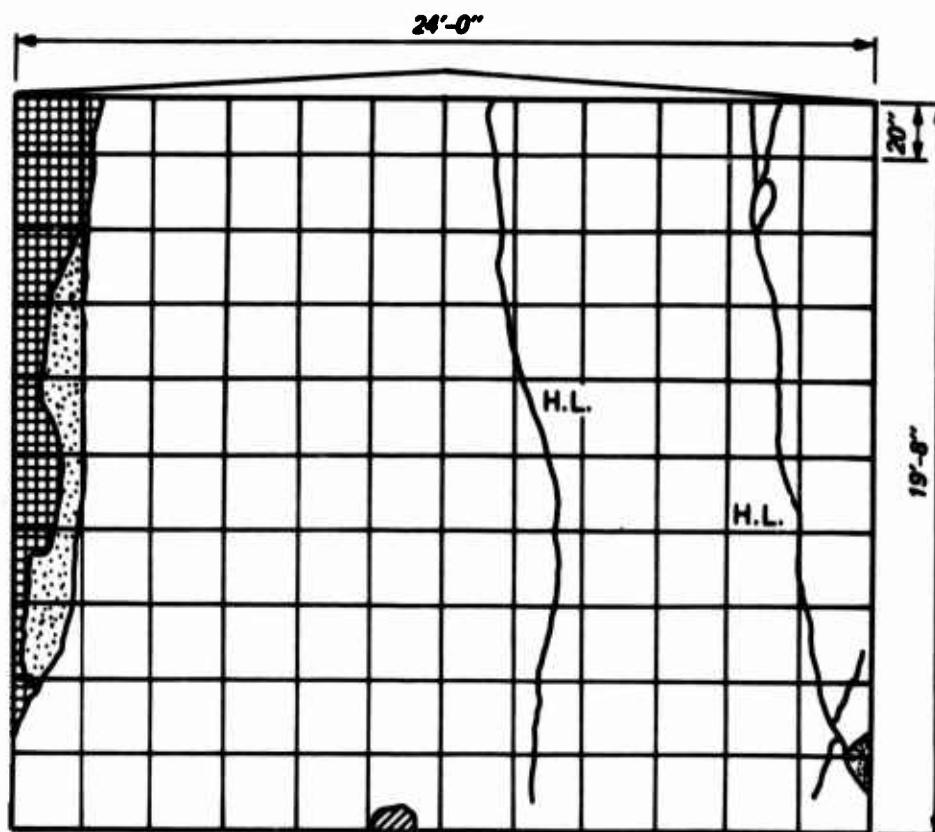
NOTE: CRACK DIMENSIONS IN INCHES

LEGEND

◼ EXPOSED REINFORCEMENT
▨ FRAGMENTED BUT NOT SPALLED
▱ SPALLED AREA
H.L. HAIRLINE CRACKS

Figure 4.15. Posttest damage to south donor bay wall.
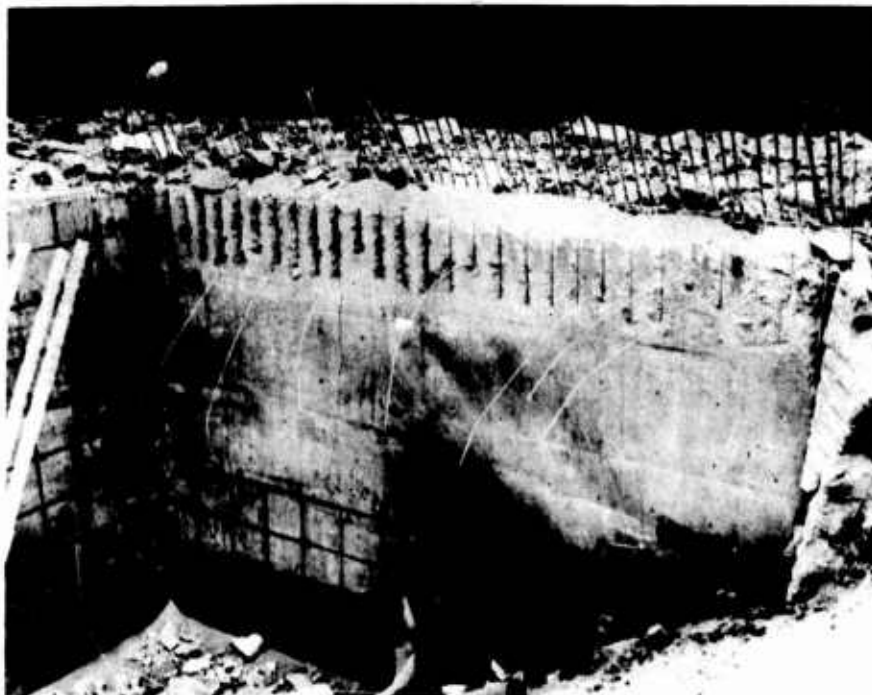
a.   Overall view.
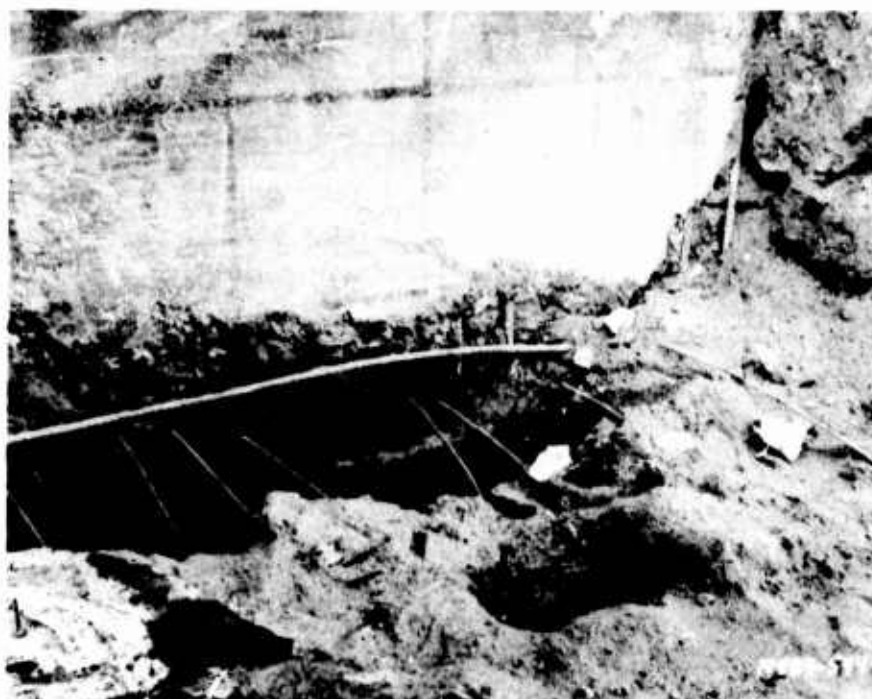
b.   Base of wall at the north end.

Figure 4.16.   Posttest damage to west donor bay wall.

143
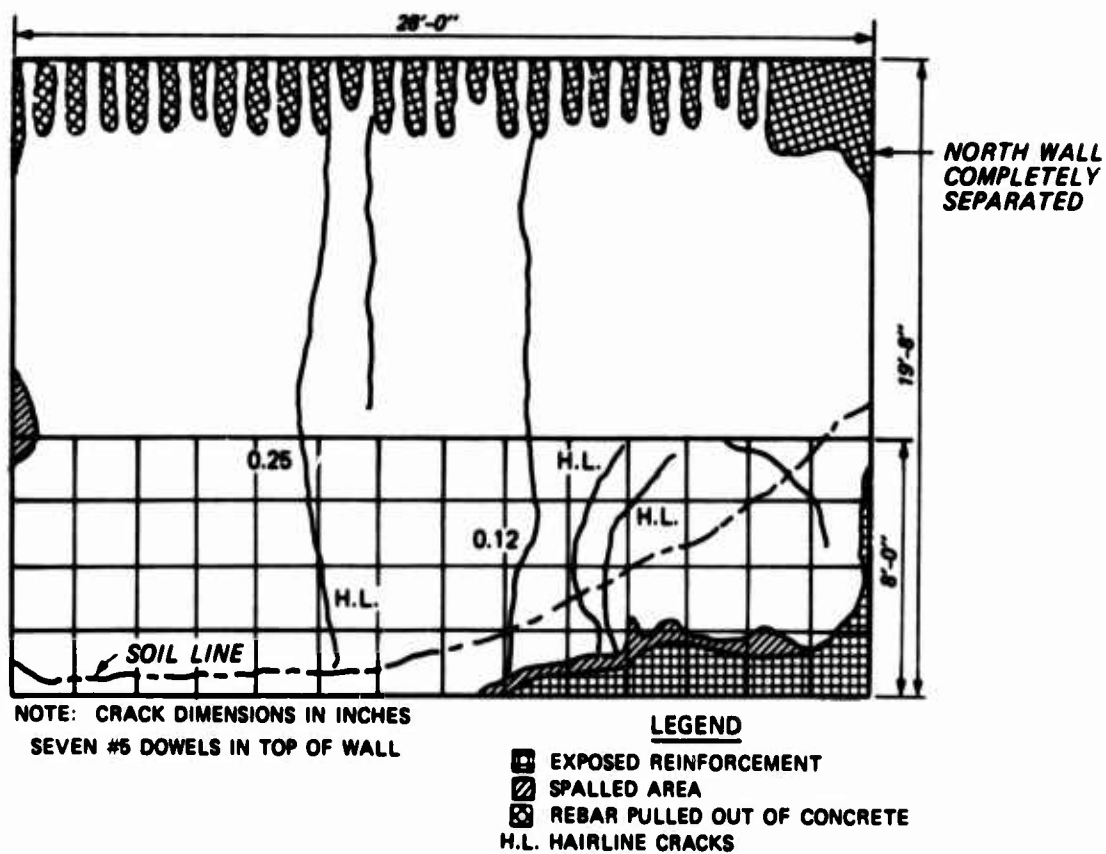
Figure 4.17.   Posttest damage to west donor bay wall.

a. Central portion of wall.
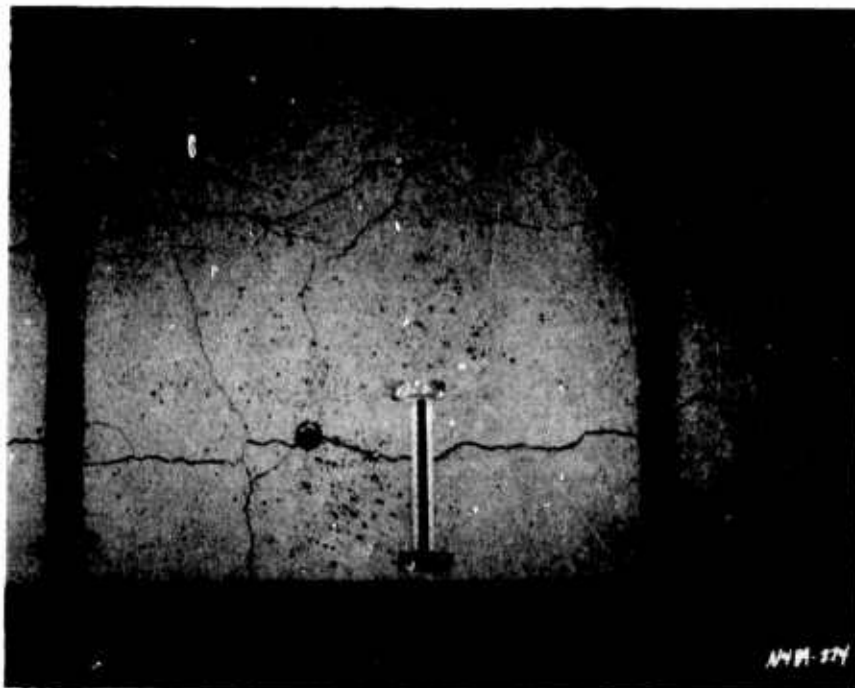
b. Detail of widest cracks.

Figure 4.18. Posttest view of acceptor bay south wall.
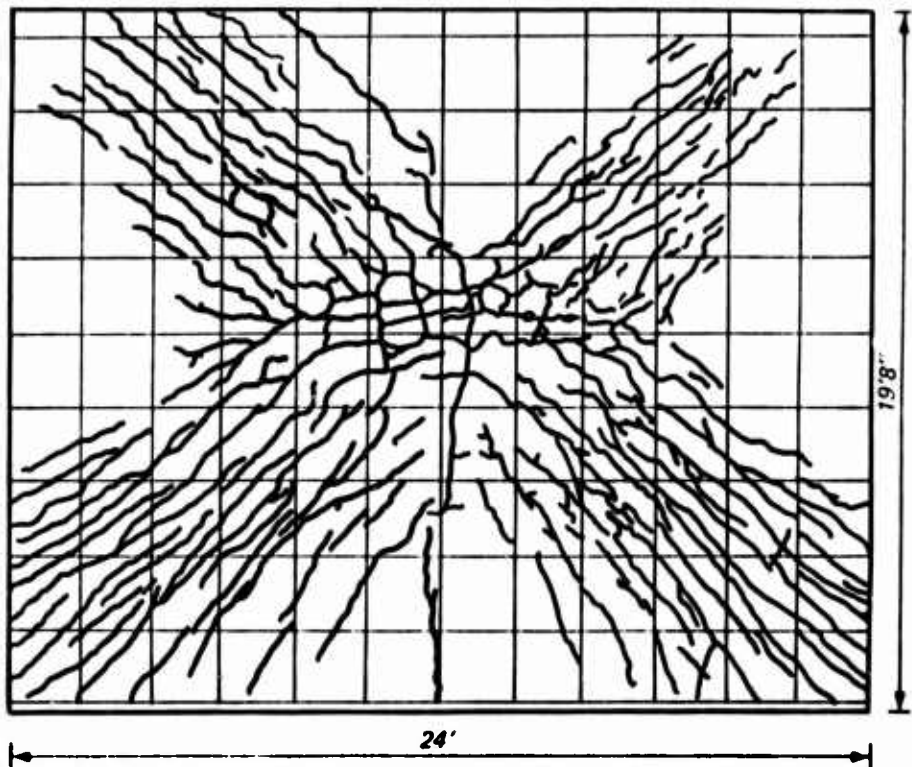
ALL CRACKS LESS THAN 1 mm WIDE
GRID IS 2 FEET ON CENTERS

Figure 4.19.   Posttest crack pattern on acceptor bay wall.

Figure 4.20.   Acceptor bay after excavation.

146

LEGEND

SYMBOL	DISPLACEMENT (FT)
0	0.00
1	0.01
2	0.02
3	0.03
4	0.04
5	0.05

NOTE: BOTTOM OF GRID REPRESENTS TOP OF 6-IN. CHAMFER AT BASE OF WALL
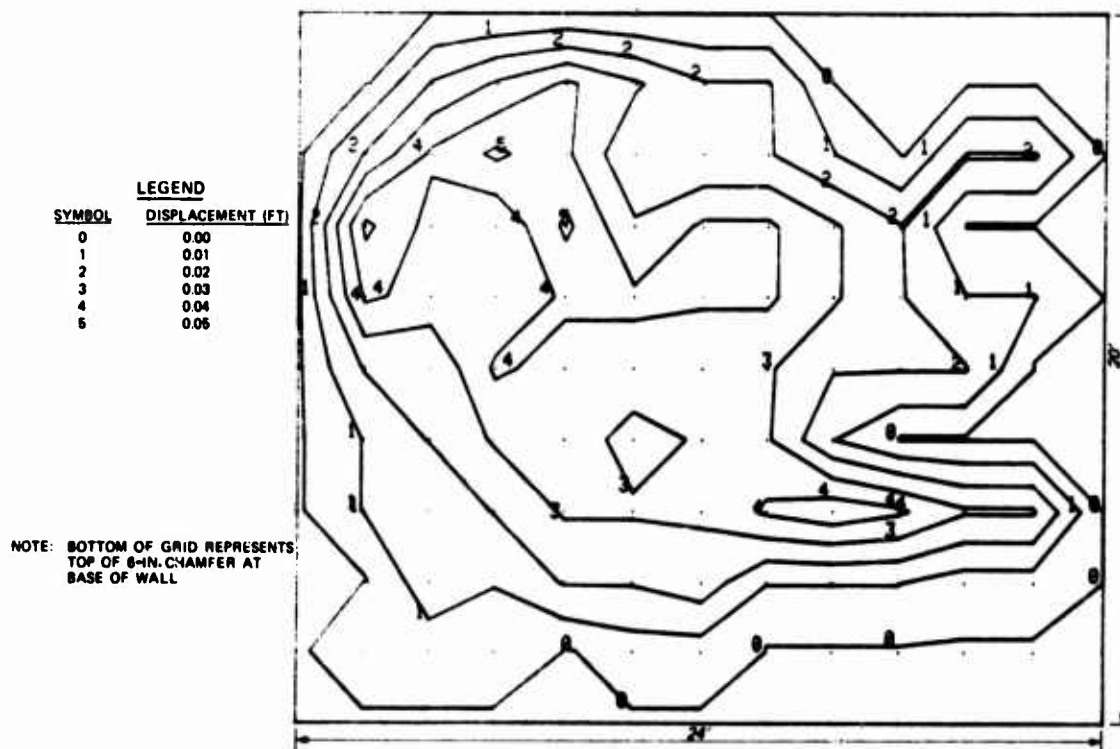
Figure 4.21. Acceptor bay wall posttest displacement contours.

Figure 4.22. Posttest view of acceptor bay north wall.

CHAPTER 5

PHASE II TEST RESULTS

5.1 STRUCTURAL VIBRATION TESTS

The four lowest resonant frequencies and associated modal damping ratios for the donor and acceptor bays are listed in Table 5.1. Typical transfer functions obtained during testing are shown in Appendix F. Data were processed with a Hewlett-Packard 5423A structural dynamics analyzer. Frequency and damping ratio values were obtained from individual transfer function records and were averaged to obtain the values shown in Table 5.1.

5.2 ELECTRONIC DATA MEASUREMENTS

Data obtained from electronic transducers are displayed in Appendix G. The heading on each data graph in the appendix includes the test name, gage number, digitizing sampling rate, and calibration value. If the record was filtered, the type of filter and frequency response after filtering are included as an additional line. The amplitude response of the LP4 filter used on some of the records is shown in Figure 4.1. All soil stress, interface pressure, and deflection records were filtered due to the low-frequency content of the recorded data. Accelerometer records were filtered to remove extraneous signals which were beyond the reliable range of the gage. Time zero on all records is the time of detonation.

Data were successfully recorded on all channels. The airblast records listed in Appendix G include 100-msec duration records for BP1-11 and BP15, with 200-msec records for BP16-29. Records for BP12-14 include 5-, 25-, and 125-msec duration records. Peak pressures on the 125-msec plots have been truncated to allow appropriate pressure scale factors to examine quasistatic pressure buildup and decay. Soil stress, interface pressure, deflection, and acceleration records have been plotted to 125 msec after detonation. Peak pressure and impulse values are listed in Table 5.2 for airblast and Table 5.3 for soil and interface pressures. Peak deflections and accelerations are listed in Table 5.4.

Posttest electronic deflection measurements for gages D-1, D-2, and D-6 were compared with physical posttest measurements to verify the validity of the electronic measurements. Physical posttest measurements at the D-1 and

148

D-2 gage locations were 0.44 in. and 0.32 in., respectively, compared with the electronic measurements of 0.482 in. and 0.346 in. The measurement differences fall well within the error associated with the physical measurements. Posttest deflection measurements for D-6 were 0.625 in. by electronic gage and 0.79 in. by physical measurement. The difference is believed to be a combination of physical measurement error and a small permanent displacement of the gage body itself. Physical measurements were not taken at gages D-3 through D-5 due to the relatively small displacements which were measured during the test event.

5.3 POSTTEST INSPECTION OF DONOR BAY

Figure 5.1 shows an overall posttest view of the donor bay. The roof disengaged during the test, with the east half separating and becoming a missile while the west half remained attached to the bay. In general, the north and south walls were the most heavily damaged, with extensive cracking and rotation near the corners in addition to spalling at the base of each wall. The east and west walls exhibited relatively minor vertical cracking but were also spalled near the base. Posttest wall displacements are listed in Table 5.5.

5.3.1 Roof Damage and Fragment Distribution

The roof slab broke into two major pieces in accordance with its design philosophy. Three planes of failure developed in the roof, all along a north-south axis. These failure planes included the center line of the roof where there was no reinforcement and at the intersection of the roof with the east and west walls. The east half of the roof completely separated from the bay while the west half remained attached to the bay and was folded over to the west side, Figure 5.1.

Details of the failure surfaces at the tops of the east and west walls are shown in Figure 5.2. The failure planes along the tops of the east and west walls were inclined at 45-deg angles.

All of the No. 5 outer face dowels which had joined the east wall to the roof remained embedded in the wall but were bent upward with all concrete cover spalled off. Fifteen of the No. 3 inner face dowels were pulled out of the inside face of the east wall while the remaining five were broken. The west side of the roof slab pulled 15 of the No. 3 dowels out of the west wall and broke 3. The No. 5 dowels remained embedded in both the wall and the

149

slab, allowing the slab to fold back over to the west side with virtually no fragment production.

As the east half of the roof slab separated from the bay, the concrete covering the bar splices between the No. 5 bars in the roof and the No. 5 dowels from the walls was spalled and fragmented. The major fragment was 15.5 by 3.54 ft in plan and weighed approximately 6550 lb. It was projected 114 ft from the bay and achieved an impact velocity of 53 fps. The force of impact fractured and twisted the slab into the shape observed in the posttest photographs (Figure 5.3). The small fragments impacted to the east of the donor bay over the simulated acceptor roof slab and the backfill slope. These areas were marked with 6-ft grids and photographed to produce Figure 5.4. No significant fragments impacted on fragment collection boxes. Fragments visible in Figure 5.4b rolled onto the box rather than impacting upon it.

A map of all major fragments and fragment grid areas is presented in Figure 5.5. In addition to the roof fragments, approximately 40 percent of the HVAC penthouse slab broke into fragments which impacted approximately 168 ft north of the bay. Fragments associated with the air lock and blast doors will be discussed in Section 5.5.2.

5.3.2 North Wall Damage

The posttest condition of the north wall is shown in Figure 5.6. The damage was mapped and the map is presented in Figure 5.7. The area adjacent to the explosive charge was badly cracked and spalled leaving a significant portion of the innerface reinforcing steel mat exposed. One vertical crack near the center extended to the top of the wall.

Damage to the northeast corner of the bay included the cracking and separation of concrete at the corner between the west and north walls plus a hinge mechanism which formed in the north wall approximately 1 ft away from the corner. The separation at the corner was on the order of 1.6 in. horizontally and 1.3 in. vertically. The No. 2 inside face horizontal reinforcing bar had failed in tension at elevations 4.5 ft and above. The No. 2 horizontal rebar on the outside face pulled out of the corner without developing the strength of the bar. Most of the No. 3 horizontal steel, turned 90 deg from the west wall as a corner detail, was bent but few bars were broken. On the outside face of the wall at ъe "hinge" location, No. 2 horizontal rebars were failed in tension.

150

The damage to the northeast corner was very similar to that of the north-west side. The corner was displaced approximately 1.5 in. horizontally and 0.35 in. vertically. No. 2 inside face horizontal rebar was broken in tension at elevations above 3 ft. The No. 2 horizontal rebar in the outer face was pulled out of the east wall without any bar failures. The No. 3 rebar from the east wall was bent, but not broken. A hinge mechanism was formed in the north wall approximately 1.5 ft from the corner. The wall had undergone a visible rotation at both the corner and this hinge. The No. 2 horizontal rebar on the outside face of the hinge had broken near the top of the wall.

5.3.3 East Wall Damage

The east wall suffered relatively minor damage during the test. Figure 5.8 shows a posttest view of the wall, and damage is detailed in Figure 5.9. The roof completely separated from the wall and 15 of the No. 3 inside face dowels pulled out of the wall. All of the outside face No. 5 roof dowels remained embedded in the wall but were rotated approximately 64 deg. The corners separated where they joined the north and south walls, but corner damage to the east wall itself was confined to minor spalling. Spalling occurred at the base of the wall, particularly at the north end, leaving some of the reinforcing steel exposed. Several vertical cracks were noted near the center of the wall.

5.3.4 South Wall Damage

Damage to the south wall was very similar to that of the north wall except there was no local spalling at the center since the charge was detonated near the north wall. The wall is shown in Figure 5.10, and posttest damage is shown in Figure 5.11. Although the corners were seriously damaged, the damage to the remainder of the wall was limited to spalling at the base of the wall and two small vertical cracks which terminated 4 ft from the floor.

Both corners of the south wall performed in an analogous manner to those of the north wall. The southeast corner separated 1.6 in. horizontally and 0.3 in. vertically. The No. 2 horizontal rebars were pulled out of the east wall between elevations 5.5 ft and 8 ft and were broken in tension above 8 ft. At the outer face reinforcement, the No. 2 and No. 3 horizontal steel merely pulled out of the fractured concrete at the corner. On the outside face of the wall adjacent to the hinge location, the No. 2 rebars were broken in tension.

The southwest corner had a horizontal displacement on the order of 2.1 in. and a 0.32-in. vertical displacement. The No. 2 horizontal rebar on the inside face broke in tension at elevations 5 to 6.5 ft and again at elevations above 8 ft. Between elevations 6.5 and 8.5 ft, these bars pulled out of the east wall and were bent. The Nos. 2 and 3 horizontal bars on the outside face of the wall were pulled out of the west wall. The No. 2 horizontal rebar on the outside face of the hinge location was broken in tension.

5.3.5 West Wall Damage

The condition of the west wall after the test is shown in Figure 5.12. Damage to the wall is displayed in Figure 5.13. The disengagement of the roof pulled the inside face No. 3 dowels out of the wall. But unlike the other side of the roof, the west half of the roof remained connected to the No. 5 outside face roof dowels and merely flipped open without tearing loose from the bay. The corners of the walls incurred only minor spalling. Significant spalling occurred at the north end of the wall near the base. The rebar was exposed at the corner of the air-lock opening and adjacent to the north wall. Numerous cracks occurred near the intersection of the bay wall and the air-lock walls.

5.3.6 Floor Slab Damage

Damage to the floor slab included hairline cracks near the location of the explosive charge and cracks adjacent to the east and west walls. Spalling was limited to an area near the northwest corner of the slab. A pictorial view of the slab is shown in Figure 5.14 and the damage is mapped in Figure 5.15.

5.4 POSTTEST INSPECTION OF ACCEPTOR BAY

Damage to the acceptor bay was primarily limited to the south wall cracking shown in Figure 5.16. All observable cracks in the photograph were highlighted with a felt-tip pen for clarity. A diagram of this crack pattern is included as Figure 5.17. Most of the cracks shown in these figures were of hairline width. The location and size of the significant cracks are shown in Figure 5.18.

The permanent displacements in the south wall are listed in Table 5.6. These deflections were measured at the locations of the grid intersections shown in Figures 5.17-5.18. Figure 5.19 is a deflection contour map of the

152

data in Table 5.6. The acceptor bay experienced a permanent rigid body displacement of 0.79 in. away from the donor bay.

The only other observable damage to the bay was the formation of a crack down the center line of the roof slab. This crack was located at the crest of the roof in the region where there was no continuous reinforcement.

5.5 POSTTEST INSPECTION OF APPURTENANT STRUCTURES

The detonation of the charge in the donor bay produced significant damage to the donor bay air lock and to the exterior ramp. All other appurtenant structures were either undamaged or suffered very minor damage.

5.5.1 Ramp and Retaining Wall

An overall posttest view of the ramp and Phase II structure is shown in Figure 5.20. All of the cemesto board on the walls and virtually all of it on the roof were destroyed during the test. All aluminum roofing material was removed. The aluminum sheets seen on the ramp in Figure 5.20 fell back to that position after the test. Figure 5.21 shows a more detailed view of the ramp damage. All of the self-tapping screws remained in place as the cemesto board fractured around them. The column in front of the donor bay was struck by debris from the air lock and broke away from the roof beam. It came to rest 417 ft east of the ramp. The girt attached to the column also broke away from the ramp and impacted several feet from the ramp. The impact load transmitted to the ramp also caused the beam and column immediately north of the donor bay air lock to break away from the retaining wall and to shear column baseplate bolts. The displacement of this member can be seen in Figure 5.21.

The retaining wall experienced minor cracking. Figure 5.22 shows a posttest view of the wall after the ramp structure and debris were removed. More detailed views of the crack patterns are given in Figure 5.23. All cracks in the photographs were less than 0.1 in. wide and were enhanced with felt-tip pens for the photographs.

5.5.2 Donor Bay Air Lock and Blast Doors

The damage to the donor air lock is shown in Figure 5.24. The air-lock walls and roof were cracked near their centers and displaced outward. Posttest displacements are listed in Table 5.7. The cover over the inside face dowels joining the walls to the roof was spalled. At the joint between the

153

air lock and the donor bay, a gap existed with a width of 0.5 in. at the floor to 1.5 in. at the roof. The dowels joining the two structures had been partially pulled out of the air lock and were bent, indicating a peak displacement somewhat larger than the posttest displacement.

The bulkhead, doorframe, and blast doors were completely removed from the air lock. The entire assembly became five separate fragments: the upper portion of the bulkhead (Figure 5.25); the south part of the bulkhead (Figure 5.26); the north part of the bulkhead with the doorframe (Figure 5.27); and the inactive blast door leaf and the active blast door leaf (Figure 5.28).

The blast doors broke away from the doorframe after breaking their hinge straps at the hinge pins. The lower locking bolt in the inactive (locked) leaf did not fail, but it rotated within the door and elongated the bolt holes in both the door and the embedded floor plate. The upper locking bolt was found undamaged and in the fully extended position. The interior skin plate on the inactive leaf was badly buckled and the entire door was severely damaged. The interior skin on the active leaf was also buckled, but the only other damage to the door was dents at the upper and lower edges. The active and inactive leafs came to rest 412.5 and 507.6 ft, respectively, from their initial position. The column broken from the ramp was found next to the active leaf as shown in Figure 5.28a.

The doorframe with the north section of the bulkhead is shown in Figure 5.27. It was located 123.1 ft from its initial position. On the south side of the frame, two of the hinge pads and pins were left intact. The bolts holding the top hinge pad failed in tension and the hinge pad was missing. Along the top and south side of the frame, the outer face shear studs failed where they were bent 90 deg. The inner face shear studs pulled out of the adjoining concrete without damage to the stud. On the north side of the frame, the bolts holding the lower hinge pad to the frame failed in tension and the hinge pad was missing. Two of the hinge pad bolts on the upper hinge also experienced tensile failure. Pieces of the door hinge strap material were still in place on the upper two hinge pins.

The two bulkhead sections on either side of the doorframe exhibited similar modes of failure. However, the south section broke away from the doorframe and landed 48.0 ft from the air lock. At the bottom, the outer (exterior) face rebars failed in shear and the inner face bars failed under combined shear and tension. Along the walls, the horizontal dowels joining

154

the walls and bulkheads failed in tension or a combined tension and shear mode. At the upper edge, approximately 4.2 ft from the air-lock floor, six of the vertical bars pulled out of the roof and the two bars next to the doorframe failed in tension.

The top bulkhead fragment was approximately 4.8 ft long and 1 ft high. It impacted 13.3 ft from its pretest location. The stirrups which joined the bulkhead to the roof failed in tension (40 percent) and shear (60 percent) along the outer face and completely pulled the inner face of the stirrup from the roof reinforcement. The four horizontal rebars pulled out of both walls.

5.5.3 Acceptor Bay Air Locks
       and Blast Door

The active blast door leaf was held closed by a 1/4-in. bolt inserted through a hasp. This was used to simulate the pneumatic door latch on the prototype. Immediately after the test the active leaf of the door was open and the bolt had been sheared off. There was no apparent damage to the doors or doorframes other than minor indentation of the outer door skin.

Both the north and south acceptor air locks were in excellent condition. The only evidence of cracking occurred at the joint between the south wall of the north acceptor air lock and the acceptor bay. The crack was less than 0.1 in. wide, and two small pieces of concrete on the joint were spalled.

Table 5.1. Lowest resonant frequencies and damping ratios of Phase II donor and acceptor bays.

Bay	Before Backfill		After Backfill	
	Frequency Hz	Damping Ratio % of Critical	Frequency Hz	Damping Ratio % of Critical
Donor	82.31	2.27	125.15	7.47
	99.64	3.92	158.18	5.10
	119.97	2.41	194.96	6.49
	156.60	1.94	209.24	5.37
Acceptor	87.73	1.31	123.55	12.25
	104.10	2.57	163.26	4.93
	125.15	3.69	196.66	13.73
	160.09	1.58	213.88	12.48

Table 5.2. Phase II peak blast pressure measurements.

Transducer	Location	Maximum Pressure psi	Time of Maximum msec	Maximum Impulse psi × sec	Time of Maximum msec
BP1	North acceptor bay wall	1.12	17.50	0.0031	78.37
BP2	East acceptor bay wall	0.94	24.51	0.0054	80.05
BP3	South acceptor bay wall	1.85	4.98	0.0038	74.51
BP4	West acceptor bay wall	2.74	4.41	0.0038	77.30
BP5	North air-lock wall	1.14	89.38	0.0057	99.15
BP6	North air-lock floor	0.81*	87.18	0.0050	99.55
BP7	North air-lock entrance	44.28	34.57	0.1431	44.01
BP8	North air-lock entrance	23.94	37.05	0.1294	45.12
BP9	Retaining wall	26.77	29.02	0.1113	43.35
BP10	Retaining wall	51.47	27.01	0.1401	37.22
BP11	Retaining wall	26.76	26.04	0.0806	29.11
BP12	East donor bay wall	817.28	1.62	3.9326	74.08
BP13	South donor bay wall	1066.80	1.77	4.8230	72.86
BP14	Center, donor bay floor	1705.5	0.35	3.7137	67.54
BP15	South air-lock entrance	14.92	36.05	0.0691	42.60
BP16	South air-lock wall	11.05	41.49	0.0916	61.30
BP17	South air-lock floor	9.16	39.00	0.0962	63.41
BP18	South air-lock floor	16.05	43.05	0.1046	58.09
BP19	South air-lock closure	15.28	46.33	0.1141	58.38
BP20	South air-lock closure	18.60	46.13	0.1137	58.40
BP21	Surface, east of donor bay	1.27*	30.28	0.0131	87.13
BP22	Surface, east of donor bay	0.99*	20.20	0.0143	81.35
BP23	Surface, east of donor bay	1.94*	17.25	0.0226	79.13
BP24	Surface, east of donor bay	0.96*	15.28	0.0154	75.39
BP25	Surface, south of donor bay	2.30*	59.10	0.0194	70.92

(Continued)

* Denotes values from filtered records, all others based on unfiltered data.

157

Table 5.2. (Concluded).

Transducer	Location	Maximum Pressure psi	Time of Maximum msec	Maximum Impulse psi × sec	Time of Maximum msec
BP26	Surface, south of donor bay	1.03*	44.23	0.0142	58.18
BP27	Surface, south of donor bay	1.13*	55.57	0.0154	71.70
BP28	Surface, south of donor bay	1.04*	59.49	0.0150	76.83
BP29	Acceptor HVAC duct	2.08*,**	25.53	0.0006	67.54

* Denotes values from filtered records, all others based on unfiltered data.
** Pressure spike at 120 msec was apparently due to particle impact on gage diaphragm.

158

Table 5.3. Phase II peak soil pressure measurements.

Transducer	Location	Maximum Pressure psi	Time of Maximum msec	Maximum Impulse psi × sec	Time of Maximum msec
SS1	Middistance between bays	98.60*	16.19*	4.584	99.66
SS2	Middistance between bays	226.92	12.95	7.876	109.85
SS3	Middistance between bays	139.96	13.93	5.250	101.20
SS4	Middistance between bays	122.42	14.17	3.937	104.02
IP1	East edge, acceptor bay wall	33.51	56.33	1.793	128.36
IP2	East edge, acceptor bay wall	45.10	54.27	2.124	135.65
IP3	East edge, acceptor bay wall	23.61	50.81	1.276	140.69
IP4	Center, acceptor bay wall	72.67	56.11	3.811	109.16
IP5	Center, acceptor bay wall	54.31	33.31	2.455	126.43
IP6	Center, acceptor bay wall	64.07	34.95	2.971	117.45
IP7	Quarter point, acceptor bay wall	47.75	56.84	2.566	113.41
IP8	Quarter point, acceptor bay wall	42.25	55.30	2.229	109.33
IP9	Quarter point, acceptor bay wall	63.13	43.65	3.139	122.76
IP10	East acceptor roof slab	1.77	47.68	0.038	90.18
IP11	East acceptor roof slab	2.10	34.93	0.042	76.35
IP12	South acceptor roof slab	7.35	23.96	0.105	70.08
IP13	South acceptor roof slab	3.06	30.24	0.017	76.33
IP14	South acceptor roof slab	1.33**	64.67**	0.036	99.04

* Peak value clipped from record.
** Spikes at 25 msec and from 112 to 150 msec due to high frequency noise.

Table 5.4. Phase II peak deflections and accelerations.

Transducer	Location	Maximum Deflection in.	Time of Maximum msec	Posttest Measurement in.
	Peak deflections			
D1	Center, south acceptor bay wall	1.367	62.30	0.482
D2	Quarter point, south acceptor bay wall	1.136	63.77	0.346
D3	Acceptor bay roof	0.211	63.82	0.091
D4	Center of acceptor bay roof	0.343	62.43	0.094
D5	Acceptor bay roof	0.133	63.50	0.089
D6	Acceptor bay floor slab	1.168	98.04	0.625

Transducer	Location	Maximum Acceleration g	Time of Maximum msec
	Peak accelerations		
A1	6-in. offset from D1	41.97	31.98
A2	6-in. offset from D2	28.67	34.27
A3	Acceptor bay floor slab	11.43	39.00

Table 5.5 Posttest donor bay wall displacements.

Location in Bay	Elevation ft	Displacement ft
Between east and west walls		
North end	2.5	0.25
	5.0	0.25
	7.5	0.21
	9.8	0.10
Center	0.0	0.00
	5.0	0.10
	9.8	0.00
South end	2.5	0.23
	5.0	0.27
	7.5	0.29
	9.8	0.25
Between north and south walls		
Center	3.0	0.42
	5.0	0.50
	9.8	0.50

Table 5.6. Acceptor bay south wall posttest deformation.

Vertical Scale ft	Horizontal Scale, ft												
	0	1	2	3	4	5	6	7	8	9	10	11	12
9.83	0.00	0.52	1.56	1.56	1.56	1.04	1.04	0.52	1.04	1.04	2.08	2.08	-0.52
9.00	0.00	1.04	1.56	0.52	1.04	1.04	1.04	0.52	0.52	0.52	1.04	1.08	-0.52
8.00	0.00	0.00	1.04	1.04	1.04	1.56	1.56	1.56	1.56	1.56	2.08	0.52	0.00
7.00	0.00	0.52	1.56	2.08	3.65	3.65	3.65	3.65	2.60	2.08	1.56	0.52	0.52
6.00	0.00	1.04	2.08	3.13	4.17	4.69	5.21	4.17	3.65	3.13	2.08	0.52	0.52
5.00	0.00	1.04	1.56	2.60	3.13	3.65	3.65	3.13	2.60	2.08	1.56	0.52	0.52
4.00	0.00	1.04	1.56	2.08	3.13	2.60	3.13	2.60	2.08	2.08	1.56	1.04	0.00
3.00	0.00	1.04	1.04	2.08	2.08	2.08	2.08	2.08	2.08	2.08	1.04	0.52	0.00
2.00	0.00	0.52	1.04	1.56	1.56	1.56	2.08	1.56	1.56	1.56	1.04	0.52	0.00
1.00	0.52	0.52	0.52	0.00	0.00	0.52	0.52	-0.52	0.00	0.00	0.00	-0.52	0.52
0.00	0.52	0.00	0.00	0.00	0.00	-0.52	-1.04	-1.56	-1.56	-1.04	-1.04	-1.04	0.52

Note: All deformations in hundredths of a foot (0.01 ft).

Table 5.7. Donor bay air-lock posttest displacements.

Distance from Donor Bay ft	Displacement at North Wall ft	Displacement at Center of Floor ft	Displacement at South Wall ft
Vertical displacements			
0.0	0.000	0.042	-0.021
6.3	0.000	0.313	0.063
12.5	0.021	0.313	0.000

Distance from Donor Bay ft	Displacement at Floor ft	Displacement at Center of Wall ft	Displacement at Roof ft
Horizontal displacements			
0.0	0.000	0.083	-0.021
6.3	0.000	0.146	0.063
12.5	0.021	0.146	-0.021

Figure 5.1. Posttest top view of donor bay.
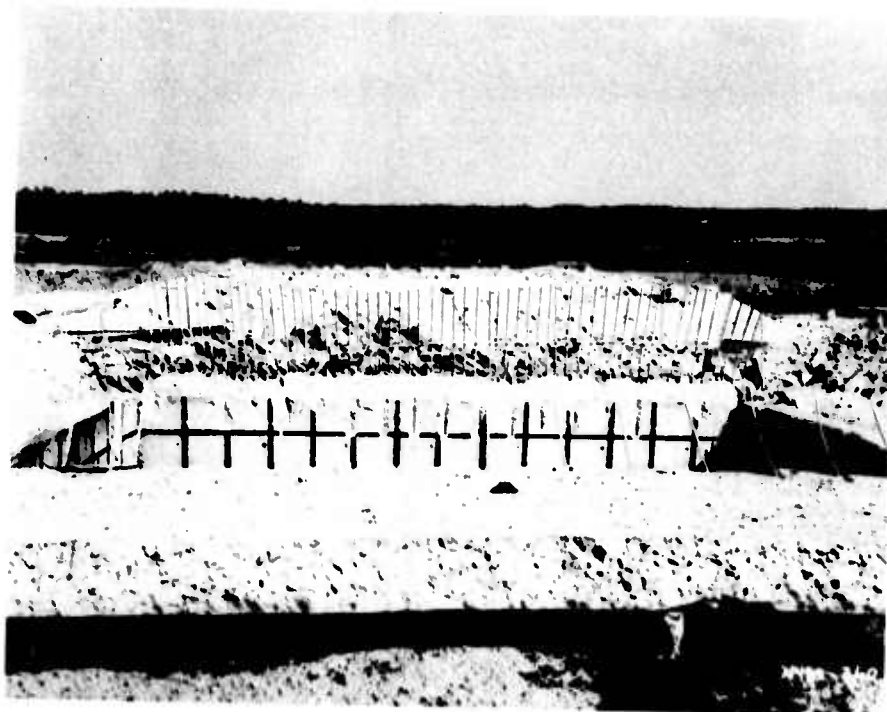
a. View facing east.

b. View facing west.

Figure 5.2. Damage to donor bay roof (Sheet 1 of 2).

165

c. Detail of west half of roof slab.

Figure 5.2. (Sheet 2 of 2).

a. View facing east.

b. View facing west.

Figure 5.3. Major donor bay roof fragment.

a. Grid over east simulated acceptor roof slab.

b. Grid over east backfill slope.

Figure 5.4. Donor bay roof fragments.
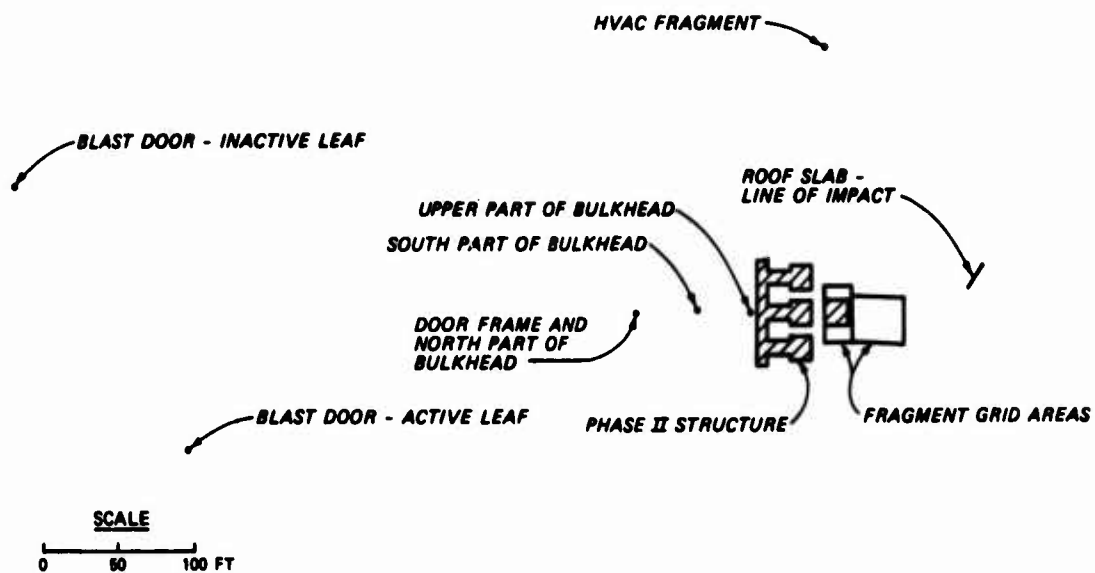
Figure 5.5. Location of significant fragments from Phase II test.

a. Overall view.
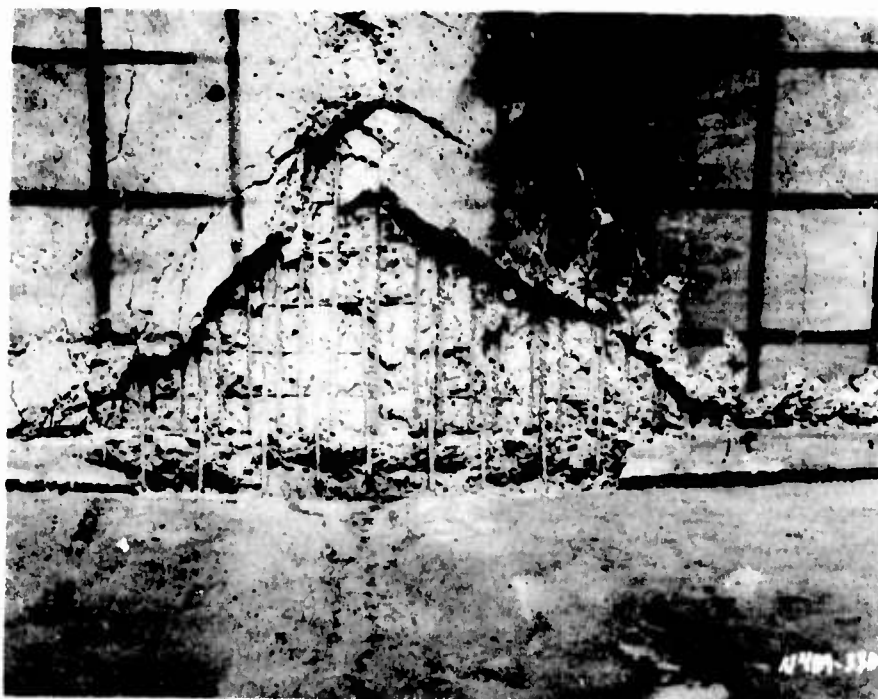
b. Damage adjacent to explosive charge.

Figure 5.6.   Posttest view of north donor bay wall
(Sheet 1 of 2).

170

c. Northwest corner.
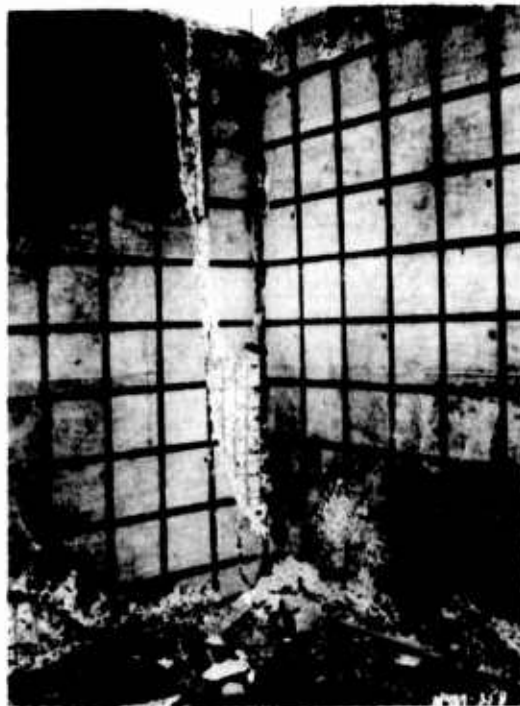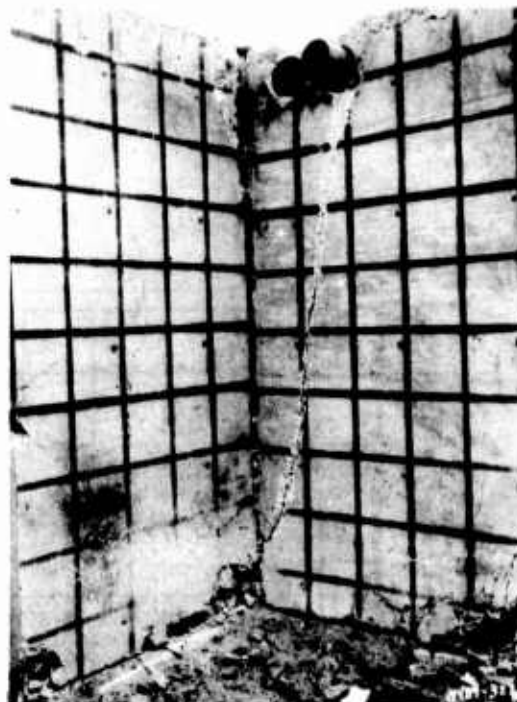
d. Northeast corner.

Figure 5.6. (Sheet 2 of 2).
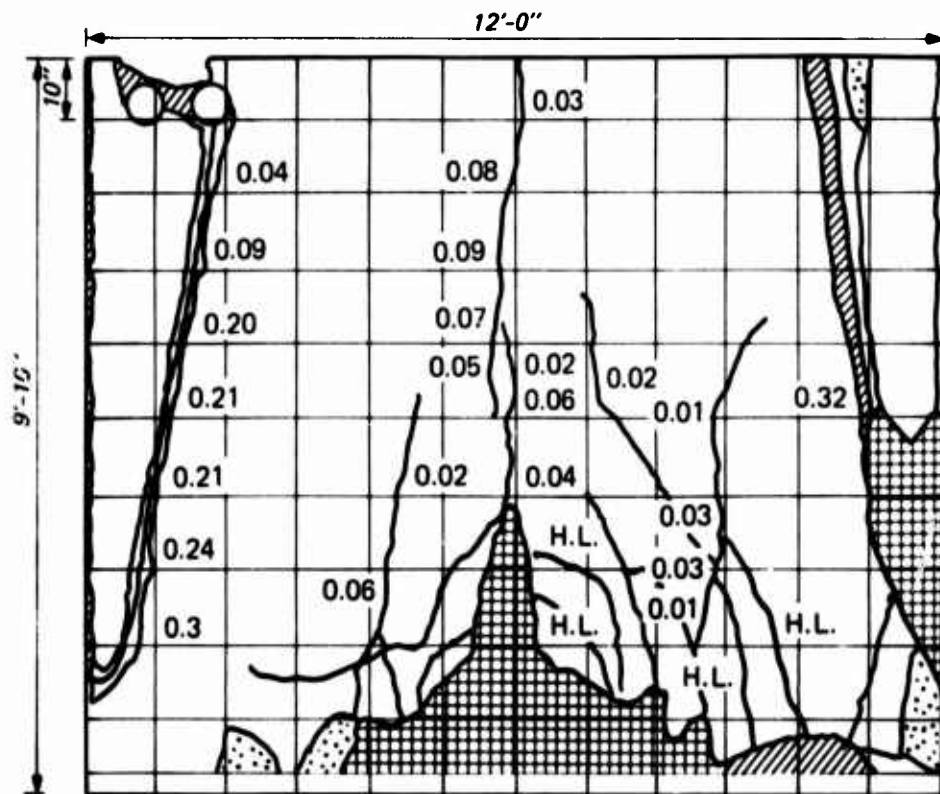
NOTE: CRACK DIMENSIONS IN INCHES

LEGEND

▦ EXPOSED REINFORCEMENT
▨ FRAGMENTED BUT NOT SPALLED
▨ SPALLED AREA
H.L. HAIRLINE CRACKS

Figure 5.7. Posttest damage to north donor bay wall.
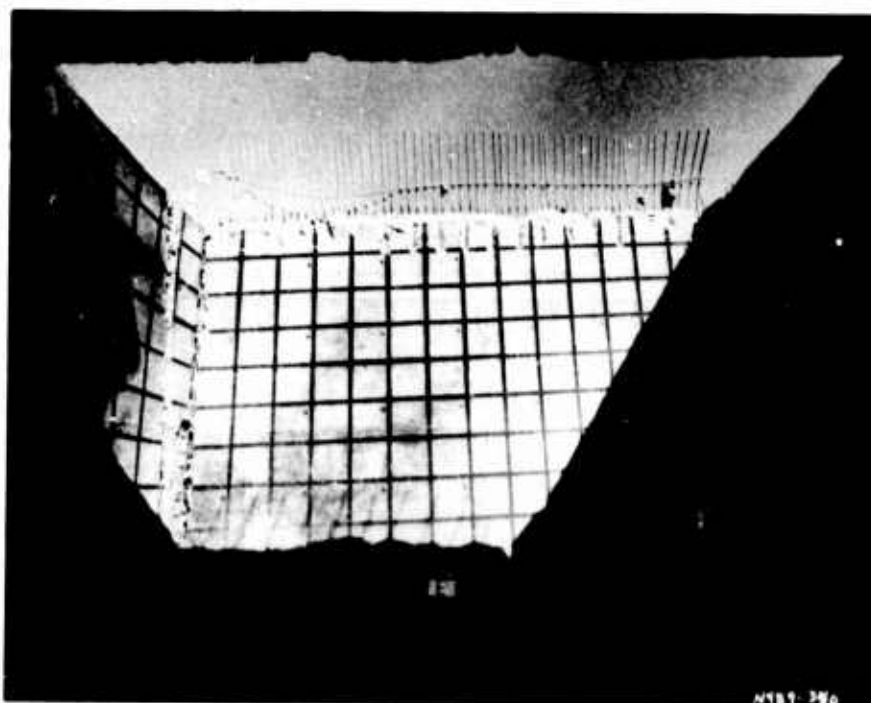
a. Overall view.

b. Damage to lower north corner.

Figure 5.8. Posttest view of donor bay east wall.

173

NOTE: CRACK DIMENSIONS IN INCHES

LEGEND

⬚ EXPOSED REINFORCEMENT
⬚ FRAGMENTED BUT NOT SPALLED
◪ SPALLED AREA
⬚ REBAR PULLED OUT OF CONCRETE
H.L. HAIRLINE CRACKS
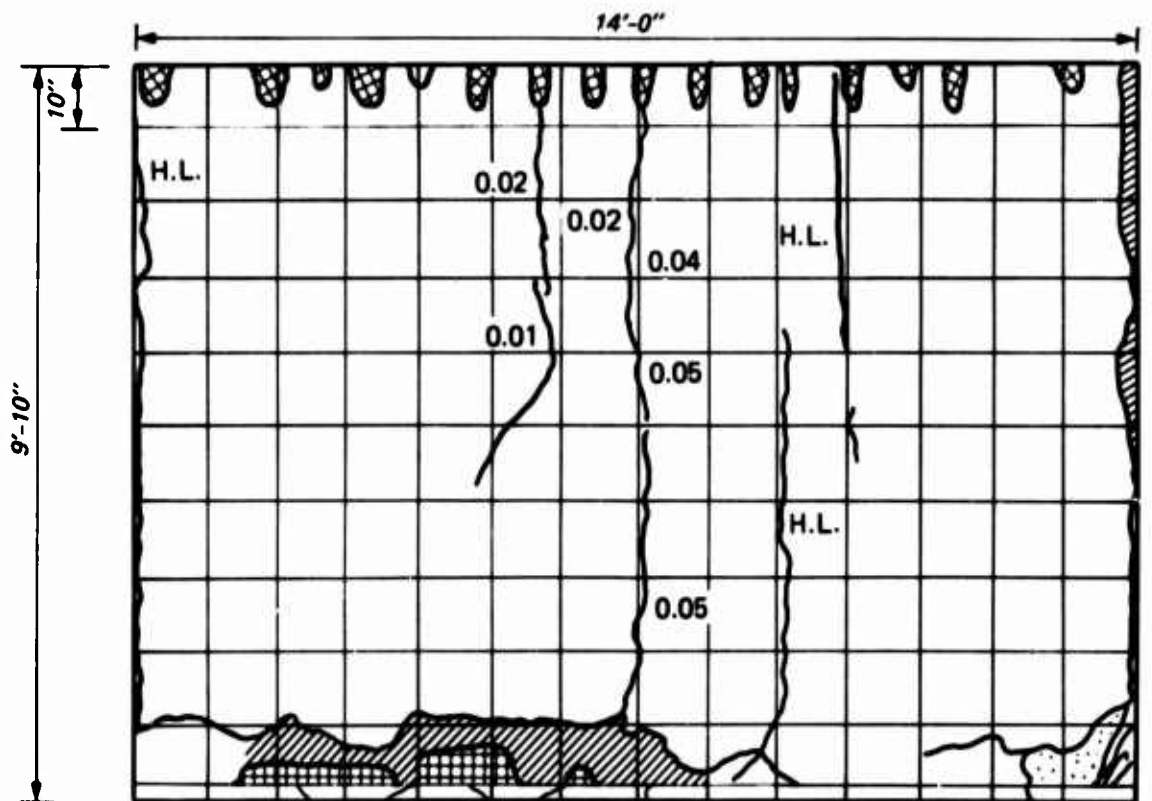
Figure 5.9.   Posttest damage to east donor bay wall.

a.   Overall view.
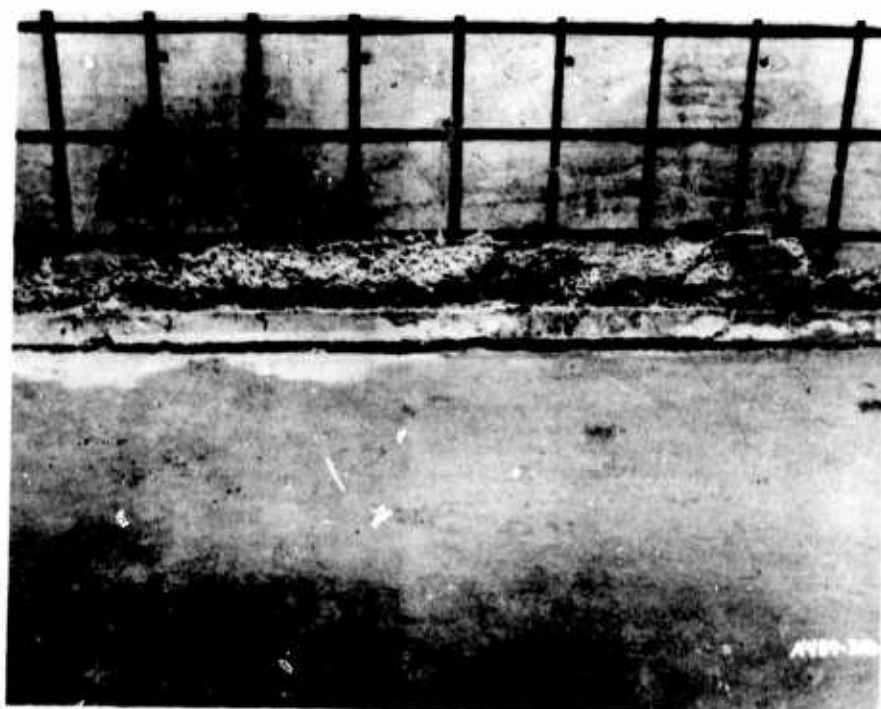
b.   Damage to lower edge.

Figure 5.10.   Posttest view of south donor bay wall
(Sheet 1 of 2).

175
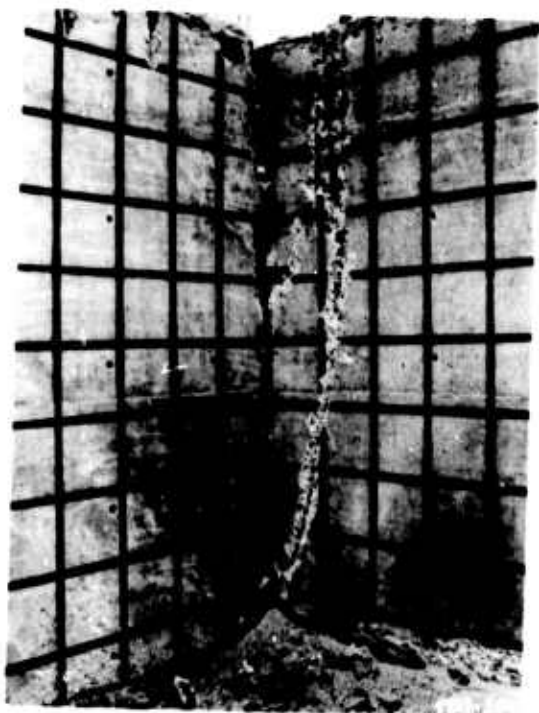
c.   Southeast corner.
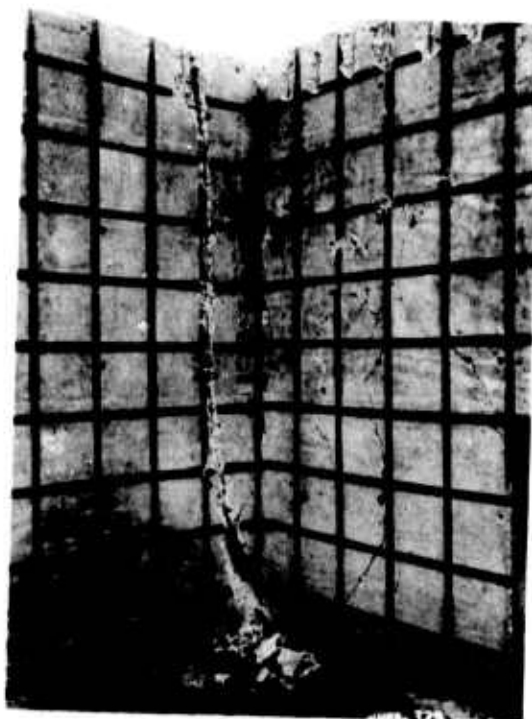
d.   Southwest corner.

Figure 5.10.   (Sheet 2 of 2).

NOTE: CRACK DIMENSIONS IN INCHES

LEGEND

⬚ EXPOSED REINFORCEMENT
⬚ FRAGMENTED BUT NOT SPALLED
▨ SPALLED AREA
H.L. HAIRLINE CRACKS
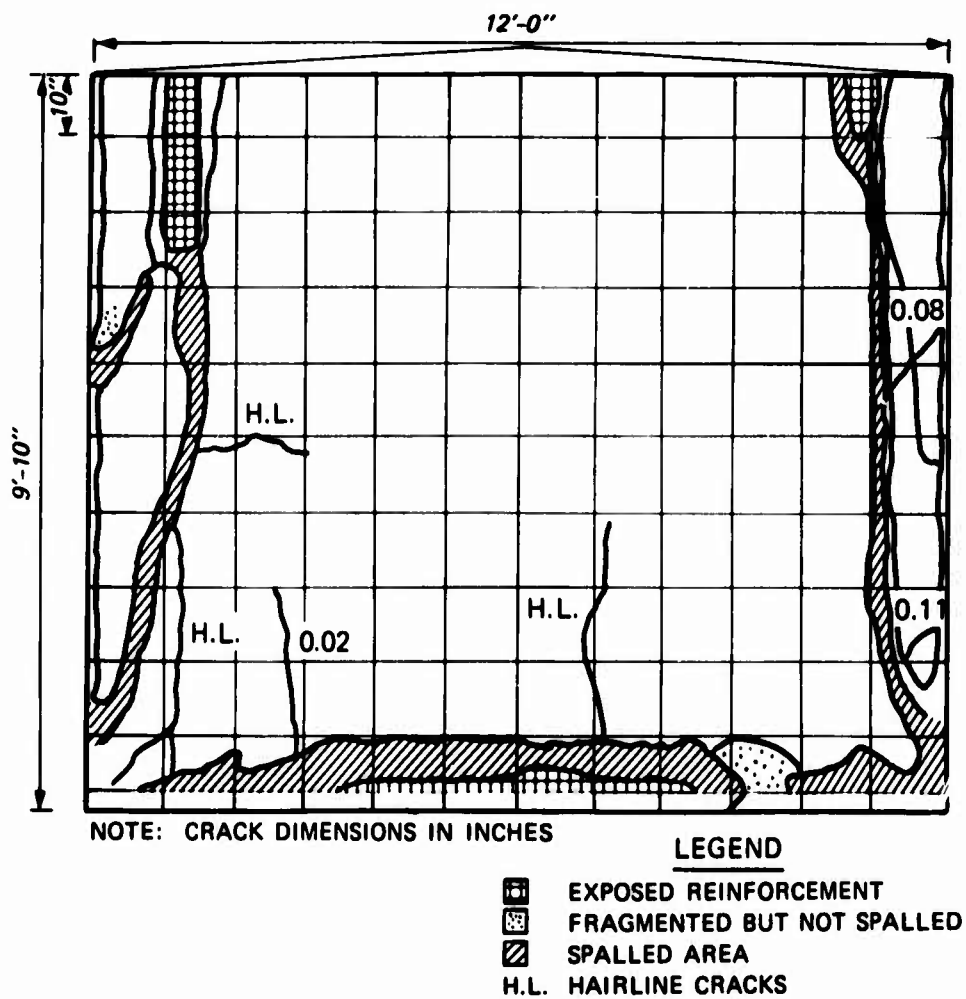
Figure 5.11. Posttest damage to south donor bay wall.

a. Overall view.
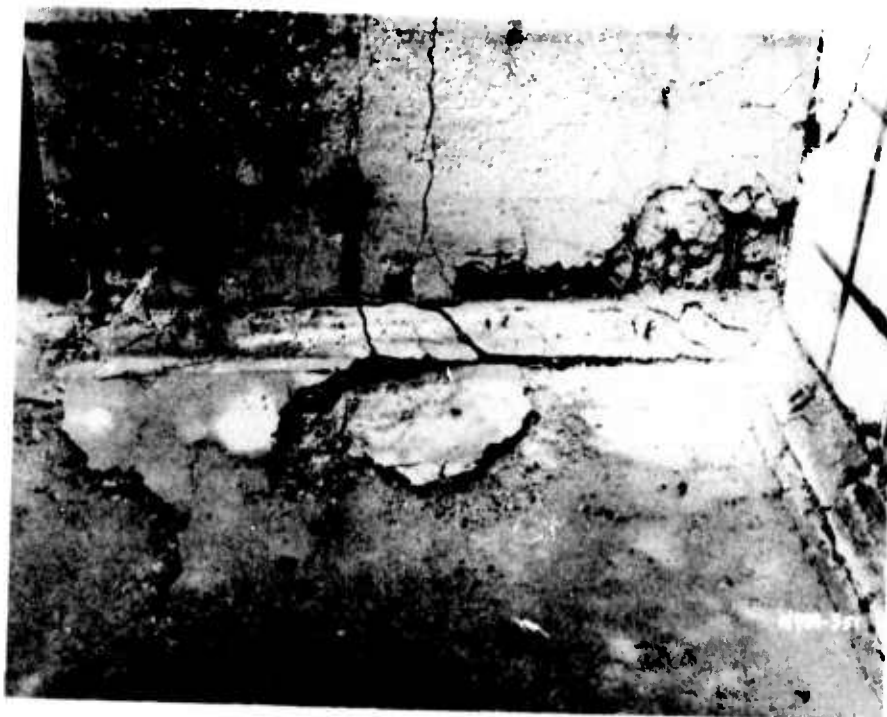
b. Damage to lower north corner.

Figure 5.12. Posttest view of west donor bay wall.

178

NOTE: CRACK DIMENSIONS IN INCHES

LEGEND

▦ EXPOSED REINFORCEMENT
▣ FRAGMENTED BUT NOT SPALLED
▨ SPALLED AREA
⊠ REBAR PULLED OUT OF CONCRETE
H.L. HAIRLINE CRACKS

Figure 5.13. Posttest damage to west donor bay wall.
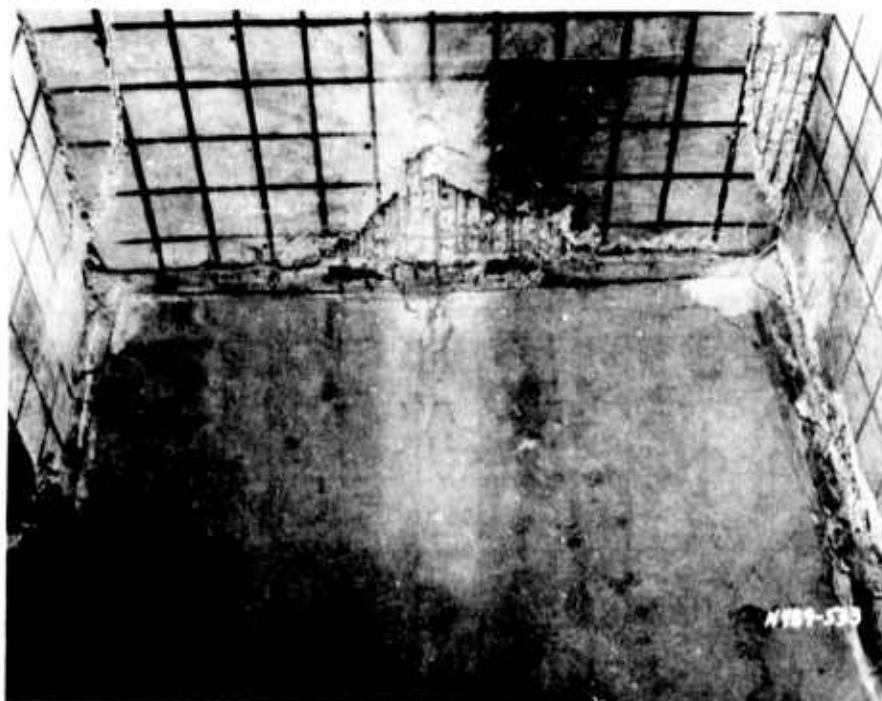
a. North end.
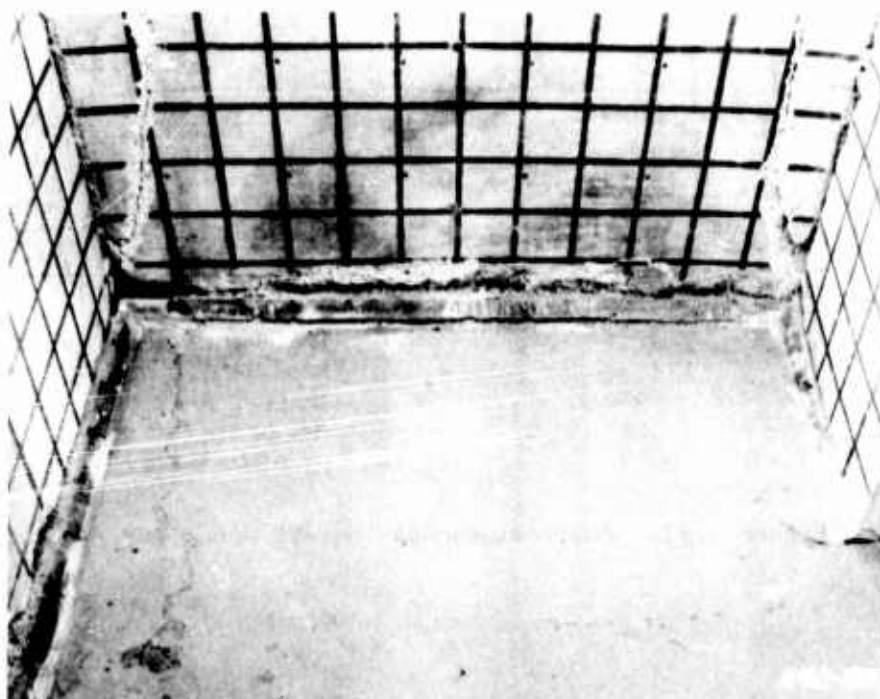
b. South end.

Figure 5.14.   Posttest view of donor bay floor
after removal of debris.
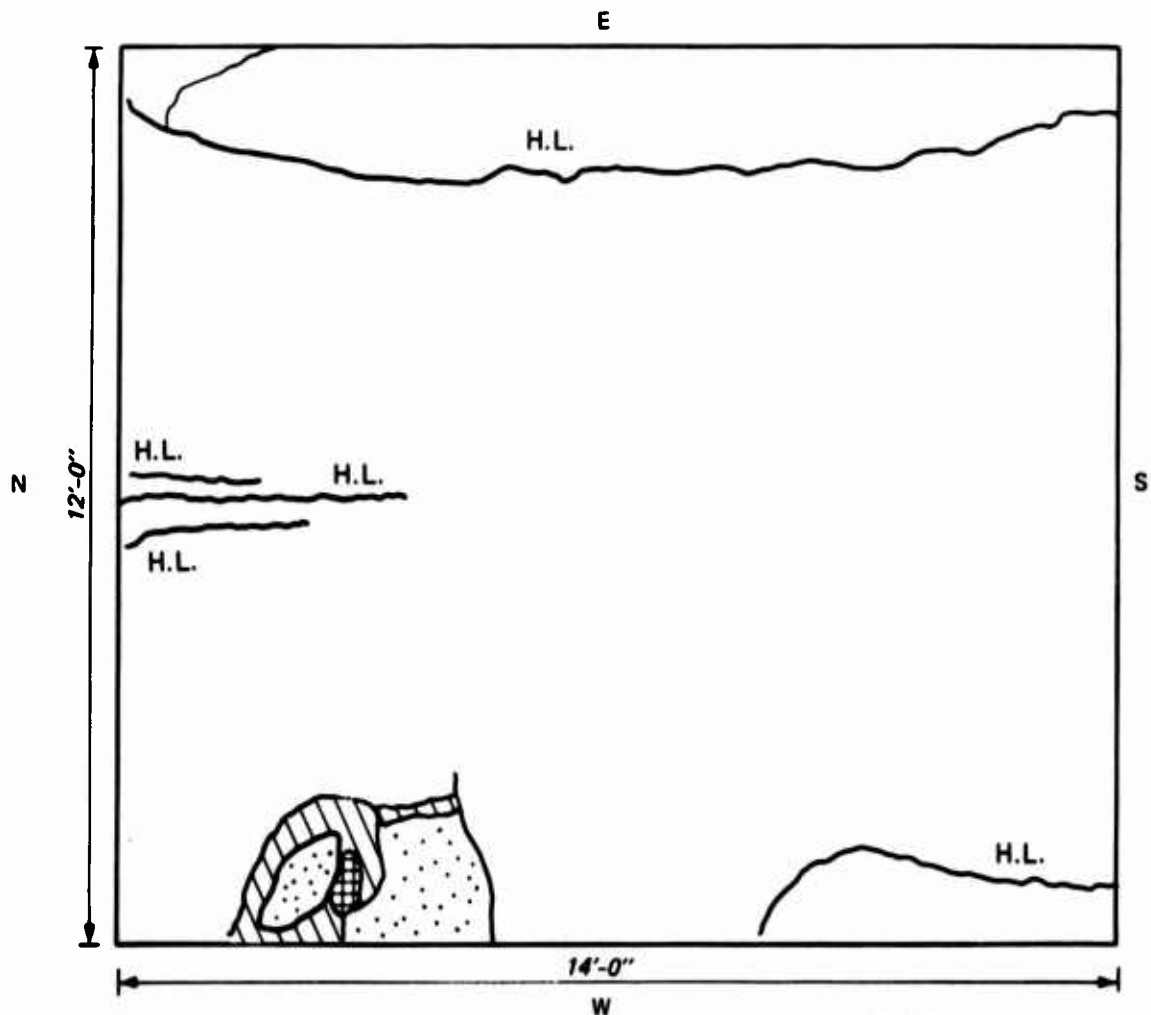
180

Figure 5.15. Posttest damage to donor bay floor.

181
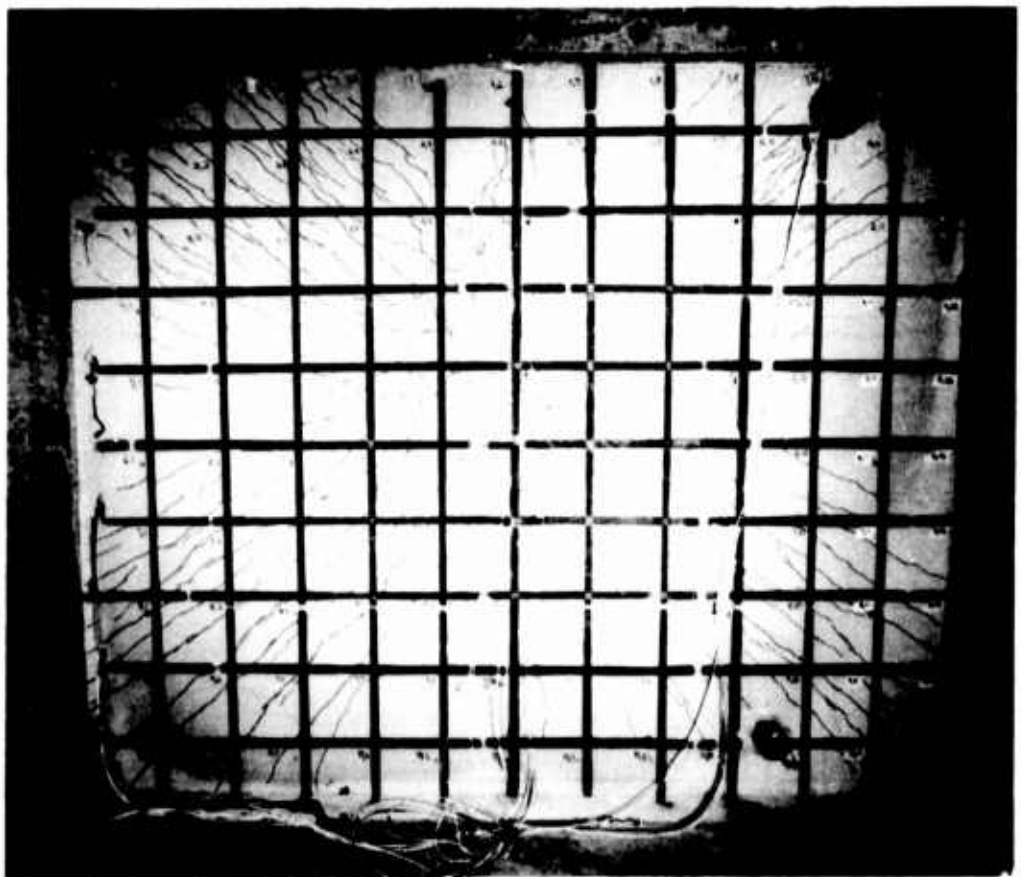
Figure 5.16.   Posttest view of cracking in acceptor bay south wall.
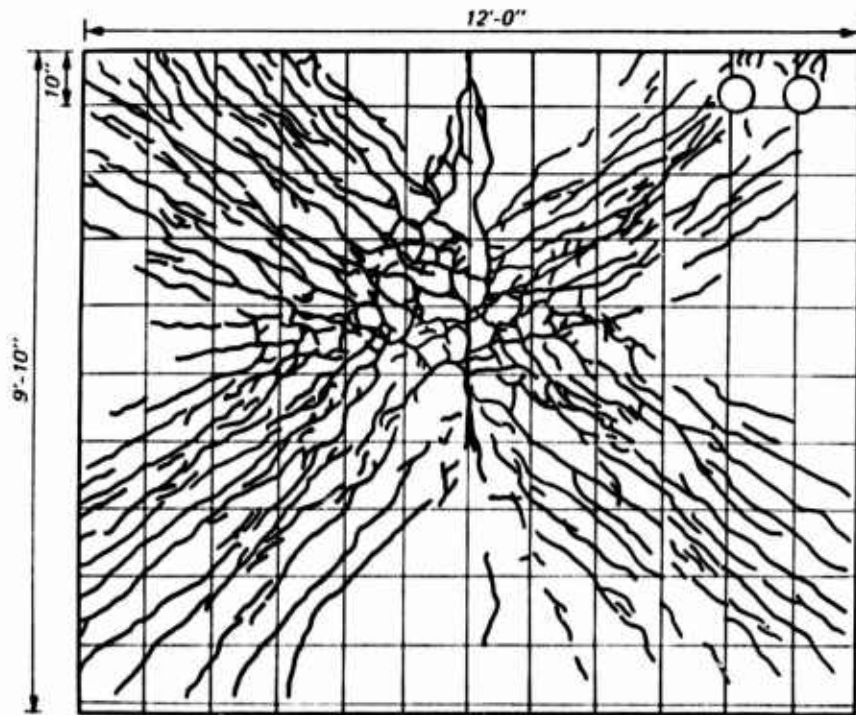
Figure 5.17. Posttest crack pattern in south acceptor bay wall.
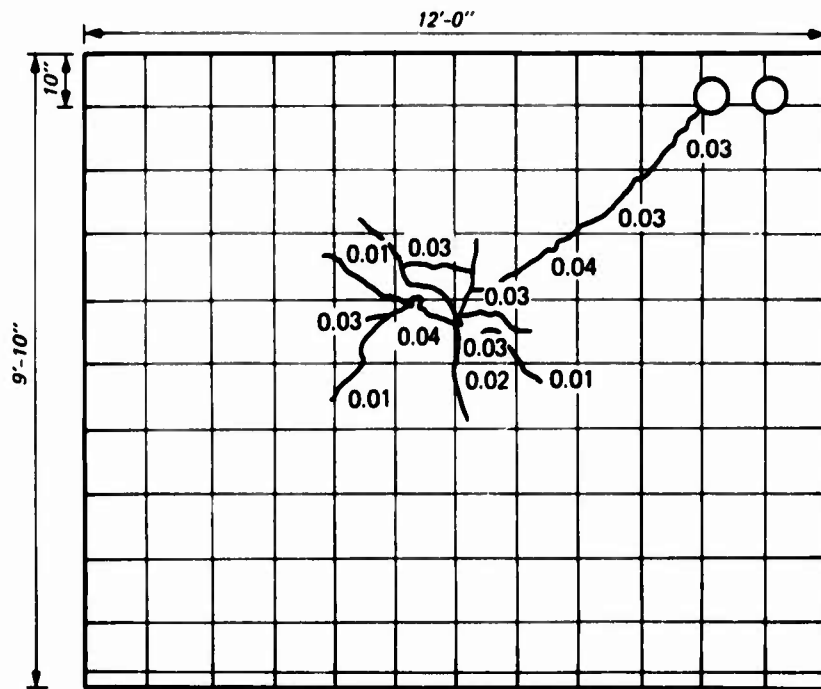
NOTE: CRACK DIMENSIONS IN INCHES

Figure 5.18. Location and size of significant cracks in south acceptor bay wall.

183
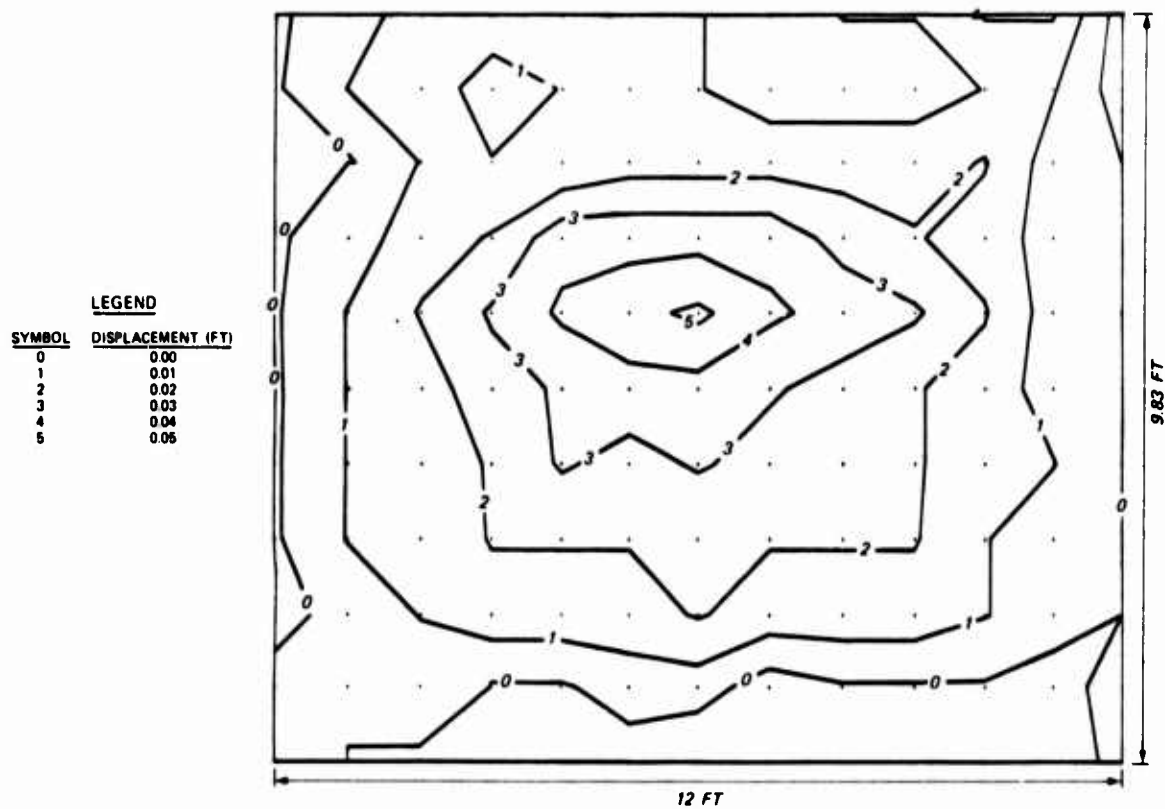
Figure 5.19.   Deflection contour map of acceptor bay south wall.
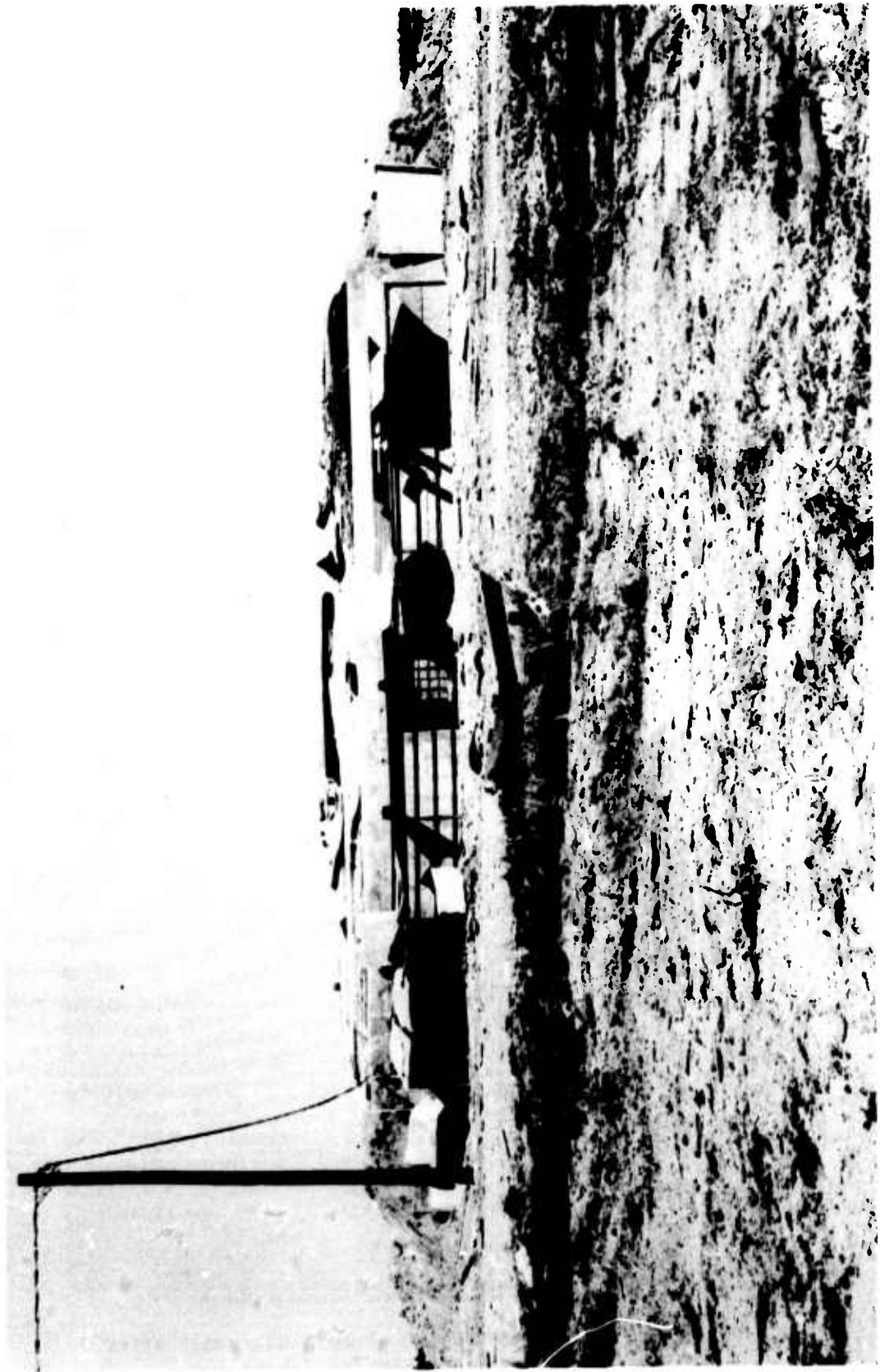
Figure 5.20. Posttest view of Phase II structure.

185
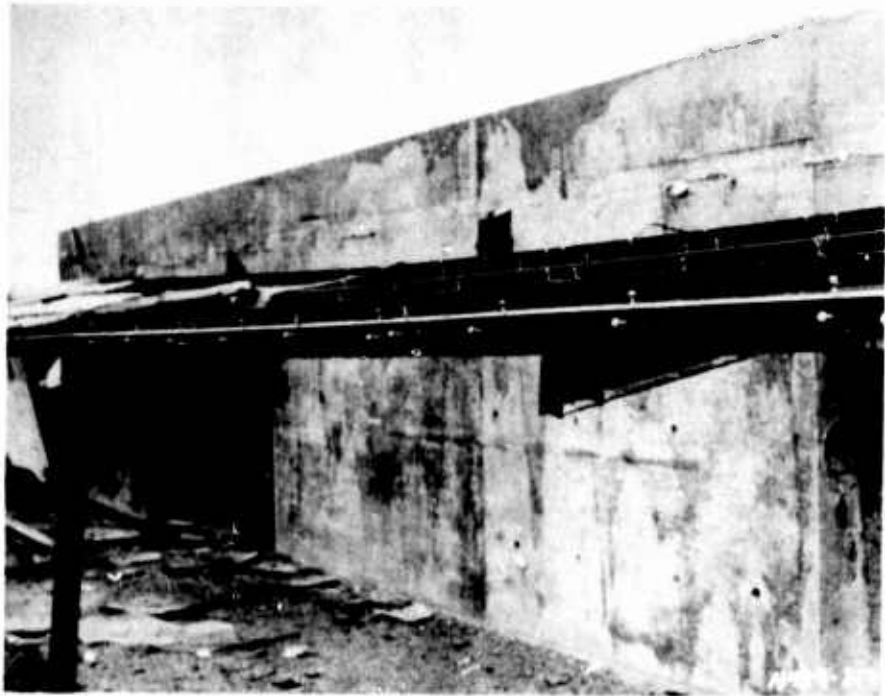
Figure 5.21.   Posttest condition of ramp.

Figure 5.22.   Posttest view of retaining wall after
removal of ramp and debris.
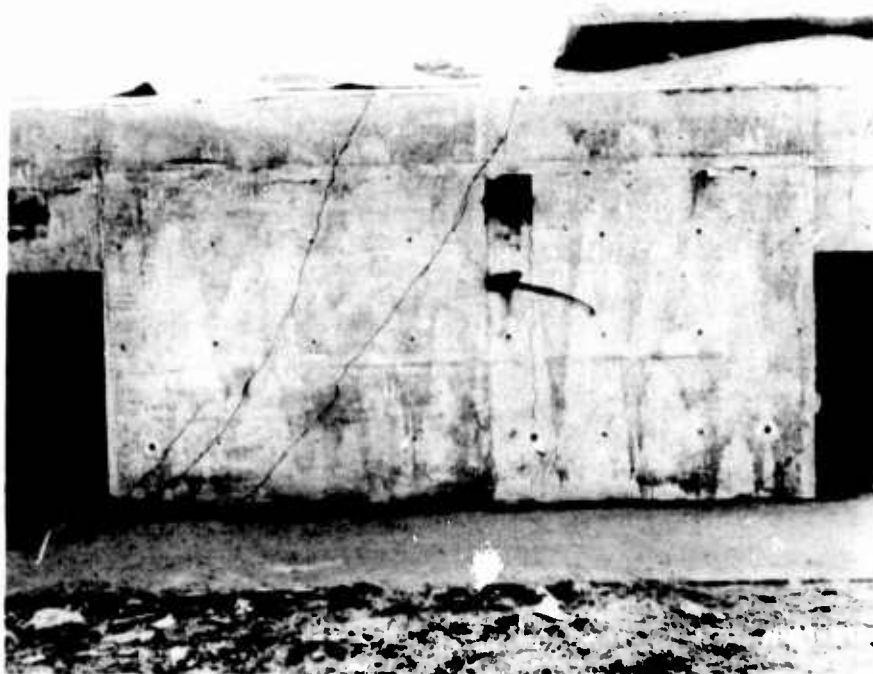
a. North of donor air lock.
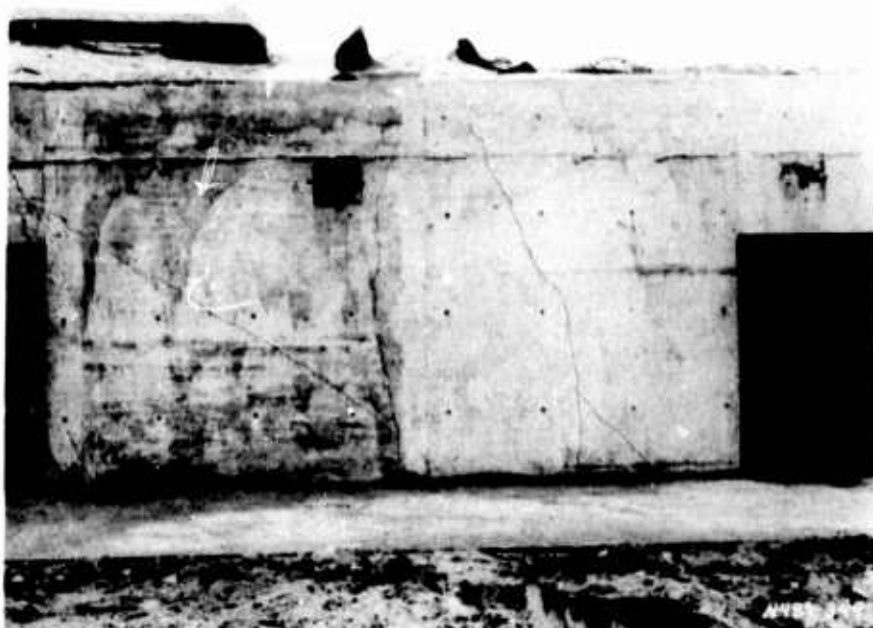
b. South of donor air lock.

Figure 5.23. Posttest cracking in retaining wall.

a. Exterior view.

b. Internal view at door bulkhead.

Figure 5.24. Damage to donor bay air lock.
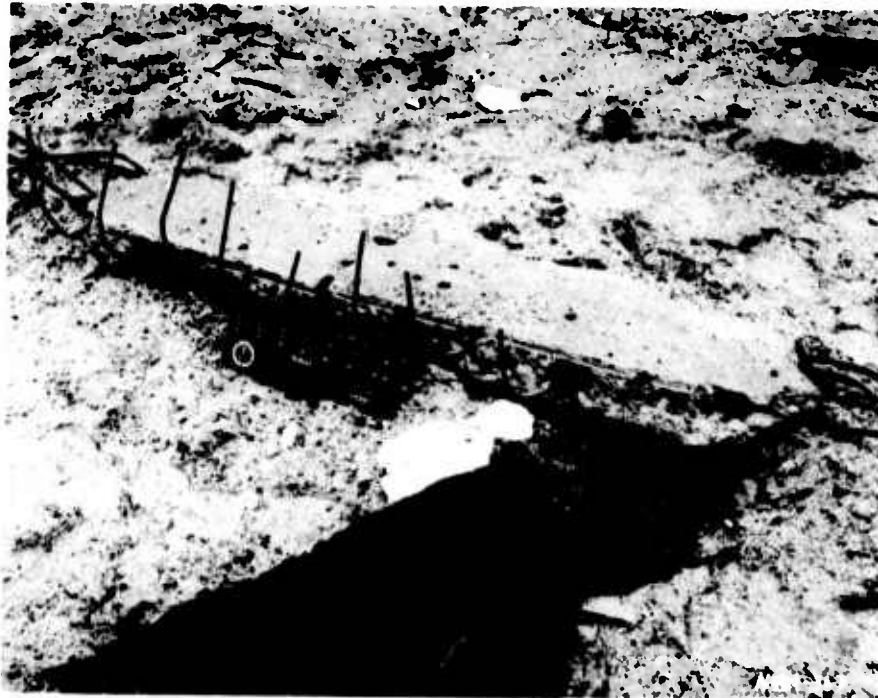
Figure 5.25.   Damage to upper part of donor bay
air-lock blast door bulkhead.
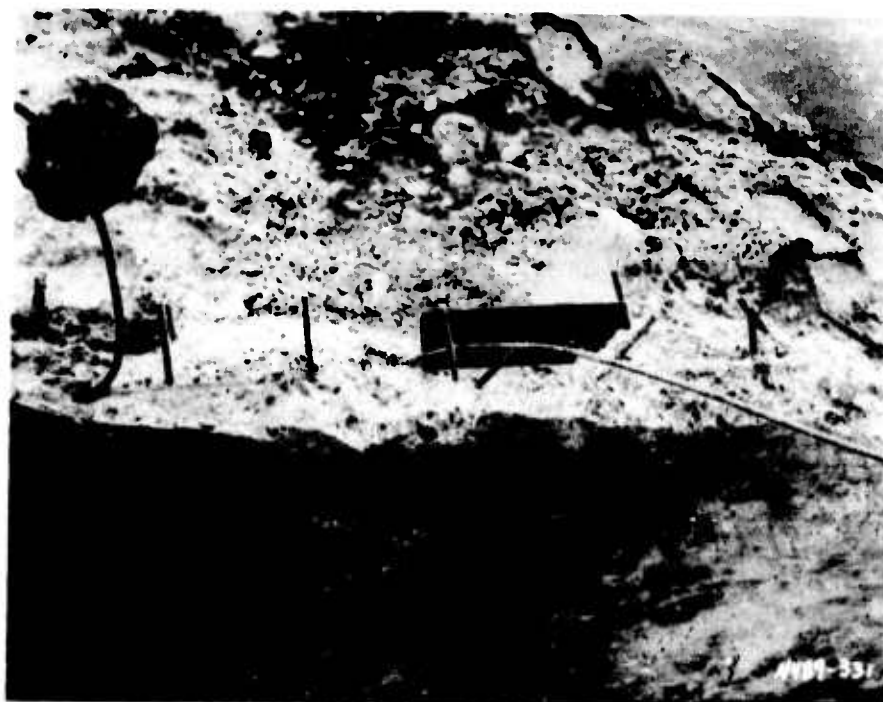
Figure 5.26.   Damage to south part of donor bay
air-lock blast door bulkhead.

189

a. Overall view.
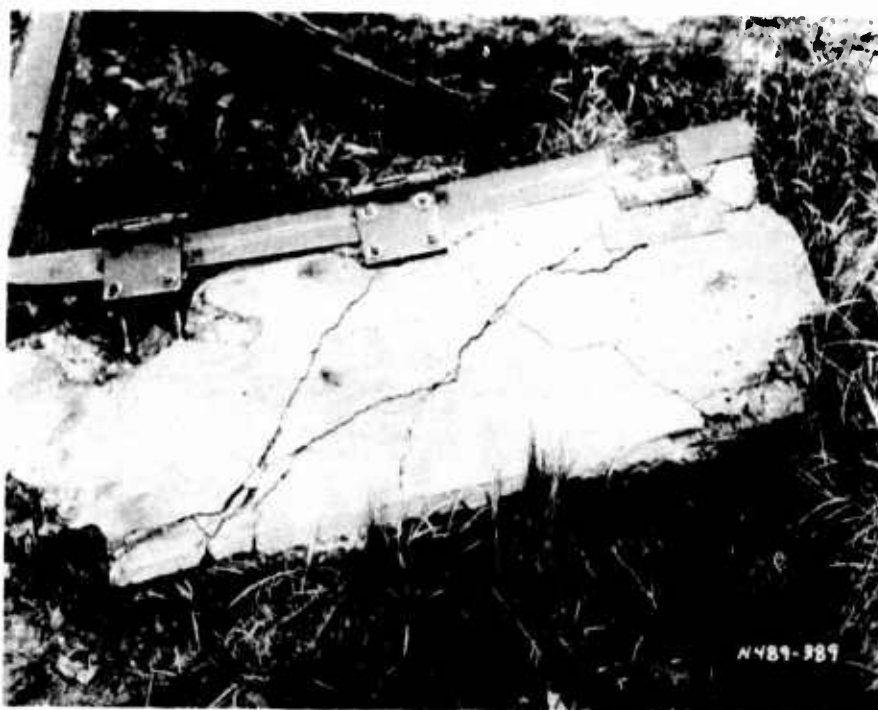
b. Detail of north side.

Figure 5.27.   Damage to donor bay blast door frame and
north part of bulkhead (Sheet 1 of 2).

c. Detail of south side.

Figure 5.27. (Sheet 2 of 2).

a.   Active leaf and ramp column.

b.   Inactive leaf.

Figure 5.28.   Posttest view of donor bay blast doors.

CHAPTER 6

DISCUSSION OF PHASE I RESULTS

6.1 VIBRATION TESTING

Comparison of frequency and damping data between the donor and acceptor bay walls shows a very good correlation both before and after backfill. This testing verifies that the stiffness of both walls was similar for excitation in the elastic behavior range.

The addition of backfill material against the walls raised the natural frequencies and increased the modal damping ratios. These trends are easily observed in a comparison of transfer functions made in the pre- and post-backfilled condition (Appendix D). Normally, backfill has little effect on frequency but does increase damping ratios. The additional stiffness added by the soil is usually offset by the added soil mass which moves with the wall. However, for the walls tested in this investigation, a 4-in.-foam layer separated the wall from the soil. The minute movements of the wall during impact excitation were absorbed in the foam rather than directly against the soil. The foam layer provided the stiffness associated with the soil, yet was very low in mass.

6.2 DONOR BAY AIRBLAST ENVIRONMENT

Pressure-time histories for the donor bay are shown in Appendix E as records BP1-5. Since three of the transducers were damaged during the test, only records from BP1 and 5 give a complete time history from charge detonation to zero pressure.

Most of the venting appeared to occur through the entrance pipe. Analysis of high-speed movies revealed that the slab blocking the entrance began to move within 12 msec of detonation and was venting significant volumes of gas by 20 msec. In contrast, the roof did not begin to vent until 61 msec. Calculations of blowdown time,[6] at which the quasistatic pressure returns to ambient, indicate that the entrance and HVAC ductwork would vent enough gas to reach blowdown time in 190 msec. Data records show blowdown times between 130 and 151 msec, indicating that the entrance is more important than the roof as a vent.

Sach's Scaling Law can be used to convert pressure data measured in the tests to pressure at sea level.[2,3] Neglecting the minor adjustments for distance and time, a good estimate of pressure can be obtained from

$$P_{sl} = \frac{(BP)_{sl}}{(BP)_{csm}} P_{csm}$$

where

P_{sl} = pressure at sea level

$(BP)_{sl}$ = barometric pressure at sea level

$(BP)_{csm}$ = barometric pressure at Camp Shelby, Miss.

P_{csm} = measured pressure at Camp Shelby, Miss.

The Phase 1 test was conducted at an uncorrected barometric pressure of 760 mm of mercury and at a temperature of 4°C. If greater accuracy is needed, then the altitude adjustment factors given in Figure 9 of Reference 2 can be used.

6.3 STRUCTURAL MODELING

The design of the donor bay was identical to that used in the prototype construction. The acceptor bay consisted of a complete wall facing the donor bay and a one-third section of a bay supporting that wall. The acceptor bay roof was not designed to vent, and the foundation was modified to resist over-turning and lateral motion. The mean 28-day concrete strength associated with the test structures is 10.9 percent less than that of the prototype. A sample of 52 concrete specimens from the prototype structure had a mean 28-day strength of 4920 psi with a standard deviation of 525 psi. The test structures had a mean 28-day strength of 4367 psi and a standard deviation of 288 psi for 44 specimens. A comparison of reinforcing steel strengths cannot be made since none of the bars in the prototype were tested during its construction.

6.3.1 Donor Bay Modeling

The use of a 9-ft-diameter corrugated metal pipe to model the entrance to the air lock created an air lock that is significantly different from that of the prototype. The prototype air lock is a rectangular concrete box section with outside dimensions of 17 ft wide and 12 ft high with 1-ft-thick sections. The concrete structure provides considerable lateral stiffness to the wall adjoining it. The corrugated pipe used on the model provided no lateral

194

stiffness to the wall. Although the prototype air lock is larger in cross-sectional area than the corrugated pipe, the actual opening into a prototype bay is 8 ft square providing a 64-sq-ft vent area. The 9-ft-diameter pipe provided a vent area of 63.6 sq ft, therefore, the corrugated pipe offered approximately the same venting area as the prototype blast doors.

The soil backfill around the south and west walls of the model was not as extensive as that of a typical prototype. Typical backfill profiles on the prototype structure are similar to those used on the north side of the model. That is, the top of the backfill is at roof level and extends to the adjacent bay. The model's south and west wall backfill extended only 2 ft away from the walls before it began to slope downward. Thus, there was less volume of earth adjacent to the south and west walls than a typical prototype bay would have.

Differences between model and prototype construction decreased the relative stiffness of the model bay. Thus, the damage sustained by the model donor bay should be more severe than that which would occur in a prototype structure. The additional stiffness contributed by a concrete air lock would have reduced the damage and rotation experienced by the east wall. The corresponding decrease in wall deflections and rotations would have minimized edge damage to the north wall.

6.3.2 Acceptor Bay Modeling

The primary objective of placing the acceptor bay in the Phase I experiment was to investigate the adequacy of the wall to withstand soil pressures generated by an explosion in the donor bay. Results of the vibration tests verify that the acceptor bay wall accurately represented the elastic stiffness of a typical bay wall. The acceptor bay foundation was designed to prevent overturning or rotation, but the total mass of the acceptor bay was slightly less than one half the mass of a typical bay. Also, the backfill around the acceptor bay was significantly less than the restraining condition surrounding a typical bay in the Building 12-64 complex. These conditions will combine to reduce the total impulse, but not the peak pressure, on the acceptor bay wall, increase rigid body motion of the acceptor bay, and decrease structural damage to the acceptor bay wall. Because structural response is accurately modeled in the Phase II experiment, the magnitude of these effects can be evaluated by comparison with Phase II test results.

195

6.4 DONOR BAY BEHAVIOR

6.4.1 Roof Behavior

Several mechanisms were involved in the donor bay roof failure. The reinforcing steel was not continuous at the center line. Thus, as it was designed to, the roof behaved as two cantilever beams. The maximum bending and shear forces due to blast pressure occurred where the roof was connected to the east and west walls. The explosion produced a relative deflection of about 2.5 ft between the east and west walls. The movement at the tops of the walls produced tensile stresses in the area that joined the roof to the walls. The No. 10 bars in the outer face of the roof reinforcement were spliced to No. 10 dowels that joined the roof to the east and west walls. Once the concrete cracked and spalled away due to combined tensile and shear forces, the splice was not strong enough to allow the roof to remain attached to the structure and fold over. Therefore, the splice failed and the two roof leaves were projected intact to the east and west of the donor bay. The fact that less than 6 percent of the No. 10 dowels broke indicates that they possessed sufficient ductility to allow the roof to fold over if the bar splices had not failed. The failure plane at the top of the walls was along a 45-deg angle. The No. 5 dowels on the inside face joining the roof to the east and west walls were pulled out of either the wall or the roof without developing the ultimate strength of the bars.

One of the principal objectives of the Phase I test was to investigate the behavior of the hinged roof. Differences between model and prototype construction had, at most, a minor effect on the total impulse imparted to the roof and on the response of the roof leaf attached to the west wall. However, the additional stiffness provided by a concrete air lock to the east wall, and the resulting decrease in response of the east wall, may have prevented the roof leaf attached to the east wall from disengaging. In every case, differences between prototype and model donor bay construction were conservative from the point of view of evaluating its design.

6.4.2 Fragment Distribution

The most serious fragment hazards to the individual bay roofs and air locks were the two roof slab fragments. Each fragment weighed approximately 46,000 lb and had a kinetic energy of 1.93×10^6 ft-lb at the time of impact.

196

Whether or not these fragments would actually impact on another bay depends
upon the orientation of the donor bay with respect to the acceptor bays.

Data from the test were used to calculate the probability of a roof frag-
ment impacting on an adjacent bays. The distances from the center of the
donor bay to the center of the lines of the roof slab impact were 104.6 ft and
105.3 ft (Figure 4.7). Lines from the center of the bay to the centers of
each line of impact formed angles of 4.83 and 14.47 deg with respect to the
center line through the east and west walls. Both slabs impacted to the north
of this center line, but SL engineers assumed that the slab could have im-
pacted on either side of the center line. From these data, they calculated
the probabilities of impact, assuming that the centroids of major roof frag-
ments will impact within a sector which has a radius of 105.5 ft and an in-
cluded angle of 29 deg. The vertex of this sector is the center of a donor
bay. The center line of the sector (the line which bisects the included angle)
is coincident with the bay center line which bisects the two walls connected
to the roof with reinforcing steel.

Once the probable impact area was established, SL personnel performed an
analysis of Building 12-64 to determine which assembly bay roofs would produce
the greatest hazard to adjacent bays due to accidental explosion. Assembly
bays 1-9 and 11-17 would project roof fragments along axes perpendicular to
each row of bays. Figure 6.1 shows the probable impact areas associated with
roof fragments from bay 3. Portions of the roof and air lock of bay 12 which
lie within the impact area have been shaded. The ratio of the shaded areas of
the bay and air lock to the total area of the impact sector is the probability
of the centroid of a major roof slab fragment impacting on the clear span of
an adjacent bay roof or air-lock roof. For all bays except bay 10, the proba-
bility of a roof impact is 0.247 and the probability of an air-lock impact is
0.160.

The roof orientation on assembly bay 10 is opposite those of the other
bays. Figure 6.2 shows the fragment impact areas associated with this bay.
Since two bay roofs fall within the impact area, the probability of hitting a
bay roof has increased to 0.536 while the probability of hitting an air-lock
roof has decreased to 0.041. Figures 6.1 and 6.2 show that only one of the
major roof slab fragments from a donor bay presents a hazard to adjacent bays.
While it is possible for the other fragment to impact on the donor bay air lock
(except bay 10), this is not considered significant since the explosion oc-
curred in that bay.

The other fragments from the donor bay were much less significant than the two major parts of the roof. A count of all fragments weighing more than 100 lb reveals that 24 landed in grid E and quadrant E while 33 landed in grid W and quadrant W (see Figures 4.7 and 4.8). Large pieces of the HVAC penthouse slab were broken off during the event, and a total of seven pieces weighing between 188 and 750 lb impacted in quadrant N (see Figures 4.7 and 4.8). Since the superstructure and mechanical equipment of the penthouse were not modeled, it is difficult to predict their influence on fragment production.

An additional concern for fragment hazards is the possible injury to persons in the open. Fragments of the size of the majority of fragments produced in this test would cause severe injury or death.

6.4.3 Wall Behavior

The internal loading of the donor bay produced large displacements of the walls, particularly near the top. These lateral displacements were accompanied by opening of the corners and the formation of hinge mechanisms near the corners in both north and south walls. Posttest measurements of wall rotations show that the east wall rotated approximately four times as much as the south and west walls. The volume of backfill against this wall was much less than that of the south and west walls. In addition, the metal entrance pipe was in the east wall, which decreased both the wall's strength and the volume of the soil adjacent to the wall.

The failure of the north wall involved several damage mechanisms. The explosive charge undoubtedly produced cracking and spalling of concrete near the bottom of the wall. The outward displacement of the wall due to internal pressure occurred simultaneously with the movements of the other walls. Thus the edges of the wall experienced inelastic rotation combined with tension. At some point in the loading or rebound cycle the wall broke away from the rest of the structure and fell back inside the bay.

6.5 ACCEPTOR BAY BEHAVIOR

6.5.1 Structural Loads

The acceptor bay was loaded by two phenomena: the initial detonation pressure wave and the quasistatic pressure within the donor bay. The initial P wave arrived at soil stress gage SS3 approximately 11 msec after detonation and reached the acceptor bay wall at interface pressure gage IP5 within 28 msec

(see Figures 2.2, 2.3, and 2.4). The arrival of the first P wave produced pressures on the order of 15 to 20 psi at locations IP2, IP5, and IP8 and is characterized by a relatively short rise time. The effects of loading produced by quasistatic pressure are much more gradual and do not reach maximum levels until at least 85 msec. Peak pressures ranged from 16 psi at IP3 to 71 psi at IP5. Maximum impulse varied from 8.1 psi-sec near the center to 1.9 psi-sec at the bottom corner.

6.5.2 Structural Behavior

The acceptor bay wall deflection records show an initial excitation at 28 msec, which corresponds to the P wave time of arrival at IP5. From 28 msec to 58 msec, the motion of the wall was characterized by a gradual increase of deflection. Deflections increased sharply from 58 msec to their peak at 130 msec.

The crack pattern and posttest deflections show that the acceptor bay wall responded in a flexural mode. This is consistent with the load distribution measured on the face of the wall. There was no indication of a punching shear failure.

Airblast transmission through the HVAC ductwork was insignificant. A peak pressure of 2.2 psi was measured in the acceptor bay ductwork (see Figure 2.5) with a maximum impulse of 0.0492 psi-sec. Since the volume of the ductwork is small compared with the volume of the bay, internal pressure change was negligible.
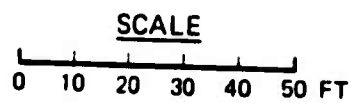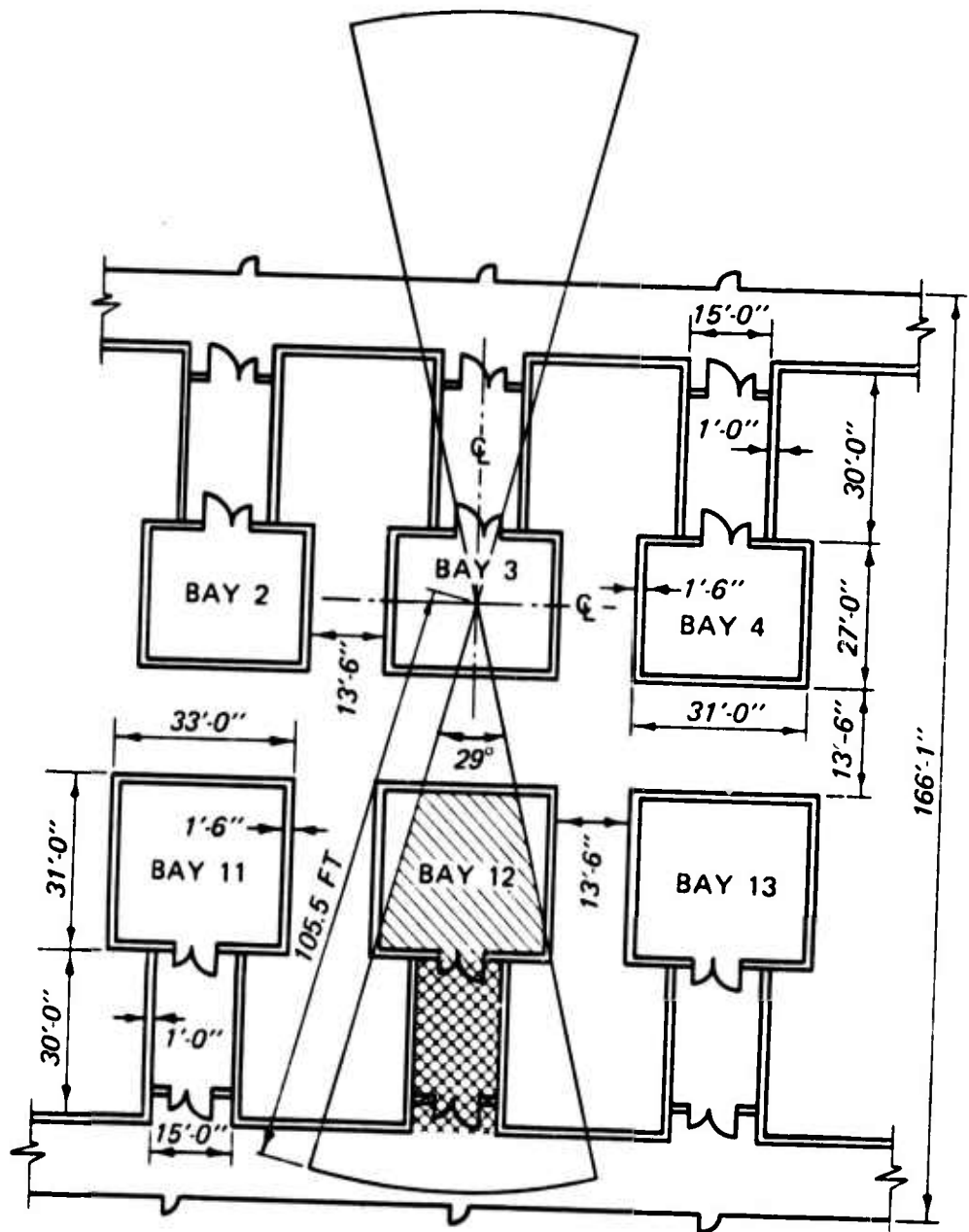
Figure 6.1. Probable impact zone for roof of bay 3, Building 12-64.
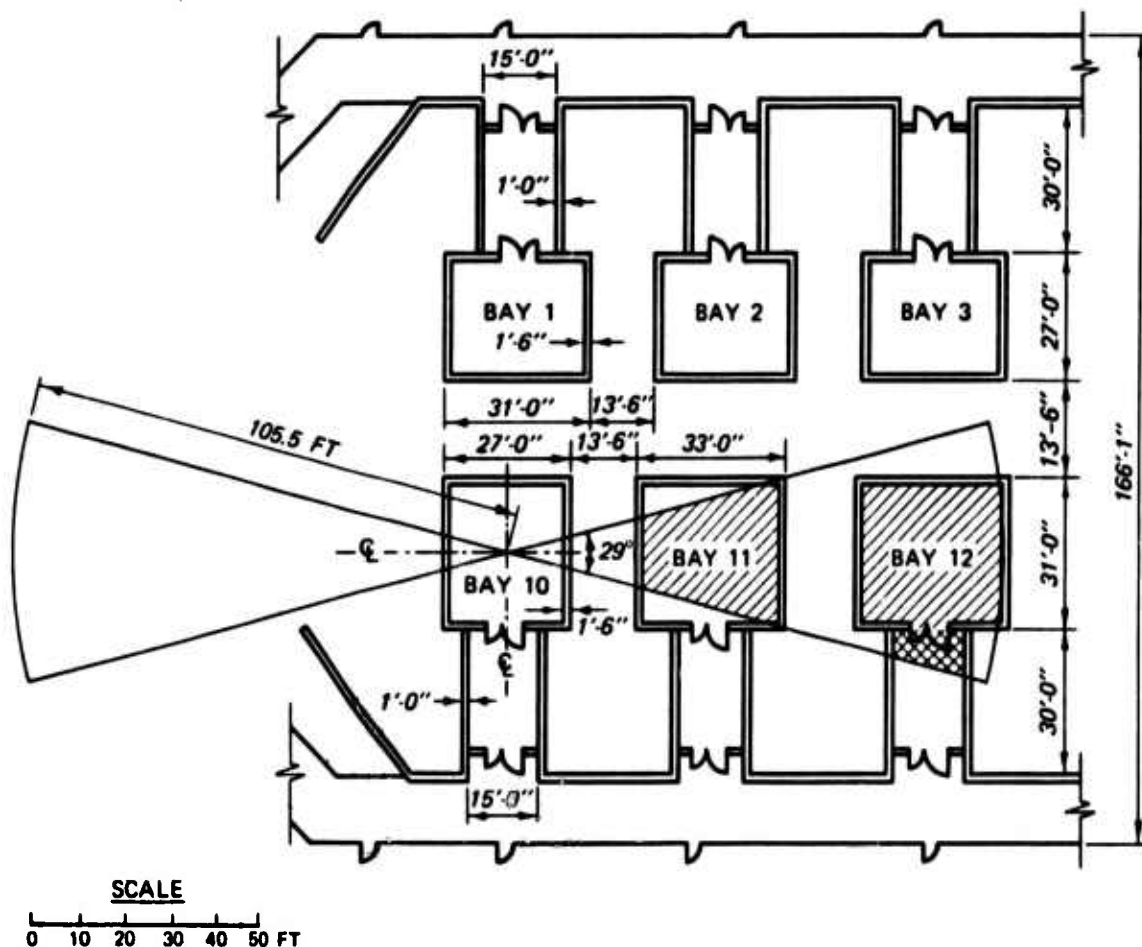
Figure 6.2. Probable impact zone for roof of bay 10, Building 12-64.

CHAPTER 7

DISCUSSION OF PHASE II RESULTS

7.1 VIBRATION TESTING

Comparison of frequency and damping ratio data for the donor and acceptor bay walls shows a good correlation both before and after backfill. Deviation of measured frequencies from a mean value was less than 4.6 percent for the first four modes both before and after backfill. Thus the similarity of mass and stiffness distribution in the two walls was verified.

The addition of backfill material dramatically increased the modal damping ratios and produced an upward shift in the measured frequencies. These trends can be observed in a comparison of transfer functions produced both before and after backfill material was added (Appendix F). Normally, the addition of soil to a structure increases the damping but has little effect on the natural frequencies.[7] The additional stiffness added by the soil is compensated by the added soil mass which moves with the wall. Because of the 2-in.- foam layer which separated the wall from direct contact with the soil very little additional mass effect was observed. The foam is relatively stiff, yet light in weight. Thus the foam layer provided additional stiffness but contributed very little additional mass to the wall as it moved.

7.2 AIRBLAST ENVIRONMENT

Airblast pressure measurements were examined to determine the blast pressure environments in and on various components of the Phase II structure. Discussion of results is focused on particular parts of the structure. Sachs's Scaling Law, given in Section 6.2 above, can be used to convert measured test pressures to pressure at sea level. The air temperature and barometric pressure at the time of the Phase II test were 12.2° C and 757 mm of mercury, respectively.

7.2.1 Donor Bay

Pressure-time histories were recorded in the donor bay by transducers BP12-14 (see Figures 3.1, 3.2, and 3.3). A peak pressure of 1706 psi was recorded at the center of the bay floor. Peak pressures of 817 and 1067 psi were recorded at the center of the east and south walls, respectively. Peak

impulses varied from 3.714 to 4.823 psi-sec. Blowdown times, i.e. times from detonation to return to ambient pressure, ranged from 67.5 to 74.1 msec at various blast gage locations.

The major portion of the donor bay venting occurred through the air lock, not the roof. Analysis of high-speed photography showed that the blast doors began venting within 20.5 msec after detonation, but the roof did not begin to vent significant quantities of gas until about 49 msec. Calculations of blowdown time using References 7 and 8 indicate that the air lock and HVAC ductwork alone would provide enough vent area to reach blowdown time within 92 msec. To achieve the blowdown times obtained during the test requires an average of only 28 percent more area than is provided by the blast doors opening into the air lock.

7.2.2 Ramp

Blast pressures in the ramp area were measured on the retaining wall at transducers BP9-11 (Figure 3.1). The initial pressure pulse reached BP11 at 12.9 msec and had traveled to BP10 and BP9 by 16.7 and 23.3 msec, respectively. Peak pressures varied from 27 psi at BP11 to 51 psi at BP10 back to 17 psi at BP9. BP11 was located near the intersection of the donor air lock and the retaining wall (Figure 3.1). The apparent reason for lower pressures and impulses being measured at BP11 than at BP10 was the gas dynamics effects associated with the sudden change in geometry near BP11.

7.2.3 Acceptor Air Locks

Blast pressures were measured in both north and south acceptor air locks. Pressure records for the north air lock are from BP5-8, while those for the south air lock are from BP15-20 (Figure 3.1). The north air lock modeled a situation in which the first set of blast doors leading to a bay was closed. The south air lock represented the inverse, where the outer doors would be open and the inner doors closed.

Pressures on the floor of the entrances to the air locks were measured at BP8 and BP15. Comparison of these records shows similar times of arrival and a similar magnitude of the initial pressure peak of approximately 12 psi at 32 msec. Between 32 and 36 msec, BP15 shows a decay in pressure, while BP8 recorded another pressure spike of 16 psi at 33 msec. This behavior is attributed to the reflection of the pressure wave off the closed blast door at BP8.

The maximum pressure at both of these transducers was recorded at about
37 msec. The wave form of this spike corresponds to the pressure spike re-
corded at 35 msec on the wall of the air lock (BP7). Thus, the peak pressure
recorded at BP8 and BP15 corresponds to the reflection of the pressure wave
off the air-lock wall. The larger pressure and impulse recorded at BP8 is at-
tributable to the reflection of pressure off the blast doors at that location.
In the portion of the airblast records after 38 msec, BP7 and BP8 exhibit a
different behavior than BP15. Once the peak pressure had been reached at the
entrance to the north acceptor air lock, the pressure decayed, exhibited a
negative pressure phase, and returned to ambient with relatively few reflec-
tions. At the south acceptor air lock, the airblast record indicates a rather
complex behavior produced by pressure waves traveling into the air lock, re-
flecting off the closed end, and traveling back to the entrance.

Peak pressures recorded within the south acceptor air lock were 11.1 psi
at the midpoint and 18.6 psi at the end of the air lock representing the
closed blast doors. Pressures measured at floor level were approximately
15 percent lower than those recorded at the midheight of the walls. All of
the records exhibited a complex pattern of reflections within the air lock.
During the 200 msec of data displayed in Appendix G, two distinct cycles of
positive and negative phase pressure are observable. Times of arrival varied
from 36 to 41 msec with the end of the first positive pressure phase occurring
between 63 and 69 msec. The first negative pressure phase lasted until
107 msec. The second positive pressure phase occurred between that time and
138 msec, with the second negative pressure phase lasting until 175 msec. At
200 msec all records were in a third positive pressure phase; however, by that
time pressures had attenuated and were near ambient.

Pressures recorded within the north acceptor air lock showed relatively
small positive pressures from about 11 msec until 51 msec at which time a net
negative pressure existed until about 73 msec. From 73 msec, pressures again
became positive and the peak pressure of 1.1 psi was recorded at 89 msec.
Comparison with records obtained in the acceptor bay and outside the blast
doors indicates the source of these pressure changes. The initial pressure
rise can be attributed either to pressure leakage through the HVAC ductwork
into the acceptor bay and the air lock or noise or a combination of both. At
the south end of the air lock, peak blast pressure reached the blast doors at
about 33 msec. The pressure impacted both doors against the door frame and,

on the rebound, the active leaf opened after the peak shock occurred. Pressure records obtained near the doors showed a negative pressure phase between 45 and 66 msec. Thus the negative pressure phase recorded inside the air lock was caused by leakage of pressure from the air lock through the open active leaf of the blast door. At the end of the negative pressure phase, air was drawn back into the air lock producing positive pressures. This effect explains how the peak positive pressure in the air lock occurred well after the peak pressures were recorded in other parts of the building.

7.2.4 Acceptor Bay

The peak positive pressures recorded in the acceptor bay were produced by pressure leakage through the HVAC ductwork. A peak pressure of 2.5 psi was recorded in the ductwork at 25.5 msec. The pressure remained positive until about 80 msec and then remained negative through 200 msec. Peak pressures measured on the bay walls were 1.1, 0.9, 1.9, and 2.7 on the north, south, east, and west walls, respectively. Times of arrival at the transducers varied with their distance from the ductwork opening. Net positive pressure was maintained in the bay until approximately 78 msec. Pressures were then vented through the ductwork and the air lock.

7.2.5 Acceptor Bay Roofs

Pressures were recorded at roof level to the east and south of the donor bay roof. All of the records were characterized by three phases. From the time of arrival to about 40 msec the records show relatively high-frequency traces associated with blast leakage from the HVAC ductwork in the donor bay. The records then display a positive pressure phase followed by a negative phase with a return to ambient pressure. The durations of these phases are somewhat different for each transducer location. The peak pressures associated with blast leakage through the ductwork were on the order of 1 to 2 psi. Peak pressures over acceptor bay roofs caused by venting of the donor roof were on the order of 1 to 1.5 psi and occurred from 55 to 72 msec after detonation. Peak impulses ranged from 0.013 to 0.023 psi-sec. These low response values confirm the observation that by the time the roof vented, most of the pressure in the donor bay had been vented through the air lock.

205

7.3 STRUCTURAL MODELING

The modeling of all forces acting on a structure subjected to blast load-ing requires that inertia, gravity, and elastic forces be correctly reproduced in the model. Since these forces scale differently in the model it is impos-sible to scale all of the forces in the same model. The modeling of the Phase II structure satisfies Cauchy's condition since the ratio of inertia forces to elastic forces is constant in the model and the prototype. Gravi-tational effects are not correctly scaled. Gravity forces will have only a negligible effect on structural load and response, but will effect fragment distribution.

The Phase II structure was constructed as a half-scale model of a portion of Building 12-64. The donor and acceptor bays, the three air locks, and the retaining wall and ramp are geometrically and structurally similar to Build-ing 12-64. The scaling relations between physical quantities of the Phase II model and the prototype are listed in Table 7.1.

7.3.1 Donor Bay Modeling

The fundamental difference between the expected performance of the model and prototype donor bays concerns the roof and simulated acceptor bays. As previously mentioned, gravity forces do not scale; thus the weight of the model roof and associated soil cover was too light. Since the opening and disengagement of the roof is a dynamics problem, the inertia of the roof is far more important in its performance; however, the resulting fragments will be brought back to earth by gravity and their distribution will not be prop-erly scaled.

The soil backfill surrounding the donor bay was confined on the north side by the acceptor bay and on the west side by the retaining wall. In the prototype, soil on the east and south sides is also confined by the other ac-ceptor bay walls which were not modeled in Phase II. The presence of the other two bays would have helped confine the soil against the east and south walls and increase their stiffness to some degree. Thus, damage to the walls of the model would be expected to be at least as severe as that expected in a prototype.

7.3.2 Acceptor Bay Modeling

The acceptor bay was identical in construction to the donor bay. The

206

soil between the donor and acceptor bays modeled the mass and stiffness of the prototype soil. Soil around the other three sides was placed to model the mass of the corresponding prototype material. Resistance of the bay to rigid body sliding is developed by the frictional resistance of the foundation, passive earth pressures on the bay, active earth pressure developed as the bay moves into the soil behind it, and inertial forces. Since frictional and passive earth pressure forces are functions of gravity as well as soil properties, these resistance forces are less than those existing in the prototype. However, active earth pressures and inertial effects are appropriately scaled. Thus rigid body sliding of the model should be slightly greater than the scaled displacement of a prototype bay. Sliding relaxes soil pressures acting on a wall facing a donor bay. But since the response time of the wall is much faster than the rigid body response of the bay, the structural damage caused by ground shock generated by an explosion in a donor bay can be accurately scaled from results in the scale model test.

7.4 DONOR BAY BEHAVIOR

Blast pressures from the explosive charge caused the opening of the roof, disengagement of the blast doors and their bulkhead from the air lock, and produced significant damage to the bay walls. The separation of the east section of the roof slab produced a large high-energy fragment capable of producing serious damage to any structure it hits. The kinetic energies of missiles produced by the separation of the donor blast door assembly from the air lock and the fragmentation of the HVAC penthouse slab are much lower than the kinetic energy of the roof.

7.4.1 Roof Behavior

Several mechanisms were involved in the donor bay roof failure. The roof slab was not reinforced at its center line; thus the east and west parts of the slab behaved as two cantilever beams spanning the distance from the walls to the center line. Maximum bending and shear forces due to internal pressure occurred where the roof was connected to the east and west walls. At the same time the roof was being moved upward, internal pressure was pushing the bay walls apart. Wall movement would also produce tensile forces at the connection between the walls and the roof.

There are two essential differences between the east and west sides of

207

the donor bay. The west wall was provided with considerable lateral stiffness by the air-lock structure. Posttest observations of crack patterns and wall deflections give an indication of the degree of restraint provided. Another difference is the presence of the air-lock opening itself and its effect in changing the blast pressure environment from one side of the bay to the other. However, there was no pressure gage on the west wall to quantify any differences in blast pressures between the east and west sides of the bay.

It is the opinion of the authors that the additional stiffness provided to the west wall by the air lock was the critical difference between the performance of the east and west parts of the roof slab. The restraint of movement near the top of the west wall minimized tensile cracking of the concrete covering the lap splice between the roof steel and dowels. This allowed the splice to develop enough force to retain the west portion of the roof slab.

7.4.2 Roof Fragment Distribution

All of the fragments produced by the breakup of the donor bay roof landed on the east side of the structure. The major roof fragment weighed approximately 4195 lb and impacted with an energy of 182,970 ft/lb. Since the scaled values of these figures are significantly higher, it is evident that the release of the roof constitutes a major hazard to adjacent structures. The other fragments from the roof were much smaller and less energetic. Interface pressures and impulses measured over the simulated acceptor bay roof slabs were very low.

The fragments torn from the HVAC penthouse slab impacted on the north side of the structure. While only a few fragments were produced, their size and range were significant. It is probable that the mechanical equipment housed in the prototype penthouses would also produce fragments in the event of an accidental explosion.

7.4.3 Wall Behavior

The donor bay walls exhibited a flexural response to the internal pressures produced by the explosion. Although the walls employed unlaced reinforcement without stirrups, there was no punching shear failure. Significant cracking and joint rotations occurred at the corners and at the hinge mechanisms which formed in the north and south walls. The formation of hinge mechanisms in the north and south walls rather than in the east and west walls is

208

due to differences in reinforcing steel. The north and south walls have 27 percent less horizontal steel area and 37 percent less vertical steel area than the east and west walls.

The air lock added considerable lateral stiffness to the west bay wall. The posttest deflections and wall crack patterns give an indication of the extent of the restraint provided. This is believed to be a key factor in the successful retention of the west portion of the roof slab.

7.4.4 Air Lock and Blast Doors

Airblast pressures in the donor air lock were not measured. However, certain aspects of the pressure distribution can be addressed. Peak pressures in the air lock were probably lower than those measured in the bay since the distance from the explosive was greater and the opening in the bay is constricted in comparison with the area of the air lock. However, since most of the quasistatic pressure was vented through the air lock, gas pressure and impulse were probably of the same order of magnitude as those measured in the bay.

The bulkhead holding the blast doors and frame failed in shear where it joined the air-lock walls, roof, and floor. The active leaf obviously opened quickly since there was relatively little pressure damage to the door. On the other hand, the inactive leaf was restrained from opening very quickly by the bolts which locked it into the floor and the doorframe. The door was severely damaged and was resisting blast pressure with membrane action. As the door bowed outward, the edges of the door and the bolts rotated laterally and enlarged the holes in the doorframe and floor. The door eventually enlarged these holes enough to open without shearing the locking bolts. Since the inactive leaf remained closed longer than the active leaf, more load was transmitted to the south side of the doorframe than the north side. This probably explains why the south portion of the bulkhead separated from the doorframe while the north portion did not. Both doors separated from the doorframes by breaking the hinge straps at the hinges.

The complete destruction of the bulkhead and door assembly produces a significant fragment hazard to personnel, vehicles, and structures located in line with the axis of the donor air lock. Since gravity forces do not scale, the scaled distances from the air lock to the points of impact of the various fragments are longer than one would expect for prototype behavior. While

pieces of the bulkhead and doorframe impacted relatively close to the donor air lock, the two door leaves traveled from 412 to 507 ft from their initial position. The initial speed of the doors could not be directly measured from the high-speed photography because they were obscured by dust and debris produced by the explosion. At a distance of approximately 30 ft from the ramp, one of the doors emerged from the dust cloud. The average of its speed, taken from two different camera locations, was 382 fps.

7.5 ACCEPTOR BAY BEHAVIOR

Data recorded from electronic transducers were used to determine the characteristics and magnitudes of loads and the response of the acceptor bay to these loads. Airblast data were examined to assess the loads resisted by the acceptor bay blast doors.

7.5.1 Structural Loads

Loading of the acceptor bay was produced by two effects: the compression or P wave produced by the explosion and the compression of soil between the donor and acceptor bay by the structural deflections of the donor bay. Pressure-time histories of the soil-stress transducers show a highly damped oscillatory pressure history for the first 50 msec and then a gradual pressure decay from about 50 to 100 msec. The pressures associated with the P wave and its reflections between the two bays account for the initial pressure oscillations. The pressure associated with donor bay deflections was a much slower phenomenon. The first 50 msec of the records are a superposition of the two mechanisms. After 50 msec, the reflections of the P wave had been attenuated. By this time gas pressures in the donor bay were falling and the donor bay walls were rebounding causing a decay in soil pressure. Soil pressures returned to zero pressure approximately 30 msec after blast pressures in the donor bay returned to ambient.

Interface pressure transducers on the face of the acceptor bay walls recorded the arrival of the initial pressure wave at approximately 8 msec. Peak pressures were recorded at gages IP5 and IP6 (Figure 3.1) near the center of the wall at approximately 34 msec. With the exception of IP9 which reached peak pressure at 44 msec, all other pressure gages recorded peak pressures at about 55 msec. Values of peak pressure ranged from 72.7 psi at IP4 to 23.6 psi at IP3. Impulses varied from a high of 3.81 psi-sec to 1.28 psi-sec

at the same two locations. The total time duration of the soil pressures on the wall was from pressure duration or time zero.

Interface pressure transducers IP10 and IP11 on the east simulated acceptor roof slab (Figure 3.1) recorded peak pressures on the order of 2 psi with a total positive impulse of approximately 0.04 psi-sec. Both records show definite positive and negative pressure phases. Airblast data over the slabs contained peak pressures of 1.3 psi and peak impulses at 0.014 psi-sec. Differences in peak interface pressure impulse versus airblast pressure impulse recorded at BP21 and BP22 are attributed to soil and roof fragments which fell onto the surface of the simulated roof and to measurement error. Shock spectra for acceleration records A1 and A2 are shown in Appendix H.

The interface pressure data records IP12, IP13, and IP14 recorded on the south simulated acceptor bay roof slab (Figure 3.1) show peak pressures between 7.4 and 1.3 psi with peak impulses varying from 0.11 to 0.04 psi-sec. Corresponding airblast data from records BP27 and BP28 show a peak pressure of 2.1 psi and a peak impulse of 0.015 psi-sec. Differences in peak impulses are also attributed to the energy of soil and debris impacting on the roof slab and measurement error. Shock spectra for the A3 acceleration record are listed in Appendix H.

7.5.2 Wall Behavior

Accelerations and deflections of the acceptor bay south wall were recorded at the center line of the wall at elevations of 5 and 7.5 ft from the floor (see Figures 3.1, 3.2, and 3.3). These locations correspond to the center and quarter point of the wall. Data records for A1 and D1 were recorded at the center and A2 and D2 at the quarter point.

The acceleration record at the center of the wall shows three distinct positive acceleration spikes. The initial acceleration measured at 8.1 msec corresponds to the time of arrival of the initial pressure wave at the interface pressure transducers. Positive accelerations of 10, 6, and 42 g's were measured at 9.3, 19.2, and 32.0 msec, respectively. The deflection at the center showed a very slow increase between 13 and 28 msec, and then a more rapid increase until a peak displacement of 1.37 in. was reached at 62.3 msec. Deflections then decreased to a posttest value of 0.48 in.

The acceleration and displacement measurements at the quarter point showed the same qualitative behavior as the records at the center. Peak

211

positive accelerations of 10.4, 5.6, and 28.7 g's were obtained at times of 10.7, 19.2, and 34.3 msec. Wall deflection increased gradually from 14 to 33 msec then increased rapidly to 1.14 in. at 63.8 msec. A permanent deflection at 0.35 in. was recorded.

Posttest inspection of wall deflections and crack patterns indicated flexural behavior. No indications of a shear failure could be detected.

7.5.3 Rigid Body Motion

Horizontal acceleration and displacement of the acceptor bay floor are shown in records A3 and D6 (Figures 3.1, 3.2, and 3.3). A peak acceleration of 11.4 g's was recorded at 39.0 msec. A peak displacement of 1.17 in. was recorded at 98.0 msec. Posttest permanent displacement was 0.79 in.

7.5.4 Blast Door Performance

While the blast pressure on the acceptor bay blast doors was not directly measured, pressure levels recorded at BP7 and BP8 (Figures 3.1, 3.2, and 3.3) indicate peak reflected pressure and impulse values on the order of 45 psi and 0.14 psi-sec, respectively. Pressure records inside the air lock show that the doors were effective in preventing positive pressure leakage into the air lock. However, posttest inspection of the doors found the active leaf in the open position. The pressure impact on the leaf and subsequent rebound sheared a 1/4-in. bolt used to hold the door shut. Use of the bolt simulated the resistance to opening provided by a pneumatic door opener on the prototype. It is not known whether the prototype mechanism would allow the door to open as the result of an impulsive load. Blast damage to the doors was limited to minor indentation of the door skin plate.

The south acceptor air lock represented a situation in which the outer blast doors are open and the inner doors to the bay are closed. Peak pressures of 46 psi were recorded at the center of the door location with peak impulses of 0.114 psi-sec.

Table 7.1. Phase II model scaling relations.

Physical Quantity	Symbol	Scaling Relation*
Length	L	$L_p = 2 \, L_m$
Time	t	$t_p = 2 \, t_m$
Frequency	f	$f_p = f_m/2$
Force	F	$F_p = 4 \, F_m$
Pressure	p	$P_p = P_m$
Impulse	I	$I_p = 2 \, I_m$
Acceleration	a	$a_p = a_m/2$
Velocity	V	$V_p = V_m$
Displacement	d	$d_p = 2 \, d_m$

* p = prototype, m = model.

CHAPTER 8

COMPARISON OF PHASE I AND PHASE II TEST RESULTS

8.1 VIBRATION TESTING

The natural frequencies of the donor and acceptor bay walls were averaged for each phase of testing and are listed in Table 8.1. Since the Phase II bays were half-scale models of the prototype, their frequencies must be halved for comparisons with full-scale data. The scaled comparisons of the Phase I and II data in Tables 8.1a and b show an average difference of 19 percent for frequencies measured before backfill but only 5 percent difference for frequencies measured after backfill.

The large difference in scaled frequencies between the two test phases in the unfilled condition was examined to find possible explanations. Since the same experimental technique was used to excite the structures in both phases, the Phase II bays received four times the scaled force that was used to excite the Phase I structure. It is possible that the impulses used to excite the Phase II bay walls were strong enough to excite a mode in the bays with a frequency lower than those associated with the walls alone. The purpose of the dynamic tests was to measure the frequencies associated with the appropriate north or south bay wall and not to measure the frequencies of the bay as a whole. Thus it is not possible to conclusively verify this belief from available data. However, comparison of data from the two test phases lends credibility to this idea.

The peak magnitudes of the transfer functions obtained during the Phase II prebackfill tests did not occur at the lowest frequencies shown in Tables 5.1 and 8.1a, but at the second frequencies listed in these tables. If the assumption is made that the second frequency listed in Table 8.1a is the lowest frequency associated with the Phase II bay walls, comparison with Phase I frequency data (extreme right column) falls more in line with comparison of postbackfill data. The difference in average scaled frequencies shrinks from 19 to 2 percent. The increase in damping associated with the postbackfill tests probably eliminated the influence of any modes not associated with the walls from those tests.

The dynamic testing of the bays verified the similarity of the donor and acceptor bay walls in each phase and also verified the scaling of wall

214

properties between the two phases. The tests provided a quality control check of geometric, material, and construction similarities.

8.2 DONOR BAY BEHAVIOR

8.2.1 Blast Environment

The three airblast transducers in the Phase II donor bay, BP12, 13, and 14, were in a location similar to BP5, 4, and 1 in the Phase I donor bay. Table 8.2 is a comparison of peak pressures, scaled impulses, and scaled time of peak values recorded with those instruments. Comparison of the scaled values is expressed as the ratio of the Phase II value to the Phase I value. The average and standard deviations for the ratios are also presented.

The average of peak Phase II pressures was 17 percent higher than those for Phase I. The pressure measured on the floor of the Phase II bay was lower than the corresponding Phase I value while the pressures measured on the walls were higher in Phase I than in Phase II. Peak pressures were recorded an average of 5 percent sooner in Phase II than in Phase I. The average of peak impulses recorded in the Phase II bay was 10 percent higher than the average Phase I peak impulse. Since BP4 was destroyed during the Phase I test, comparison for this transducer was made at a time prior to failure. The impulse value for BP13, the corresponding transducer in Phase II, was obtained at the same scaled time as that used for BP4. Peak impulse was reached only 1 percent faster in Phase II than in Phase I.

Comparison of donor bay airblast data shows that the Phase II explosive charge generated higher peak pressures and impulses than the Phase I charge. However, comparison of times of arrival and times of peak pressures and impulses shows a close correlation which would be expected due to the geometric similarity of the bays and charge locations. The similarity of the scaled times to reach peak impulse (or zero ambient pressure) shows that venting occurred at approximately the same rate in both donor bays.

8.2.2 Wall Response

In general, the damage mechanisms in the two donor bays were similar, but the magnitude of the damage was greater in the Phase I bay. The separation and collapse of the north wall and the large rotation of the east wall did not occur in the Phase II test. Posttest displacements between the east and west

215

walls of the two bays are compared in Table 8.3. The average scaled Phase II displacements were 37 percent of the average Phase I values at the middle of the walls and only 9 percent of Phase I displacements at the top. Since the relative locations of the bay entrances were reversed, the east wall of the Phase I structure should be compared with the west wall of the Phase II structure and vice versa. The north and south walls are directly comparable.

Damage to the north walls of the two bays can be compared using Figures 4.11 and 5.6. Both walls experienced cracking at the corners and the development of hinge mechanisms a small distance from each corner. But the large displacements of the walls in the Phase I structure produced much more severe damage and resulted in the collapse of the wall.

The east wall of the Phase I bay also experienced more displacement and damage than the corresponding west wall of the Phase II bay. Damage can be compared using Figures 4.16 and 4.17 versus Figures 5.8 and 5.9. The east Phase I wall suffered a large outward rotation with subsequent separation of reinforcing steel near the bottom of the wall. When most of the earth backfill was removed from the wall during site clean up, it collapsed outward under its own weight. The west Phase II wall did not exhibit such serious damage. The presence of the air lock added considerable lateral support to the Phase II wall which was not present in the Phase I structure. The mid-height displacements in the center of the Phase II bay were smaller than those measured at the ends. The corresponding Phase I measurements show the opposite trend.

Damage to the south and west walls of the Phase I donor bay is very similar to the damage to the Phase II south and east bay walls. South wall damage can be compared using Figures 4.14 and 4.15 for Phase I and Figures 5.10 and 5.11 for Phase II. The formation of hinge mechanisms and cracking at the corners are very similar. The southeast corner of the Phase I wall was more heavily damaged in the Phase I bay due to large rotation of the east wall. The posttest condition of the west Phase I wall and the east Phase II wall can be compared using Figures 4.16 and 4.17 versus Figures 5.8 and 5.9. The crack and damage patterns are similar.

The use of a corrugated metal pipe to model the concrete air-lock structure and the omission of a retaining wall significantly altered the behavior of the Phase I donor bay walls in comparison with the Phase II structure. The Phase II structure provided a more accurate model of the total stiffness of

Building 12-64. Thus, the damage to the Phase II donor bay is more represen-
tative of the damage to be expected in a prototype bay.

8.2.3 Roof Response

The most significant difference between the behavior of the roof in the
two phases was the separation of both east and west parts of the roof in
Phase I while only the east part of the Phase II roof separated from the bay
to produce missiles. The scaled size and the velocities of the major roof
fragments were similar in both test phases. However, the fragment distribu-
tion from the Phase II test is not comparable with the Phase I results since
gravity was not scaled in the Phase II test. Note that fragment velocities
were determined using high speed film from impact velocities. Neglecting air
drag forces, initial fragment velocity magnitudes should be the same as impact
velocity magnitudes. The retention of the west part of the Phase II donor
roof is attributed to additional stiffness provided to the west wall by the
air-lock structure. The restraint of movement near the top of the west wall
minimized tensile cracking of the concrete covering the lap splice between
the roof steel and dowels from the walls. This allowed the splice to develop
enough force to retain the west portion of the roof slab.

The probability of major portions of a donor bay roof impacting on adja-
cent bays has been discussed in Section 6.4.2. The Phase II test showed that
the section of the roof adjacent to the air lock may not separate from the bay
to become a missile. However, Figure 6.1 shows that the section of the roof
adjacent to the air lock does not present a threat to other bays in Build-
ing 12-64 even if it is released. Therefore, the probability of hit values
developed in Section 6.4.2 are still applicable. The retention of half of the
roof does reduce the missile threat to other buildings and personnel in the
open. Since the roof of bay 10 is oriented differently than those of the
other bays, the air lock does not stiffen either of the walls to which the
roof is attached. Thus both parts of the bay 10 roof would probably be re-
leased in an accidental explosion as shown in Figure 6.2.

8.3 ACCEPTOR BAY BEHAVIOR

8.3.1 Acceptor Bay Loads

Soil pressures acting on acceptor bays were measured between the bays and

217

on the face of the acceptor bay wall. Four soil stress transducers were placed halfway between the donor and acceptor bays to measure free-field soil pressures. A total of nine interface pressure gages measured pressures on the acceptor bay south wall. The transducer designations correspond to approximately the same locations in both phases. The soil stress instruments' locations were exactly scaled, but there were differences in the elevations of the interface pressure transducers. All of the interface pressure transducers in Phase II were located at higher scaled elevations than those of Phase I as specified in the test plan (see Figures 2.4 and 3.2).

A comparison of peak pressures and the elapsed time to peak pressures is presented in Table 8.4. A similar comparison of peak impulses and associated times is presented in Table 8.5. The comparisons are in the form of ratios of scaled Phase II quantities to those of Phase I. Average values of the ratios and associated standard deviation are also listed.

Pressures and impulses recorded for the Phase II soil stress transducers are 70 and 153 percent higher, respectively, than the Phase I values. The times at which the peak values were obtained vary only 7 percent between the two phases. The consistently higher values may be partly attributed to higher average pressures and impulses generated in the Phase II donor bay. However, the majority of the difference is believed to be caused by experimental error associated with the soil stress gages. The pressure registrations of these instruments are a function of placement, distance from pressure source, and the medium in which the gages are placed. Even under controlled laboratory conditions, registration differences of 25 percent between gages in the same approximate location are not uncommon.[9] Field conditions and differences in donor bay pressures certainly increased registration differences.

Comparisons of average values of pressures, impulses, and the time of peak values show that higher peak interface pressures were developed in Phase II but for a shorter duration than those of Phase I. The average scaled impulse values are only 3 percent higher for Phase II than for Phase I. Peak pressures at transducers IP1-3, 6, and 9 were higher in Phase II than in Phase I. Conversely, peak pressures for gages IP5, 7, and 8 were lower in Phase II. Specific Phase II peak pressures varied from 24 percent below Phase I peaks at IP5 to 94 percent above Phase I peaks at IP9. Peak impulse values followed the same trends as the pressure values except that IP2 had a lower scaled impulse in Phase II. Scaled impulses for Phase II varied from

218

41 percent below Phase I at IP5 to 52 percent above at IP9.

The average variation in pressures and impulses between the two phases was fairly consistent. Specific pressure variations between individual transducers were much greater. One significant difference in the acceptor bay behavior between the two phases was the rigid body displacement of the bays. Comparing scaled rigid body displacements, the Phase II acceptor bay translated 29 percent less than the Phase I bay. Because the Phase II bay was effectively "stiffer" than the Phase I bay, passive soil arching was undoubtedly greater. Passive arching becomes a factor when a structure is stiffer than the surrounding soil. Blast pressures acting around the periphery of the bay were "arched" onto the relatively stiff structure, particularly the edges of it. This phenomenon would explain the increased pressures at IP1 and 2 and, to a smaller degree, the increased pressures at IP3, 6, and 9.

Another significant difference in the performance of the two test phases was the behavior of the donor bay north wall. In the Phase I test, the north wall broke away from the rest of the bay. The increased flexibility allowed the wall to displace farther into the soil than the more restrained Phase II wall. This would cause higher pressures near the center of the Phase I acceptor bay which is consistent with data measured at IP5, 7, and 8.

8.3.2 Acceptor Bay Response

Only two electronic data measurements for the acceptor bays are directly comparable between the Phase I and Phase II tests. Channel D1 was used in both phases to measure the midspan displacement of the south wall. Channel D3 in Phase I and D6 in Phase II were used to measure the translation of the acceptor bay floor. The scaled peak displacement at the center of the south wall (facing the donor bay) was 35 percent greater in Phase II than in Phase I. Scaled rigid body translation of the Phase II acceptor bay was no more than 71 percent of the Phase I value. Comparison of electronic and physical posttest measurements in Phase I indicate that the peak displacements electronically measured in that phase may have been less than the actual displacements. Posttest displacements of the acceptor bay wall are listed in Tables 4.11 and 5.6. Displacement contours drawn from these data are presented in Figures 4.21 and 5.19. The scaled posttest displacements for Phase I are less than half of those recorded in Phase II. While the peak Phase I displacements were only 74 percent of the scaled Phase II values, there is still a large discrepency.

One possible explanation is the difference in the behavior of the north donor
bay wall which collapsed during the Phast I test. This may have influenced
the posttest displacements of the Phase I acceptor bay wall. A qualitative
comparison of the damage similarities in the two phases can be seen in the
crack patterns in Figures 4.19 and 5.17. The patterns in both figures are
typical of a flexural behavior mode.

The modeling of the Phase I and II acceptor bays has been discussed in
Sections 6.3.2 and 7.3.2. In general, the Phase I acceptor bay was less re-
sistant to rigid body translation than the Phase II acceptor bay. Much of the
difference between the displacements of the two walls can be attributed to
this fact. The average impulse recorded to the face of both bays was approx-
imately the same. However in Phase I, more energy was dissipated in rigid
body movement of the bay than in Phase II. Thus, the Phase II bay suffered
more wall damage than in Phase I. Since the Phase II structure more closely
modeled the features of the prototype, displacements and damage recorded in
that test phase are considered to be more representative of prototype behavior.

Table 8.1. Comparison of natural frequencies for Phase I and II bay walls.

a. Frequencies before backfill.

| Frequency No. | Phase I | | Phase II | | Phase II Frequency 2 × Phase I Frequency | Phase II Frequency (n + 1)* 2 × Phase I Frequency (n) |
	Average Frequency Hz	Standard Deviation σ	Average Frequency Hz	Standard Deviation σ		
1	48.31	0.16	85.02	2.71	0.880	1.054
2	58.47	4.92	101.87	2.23	0.871	1.048
3	82.65	0.18	122.56	2.59	0.741	0.958
4	104.44	4.80	158.35	1.74	0.758	--
					Avg 0.813	Avg 1.020
					σ 0.063	σ 0.044

b. Frequencies after backfill.

| Frequency No. | Phase I | | Phase II | | Phase II Frequency 2 × Phase I Frequency |
	Average Frequency Hz	Standard Deviation σ	Average Frequency Hz	Standard Deviation σ	
1	63.94	2.56	124.35	0.80	0.972
2	81.36	1.73	160.72	2.54	0.988
3	101.31	0.75	195.81	0.85	0.966
4	118.99	4.72	211.56	2.32	0.889
					Avg 0.954
					σ 0.038

* This comparison was made with the assumption that the lowest comparable frequency for the Phase II bays before backfill was 101.87 Hz.

Table 8.2. Donor bay airblast comparison.

a. Peak pressure.

Transducer Location	Phase I			Phase II			Ratio of Phase II Quantity to Phase I	
	Transducer	Peak Pressure psi	Time of Peak msec	Transducer	Peak Pressure psi	Time of Peak msec	Pressure	Scaled Time of Peak
Center of floor	BP1	2323.4	0.74	3P14	1705.5	0.35	0.734	0.946
South wall	BP4	794.7	3.84	BP13	1066.80	1.77	1.342	0.922
Wall opposite air lock*	BP5	571.3	3.28	BP12	817.28	1.62	1.431	0.988
							Avg 1.169	0.952
							Std deviation 0.310	0.027

b. Impulse.

Transducer	Phase I		Phase II			Ratio of Phase II Quantity to Phase I	
	Maximum Impulse psi-sec	Time of Peak msec	Transducer	Maximum Impulse psi-sec	Time of Peak msec	Scaled Impulse	Scaled Time of Peak
BP1	7.969	129.33	BP14	3.7137	67.54	0.932	1.045
BP4	4.129**	50.00**	BP13	2.669**	25.00**	1.293**	--
BP5	7.289	150.99	BP12	3.9326	74.08	1.079	0.981
						Avg 1.101	1.013
						Std deviation 0.148	0.032

* West wall for Phase I, east wall for Phase II.
** Transducer BP4 failed during the test. Records were compared at 50 msec for Phase I and 25 msec for Phase II.

222

Table 8.3. Comparison of posttest donor bay displacements between east and west walls.

Location	Phase I Displacement ft		Phase II Displacement ft		2 × Phase II Displacement ÷ Phase I Displacement	
	Midheight	Top	Midheight	Top	Midheight	Top
North end	1.75	2.38	0.25	0.10	0.29	0.08
Center	2.08	2.71	0.10	0	0.10	0
South end	0.75	2.83	0.27	0.25	0.72	0.18
					Avg 0.37	0.09

Table 8.4. Comparison of peak soil and interface pressures.

| Transducer | Phase I | | Phase II | | Ratio of Phase II Value to Phase I Value | |
	Peak Pressure psi	Time of Peak msec	Peak Pressure psi	Time of Peak msec	Pressure	Scaled Time
a. Soil stress transducers.						
SS1	36.35	26.68	--*	--*	--	--
SS2	117.45	23.72	226.92	12.95	1.932	1.092
SS3	94.50	26.46	139.96	13.93	1.481	1.053
SS4	72.59	26.82	122.42	14.17	1.687	1.057
				Avg	1.700	1.067
				Std deviation	0.184	0.018
b. Interface pressure transducers.						
IP1	27.09	108.57	33.51	56.33	1.237	1.038
IP2	36.97	108.56	34.10	54.27	1.220	1.000
IP3	15.82	97.18	23.61	50.81	1.492	1.046
IP4	--**	--**	72.67	56.11	--	--
IP5	71.33	84.89	54.31	33.31	0.761	0.785
IP6	43.45	94.63	64.07	34.95	1.475	0.739
IP7	51.77	108.57	47.75	56.84	0.922	1.047
IP8	51.39	88.50	42.25	55.30	0.822	1.250
IP9	32.62	98.68	63.13	43.65	1.935	0.885
				Avg	1.233	0.974
				Std deviation	0.372	0.154

* Peak values not recorded.
** Transducer failed to operate.

Table 8.5. Comparison of peak impulses from soil and interface pressure transducers.

Transducer	Phase I Peak Pressure psi-sec	Phase I Time of Peak msec	Phase II Peak Pressure psi-sec	Phase II Time of Peak msec	Ratio of Phase II Value to Phase I Value Scaled Impulse	Ratio of Phase II Value to Phase I Value Scaled Time
a. Soil stress transducers.						
SS1	2.338	204.8	4.584	99.66	3.921	0.973
SS2	6.583	194.2	7.876	109.85	2.393	1.131
SS3	5.036	196.9	5.250	101.20	2.085	1.028
SS4	4.571	193.9	3.937	104.02	1.723	1.073
				Avg	2.531	1.051
				Std deviation	0.837	0.058
b. Interface pressure transducers.						
IP1	3.021	305.8	1.793	128.36	1.187	0.840
IP2	4.755	345.8	2.124	135.65	0.893	0.785
IP3	1.962	293.4	1.276	140.69	1.300	0.959
IP4	--	--	3.811	109.16	--	--
IP5	8.285	326.2	2.455	126.43	0.593	0.775
IP6	5.477	314.7	2.971	117.45	1.085	0.746
IP7	5.908	292.9	2.566	113.41	0.869	0.774
IP8	5.873	276.8	2.229	109.33	0.759	0.790
IP9	4.124	262.1	3.139	122.76	1.522	0.937
				Avg	1.026	0.826
				Std deviation	0.286	0.075

225

CHAPTER 9

CONCLUSIONS AND RECOMMENDATIONS

9.1 CONCLUSIONS

From the data and information obtained in this test, the following conclusions can be drawn:

a. The separated bay configuration, as it exists in the Building 12-64 Complex, will prevent structural failure from ground shock or airblast in bays surrounding a bay in which an accidental explosion occurs.

b. The reinforcing steel details which are used to join the bay walls to the roof slab are not reliable in preventing separation of roof sections from the bay due to an accidental explosion of 300 lb of PBX 9501.

c. The separation of a portion of the roof slab produces a missile threat to other bays in Building 12-64.

d. The outer bulkhead and the blast door assembly in the air locks are inadequate to resist the effects of an internal explosion. Separation of these components from the donor bay air lock produces missiles of significant size and range.

e. Existing blast doors are effective in preventing blast leakage into acceptor bays.

f. Airblast leakage into acceptor bays through vents and the HVAC ductwork modeled in the test is negligible.

9.2 RECOMMENDATIONS

Test results have identified problem areas associated with donor bay roof design and the performance of air-lock bulkheads and blast doors subjected to internal explosion. Since new facilities are to be designed and constructed, design changes can reduce or eliminate these problems. However, continued safe use of existing facilities is also desired.

The performance of the donor roof suggests that the lateral support provided by the air lock was a key factor in the retention of the roof slab on the west side of the structure. Construction of a collar around the top of bay walls would stiffen the roof-to-wall connections and could possibly prevent the release of large roof fragments. An alternative would be the

226

installation of high-strength steel cables from the roof to the walls to "catch" a separated roof segment.

An earth berm, reinforced concrete wall, or steel I-beam grid or mat could be used to stop fragments coming from the air lock. The earth berm, in front of the air lock, against the frangible ramp, would be an effective and economical solution. However, the earth berm would require a larger area than other solutions. A reinforced concrete wall, installed as part of the ramp, would be effective provided the excess reflected pressure from the blast pressure venting the air lock is not a problem. The steel I-beam grid may not produce as great a reflected pressure as the concrete wall; however, some small fragments may penetrate the grid unless the I-beams are staggered in more than one layer.

The design of new facilities can correct the problems identified in Building 12-64 with relatively minor modifications. The roof steel could be modified by making the principal reinforcement continuous in each part of the roof and including vertical stirrups to prevent the reinforcement from pulling out of the roof slab and, thus, prevent the disengagement of the roof. Since much of the early venting occurs through the air lock, enlargement of blast doors would allow quicker venting of the donor bay and, thus, less impulse on the roof and walls. The reinforced concrete bulkheads supporting the blast door assembly should be redesigned or eliminated to prevent failure and, thus, prevent the fragment hazard they cause when they fail. A wall, berm, or fragment trap should be included to stop fragments projected through the air lock. The reinforcing steel details at the corners of the bay could be improved to decrease structural damage and motion and, thus, reduce loads transmitted through the soil to adjoining bays.

There are a few construction features used for the existing Building 12-64 Complex that will not, or should not, be used in any new construction. Rebar mats should not be welded because welding reduces rebar ductility. Grade 40 rebars are no longer generally available for construction; using Grade 60 bars will result in a stronger structure and less structural damage in case of an accidental explosion. There should be no rebar laps in the roof because the large roof rotations will cause failure at the laps. Use of a non-cohesive sand backfill material between the bays in any new construction should be continued because this material rapidly attenuates soil stress. In general, the separated bay concept has been validated, and is strongly recommended for new construction.

227

REFERENCES

1. Gibbs & Hill/Ammann & Whitney; "Test Plan and Specifications for Determining the Blast-Resistant Capability of Building 12-64"; Feb 1981; New York, N. Y.

2. M. M. Swisdak, Jr.; "Explosion Effects and Properties: Part I - Explosion Effects in Air"; NSWC/WOL/TR 75-116 (supersedes Section A, NOLTR 65-218), Oct 1975; Naval Surface Weapons Center, White Oak, Silver Spring, Md.

3. Headquarters, U. S. Army Materiel Command; "Engineering Design Handbook, Explosions in Air, Part One"; AMC Pamphlet No. 706-181, 15 Jul 1974; Alexandria, Va.

4. Bernard Ray Tillery; "Sub-Soil Investigation Top Roof, Building 12-64, Pantex Plant"; 1 Aug 1981; Amarillo Testing and Engineering, Inc., Amarillo, Tex.

5. George T. West; "PBX 9501 Air Blast Experiments"; MHSMP-82-09, Feb 1982; Mason & Hanger, Silas Mason Co., Inc., Amarillo, Tex.

6. U. S. Army Engineer Division, Huntsville; "Suppressive Shields Structural Design and Analysis Handbook"; HNDM-1110-1-2, 18 Nov 1977; Huntsville, Ala.

7. R. D. Crowson; "Essex-Diamond Ore Research Program; Vibration Tests and Analyses of ESSEX V Model Structures"; Technical Report N-78-2, Aug 1978; U. S. Army Engineer Waterways Experiment Station, CE, Vicksburg, Miss.

8. U. S. Department of Energy; "A Manual for the Prediction of Blast and Fragment Loadings on Structures"; DOE/TIC-11268, Nov 1980; Albuquerque Operations Office, Amarillo Area Office, Amarillo, Tex.

9. J. K. Ingram; "Development of a Free-Field Soil Stress Gage for Static and Dynamic Measurements"; Technical Report No. 1-814, Feb 1968; U. S. Army Engineer Waterways Experiment Station, CE, Vicksburg, Miss.

APPENDIX A

DEPARTMENT OF ENERGY BUILDING 12-64
TEST EVENT CALENDAR

Date 1981	Event
Sep 11	Concrete placed in Phase II retaining wall footing and bay floor slabs.
Sep 15	Phase I acceptor bay floor slab placed.
Sep 18	Phase I donor bay floor slab placed.
Sep 28	Concrete placed in Phase II donor and acceptor bay walls.
Oct 16	Phase I donor bay walls placed.
Oct 20	Blast door fabrication completed.
Oct 27	Concrete placed in Phase II retaining wall.
Oct 28	Phase I acceptor bay walls placed.
Nov 4	Concrete placed in Phase II donor and acceptor bay roofs.
Nov 9	Concrete placed in air-lock floor slabs.
Nov 18	Concrete placed in ramp slab.
Nov 18	Phase I donor and acceptor bay roof slabs placed.
Nov 23	Backfill around Phase I bay walls started.
Nov 25	Blast doors and frames set in place.
Nov 26	Phase I acceptor bay back wall completed.
Dec 1	Concrete placed in air-lock walls and roofs.
Dec 4	Phase I backfill completed and HVAC slab placed.
Dec 8	Phase I Gulf Seal installation completed.
Dec 18	Phase I Event.

1982	
Jan 12	Backfill of Phase II bay walls completed.
Jan 16	Phase II ramp completed.
Jan 19	Concrete placed in Phase II simulated acceptor bay roof slabs and HVAC slab.
Jan 20	Backfill over Phase II roofs completed.
Jan 21	Phase II "Gulfseal"-type panels installed.
Jan 21	Phase I roof fragment data collection completed.
Jan 27	Phase II Event.
Jan 29	Phase II data collection completed.
Jan 29	Phase I donor bay interior excavation and data collection completed.

APPENDIX B

CONCRETE REINFORCING STEEL STRESS-STRAIN DATA

The following figures show the stress-strain curves for the different re-
inforcing bar sizes used. The vertical axis measures stress (in psi) and the
horizontal axis measures strain (in μ-in./in.). The specimen number indicates
bar size followed by sample number. The strain was measured using electronic
gages. These curves show the strain plotted until the gage failed or the
strain reached 24,000 μin./in. They do not show bar failure.

SPEC - #2-2

SPEC - #2-1

B3

SPEC - #3-1

GUAGE OUT

SPEC - #2-3

B4

SPEC - #3-3

MICRO-INCHES/INCH

STRESS, PSI

GUAGE OUT

SPEC - #3-2

MICRO-INCHES/INCH

STRESS, PSI

B5

SPEC - #4-2

SPEC - #4-1

B6

SPEC - #5-1

SPEC - #4-3

B7

SPEC - es-3

SPEC - es-2

B8

SPEC - r6-1

SPEC - r5-4

SPEC - #6-3

SPEC - #6-2

B10

SPEC - s6-1

MICRO-INCHES/INCH

STRESS, PSI

SPEC - s6-4

MICRO-INCHES/INCH

STRESS, PSI

B11

SPEC - #6-3

SPEC - #6-2

B12

SPEC - #8-1 REBAR

MICRO-INCHES/INCH

STRESS, PSI

SPEC - #8-4

MICRO-INCHES/INCH

STRESS, PSI

B13

SPEC - #9-3

SPEC - #9-2 REBAR

B14

SPEC - #10-1 REBAR

SPEC - #5-1

B15

SPEC - #10-3 REBAR

SPEC - #10-2 REBAR

B16

SPEC - #18-4 REBAR

APPENDIX C

STRUCTURAL STEEL STRESS-STRAIN DATA

The following figures represent the stress-strain curves for the structural steel used in model structures. Specimens 1-3 are from 16-gage sheet steel and specimens 4-6 are from 10-gage. Specimens 7-9 are from 3/16-in.-thick plate and specimens 10-12 are from 1/4-in.-thick plate.

SPECIMEN NO. 1

SPECIMEN NO. 2

C3

SPECIMEN NO. 3

SPECIMEN NO. 4

C4

SPECIMEN NO. 7

SPECIMEN NO. 8

C6

SPECIMEN NO. 9

SPECIMEN NO. 10

SPECIMEN NO. 11

SPECIMEN NO. 12
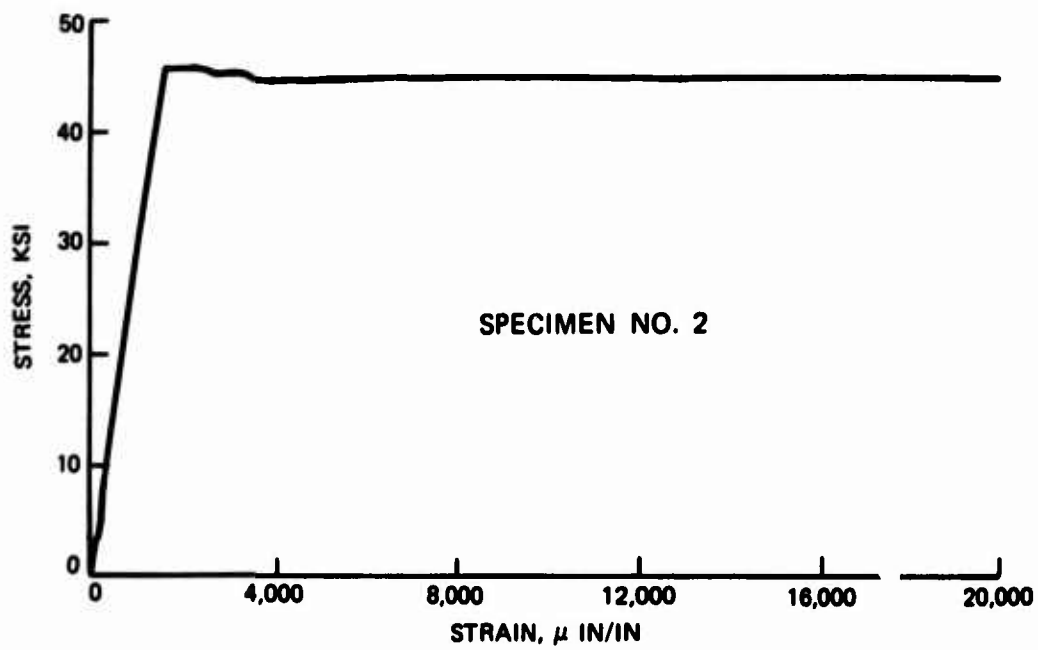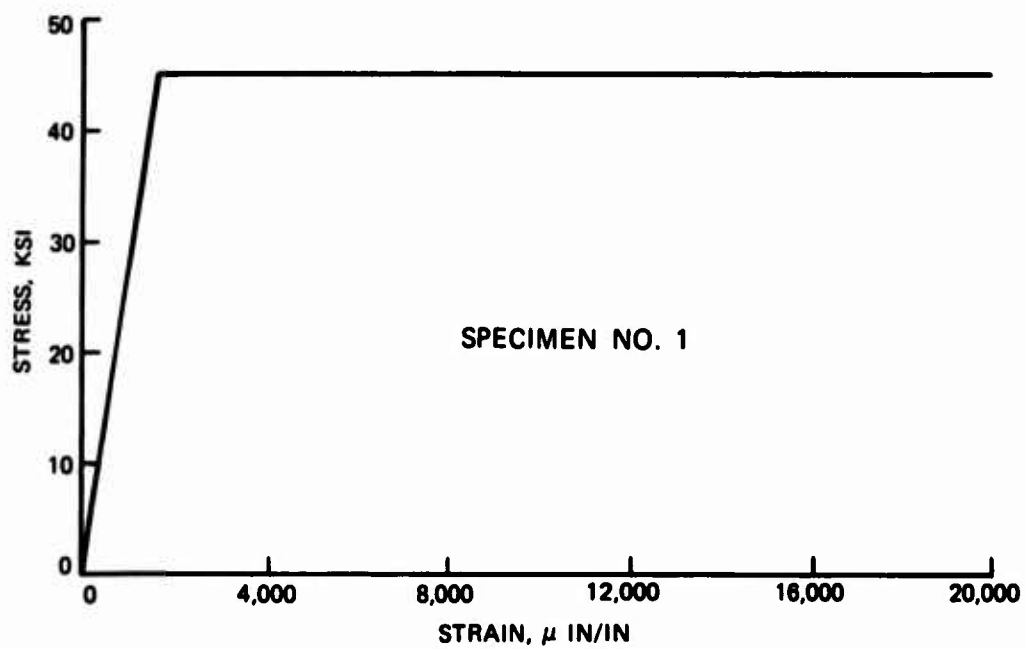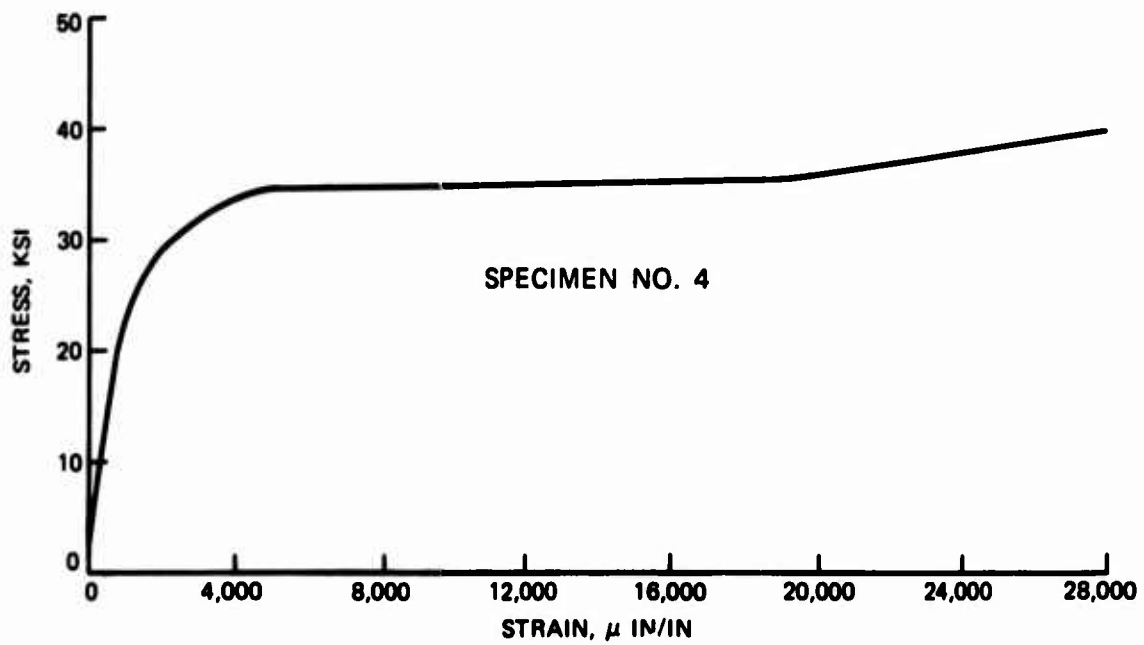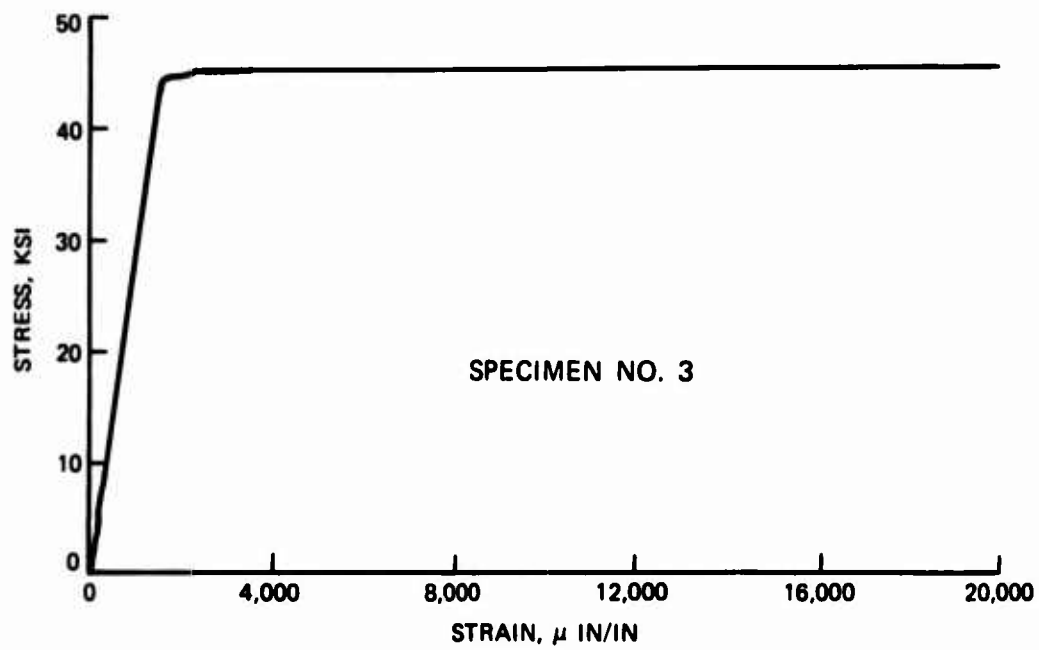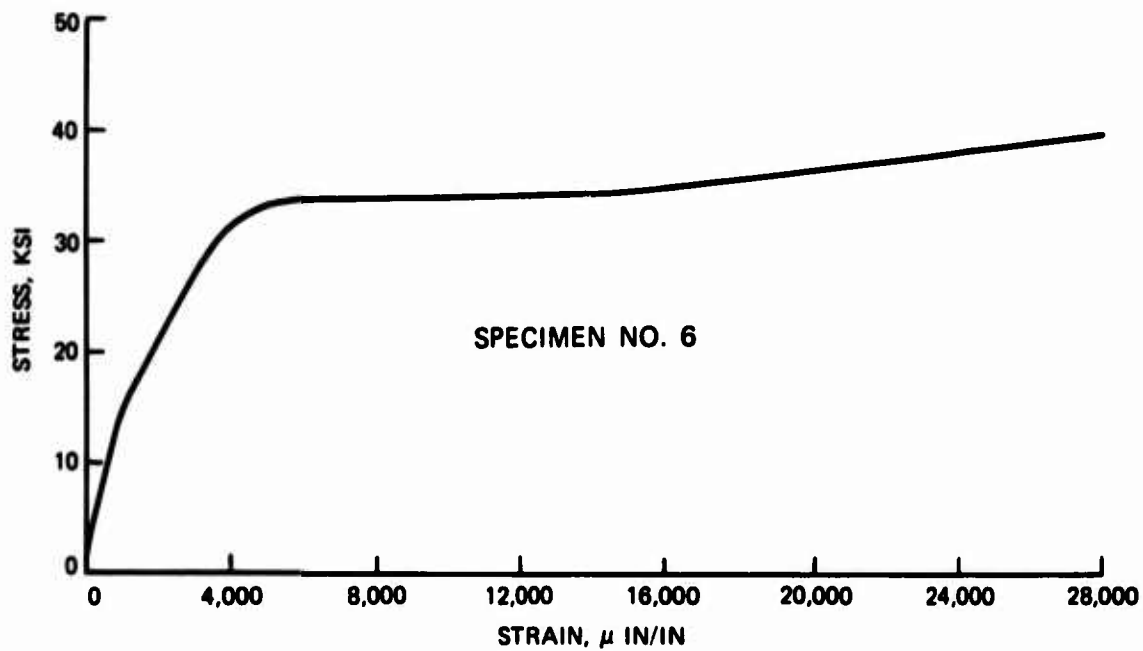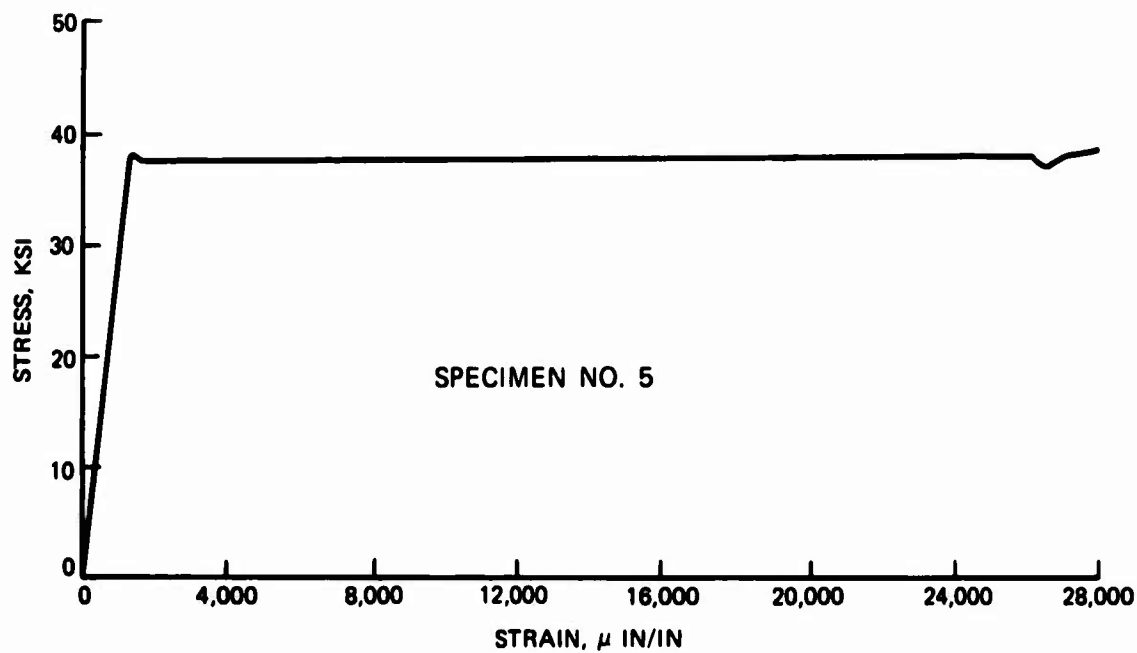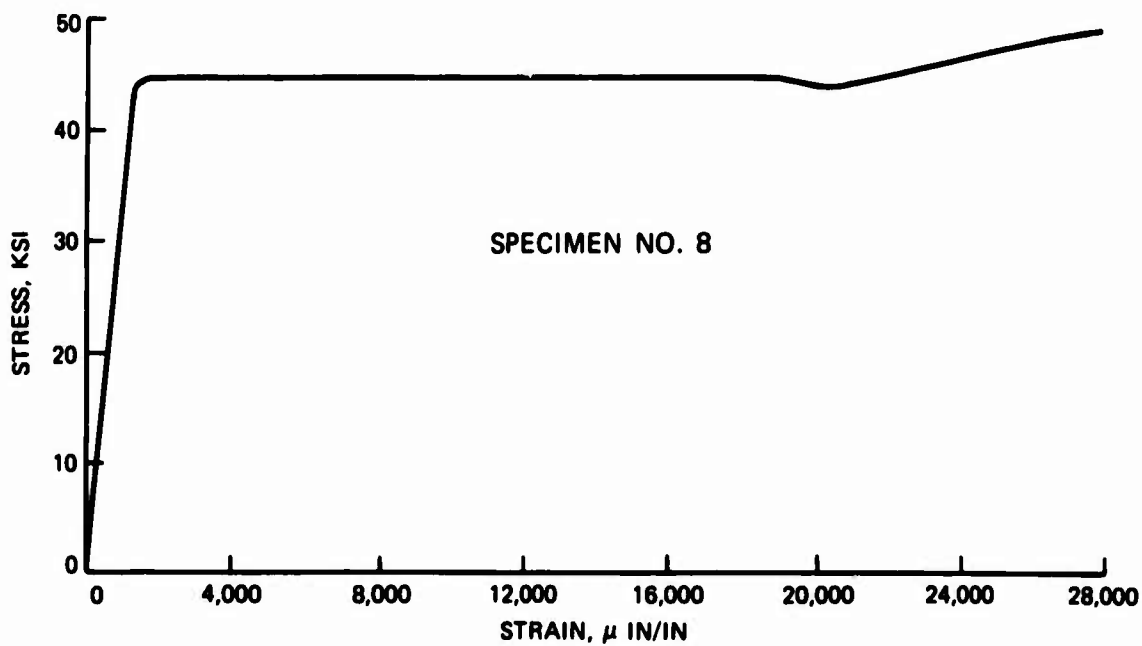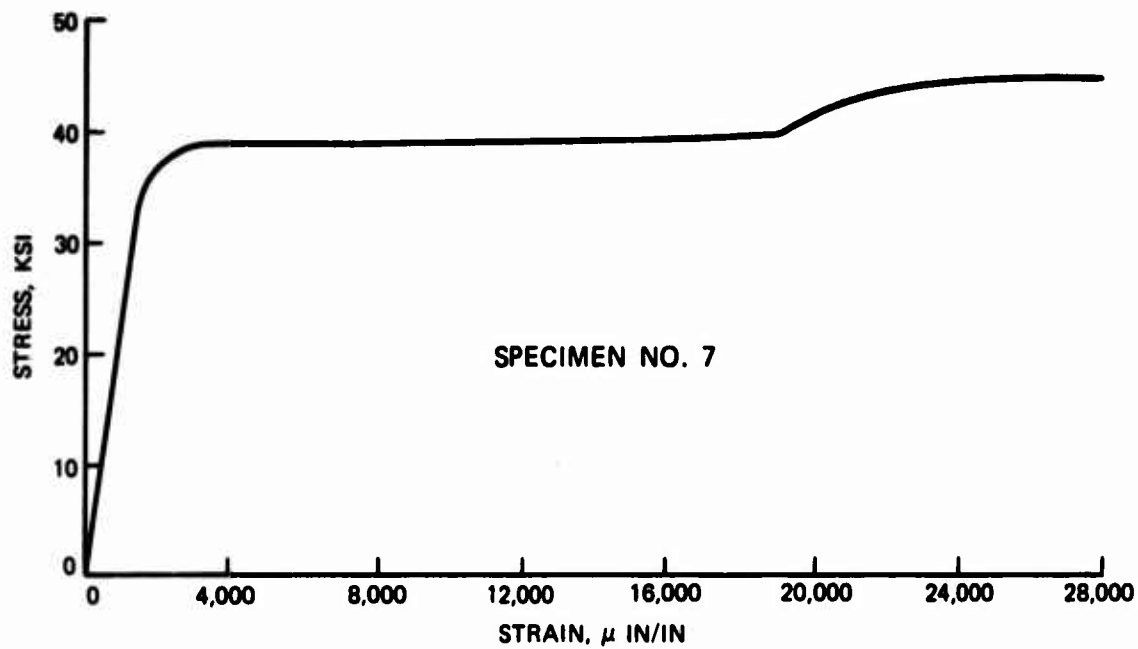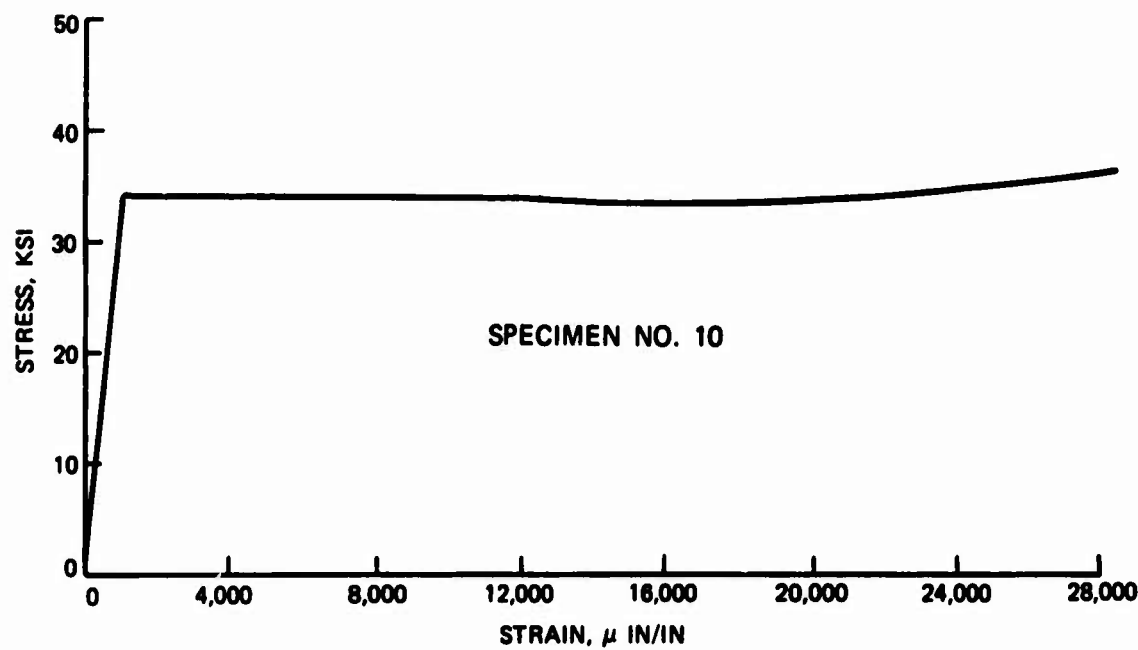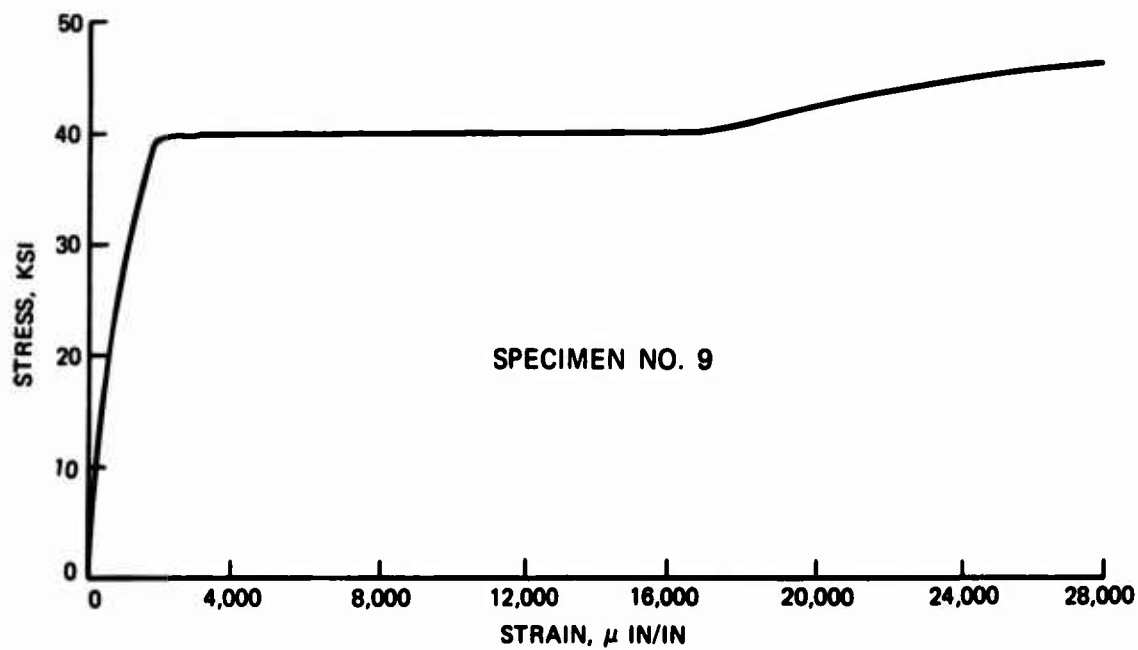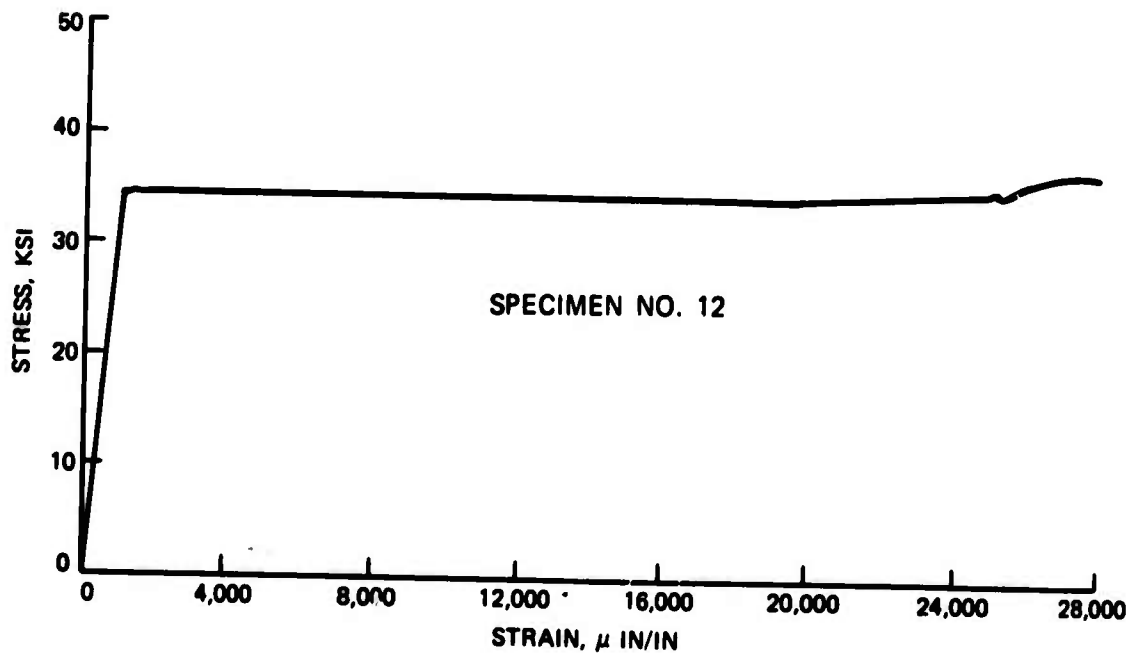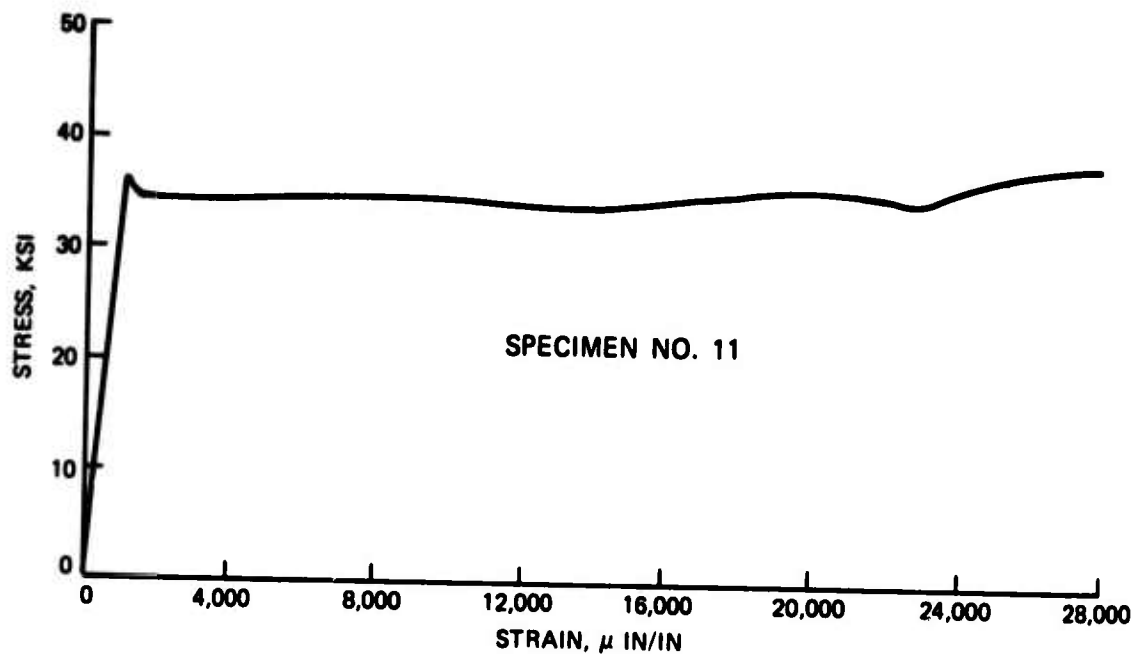
APPENDIX D

PHASE I STRUCTURAL VIBRATION TEST DATA

Typical transfer functions obtained during model testing are shown in Figures D1, D2, and D3. Each function is a graph of response magnitude (acceleration normalized with respect to force) versus frequency of excitation. All of the transfer functions in Figure D1 are for the same drive point and accelerometer locations and are directly comparable. Thus, comparisons between donor and acceptor bay dynamic responses are possible as well as comparisons between the pre- and post-backfilled structures.

Figure D2 contains transfer functions for the donor bay with different drive point and accelerometer locations from those in Figure D1a and D1b. Thus some of the resonant frequencies visible in one figure are not visible in the other and vice versa. The effects of backfill are visible by comparing the two graphs.

The transfer functions in Figure D3 are for the acceptor bay and are similar to those in Figure D2. The two figures are not directly comparable because the accelerometer locations are slightly different. Several of the frequencies shown in Figure D3 are different from those of Figure D1c and D1d for the same reasons previously mentioned.

a. Donor bay before backfill, point 1, accelerometer at point 7.

b. Donor bay after backfill, point 1, accelerometer at point 7.
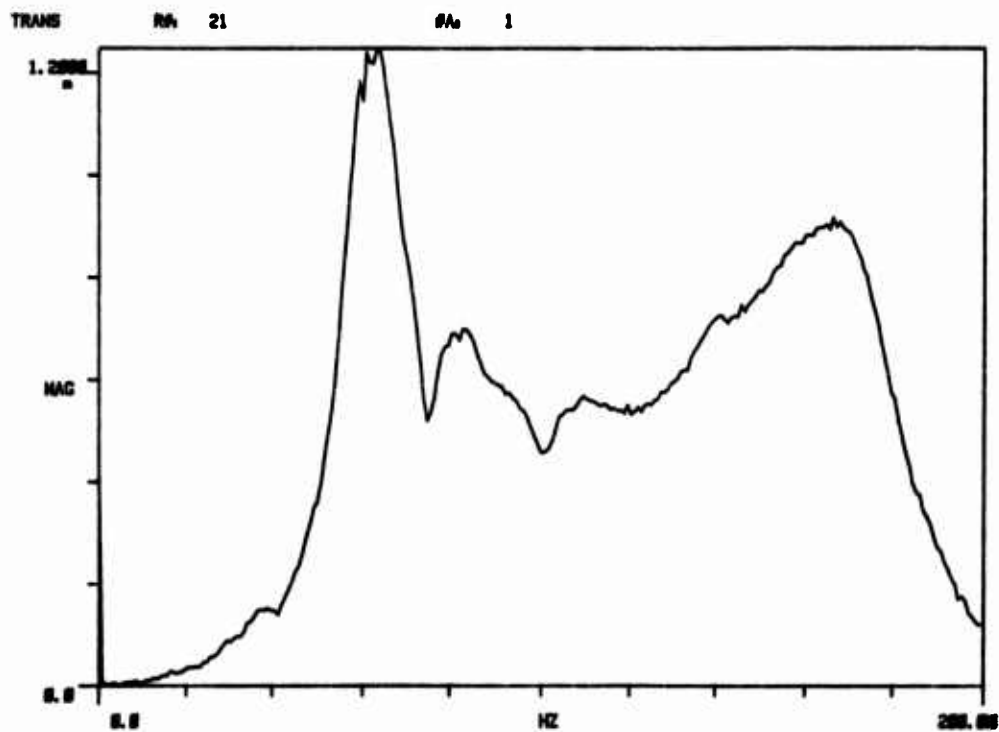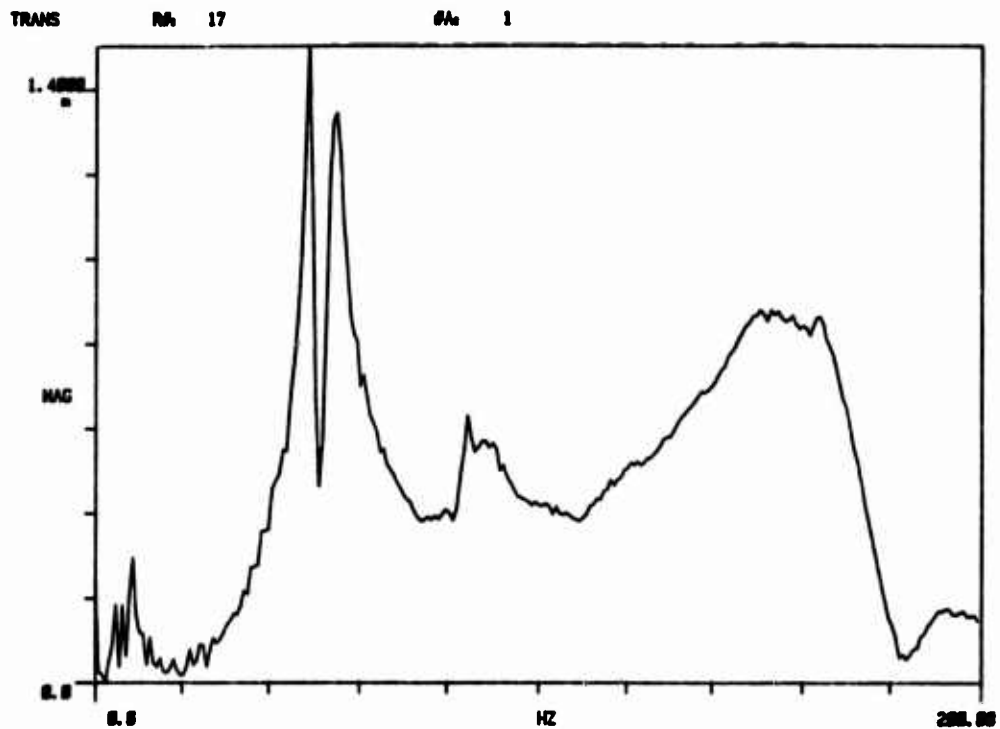
Figure D1. Comparison of transfer functions (Continued).
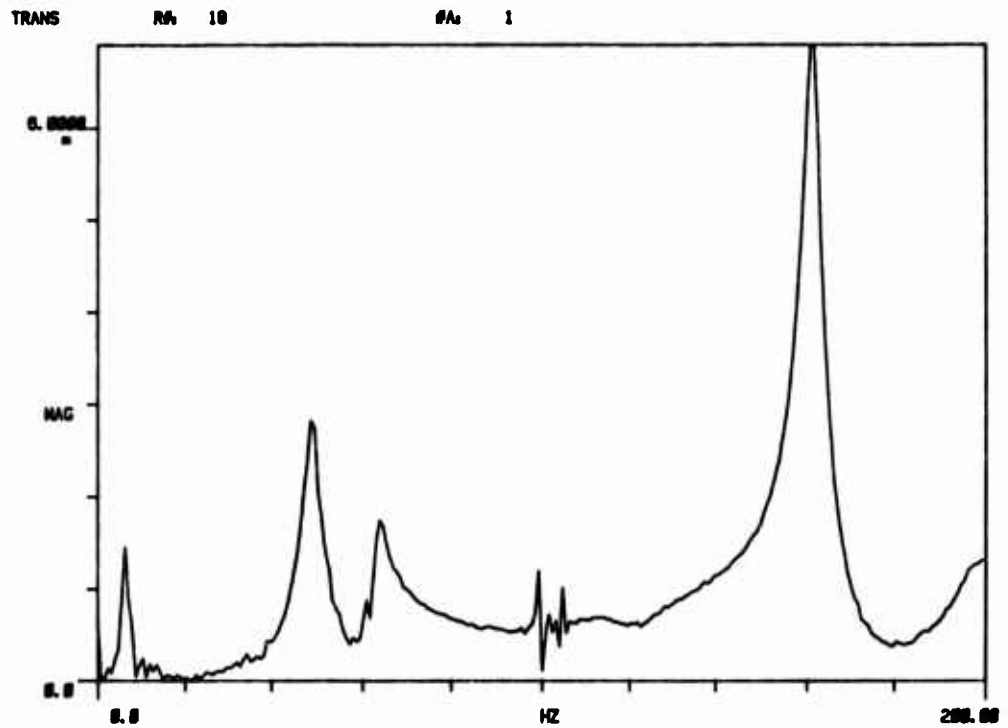
c. Acceptor bay before backfill, point 1, accelerometer at point 7.
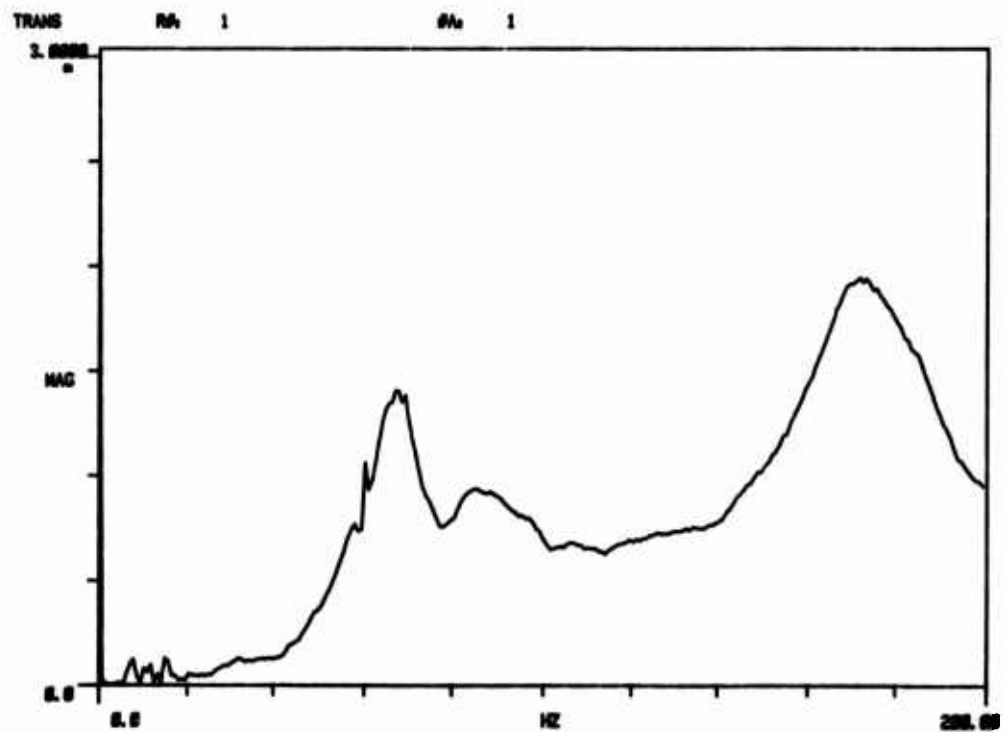
d. Acceptor bay after backfill, point 1, accelerometer at point 7.

Figure D1. (Concluded).
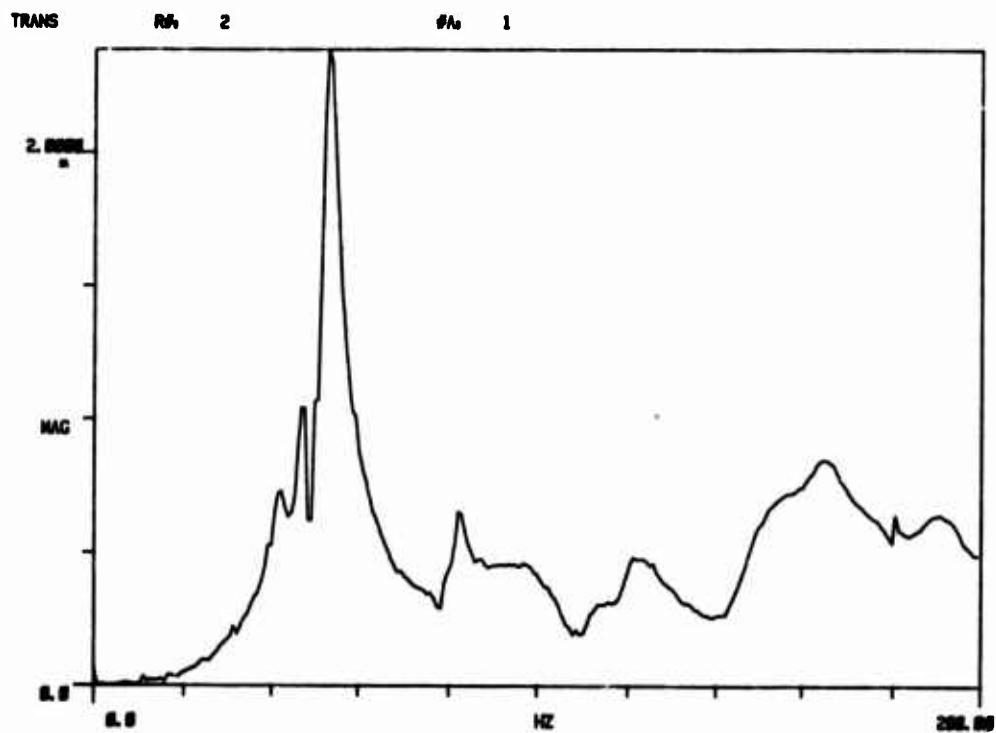
a. Before backfill, point 2, accelerometer at point 13.
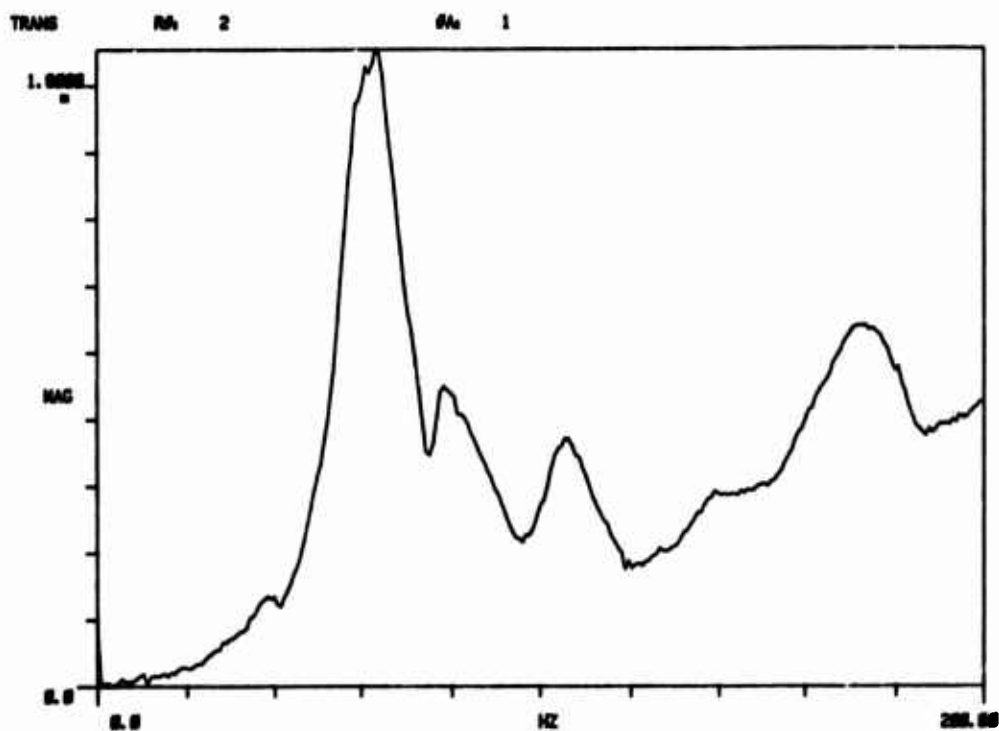
b. After backfill, point 2, accelerometer at point 13.

Figure D2. Donor bay transfer functions.

D5
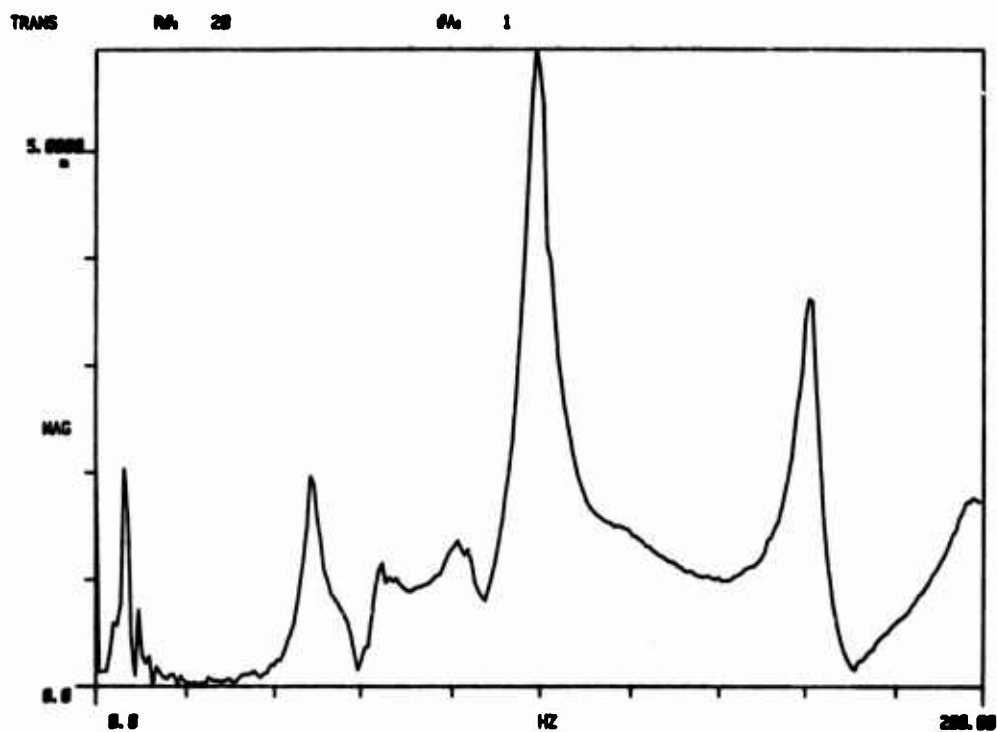
a. Before backfill, point 3, accelerometer at point 7.
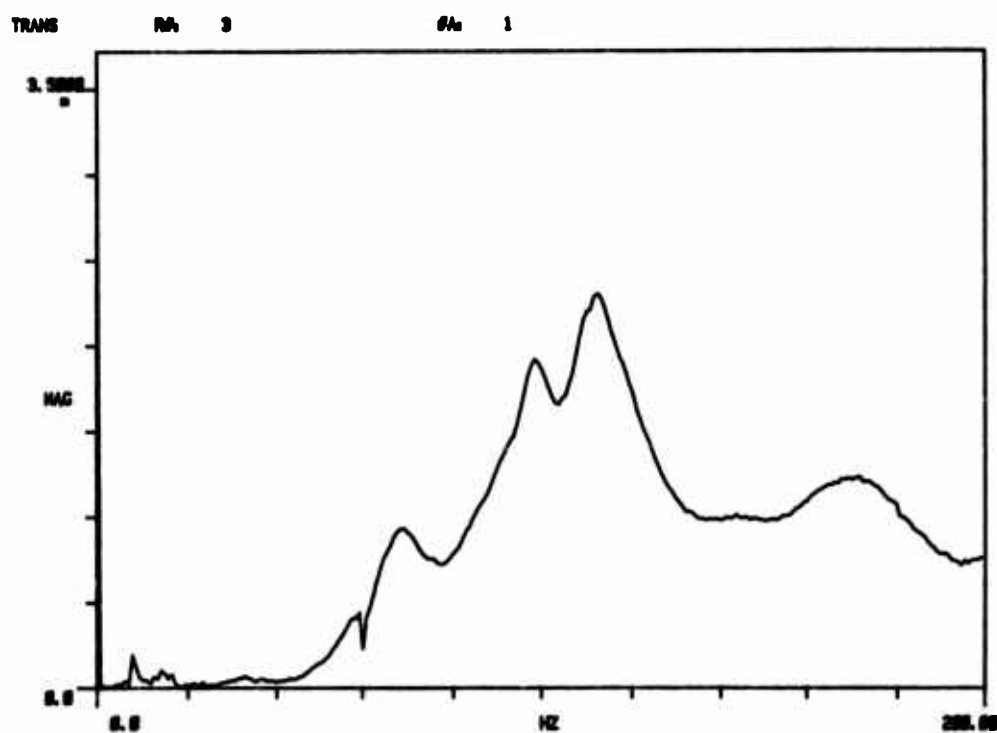
b. After backfill, point 3, accelerometer at point 7.

Figure D3. Acceptor bay transfer functions.

APPENDIX E

PHASE I TEST DATA

In this appendix, electronic data are shown with one of five different time scales. Unfiltered airblast data for gages BP1-5 are plotted for 10 msec. These graphs show the time of arrival of the shock wave and peak pressures recorded at the transducers inside the donor bay. Gages BP2 and 6 were damaged within 20 msec, so unfiltered records of these gages are plotted to the time of failure on a 20-msec scale. All of the aforementioned records were processed to obtain an 80-kHz frequency response.

Filtered blast pressure records for transducers BP1, BP3, BP4, and BP5 are shown with a 50-msec time scale. They are useful in viewing the attenuation of reflected shocks and the buildup of quasistatic pressure. The frequency response of these records is on the order of 22.5 kHz, so the peak values shown on these records are lower than those of the unfiltered records.

The long-duration (100 and 250 msec) records were digitized at a lower sampling frequency and were filtered to yield a frequency response of 4.5 kHz. These records show relatively low frequency phenomenon such as quasistatic pressure decay, soil pressures, and deflections. All data except peak blast pressures are accurately reproduced within this frequency response.

DOE BLDG 12-64 PI
BP-1-S
500000. HZ CAL= 1001.
LP4 70% CUTOFF= 22500. HZ
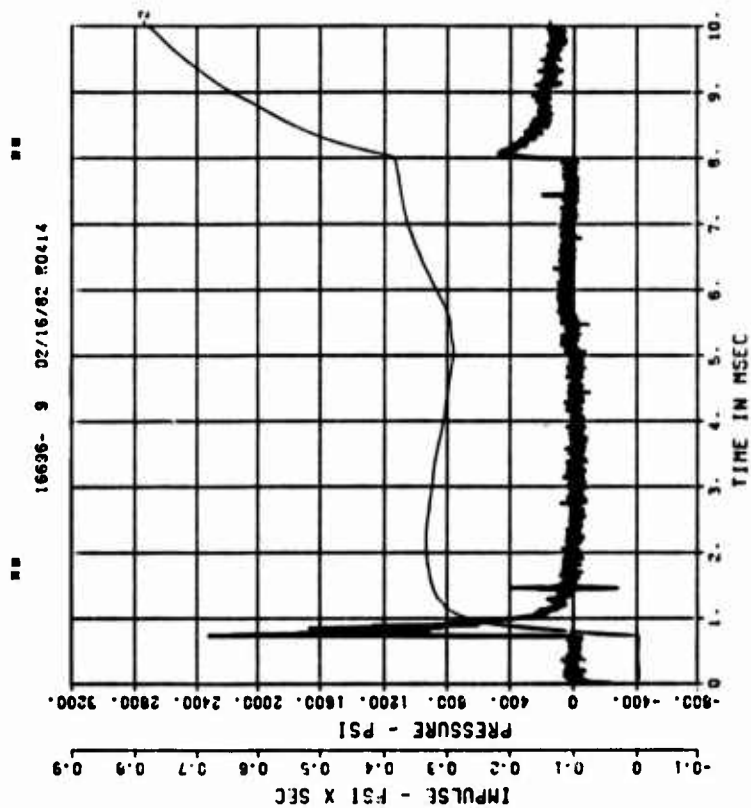
16695- 9 02/23/92 80P5:

PRESSURE - PSI

IMPULSE - PSI X SEC

TIME IN MSEC

** PEAK VALUE IS 75   % OVER CALIBRATION **

DOE BLDG 12-64 PI
BP-1-S
500000. HZ CAL= 1001.

16696- 9 02/16/82 80414

PRESSURE - PSI

IMPULSE - PSI X SEC

TIME IN MSEC

** PEAK VALUE IS 132 % OVER CALIBRATION **

E3

DOE BLDG 12-64 PI
BP-2-S
500000. HZ CAL= 188.3

16696- 10   01/05/92 ROP23

TIME IN MSEC

STRESS - PSI

IMPULSE - PSI X SEC
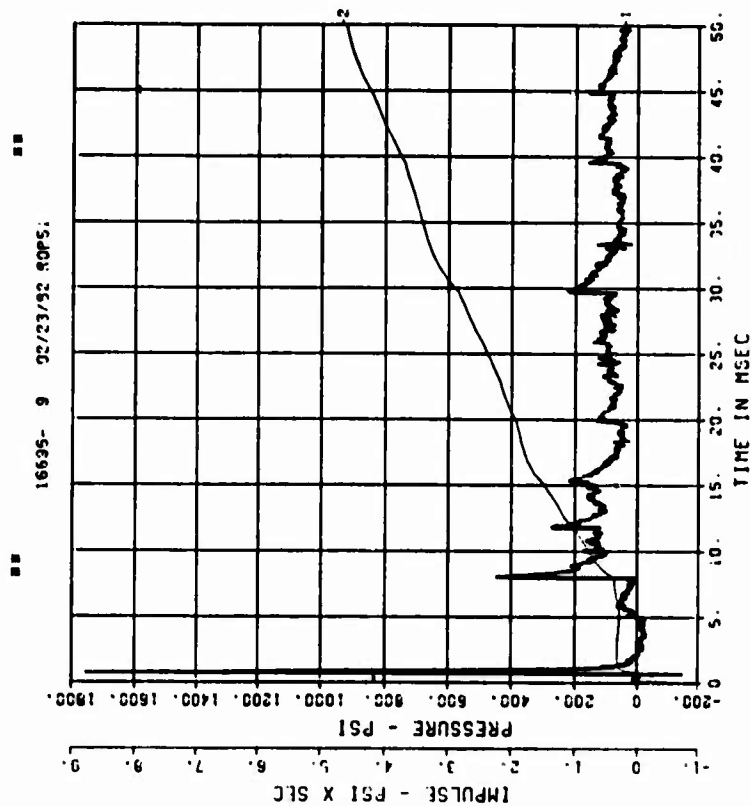
** PEAK VALUE IS 420 % OVER CALIBRATION **

DOE BLDG 12-64 PI
BP-1
100000. HZ CAL= 1001.
LP4 70% CUTOFF= 4500. HZ
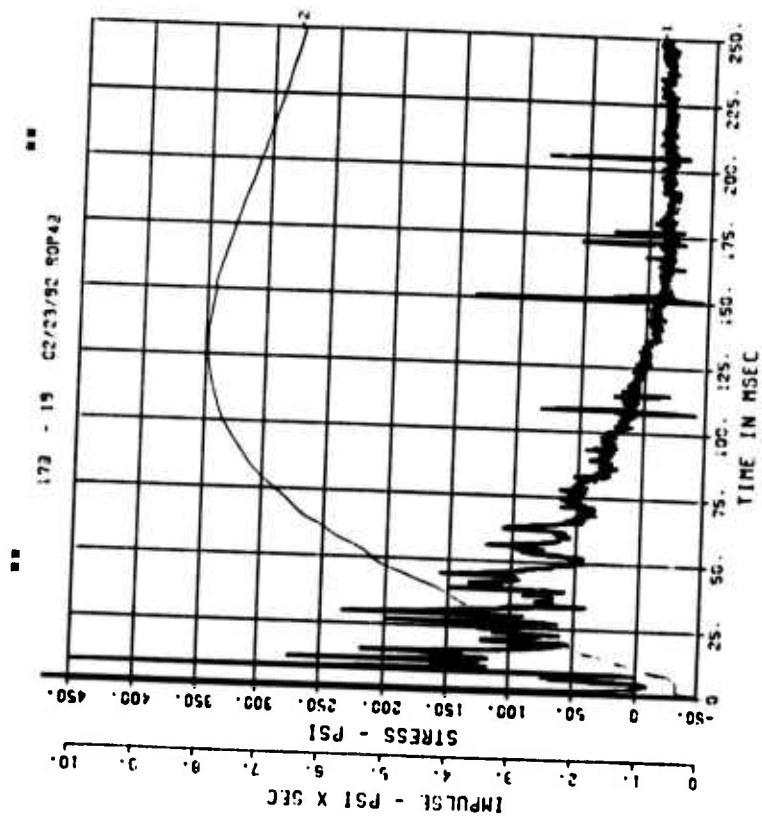
172 - 19   02/23/92 ROP42

TIME IN MSEC

STRESS - PSI

IMPULSE - PSI X SEC

** PEAK VALUE IS 23 % OVER CALIBRATION **

E4

DOE BLDG 12-64 PI
BP-3-S
500000. HZ   CAL= -176.0

DOE BLDG 12-64 PI
BP-2-S
500000. HZ   CAL= 188.3

E5
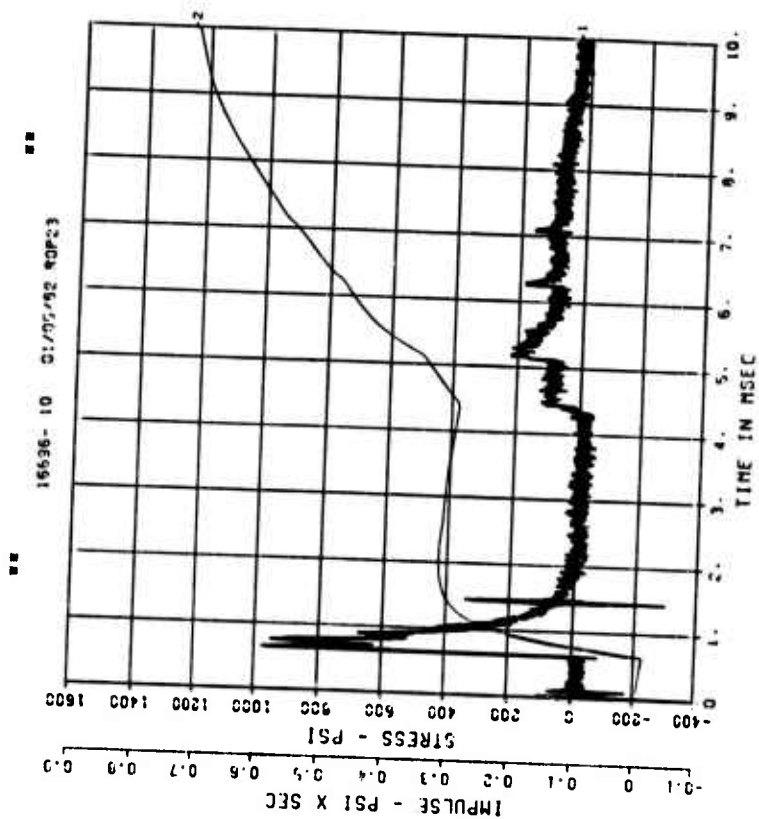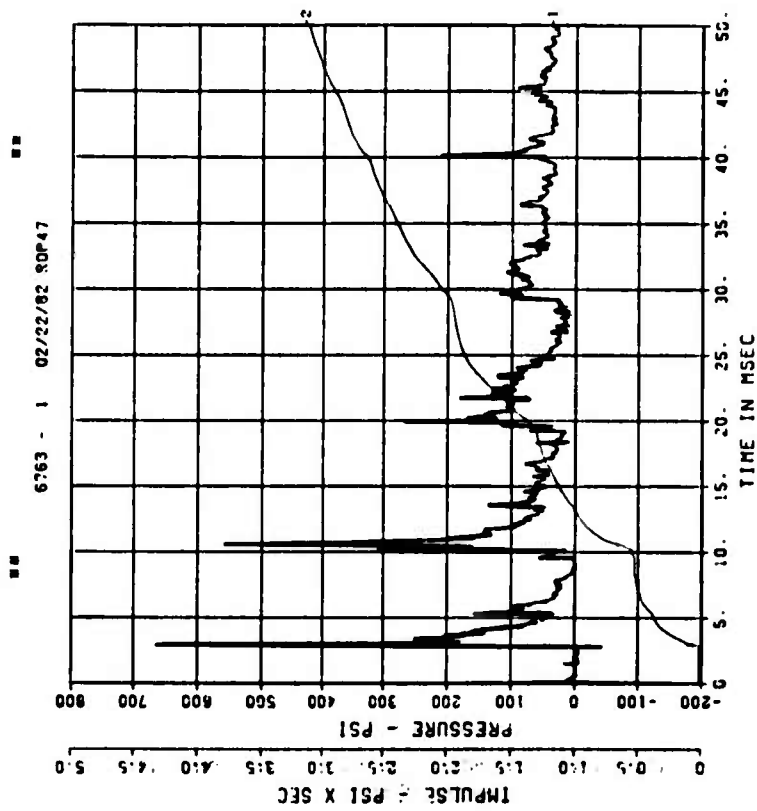
DOE BLDG 12-64 PI
BP-3-S
100000. HZ CAL= -176.0
LP4 70% CUTOFF= 4500. HZ
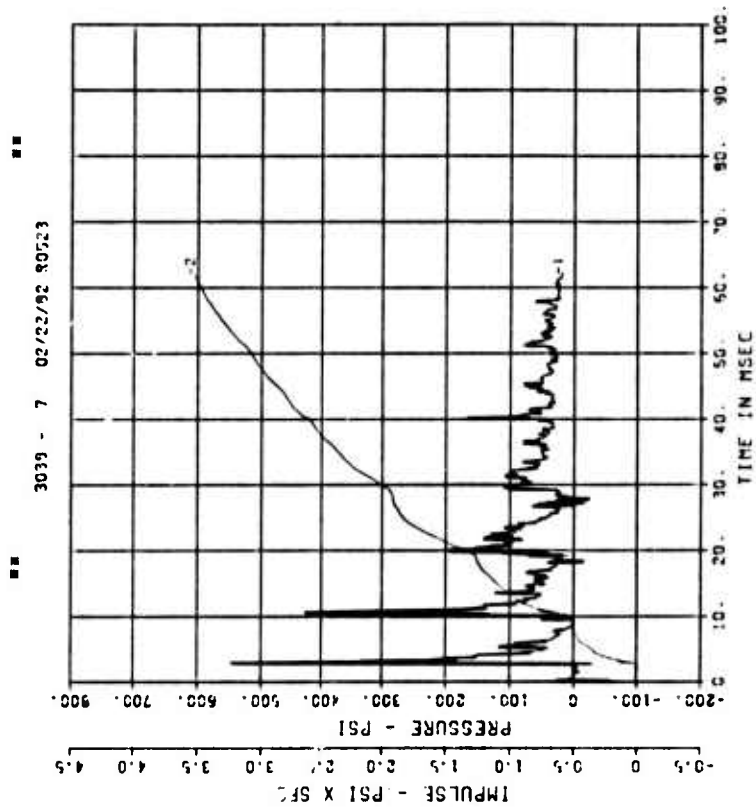
3039 - 7   02/22/82 80S23

** PEAK VALUE IS 610 % OVER CALIBRATION **

DOE BLDG 12-64 PI
BP-3-S
500000. HZ CAL= -176.0
LP4 70% CUTOFF= 22500. HZ

6763 - 1   02/22/82 80P47

** PEAK VALUE IS 630 % OVER CALIBRATION **

E6

DOE BLDG 12-64 PI
BP-4-S

500000. HZ CAL= -177.2
LP4 70% CUTOFF= 22500. HZ

6763 - 2   02/22/82 ROP45

** PEAK VALUE IS 314 % OVER CALIBRATION **

DOE BLDG 12-64 PI
BP-4-S

500000. HZ CAL= -177.2

6763 - 2   02/22/82 ROP45
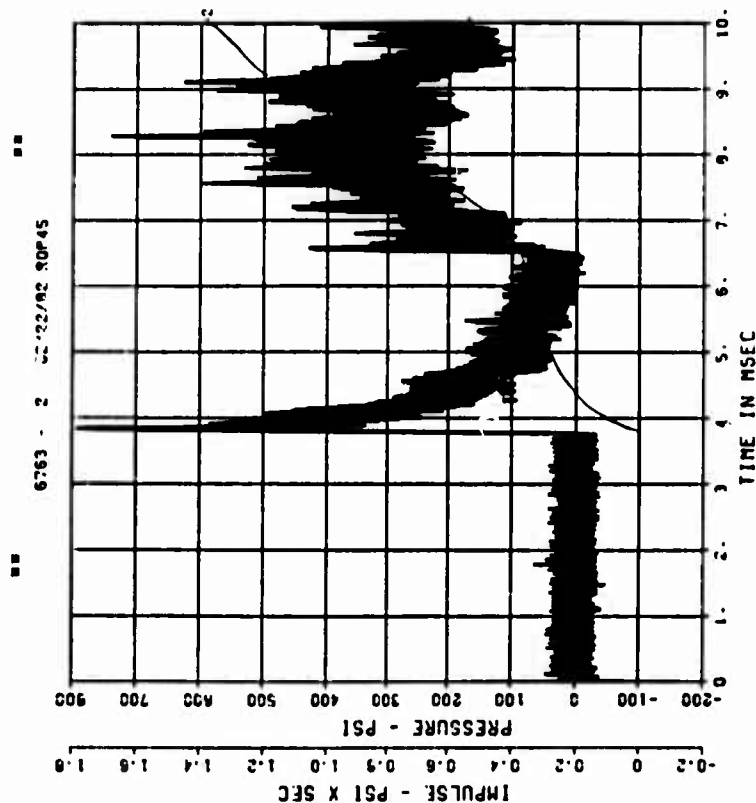
** PEAK VALUE IS 349 % OVER CALIBRATION **

E7
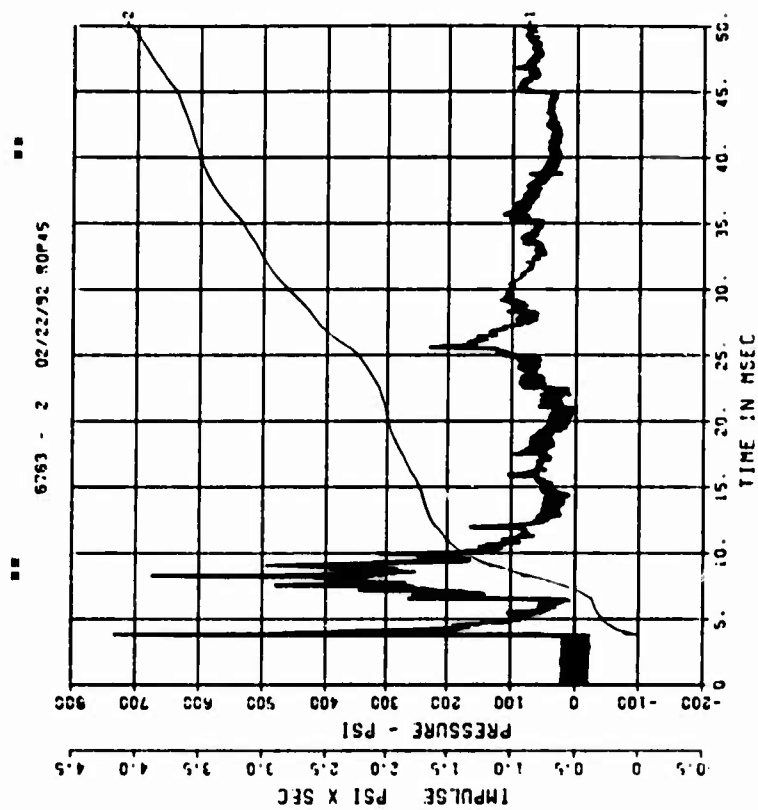
DOE BLDG 12-64 PI
BP-5-S
500000. HZ CAL= 241.3

DOE BLDG 12-64 PI
BP-4-S
100000. HZ CAL= -177.2
LP4 70% CUTOFF= 4500. HZ
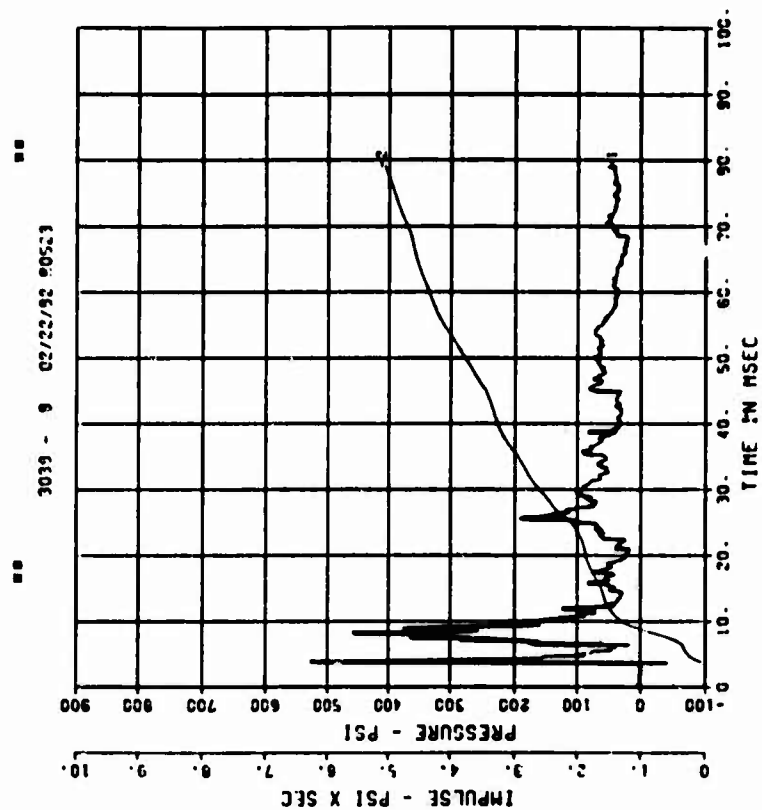
DOE BLDG 12-64 PI
BP-5
100000. HZ CAL= 241.3
LP4 70% CUTOFF= 4500. HZ

17311- 4 01/21/92 ROC:5
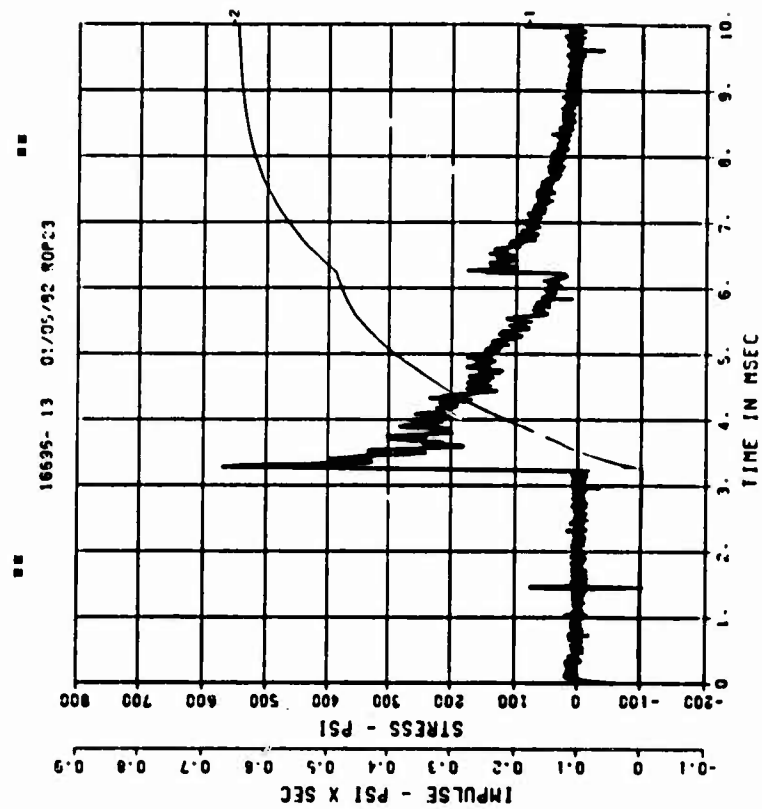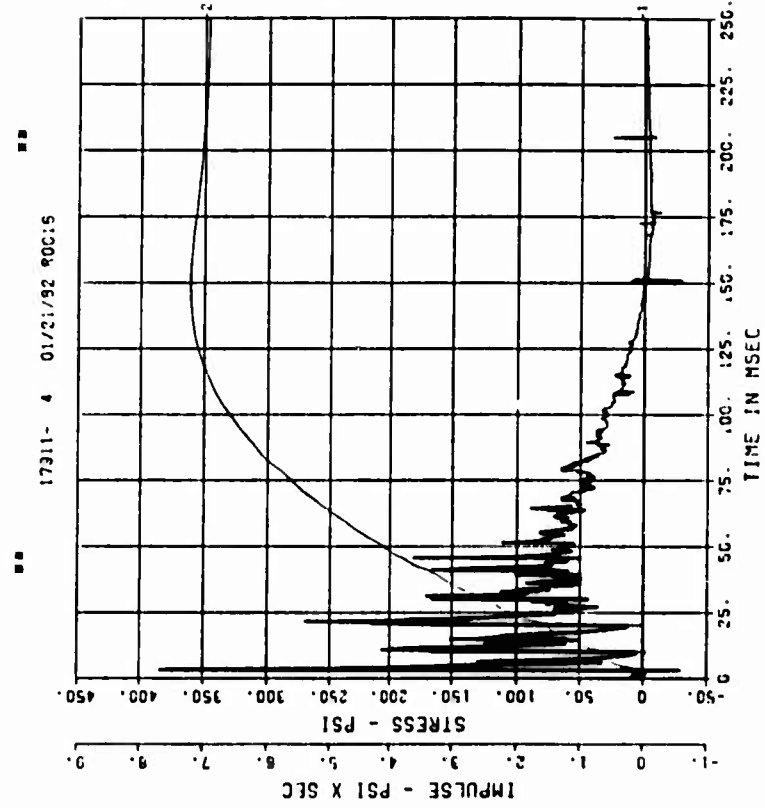
** PEAK VALUE IS 53 % OVER CALIBRATION **

DOE BLDG 12-64 PI
BP-5-S
500000. HZ CAL= 241.3
LP4 70% CUTOFF= 22500. HZ

16695- 13 01/05/92 ROP:6

** PEAK VALUE IS 123 % OVER CALIBRATION **

DOE BLDG 12-64 PI
BP-7

100000. HZ CAL= 25.70
LP4 70% CUTOFF= 4500. HZ

DOE BLDG 12-64 PI
BP-6-S

500000. HZ CAL= 70.70

** PEAK VALUE IS 5.1 % OVER CALIBRATION **

E10

013

DOE BLDG 12-64 PI
BP-9

100000. HZ CAL= 10.10
LP4 70% CUTOFF= 4500. HZ

DOE BLDG 12-64 PI
BP-8

100000. HZ CAL= 24.50
LP4 70% CUTOFF= 4500. HZ

DOE BLDG 12-64 PI
SS-2-S

100000. HZ   CAL= 53.20
LP4 70% CUTOFF= 4500. HZ

DOE BLDG 12-64 PI
SS-1

100000. HZ   CAL= 69.60
LP4 70% CUTOFF= 4500. HZ
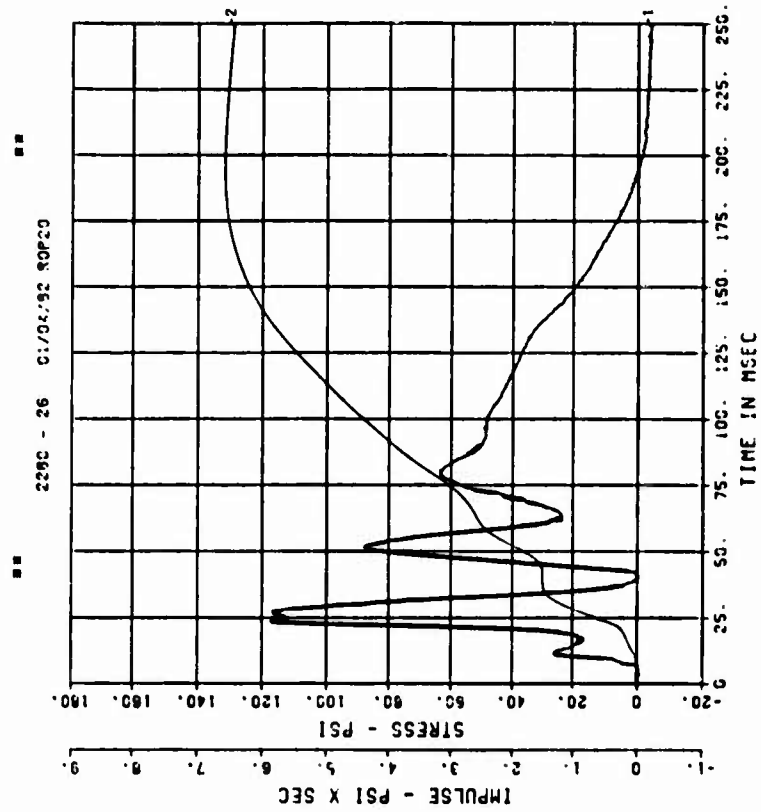
** PEAK VALUE IS 121 % OVER CALIBRATION **

E12

DOE BLDG 12-64 PI
SS-4

100000. HZ CAL= 70.30
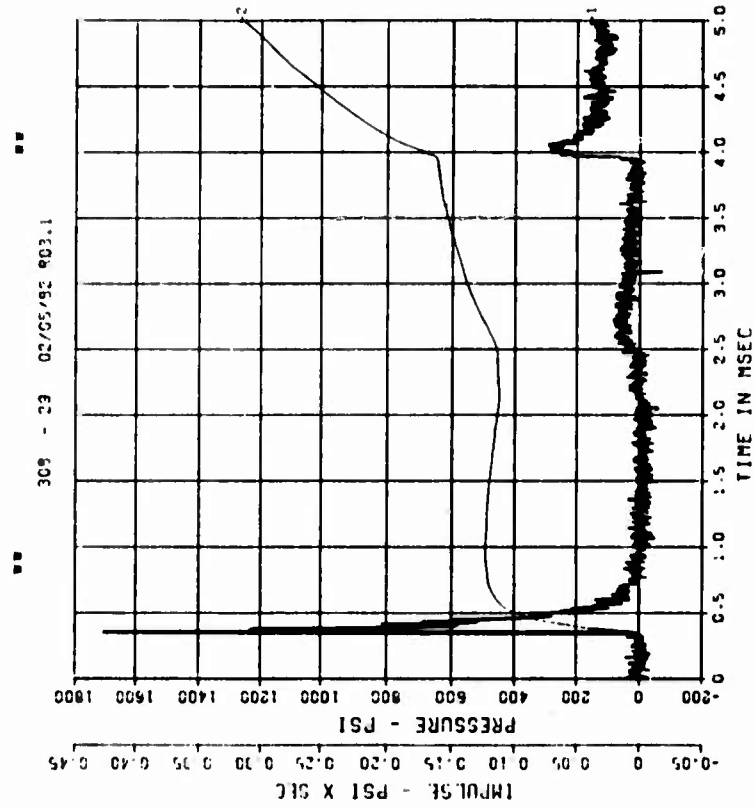LP4 70% CUTOFF= 4500. HZ

2290 - 13   01/04/92 ROPCO

** PEAK VALUE IS 5   % OVER CALIBRATION **

DOE BLDG 12-64 PI
SS-3

100000. HZ CAL= 69.20
LP4 70% CUTOFF= 4500. HZ

2290 - 12   01/04/92 ROPCO
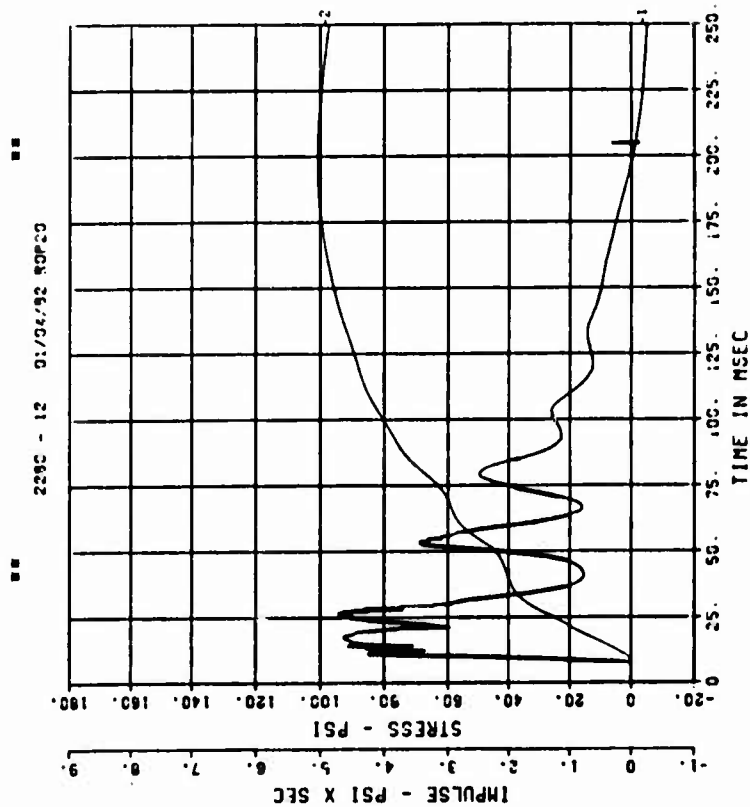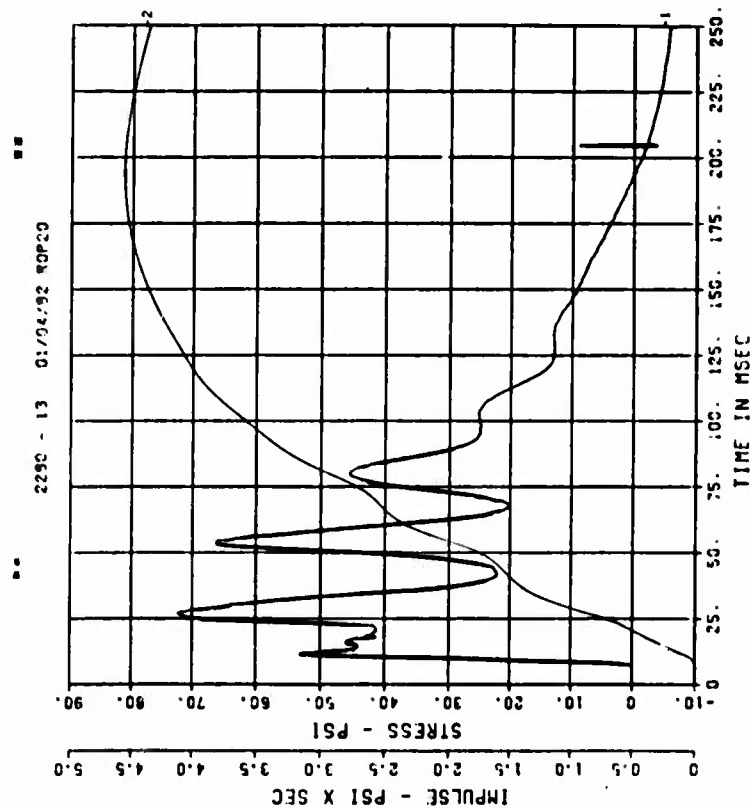
** PEAK VALUE IS 97   % OVER CALIBRATION **

DOE BLDG 12-64 PI
IP-2-S
100000. HZ CAL= 14.10
LP4 70% CUTOFF= 4500. HZ

2280 - 18   01/04/92 80P20
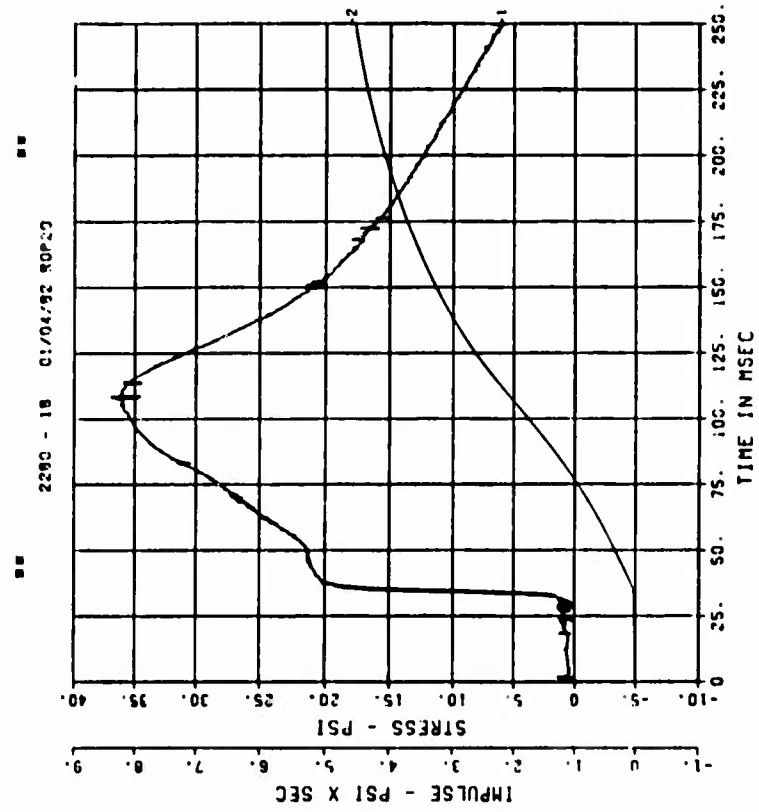
** PEAK VALUE IS 162 % OVER CALIBRATION **

DOE BLDG 12-64 PI
IP-1-S
100000. HZ CAL= 9.900
LP4 70% CUTOFF= 4500. HZ

2280 - 17   01/04/92 80P20

** PEAK VALUE IS 174 % OVER CALIBRATION **

E14

DOE BLDG 12-64 PI
IP-5

100000. HZ CAL= 28.70
LP4 70% CUTOFF= 4500. HZ

2290 - 32   01/04/82 ROP20

STRESS - PSI

IMPULSE - PSI X SEC

TIME IN MSEC
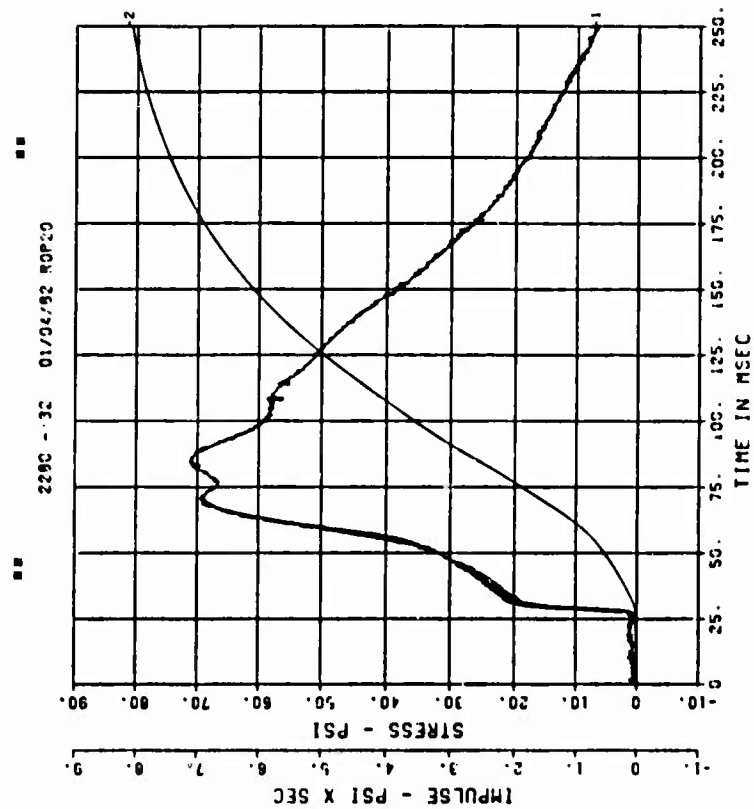
** PEAK VALUE IS 143 % OVER CALIBRATION **

DOE BLDG 12-64 PI
IP-3

100000. HZ CAL= 12.60
LP4 70% CUTOFF= 4500. HZ

2405 - 3   02/03/82 RO340

STRESS - PSI

IMPULSE - PSI X SEC

TIME IN MSEC

** PEAK VALUE IS 25 % OVER CALIBRATION **

E15

DOE BLDG 12-64 PI
IP-7-S
100000. HZ CAL= 12.40
LP4 70% CUTOFF= 4500. HZ

2290 - 22 02/12/82 ROP12

STRESS - PSI

IMPULSE - PSI X SEC

TIME IN MSEC

** PEAK VALUE IS 58.9 % OVER CALIBRATION **

DOE BLDG 12-64 PI
IP-6
100000. HZ CAL= 30.00
LP4 70% CUTOFF= 4500. HZ

2485 - 8 03/09/82 ROP30

STRESS - PSI

IMPULSE - PSI X SEC

TIME IN MSEC
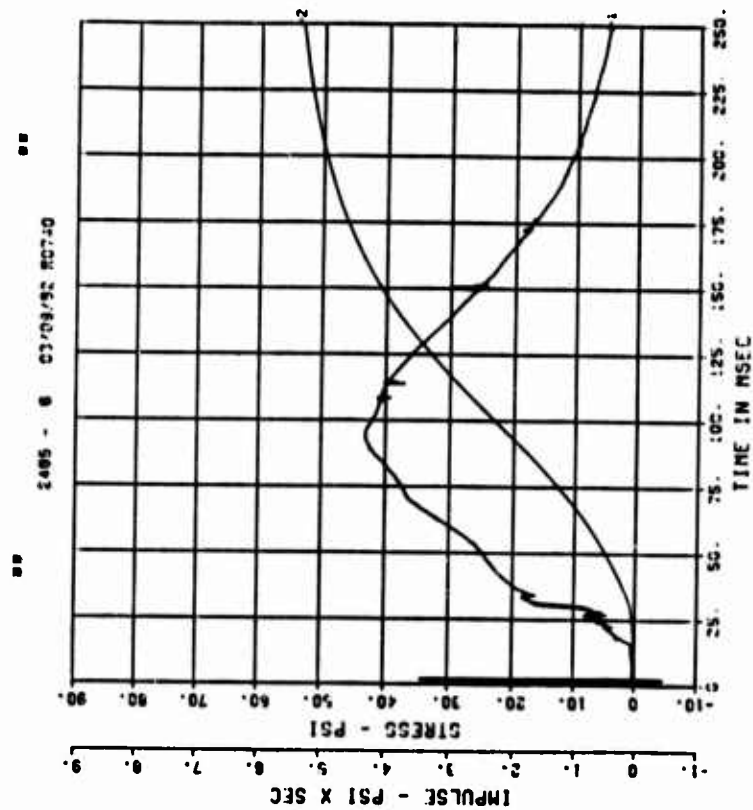
** PEAK VALUE IS 45 % OVER CALIBRATION **

E16

DOE BLDG 12-64 PI
IP-9

100000. HZ CAL= 26.70
LP4 70% CUTOFF= 4500. HZ

2495 - 3   01/05/92 POP24

STRESS - PSI

IMPULSE - PSI X SEC

TIME IN MSEC
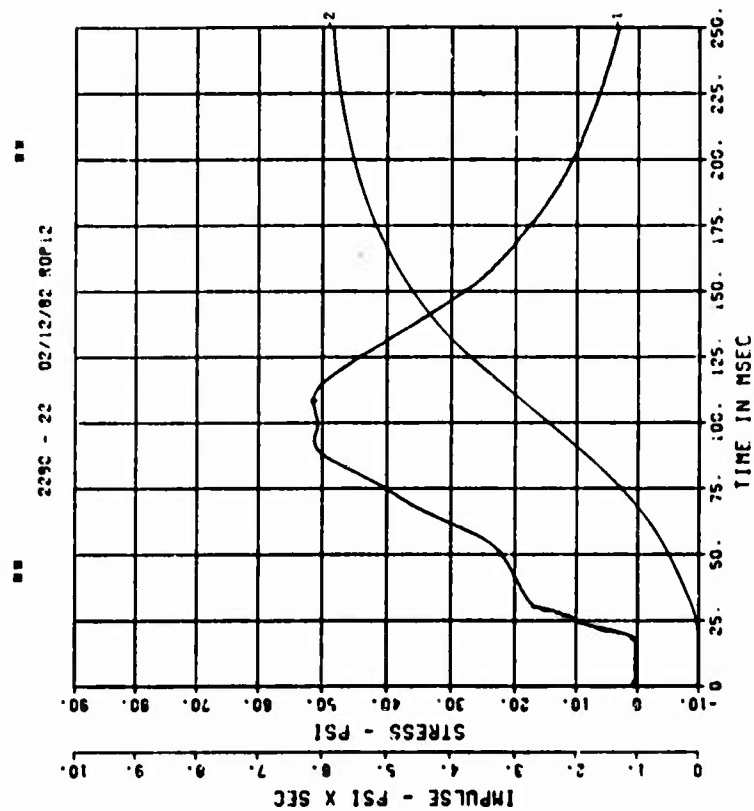
** PEAK VALUE IS 22   % OVER CALIBRATION **

DOE BLDG 12-64 PI
IP-8-S

100000. HZ CAL= 18.30
LP4 70% CUTOFF= 4500. HZ

2290 - 23   01/04/92 POP20

STRESS - PSI

IMPULSE - PSI X SEC

TIME IN MSEC

** PEAK VALUE IS 18%   % OVER CALIBRATION **

E17

DOE BLDG 12-64 PI
D-2

100000. HZ CAL= -1.800
LP4 70% CUTOFF= 4500. HZ

2290 - 15   02/06/92 R0333

DISPLACEMENT-INCHES

TIME IN MSEC
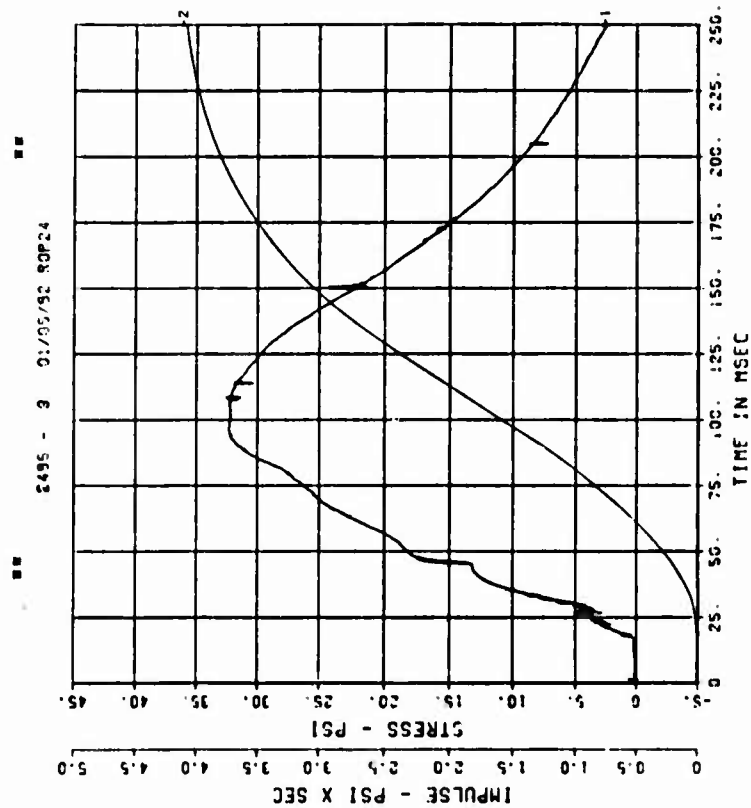
** PEAK VALUE IS 12   % OVER CALIBRATION **

DOE BLDG 12-64 PI
D-1

100000. HZ CAL= -1.900
LP4 70% CUTOFF= 4500. HZ

2290 - 14   02/12/92 R0P12

DISPLACEMENT-INCHES

TIME IN MSEC
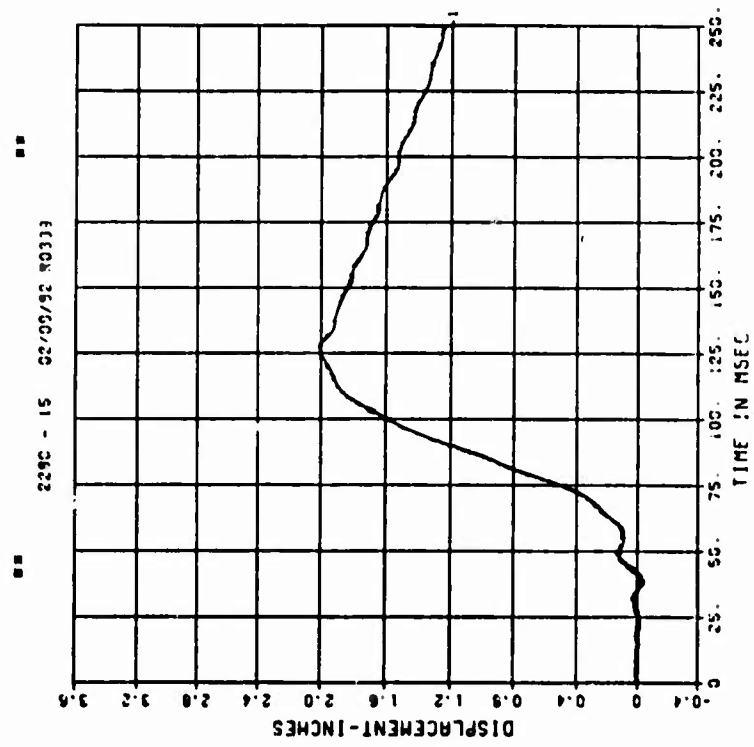
DOE BLDG 12-64 PI
D-3-S
100000. HZ   CAL= -1.610
LP4 70% CUTOFF= 4500. HZ

2280 - 31   02/09/82 R0339
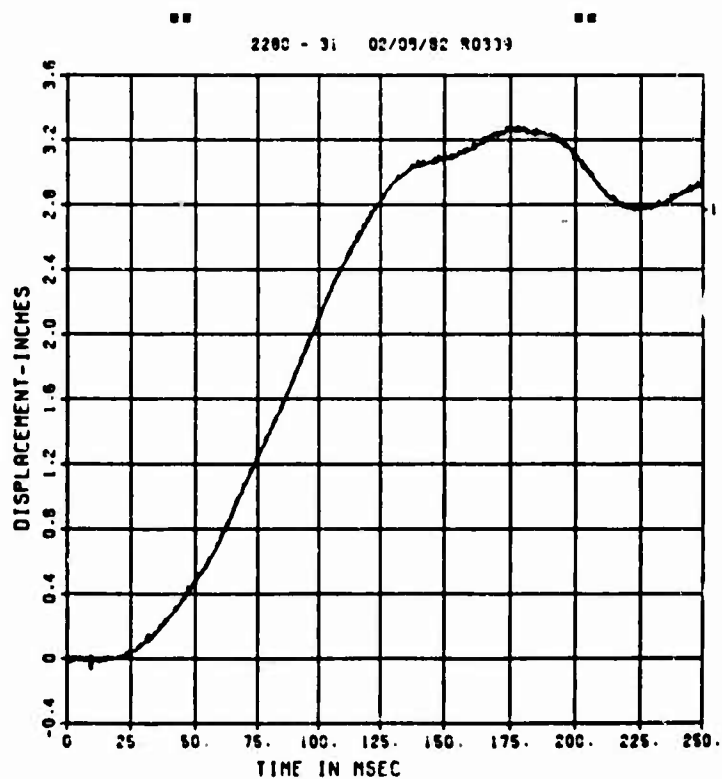
** PEAK VALUE IS 109 % OVER CALIBRATION **

E19

APPENDIX F

PHASE II STRUCTURAL VIBRATION TEST DATA

Figures F1 and F2 depict typical transfer functions obtained during dynamic testing. Each figure is a graph of response magnitude (acceleration normalized with respect to force) versus frequency of excitation. All of the functions in this appendix were obtained for the same drive point and accelerometer locations and are directly comparable. Differences in smoothness of the pre- and post-backfill functions are due to the use of a different type of accelerometer for the post-backfill tests.
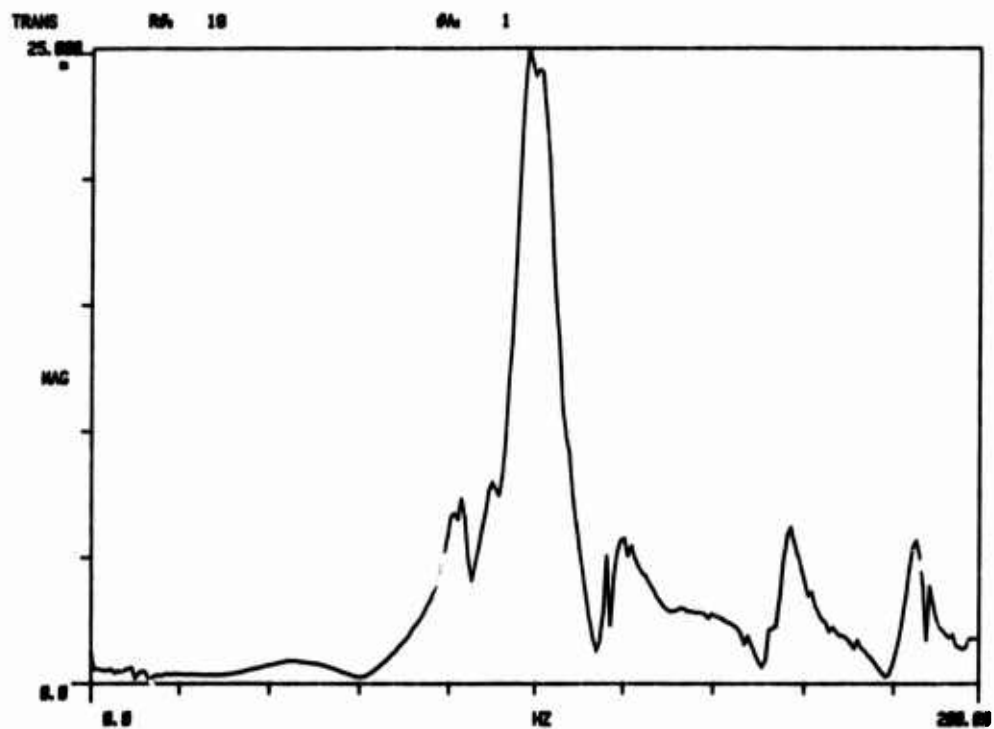
a. Before backfill.
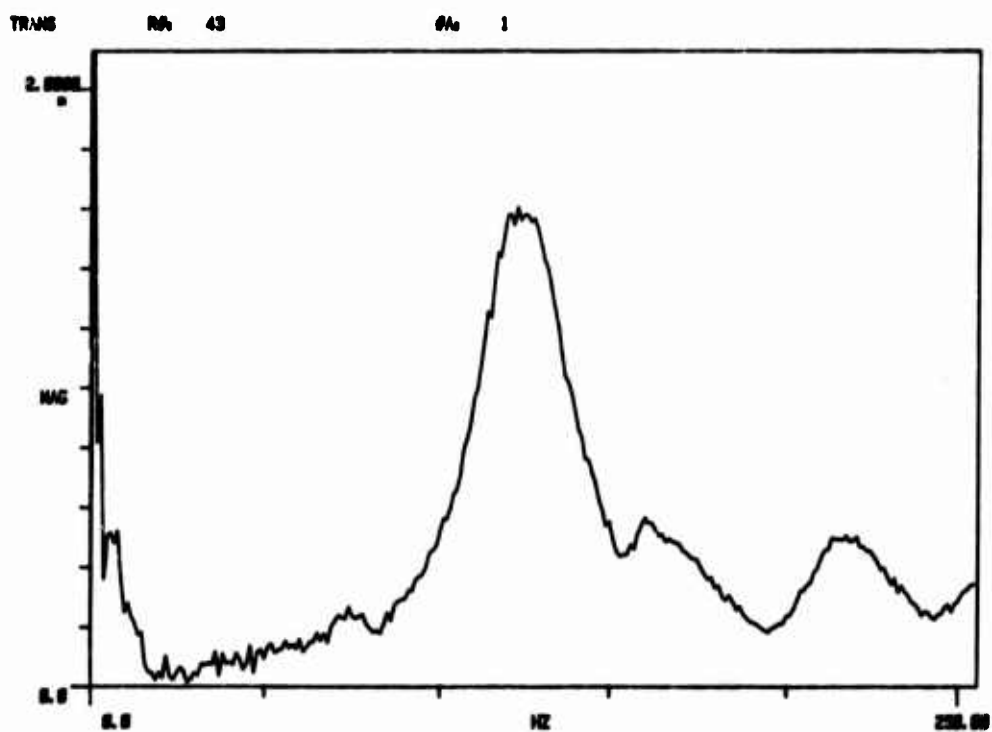
b. After backfill

Figure F1. Transfer functions for donor bay.

F3
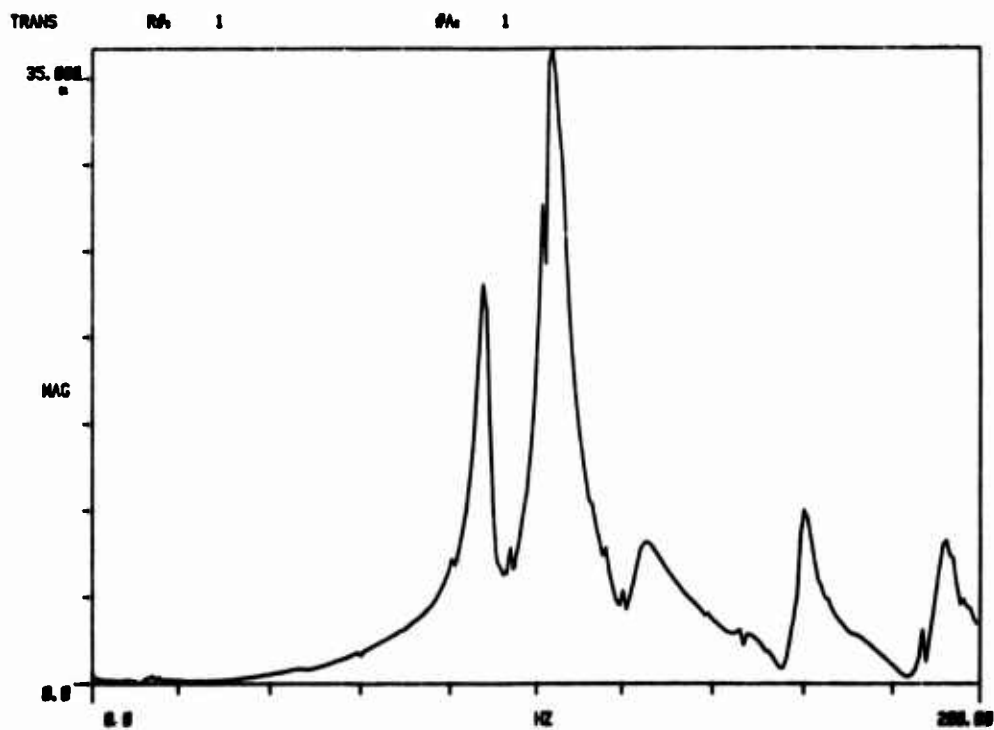
a. Before backfill.
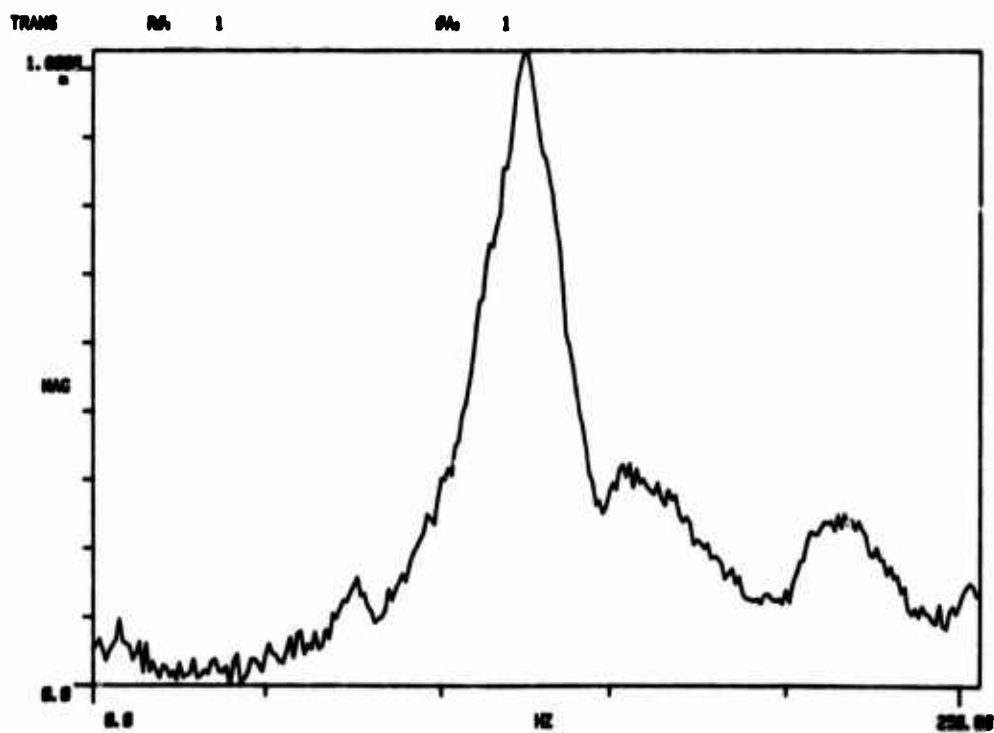
b. After backfill.

Figure F2. Transfer functions for acceptor bay.

APPENDIX G

PHASE II TEST DATA

Electronic data are shown with one of six different time scales. Air-blast data shown with time scales of 5 and 25 msec were recorded and processed to obtain a system frequency response of 80 kHz. The remaining records were recorded and digitized to achieve frequency response on the order of 20 kHz for unfiltered records and 4.5 kHz for filtered records.

The 5- and 25-msec records from BP12-14 show the time of arrival of the initial shock wave and peak pressures. The attenuation of the reflected shocks and the buildup of quasistatic pressure can be observed in the 25-msec records. The 125-msec records for these transducers show the quasistatic pressure buildup and decay. Peak pressures are not shown on these records due to reduced frequency response and the use of a scale factor appropriate for quasistatic pressures.

All other data are shown with a time scale appropriate for the phenomenon recorded. Blast pressure data are shown with either 100- or 200-msec scales. Interface and soil stress data records have either 125- or 150-msec scales. Deflection and acceleration data are shown with 125-msec durations.

DOE BLDG 12-64 PII
BP-2
100000. HZ CAL= 17.80

01994- 29   02/05/92 POP31

** PEAK VALUE IS 95   % UNDER CALIBRATION **

DOE BLDG 12-64 PII
BP-1
100000. HZ CAL= 17.00

01994- 27   02/03/92 POP37

** PEAK VALUE IS 86   % UNDER CALIBRATION **

G3

DOE BLDG 12-64 PII
BP-4
100000. HZ CAL= 20.80

0:994- 33   02/05/82 ROP31

** PEAK VALUE IS 57   % UNDER CALIBRATION **

TIME IN MSEC

PRESSURE - PSI

IMPULSE - PSI X SEC
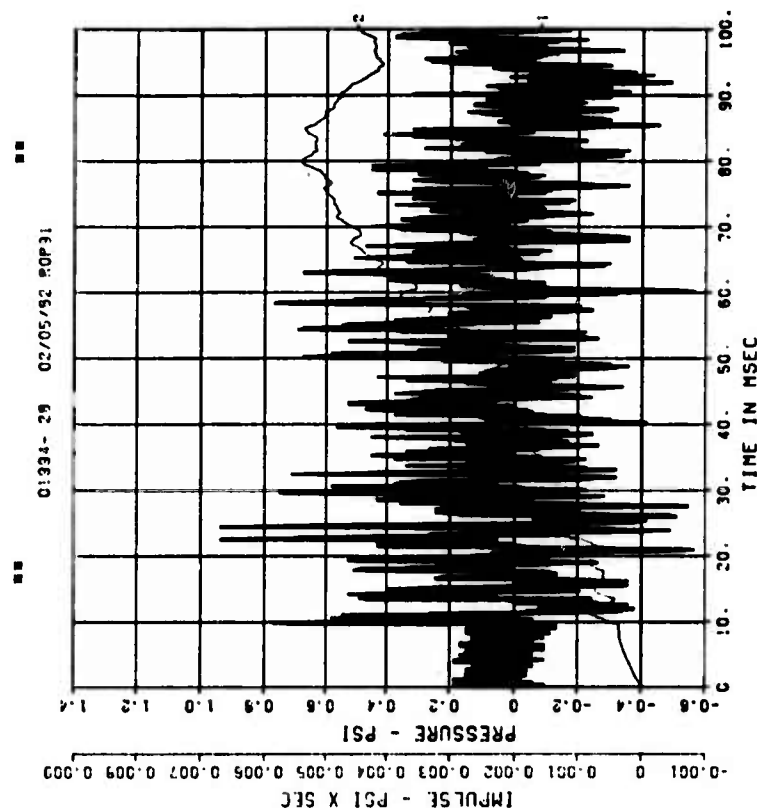
DOE BLDG 12-64 PII
BP-3
100000. HZ CAL= 15.50

0:994- 32   02/05/82 ROP31

** PEAK VALUE IS 91   % UNDER CALIBRATION **

TIME IN MSEC

PRESSURE - PSI

IMPULSE - PSI X SEC

G4

DOE BLDG 12-64 PII
BP-6
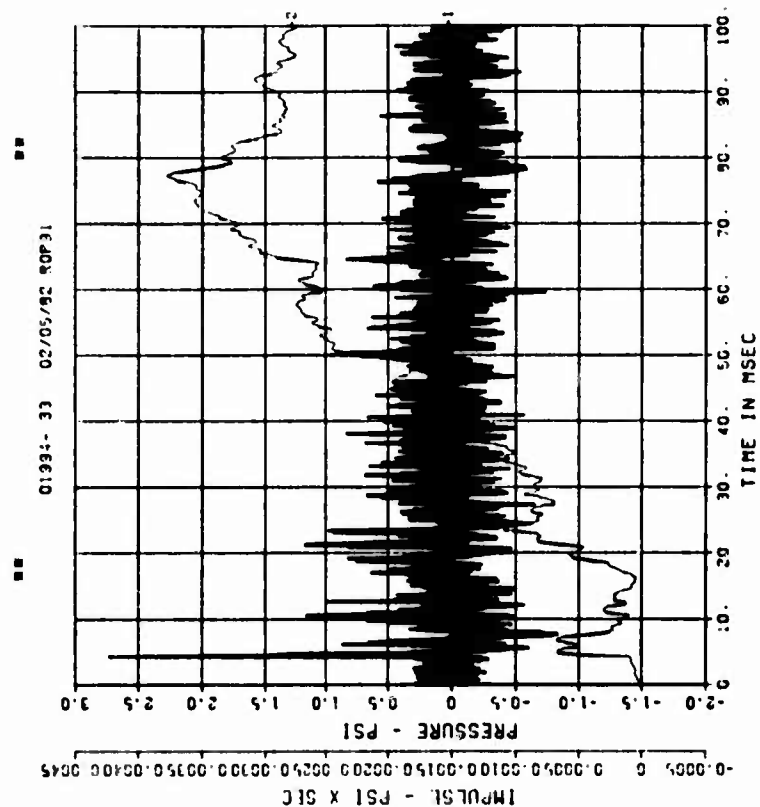
100000. HZ CAL= 27.80
LF4 70% CUTOFF= 4500. HZ

DOE BLDG 12-64 PII
BP-5-S

100000. HZ CAL= 6.800

G5

DOE BLDG 12-64 PII
BP-8
100000. HZ CAL= 57.50
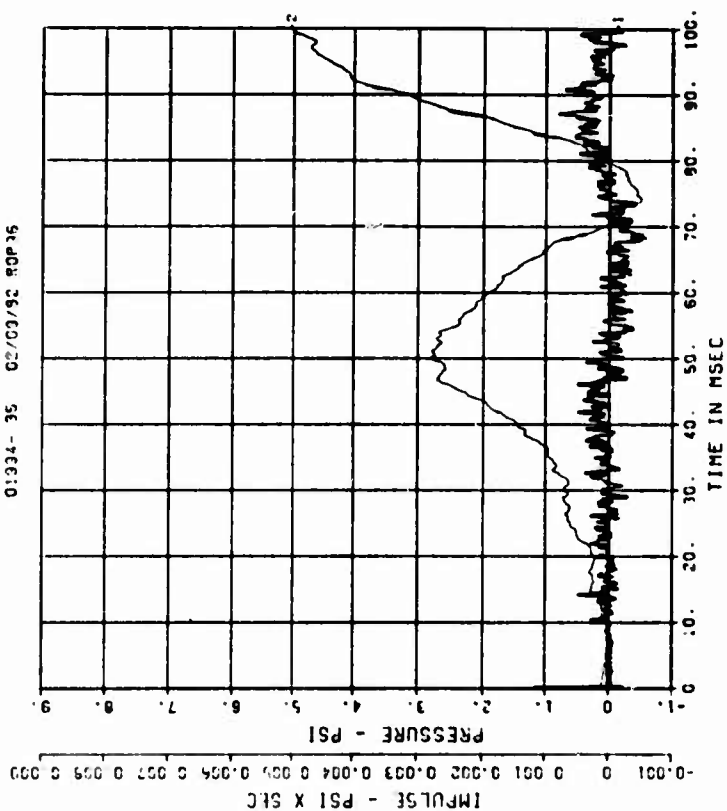
DOE BLDG 12-64 PII
BP-7
100000. HZ CAL= 77.90

G6

DOE BLDG 12-64 PII
BP-10
100000. HZ CAL= 116.2
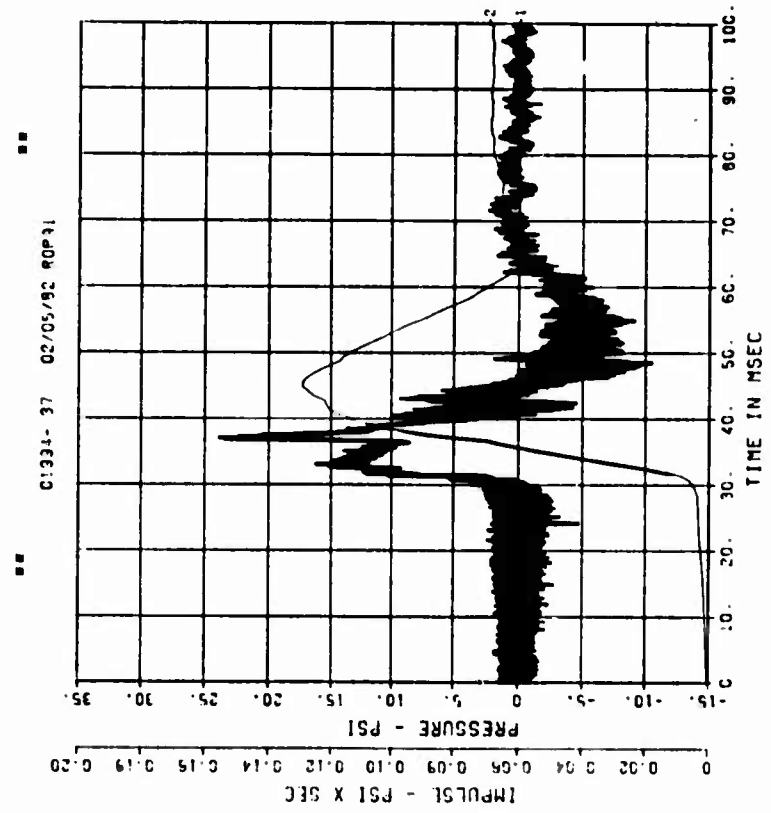
DOE BLDG 12-64 PII
BP-9
100000. HZ CAL= 77.10

G7

DOE BLDG 12-64 PII
BP-12-S
500000. HZ CAL= -304.7
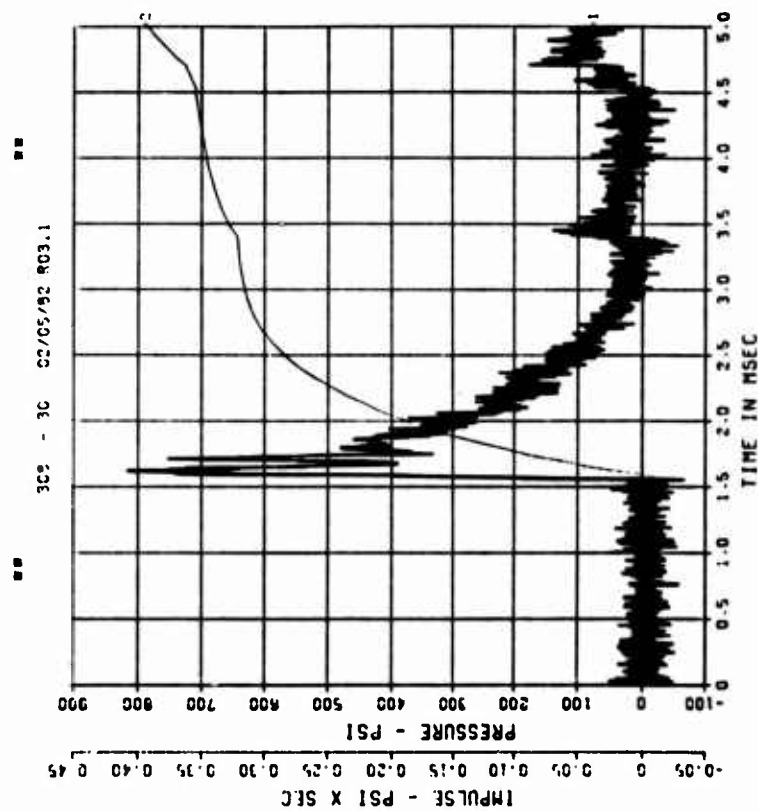
** PEAK VALUE IS 168 % OVER CALIBRATION **

DOE BLDG 12-64 PII
BP-11
100000. HZ CAL= 114.7

G8

DOE BLDG 12-64 PII
BP-12

100000. HZ CAL= 304.7
LF4 70% CUTOFF= 4500. HZ

01994-41   02/03/92 ROP37

PRESSURE - PSI

IMPULSE - PSI X SEC

TIME IN MSEC

** PEAK VALUE IS 44   % OVER CALIBRATION **

DOE BLDG 12-64 PII
BP-12

100000. HZ CAL= 304.7

01994-41   02/03/92 ROP37

PRESSURE - PSI

IMPULSE - PSI X SEC

TIME IN MSEC

** PEAK VALUE IS 35   % OVER CALIBRATION **

DOE BLDG 12-64 PII
BP-13-S
500000. HZ CAL= 355.9

3603 - 1 02/03/92 ROP39

STRESS - PSI
IMPULSE - PSI X SEC
TIME IN MSEC

** PEAK VALUE IS 200 % OVER CALIBRATION **

DOE BLDG 12-64 PII
BP-13-S
500000. HZ CAL= 355.9

3603 - 1 02/03/92 ROP33

STRESS - PSI
IMPULSE - PSI X SEC
TIME IN MSEC

** PEAK VALUE IS 200 % OVER CALIBRATION **

G11
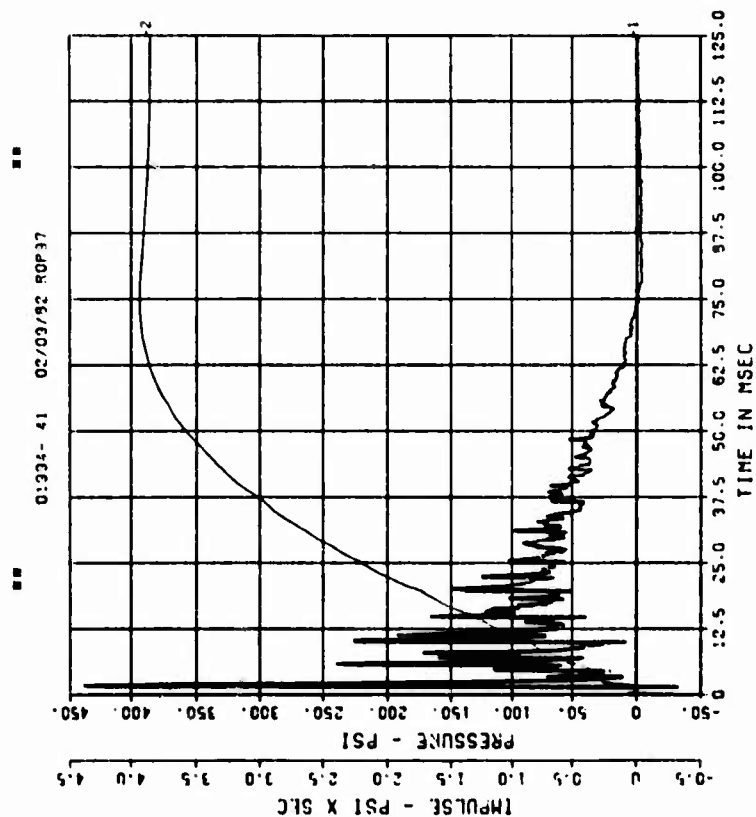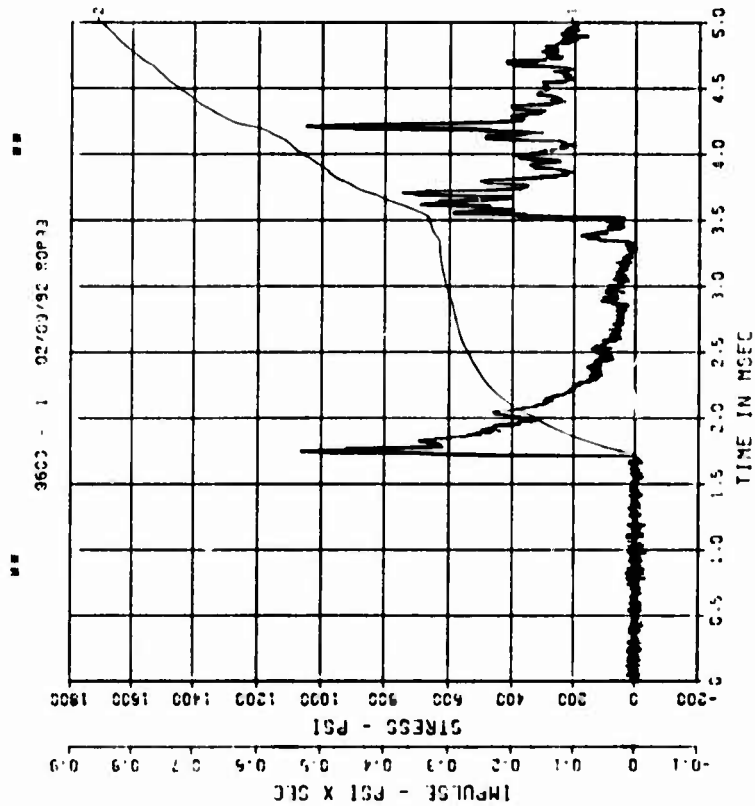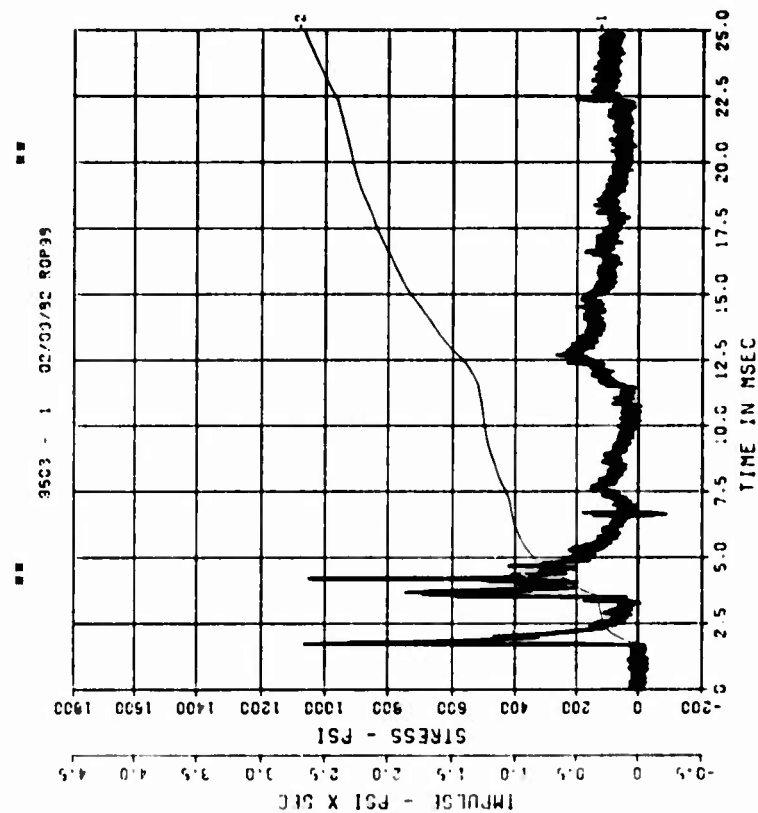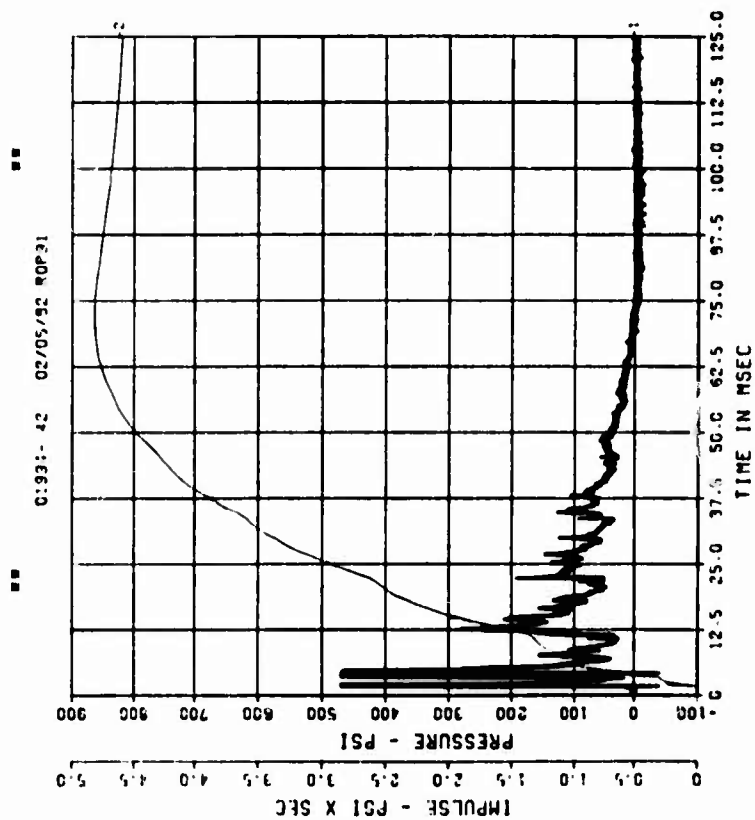
DOE BLDG 12-64 PII
BP-13
100000. HZ CAL= 355.9
LP4 70% CUTOFF= 4500. HZ
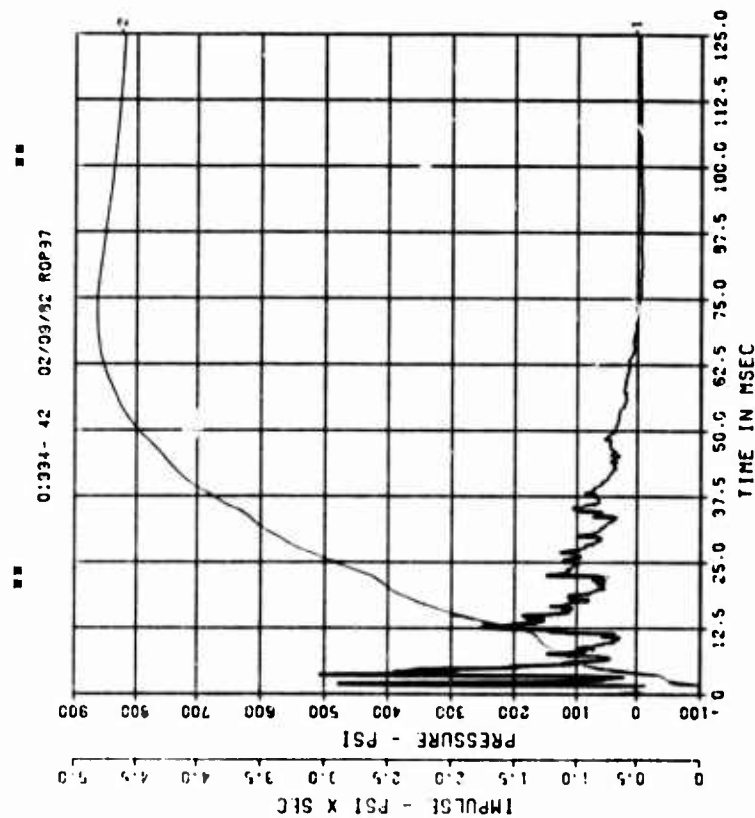
DOE BLDG 12-64 PII
BP-13
100000. HZ CAL= 355.9

G12

DOE BLDG 12-64 PII
BP-14-S
500000. HZ CAL= 341.1

DOE BLDG 12-64 PII
BP-14-S
500000. HZ CAL= 341.1

G13

DOE BLDG 12-64 PII
BP-14
100000. HZ CAL= 341.1
LF4 75% CUTOFF= 4500. HZ

DOE BLDG 12-64 PII
BP-14
100000. HZ CAL= 341.1

G14
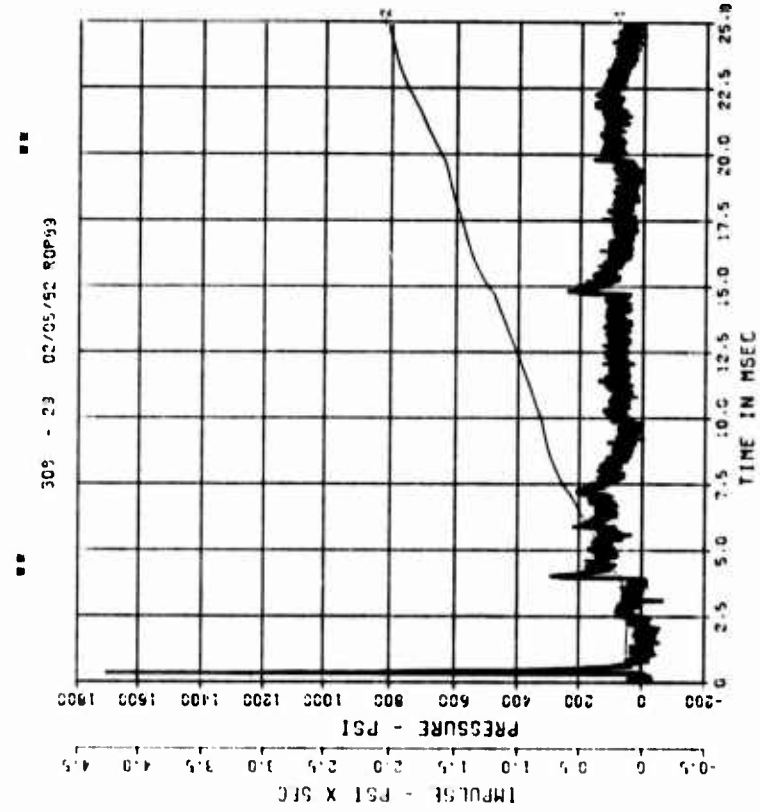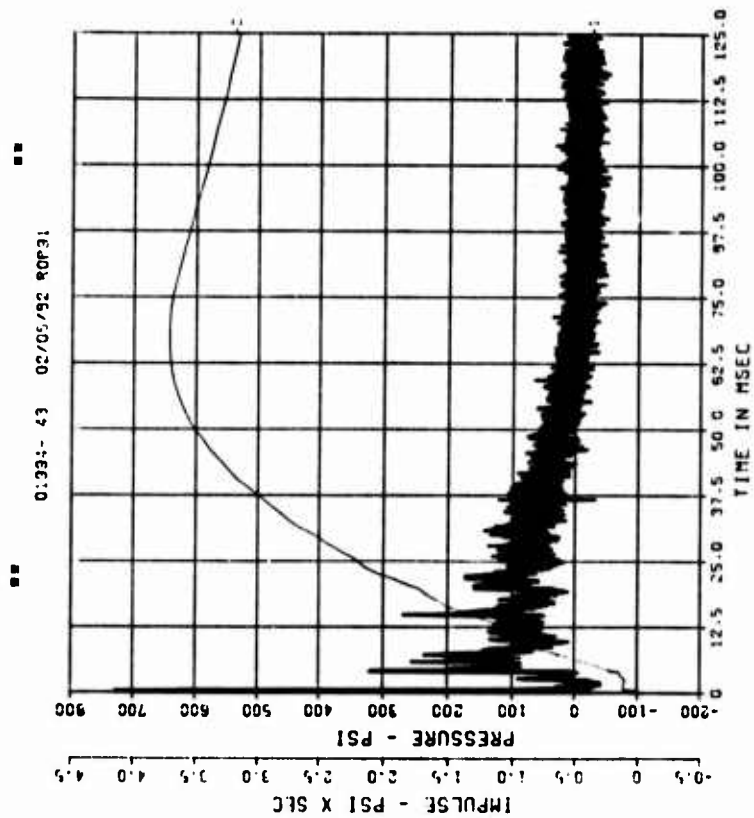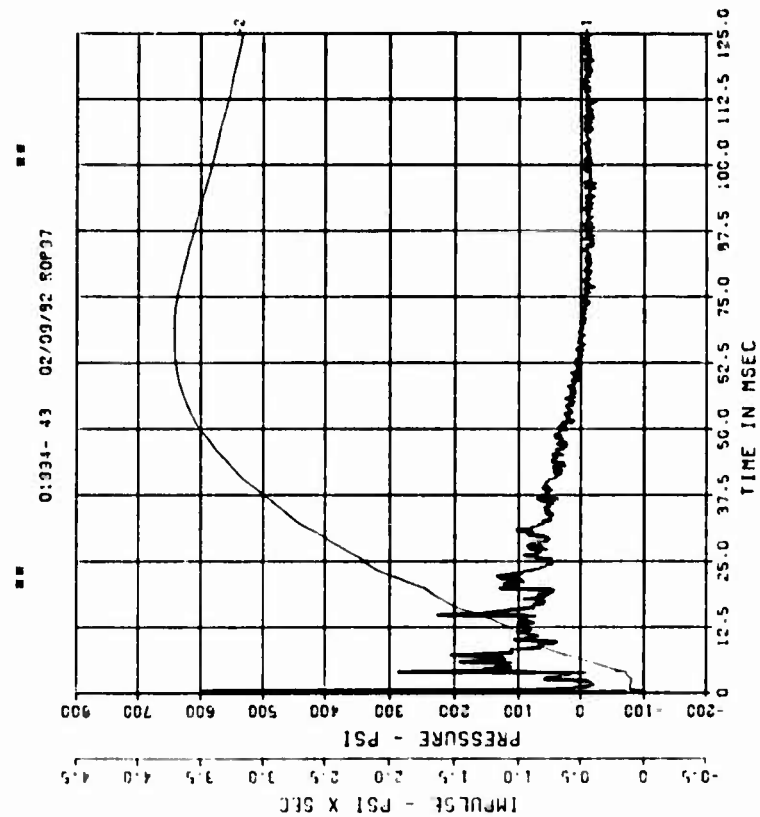
DOE BLDG 12-64 PII
BP-16
100000. HZ CAL= 32.50

DOE BLDG 12-64 PII
BP-15
100000. HZ CAL= 55.00

G15

DOE BLDG 12-64 PII
BP-18
100000. HZ CAL= 34.10
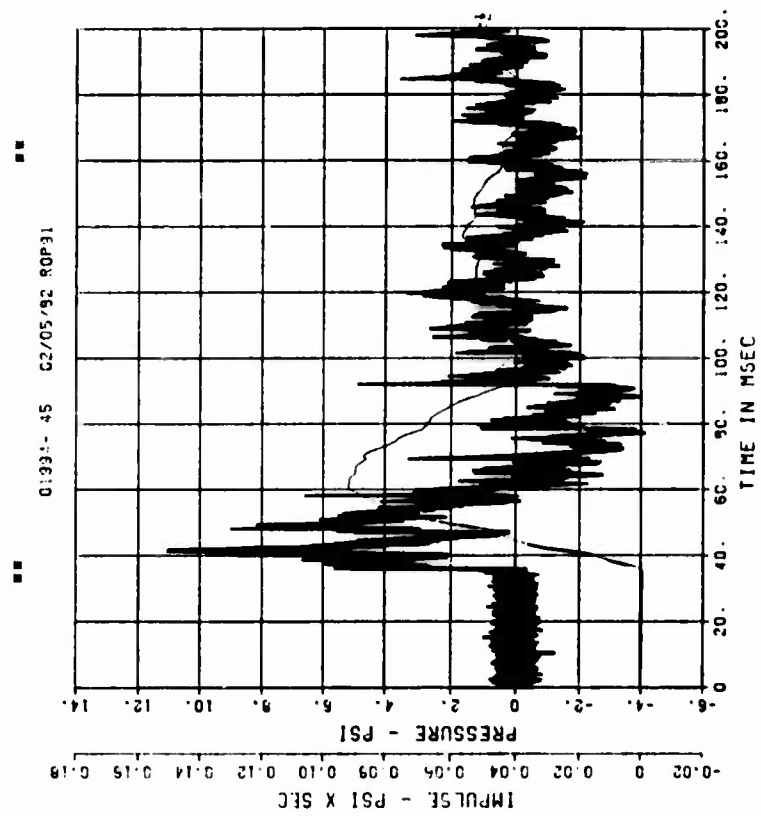
DOE BLDG 12-64 PII
BP-17
100000. HZ CAL= 32.10

G16

DOE BLDG 12-64 PII
BP-20
100000. HZ CAL= 31.90
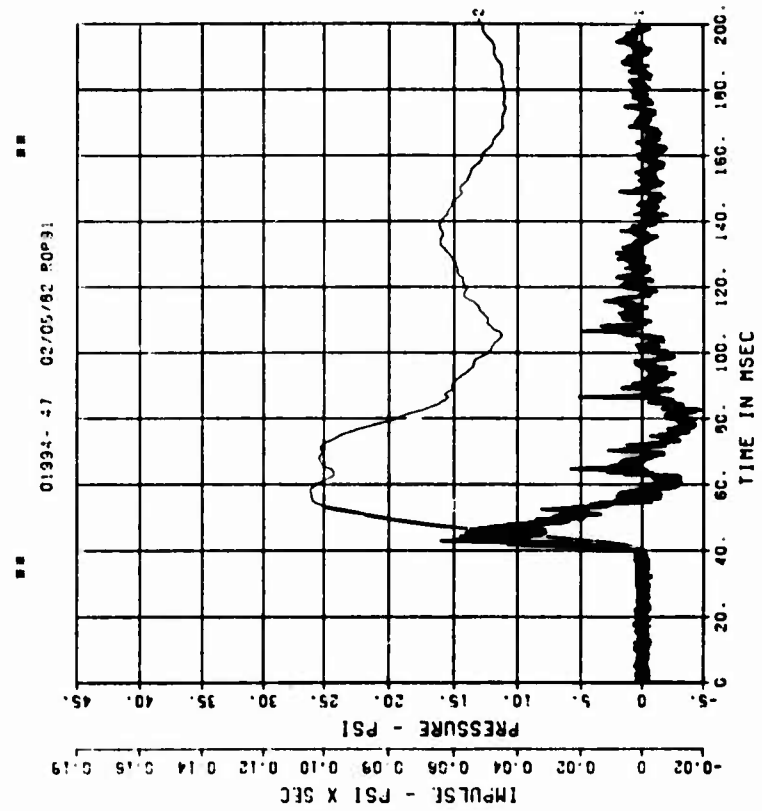
DOE BLDG 12-64 PII
BP-19
100000. HZ CAL= 34.70

G17

DOE BLDG 12-64 PII
BP-22

100000. HZ CAL= 24.40
LP4 70% CUTOFF= 4500. HZ

0:93:- S: 02/03/92 ROP96

** PEAK VALUE IS 36   % UNDER CALIBRATION **

DOE BLDG 12-64 PII
BP-21

100000. HZ CAL= 12.40
LP4 70% CUTOFF= 4500. HZ

0:93:- 50 02/03/92 ROP96

G18

DOE BLDG 12-64 PII
BP-24
100000. HZ CAL= 51.97
LP4 70% CUTOFF=4500. HZ

0:334-53   02/03/92 ROP36

PRESSURE - PSI
IMPULSE - PSI X SEC
TIME IN MSEC
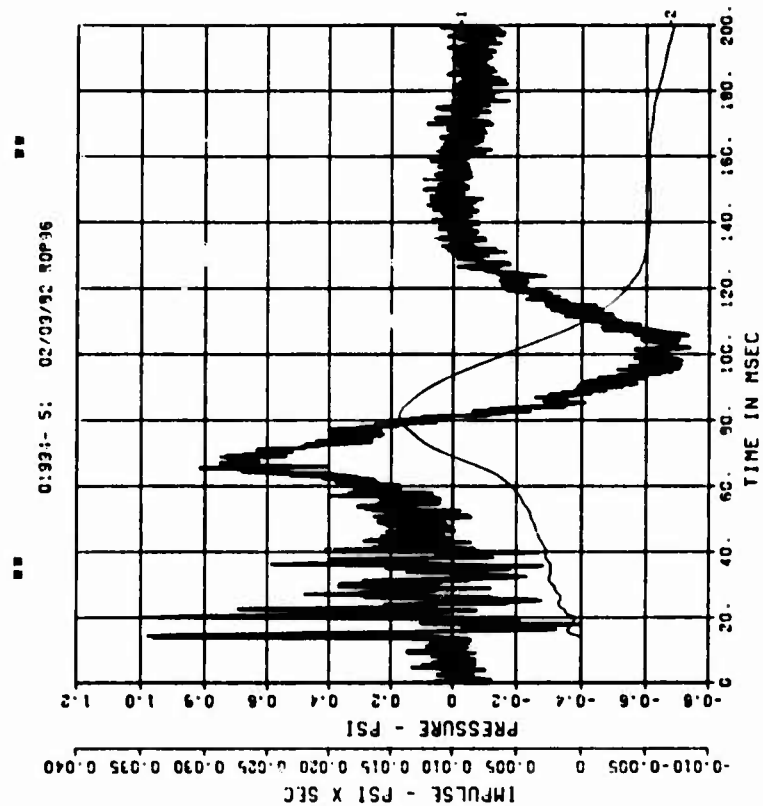
** PEAK VALUE IS 98   % UNDER CALIBRATION **

DOE BLDG 12-64 PII
BP-23
100000. HZ CAL= 33.60
LP4 70% CUTOFF=4500. HZ

0:334-52   02/03/92 ROP36

PRESSURE - PSI
IMPULSE - PSI X SEC
TIME IN MSEC

** PEAK VALUE IS 92   % UNDER CALIBRATION **

DOE BLDG 12-64 PII
BP-26

100000. HZ CAL= 45.70
LP4 70% CUTOFF= 4500. HZ

** PEAK VALUE IS 93   % UNDER CALIBRATION **
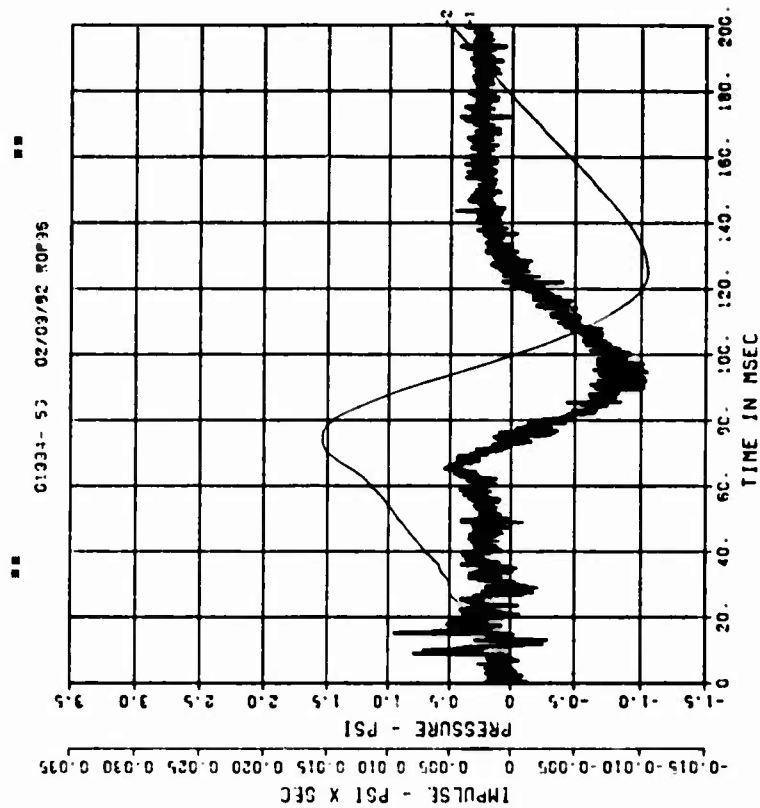
DOE BLDG 12-64 PII
BP-25

100000. HZ CAL= 76.40
LP4 70% CUTOFF= 4500. HZ

** PEAK VALUE IS 57   % UNDER CALIBRATION **

G20

DOE BLDG 12-64 PII
BP-28
100000. HZ CAL= 18.50
LP4 70% CUTOFF= 4500. HZ
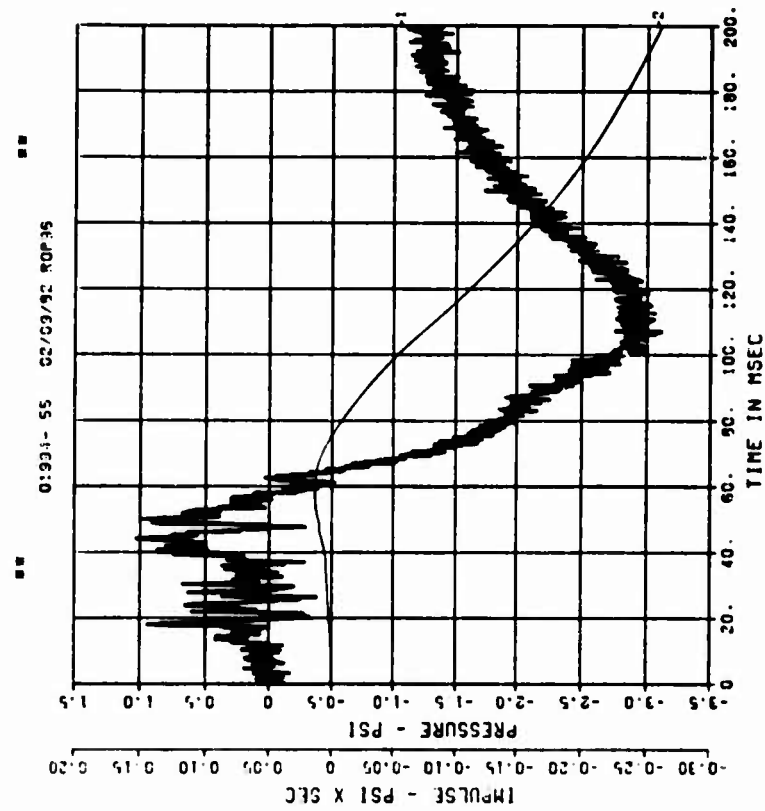
** PEAK VALUE IS 94   % UNDER CALIBRATION **

DOE BLDG 12-64 PII
BP-27
100000. HZ CAL= 25.20
LP4 70% CUTOFF= 4500. HZ

** PEAK VALUE IS 97   % UNDER CALIBRATION **

G21

DOE BLDG 12-64 PII
SS-1

100000. HZ CAL= 72.50
LP4 70% CUTOFF= 4500. HZ

DOE BLDG 12-64 PII
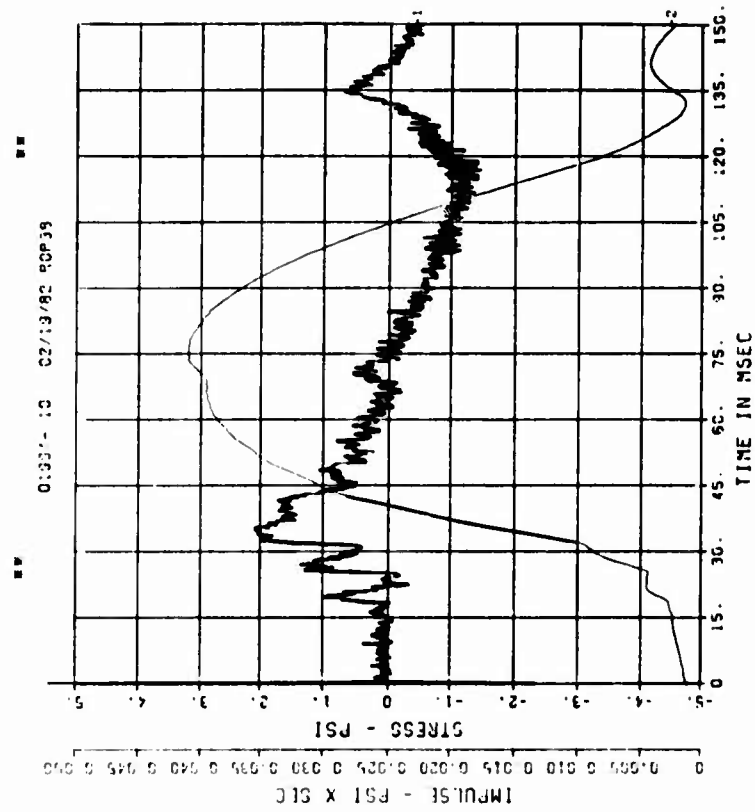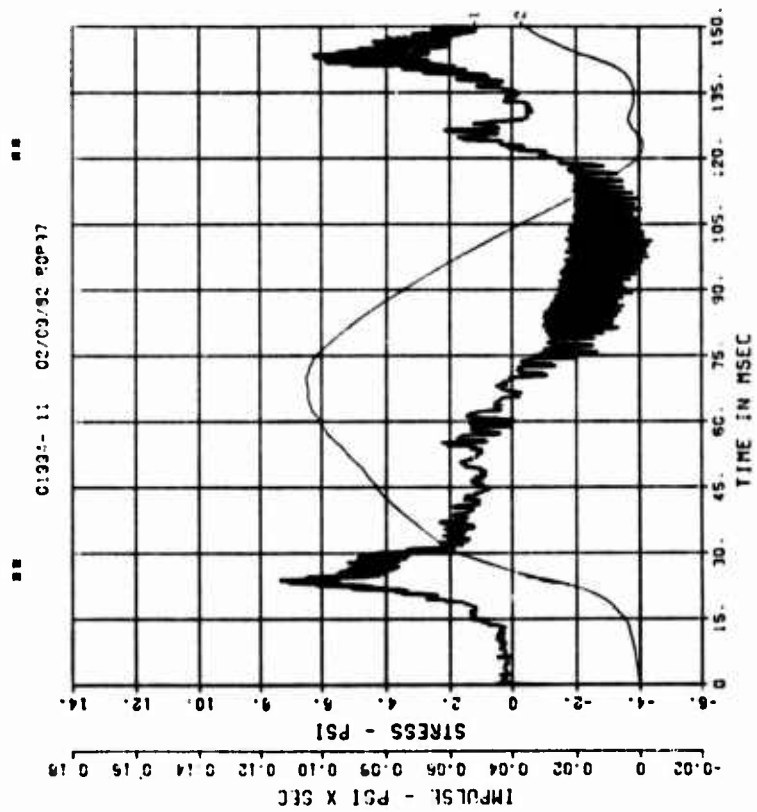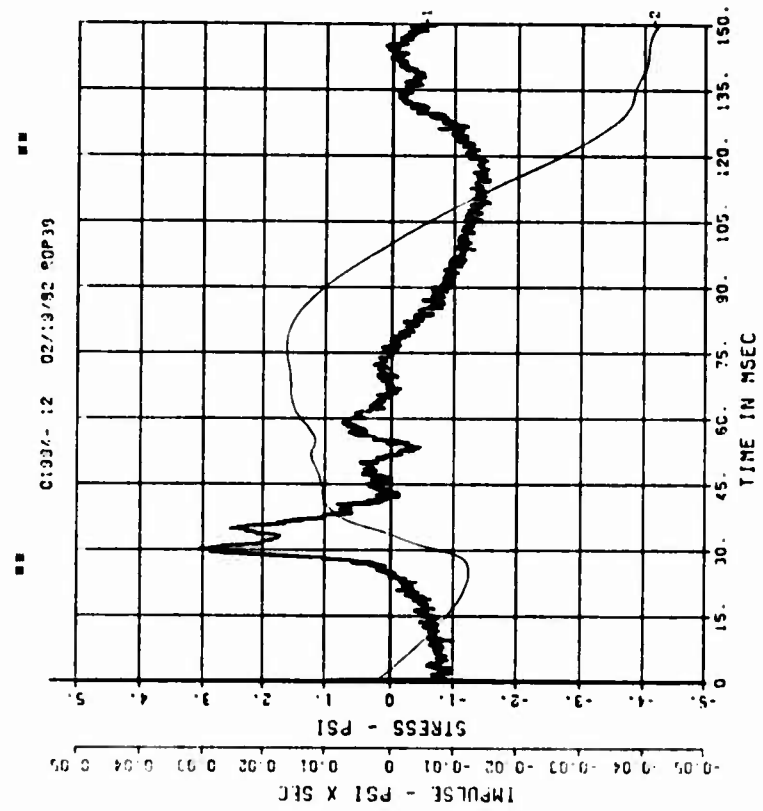BP-29

100000. HZ CAL= 12.70
LP4 70% CUTOFF= 4500. HZ

G22

DOE BLDG 12-64 PII
SS-3
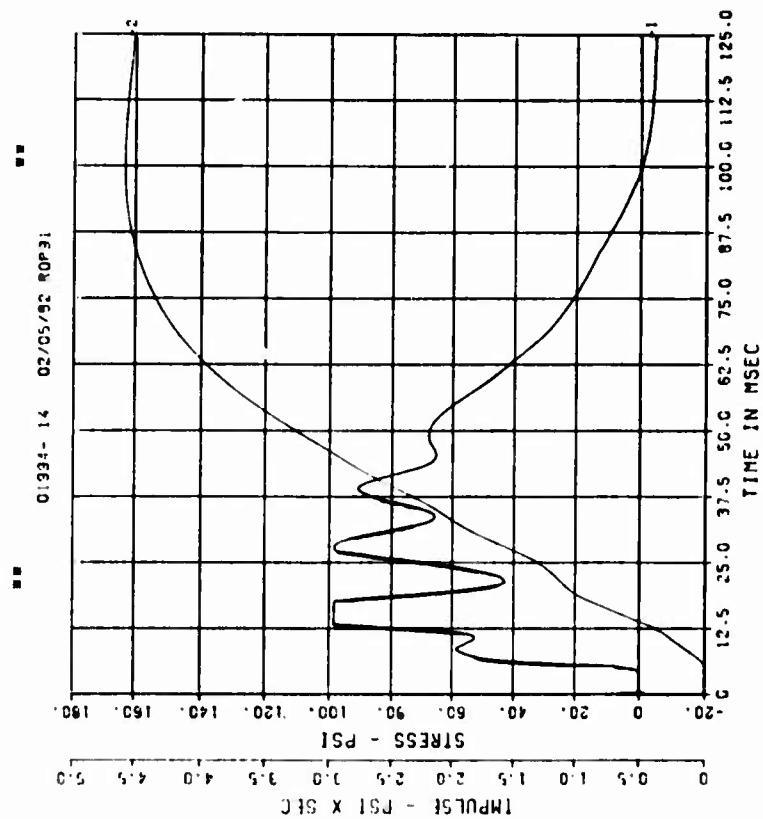
100000. HZ   CAL= 163.9
LP4 70% CUTOFF= 4500. HZ

DOE BLDG 12-64 PII
SS-2

100000. HZ   CAL= 202.2
LP4 70% CUTOFF= 4500. HZ
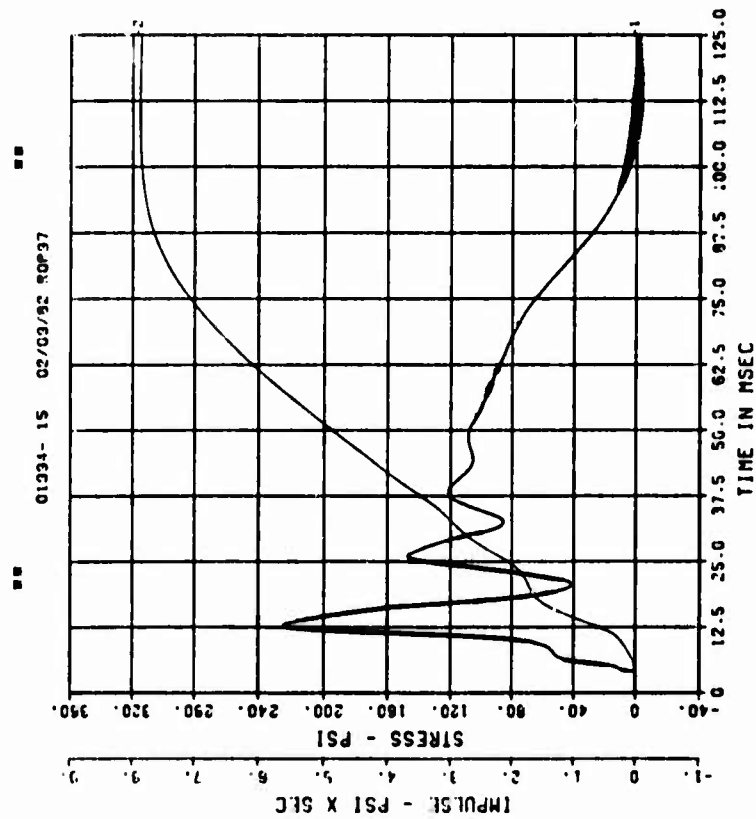
** PEAK VALUE IS 11 % OVER CALIBRATION **

G23

DOE BLDG 12-64 PII
IP-1

100000. HZ CAL= 63.97
LP4 70% CUTOFF= 4500. HZ

01994- 1   02/05/82 ROP31

DOE BLDG 12-64 PII
SS-4

100000. HZ CAL= 170.6
LP4 70% CUTOFF= 4500. HZ

01994- 17   02/05/82 ROP31
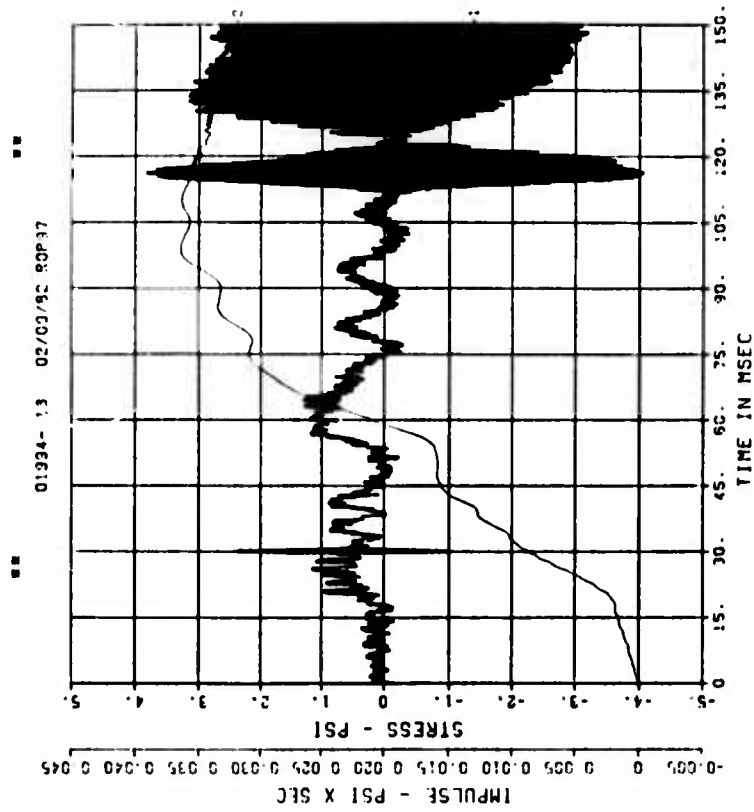
DOE BLDG 12-64 PII
IP-3

100000. HZ CAL= 51.90
LP4 70% CUTOFF= 4500. HZ

DOE BLDG 12-64 PII
IP-2

100000. HZ CAL= 86.70
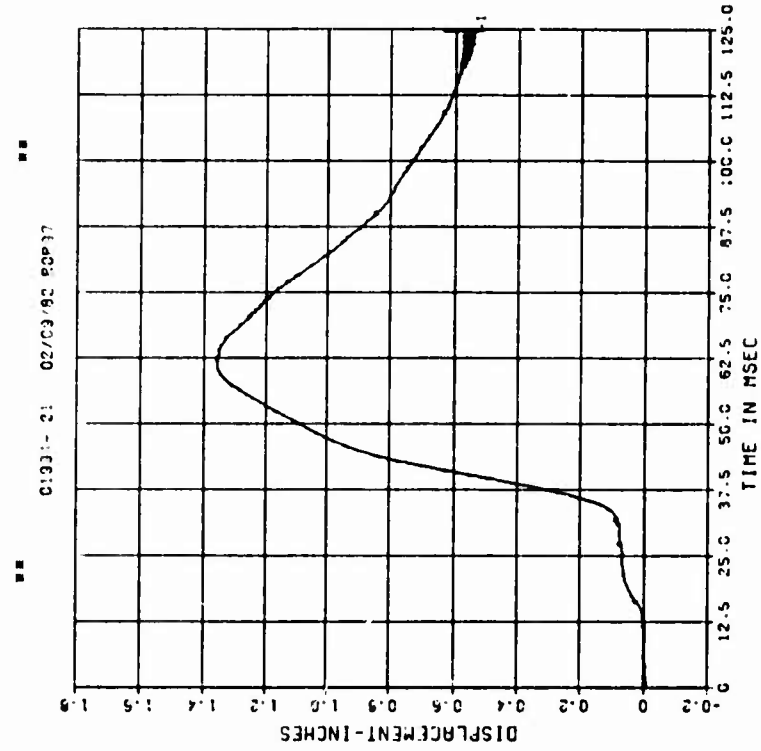LP4 70% CUTOFF= 4500. HZ

G25

DOE BLDG 12-64 PII
IP-5

100000. HZ CAL= 129.2
LP4 70% CUTOFF= 4500. HZ

01994- 5   02/05/92 ROP31

DOE BLDG 12-64 PII
IP-4

100000. HZ CAL= 104.4
LP4 70% CUTOFF= 4500. HZ

01994- 4   02/05/92 ROP31

DOE BLDG 12-64 PII
IP-7

100000. HZ CAL= 98.90
LP4 70% CUTOFF= 4500. HZ
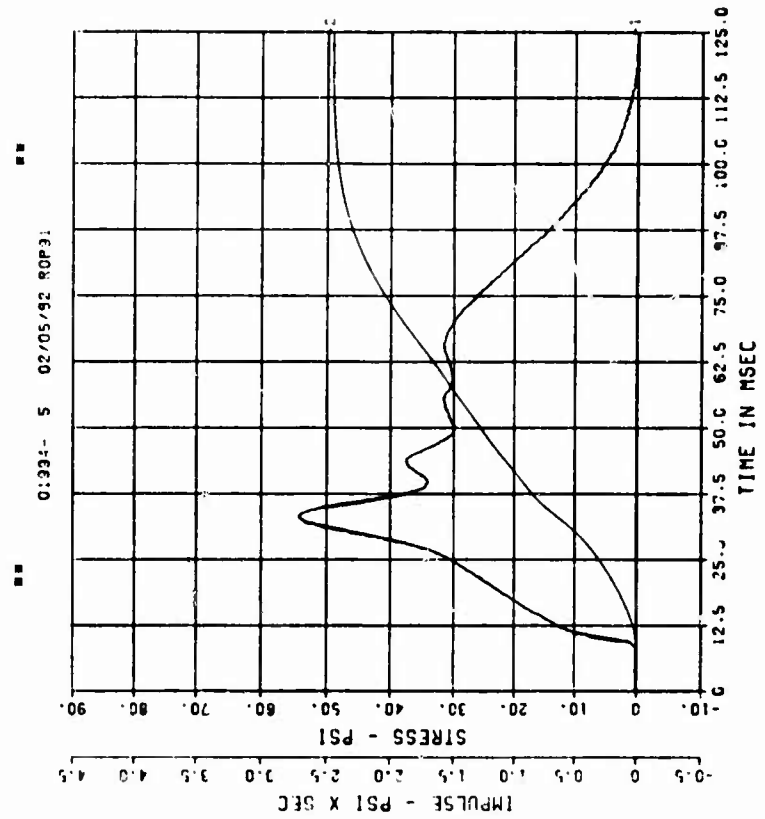
DOE BLDG 12-64 PII
IP-6

100000. HZ CAL= 102.2
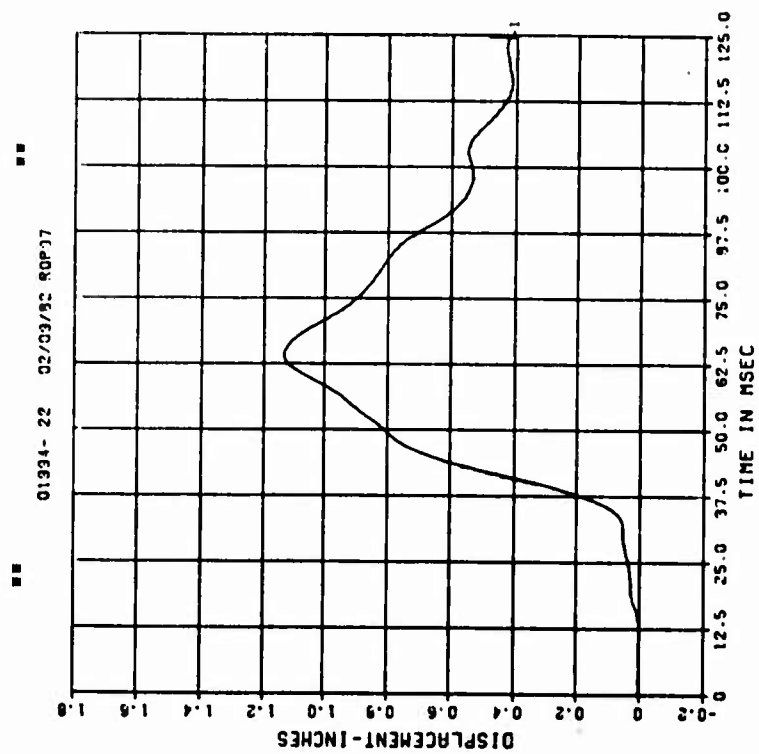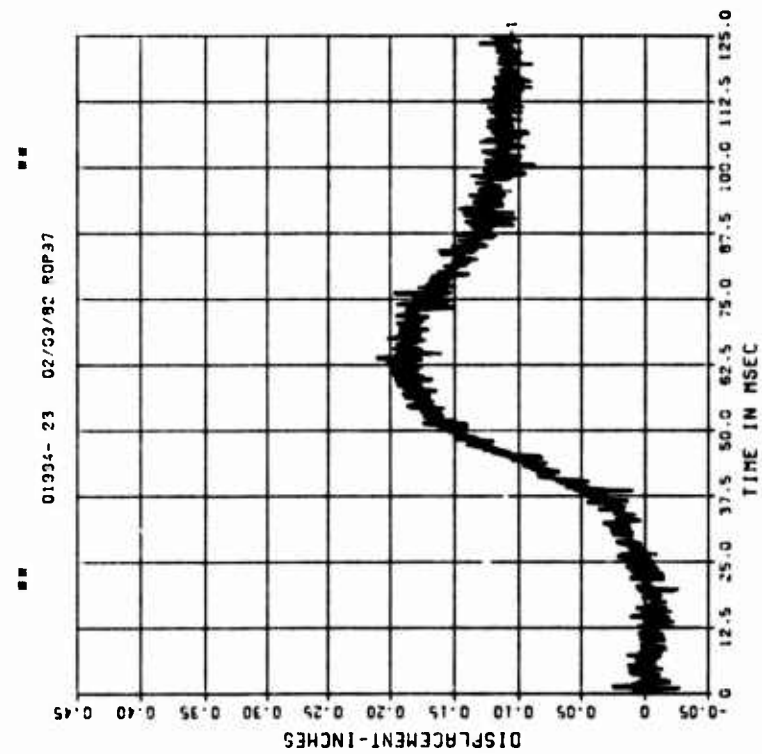LP4 70% CUTOFF= 4500. HZ

DOE BLDG 12-64 PII
IP-9
100000. HZ CAL= 87.50
LP4 70% CUTOFF= 4500. HZ

DOE BLDG 12-64 PII
IP-8
100000. HZ CAL= 99.90
LP4 70% CUTOFF= 4500. HZ

G28

DCE BLDG 12-64 PII
IP-11

100000. HZ CAL= 117.2
LP4 70% CUTOFF= 4500 HZ
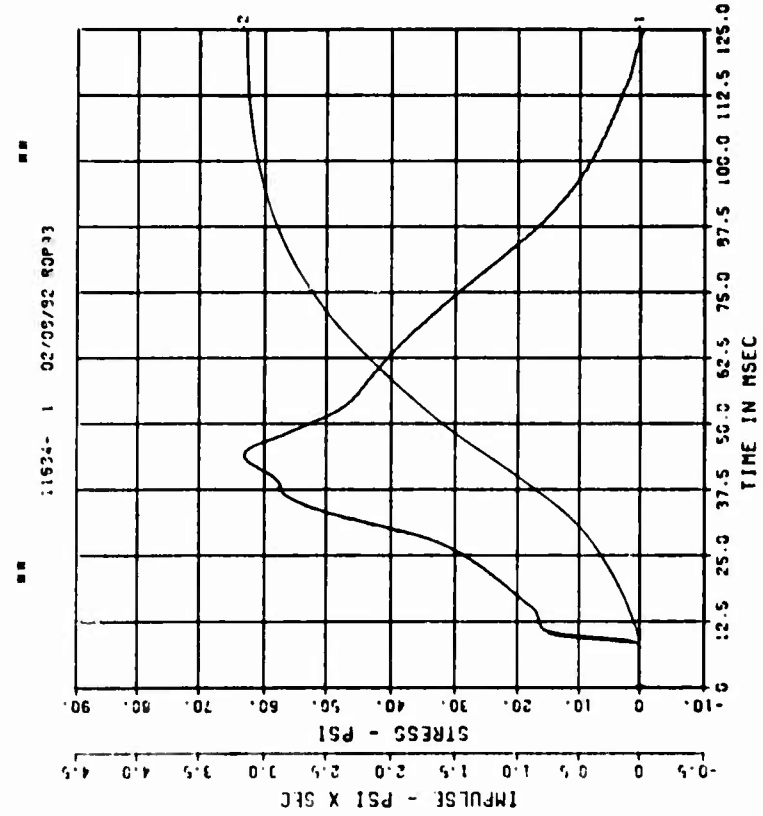
DCE BLDG 12-64 PII
IP-10

100000. HZ CAL= 94.70
LP4 70% CUTOFF= 4500 HZ

DOE BLDG 12-64 PII
IP-13

100000. HZ CAL= 111.8
LP4 70% CUTOFF= 4500. HZ

DOE BLDG 12-64 PII
IP-12

100000. HZ CAL= 129.8
LP4 70% CUTOFF= 4500. HZ

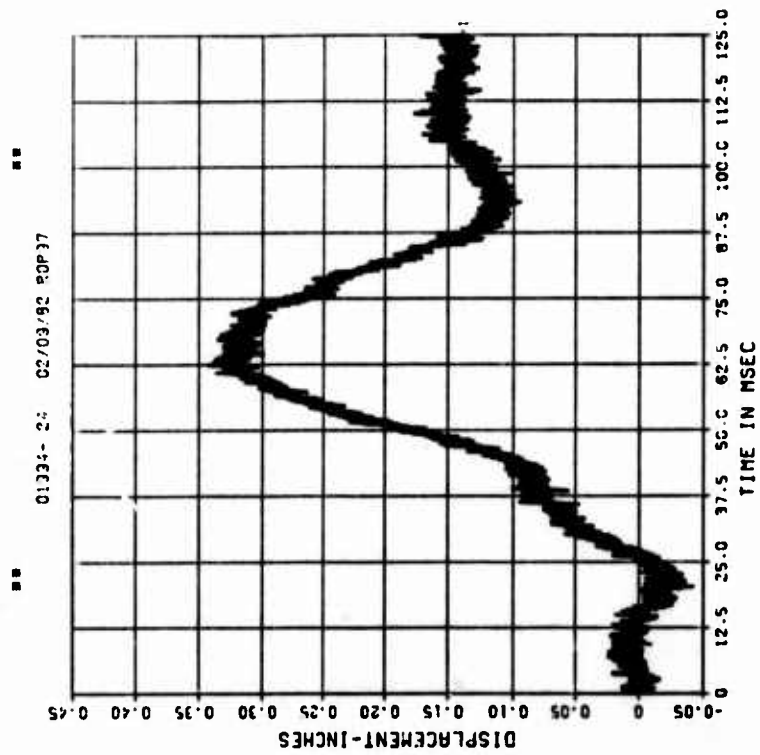** PEAK VALUE IS 94   % UNDER CALIBRATION **

G30

DOE BLDG 12-64 PII
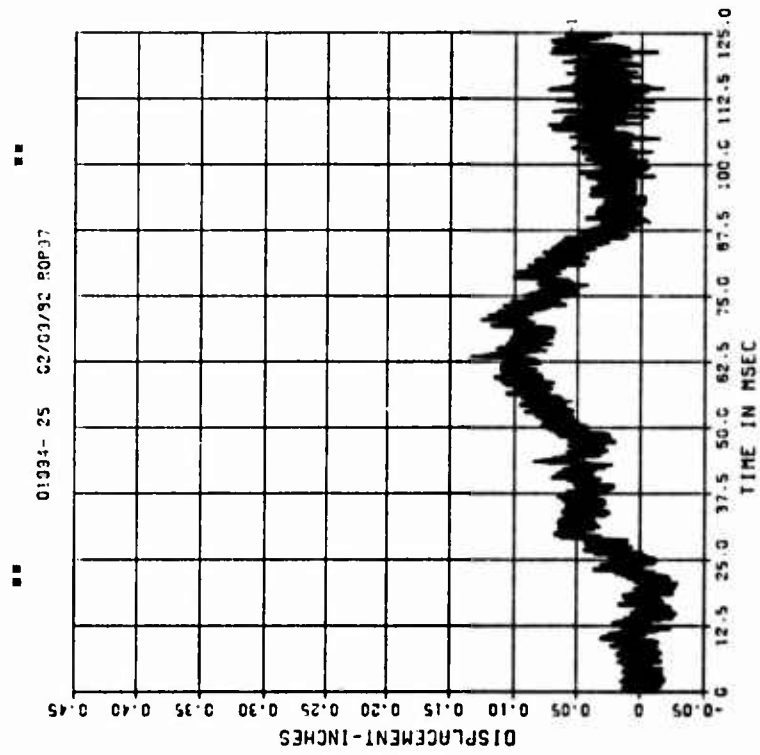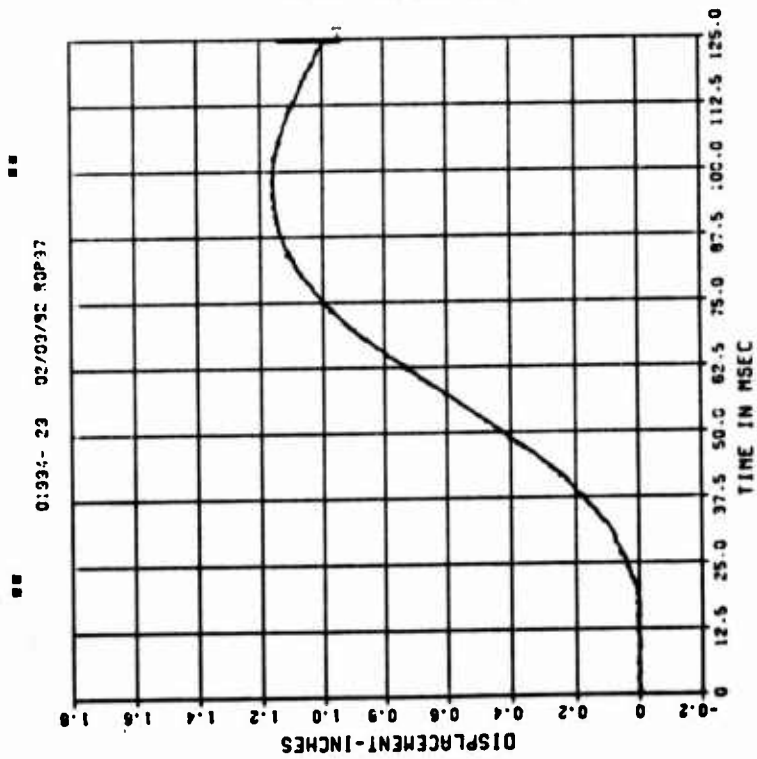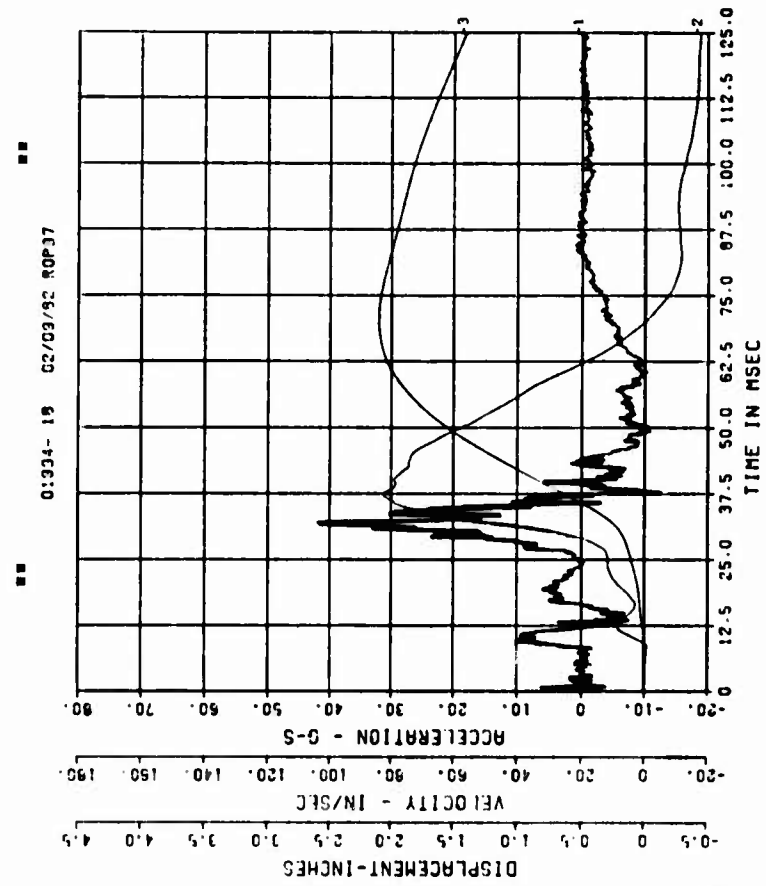D-1

100000. HZ CAL= -2.610
LP4 70% CUTOFF= 4500. HZ

01934-21   02/03/92 ROP37

DOE BLDG 12-64 PII
IP-14

100000. HZ CAL= 129.0
LP4 70% CUTOFF= 4500. HZ

01934-13   02/03/92 ROP37

** PEAK VALUE IS 97   % UNDER CALIBRATION **

DOE BLDG 12-64 PII
D-3

100000. HZ CAL= 6.590
LP4 70% CUTOFF= 4500. HZ

01994- 23   02/03/82 ROP37

TIME IN MSEC

DISPLACEMENT-INCHES

** PEAK VALUE IS 37   % UNDER CALIBRATION **

DOE BLDG 12-64 PII
D-2

100000. HZ CAL= -1.660
LP4 70% CUTOFF= 4500. HZ

01994- 22   02/03/82 ROP37

TIME IN MSEC

DISPLACEMENT-INCHES

G32

DOE BLDG 12-64 PII
D-5

100000. HZ CAL= 6.410
LP4 70% CUTOFF= 4500. HZ

01094- 25   02/03/92 POP37

** PEAK VALUE IS 99   % UNDER CALIBRATION **

DISPLACEMENT-INCHES
TIME IN MSEC

DOE BLDG 12-64 PII
D-4

100000. HZ CAL= 6.280
LP4 70% CUTOFF= 4500. HZ

01094- 24   02/03/92 POP37

** PEAK VALUE IS 95   % UNDER CALIBRATION **

DISPLACEMENT-INCHES
TIME IN MSEC

DOE BLDG 12-64 PII
A-1

100000. HZ CAL= 254.9
LP4 70% CUTOFF= 4500. HZ

0:334- 18 02/03/92 ROP37

** PEAK VALUE IS 94   % UNDER CALIBRATION **

DOE BLDG 12-64 PII
D-6

100000. HZ CAL= -4.000
LP4 70% CUTOFF= 4500. HZ

0:334- 23 02/03/92 ROP37

DOE BLDG 12-64 PII
A-3

100000. HZ CAL= 157.2
LP4 70% CUTOFF= 4500. HZ

G:004-20   02/03/92 RQP17

ACCELERATION - G-S

VELOCITY - IN/SEC

DISPLACEMENT-INCHES

TIME IN MSEC

** PEAK VALUE IS 91   % UNDER CALIBRATION **

DOE BLDG 12-64 PII
A-2

100000. HZ CAL= 219.6
LP4 70% CUTOFF= 4500. HZ

G:004-19   02/03/92 RQP17

ACCELERATION - G-S

VELOCITY - IN/SEC

DISPLACEMENT-INCHES

TIME IN MSEC

** PEAK VALUE IS 97   % UNDER CALIBRATION **

G35
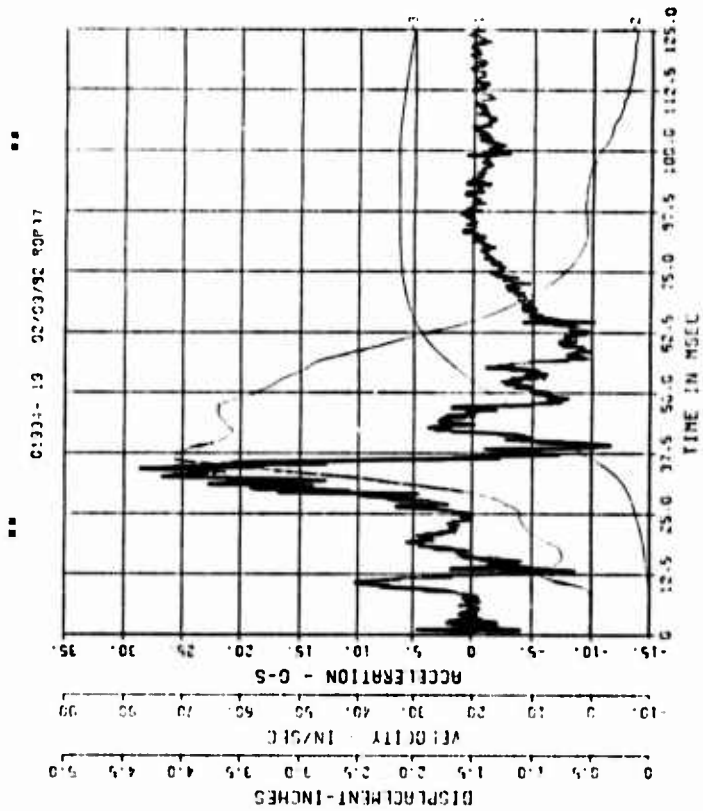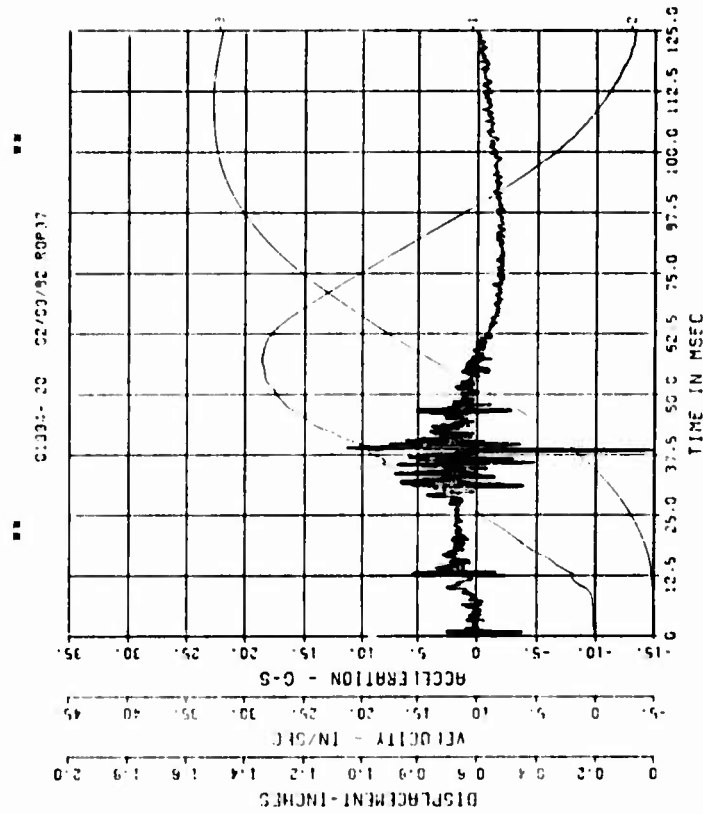
APPENDIX H

SHOCK SPECTRA FOR PHASE II ACCELEROMETER RECORDS

The shock spectra for accelerometer records A1, A2, and A3 are presented in this appendix for damping values of 0, 5, and 10 percent of critical. Each spectrum is a graph of peak pseudo-velocity in units of in./sec (labeled SSP Amplitude) versus frequency in Hz. The spectrum represents the peak response of a single-degree-of-freedom (SDOF) system of a particular frequency to the given acceleration record.

The Fast Fourier Transform (FFT) algorithm was used to determine acceleration amplitude as a function of frequency for each acceleration record. The FFTs were used to select frequencies associated with peak acceleration amplitudes. A total of 28 frequencies were selected for the A1 and A2 spectra and 26 frequencies for the A3 spectra, all between 1 and 1000 Hz. The peak SDOF responses to the acceleration records were calculated for each of these frequencies. Each spectrum is a piece-wise linear curve through these points.

Peak displacements and accelerations are easily obtained from the pseudo-velocities shown in spectra using the following relationships:

$$d = \frac{V}{2\pi f} \qquad\qquad a = \frac{2\pi f V}{12(32.2)}$$

where

    d = maximum displacement, in.

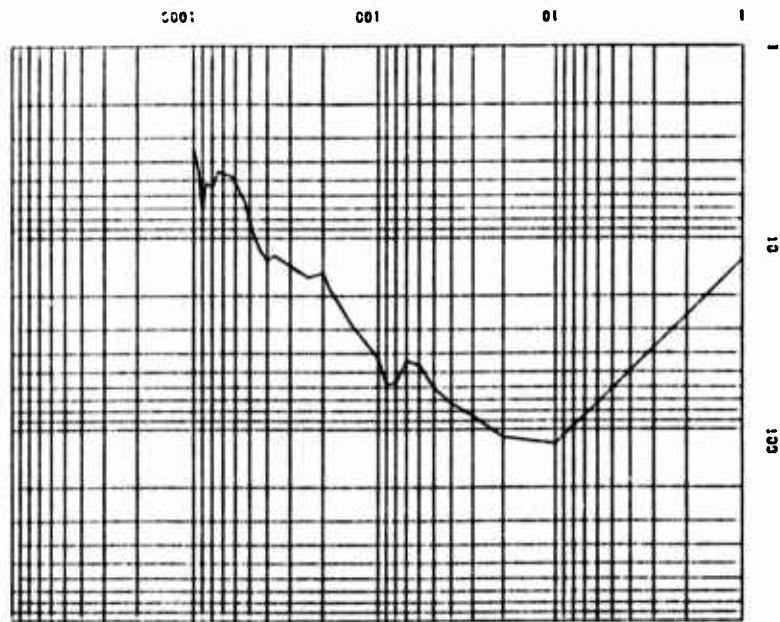   V = peak pseudo-velocity, in./sec.

    f = frequency, Hz

    a = maximum acceleration, "g's"

DOE BLDG 12-64 PII
A-1
100000. HZ CAL= 254.9
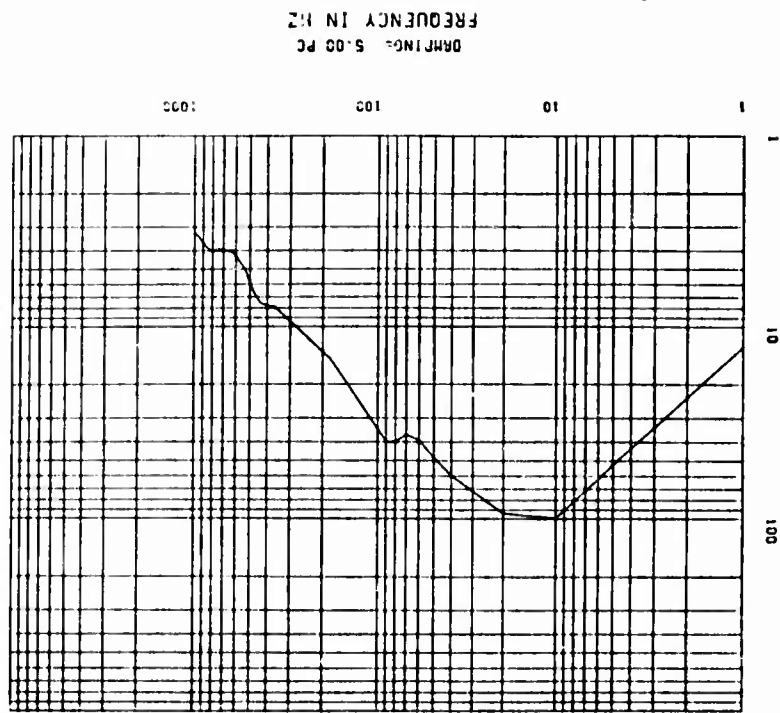LF4 70% CUTOFF= 4500. HZ

SSP

0:991:-19 04/30/92 #0209

SSP
AMPLITUDE

FREQUENCY IN HZ
DAMPING= 5.00 PC

DOE BLDG 12-64 PII
A-1
100000. HZ CAL= 254.9
LF4 70% CUTOFF= 4500. HZ

SSP

0:991:-19 04/30/92 #0209

SSP
AMPLITUDE

FREQUENCY IN HZ
DAMPING= 0. PC

H3

DOE BLDG 12-64 PII
A-2

100000. HZ   CAL= 219.6
LP4 70% CUTOFF= 4500. HZ

SSF

0:331- 19   04/30/92 R0203

DAMPING= 0.   PC

FREQUENCY IN HZ

■ SSP ■
AMPLITUDE

DOE BLDG 12-64 PII
A-1

100000. HZ   CAL= 254.9
LP4 70% CUTOFF= 4500. HZ

SSF

0:331- 19   04/30/92 R0203

DAMPING= 10.00 PC

FREQUENCY IN HZ

■ SSP ■
AMPLITUDE

DOE BLDG 12-64 PII
A-2

100000. HZ CAL= 219.6
LP4 70% CUTOFF= 4500. HZ

SSP

0:931- 19   04/30/92 R0203

FREQUENCY IN HZ
DAMPING= 10.00 PC

AMPLITUDE

■ SSP ■

1000

100

10

1

DOE BLDG 12-64 PII
A-2

100000. HZ CAL= 219.6
LP4 70% CUTOFF= 4500. HZ

SSP

0:931- 19   04/30/92 R0203

FREQUENCY IN HZ
DAMPING= 5.00 PC

AMPLITUDE

■ SSP ■

DOE BLDG 12-64 PII
A-3
100000. HZ CAL= 157.2
LP4 70% CUTOFF= 4500. HZ

SSP

0:393:-20 04/30/92 #0200

FREQUENCY IN HZ
DAMPING= 5.00 PC

■ SSP ■
AMPLITUDE

DOE BLDG 12-64 PII
A-3
100000. HZ CAL= 157.2
LP4 70% CUTOFF= 4500. HZ

SSP

0:393:-20 04/30/92 #0200

FREQUENCY IN HZ
DAMPING= 0. PC

■ SSP ■
AMPLITUDE

H6

DOE BLDG 12-64 P I
A-3
100000. HZ   CAL= 157.2
LF4 70% CUTOFF= 4500. HZ

DAMPING: 10.00 PC
FREQUENCY IN HZ

AMPLITUDE
* SSP *